Albert A. Lysko

On Multiple Domain Basis Functions and Their Application to Wire Radiators

Thesis for the degree of Philosophiae Doctor

Trondheim, May 2010

Norwegian University of Science and Technology
Faculty of Information Technology, Mathematics
and Electrical Engineering
Department of Electronics and Telecommunications

NTNU
Norwegian University of
Science and Technology

NTNU
Norwegian University of Science and Technology

Thesis for the degree of Philosophiae Doctor

Faculty of Information Technology, Mathematics and Electrical Engineering
Department of Electronics and Telecommunications

ISBN 978-82-471-2168-9 (printed ver.)
ISBN 978-82-471-2169-6 (electronic ver.)
ISSN 1503-8181

Doctoral theses at NTNU, 2010:102

Printed by NTNU-trykk

Dedication

Эта работа посвящается моей дорогой маме Елене Алексеевне Лыско. Ты посвятила свою жизнь моему развитию и обучению. Я посвящаю мою жизнь сохранению твоих духовных ценностей.

Dette arbeidet er dedikert til min kjære Mamma, Elena Alekseevna Lysko. Du viet ditt liv til min utvikling og utdannelse. Jeg vier mitt liv til å videreføre dine åndelige idealer og verdier.

This work is dedicated to my dear mummy, Elena Alekseevna Lysko. You dedicated your life to my development and education. I devote my life to uphold your virtues.

Abstract

The Method of Moments (MoM) is a general method for solving linear problems, including electromagnetic problems, such as radiation and scattering of electromagnetic waves. The applications of the method include analysis and design of antennas and scatterers and electromagnetic compatibility. This work develops several new extensions to the traditional framework of the method of moments, addressing memory savings, problem conditioning, and acceleration of computations.

The MoM's groundwork in this thesis is based on the works by Professor B.M. Kolundzija. The theory from his books and papers was implemented in a Matlab programming code, within the thin-wire kernel. Several new features, core to this thesis, were then devised, including an improvement to the condition number of impedance matrix, analytical computation of radiation pattern, and piecewise-linearly interpolating multiple domain basis functions (MDBF).

This work includes a study into new possibilities to minimize the impedance matrix's condition number with non-to-little computational overhead. The approach devised involves an appropriate selection of a common/reference wire at a junction with multiple wires attached. It is shown that the choice is frequency dependent. Several solutions with different degrees of optimality and complexity are introduced. A proposed simplistic method ensures that the maximum condition number is never encountered. On the other extreme, another new but more computationally demanding method minimizes the condition number. The technique proposed has demonstrated an order of magnitude reduction in the condition number.

The work also proposed a novel method for an accelerated computation of radiation patterns. The method is based on analytical techniques. At low frequencies, the method employs Taylor's expansion of the oscillating exponential term. At higher frequencies, the method uses integration by parts. Estimates for errors are derived and used to establish the boundary between the Taylor's expansion and the integration by parts. At this boundary, the method has a limitation on the best achievable accuracy. However, this limit is found to be sufficient for most practical applications. The speed and accuracy of a Matlab realization of the method were found matching commercial

software, indicating further acceleration potential through coding in a lower level programming language.

The bulk of this thesis is on the realisation of multiple domain basis functions (MDBF). MDBF are be defined over a chain of several wire segments. The proposed extension to the traditional MoM decouples the requirements for the mesh of the geometrical model from the requirements for the representation of current distribution. This separation permits to treat curved structures more efficiently, as well as also extends the boundaries of the thin wire approximation. The presented treatment of the problem includes the development and testing of several original automatic algorithms for generating appropriate meshes of chains of wires. The concept of linearly interpolated MDBFs is developed, implemented and tested on piecewise linear (PWL) and piecewise sinusoidal (PWS) MDBFs. Several examples ranging from a short monopole to a resonant coil-loaded antenna were used to illustrate the techniques devised. The application of the technique to the latter example has shown an order of magnitude improvement in the number of the unknowns, as compared to a traditional MoM formulation. This translates into two orders of magnitude in memory savings.

Furthermore, a theoretical basis for applying higher order polynomial basis functions to chains of wire segments has been developed, and can be readily extended onto other shapes of basic geometrical element than wire segments. An estimate for computational complexity associated with the higher order hierarchical polynomial basis functions has been derived, quantifying the available potential for a reduction in the number of unknowns.

A composition of these individual improvements covers the wide spectrum of a MoM based solution to a multitude of practical problems. It is expected to provide a next step in the reduction of the time and other resources required to solve large problems, towards a numerical electromagnetic synthesis of antennas.

Acknowledgements

This thesis is the culmination of several years of work. Throughout these years I have received moral, academic and financial support, and there are many people to whom I am very grateful.

First of all, I would like to thank my first scientific advisor Professor Jon Anders Aas. His infinite patience and his support permitted me to complete the work. His efforts in reviewing the chapters are also appreciated very much. Professor Aas's attention to detail helped me to learn and also to become more independent. I cherish the friendship, in addition to the personal and character examples he has displayed over the years.

I greatly appreciate the confidence, guidance and assistance provided by my second scientific advisor, Professor Guennadi Kouzaev, in the completion phase of the thesis. His suggestions for the thesis have been very valuable and are also sincerely acknowledged.

The help and various forms of support from many of the staff at the Department of Electronics and Telecommunications, NTNU and SINTEF are truly appreciated. The examples of Bjørn Uno Kolstad, Egil Eide, Jacob Kuhnle and many others will always stay with me. The sincere friendliness, openness and honesty of Norwegians have become a reference to me.

I would like to express my gratitude to the Faculty of Information Technology, Informatics, Mathematics and Electrical Engineering (IME), who took me as a student and co-funded the studies. The financial support via the Norwegian Quota programme and Lånekassen, Norway is also gratefully acknowledged.

The last parts of the thesis I completed whilst I was working as a researcher at the Meraka Institute, CSIR. I am very grateful to the Meraka Institute and, personally, to my managers, Kobus Roux and Ntšibane Ntlatlapa for the support and motivation.

The help in the form of a special version of modelling software WIPL-D, received from WIPL-D d.o.o., Serbia, is gratefully acknowledged. The WIPL-D's efficiency in generation of large impedance matrices has been very valuable.

This long list would never be whole without showing my deep and sincere appreciation to my family and our fiends. I am grateful to my parents-in-law, Sewsunker and Sabita Dhavraj, for the support received from them. The Aasens, Løvseths, Pilipenkos, Gamages and several other families have always been very loyal and caring friends to us. I thank them for their genuine love and friendship. My brother Aleksey's frequent motivational talks and reminders are honoured with gratefulness and love. The kind help in polishing parts of the text, received from Indru Olivier, Artem Pilipenko and Vadim Makarov is appreciated very much.

My wife, Meena Lysko has edited English of many parts of the thesis, and has also helped with great suggestions. I truly appreciate your thoughtful and loveful efforts. Also, I must admit that the treasured lives of both my wife and my daughter Yulia have been tightly coupled and entangled with this work. Their sacrifice, love, care, support and encouragement will be always remembered.

Contents

Chapter 1. Introduction

The *Method of Moments* (MoM) is a general method for solving linear problems, including electromagnetic problems, such as radiation and scattering of electromagnetic waves. The method has many applications including antenna design and analysis, and electromagnetic compatibility.

This work establishes an extension for the method of moments, separating the requirements on the geometrical model from the requirements on the current representation. This permits to treat curved structures more efficiently and also extends the boundaries of the thin wire approximation.

This introductory chapter starts with an overview of the historical developments related to the method of moments. It then proceeds with a comparison of several other methods of computational electromagnetics, namely FDTD, and FEM, against the method of moments and one another. This is followed by a motivation for the work done, statements concerning the originality and novelty of the work, and a relevant chronology and key elements in the developments towards the concept of "chains". An outline of the thesis concludes this chapter.

1.1 Brief Historical Background of the Method

The path to the modern method of moments in the field of electromagnetics began with theoretical works more than a century ago [Collin, 11].

Maxwell presented his theory of electromagnetic waves in 1864 [Maxwell, 70]. Only much later, the problem of evaluating the current distribution that is induced on a thin straight-wire radiator by a time-harmonic electromagnetic field was described by Pocklington [Pocklington, 87]. He published what became [Balanis, 4] known as Pocklington's Equation. In 1898, Abraham succeeded in calculating the radiated field from a half wave dipole. He obtained an exact solution for a freely oscillating elongated ellipsoid of revolution [Abraham, 1]. Much later, in the 1930s, a cylindrical centre-driven antenna was considered by King [King, 38] and Hallén [Hallén, 26].

The exact nature of formulation for the complex problem in terms of mathematical physics places a restriction on the geometries that can be investigated. Asymptotic methods such as the method of steepest descent [Balanis, 4], as well as perturbation methods furthered the reach of science towards finding approximate solutions to many practical problems. Although these methods have been instrumental in extending the range of the problems that could be treated, they are complex, and are still not able to address an arbitrary geometry in a systematic manner. A more universal, although approximate, solution was needed.

Following the works on a variational method by a Swiss theoretical physicist Walter Ritz, the first steps towards the modern method of moments (MoM) were taken by a Russian mathematician and engineer Boris Grigoryevich Galerkin just before 1920-s. His name has been used with in conjunction with the name MoM to denote the most frequently use scenario where the sets of basis and testing functions are the same.

In electromagnetics, a version of MoM was first utilized by Nomura in 1952 [Nomura, 81] and Storm in 1953 [Storm, 103]. The both cases dealt with linear antennas[1]. Consequently, the mathematical foundations of the MoM were set out in 1964 in works by Kantorovich, Krylov, Akilov [Kantorovich et al., 36], [Kantorovich et al., 37].

The method of moments became popular after the publications by Harrington in 1967-1968 [Harrington, 27], [Harrington, 28], whose systematic approach brought unification into the method. Even now, his book on the MoM [Harrington, 28] is perhaps the most cited reference for this technique.

Today several variations[2] of the MoM technique are in extensive use by scientists and engineers. There exist many publications, including a number of excellent books specifically focusing on the method and its applications in electromagnetics, such as

[1] The term linear antenna refers to a straight wire.

[2] The specialist areas include frequency domain realizations for general problems, spectral domain approaches for multilayered structures (e.g. in design of multilayered printed circuit boards), and the time domain techniques (a new trend for ultra wide bandwidth applications).

[Mittra, 76], [Wang, 110], [Miller et al, 75], [Morita et al, 78], [Peterson et al, 85], and [Makarov, 67]. The method is widely accepted. Many textbooks on antennas and electromagnetics include simple codes realising the MoM, for example [Balanis, 5], [Stutzman, 104], and [Makarov, 67].

There are also a number of software packages realising MoM and are available either freely or commercially. The freely available codes gained momentum in 1980s with the Numerical Electromagnetic Code (NEC) [Burke and Poggio, 7] developed at the Lawrence Livermore National Laboratory [Burke et al., 6] and now includes many other freely available codes [http://www.cvel.clemson.edu/modeling/EMAG/free-codes.html]. There are many commercial programs as well. Some of the popular names include:

- Momentum (by Agilent Technologies, USA) [http://eesof.tm.agilent.com/products/momentum_main.html],
- Sonnet (by Sonnet Software Inc., USA) [http://www.sonnetusa.com/],
- WIPL-D (by WIPL-D d.o.o., Serbia) [http://www.wipl-d.com],
- FEKO (by EM Software & Systems, South Africa) [http://www.feko.info],
- IE3D (by Zeland Software, USA) [http://www.zeland.com/ie3d.htm]
- SuperNEC (by Poynting Software, South Africa), [http://www.supernec.com]
- and others.

There are comprehensive lists available on-line at the web pages [http://www.cvel.clemson.edu/modeling/EMAG/csoft.html] of the Clemson University Vehicular Electronics Laboratory and the "EMLIB (Electromagnetics software and databases)" web pages at [http://www.ieeeaps.org/emlib/emlib.html].

Each package has its advantages and restrictions. A detailed comparison of the programs is a challenging topic that is further complicated by constant developments in the field.

1.2 Computational Electromagnetics Methods

The field of computational electromagnetics has become a fast-paced discipline. The method of moments was particularly popular in the past, probably due to memory limitations in digital computers. Today the technology has improved dramatically, the random access memory has become relatively inexpensive, and there are several other methods that have become practicable and compete with the method of moments.

There exist a number of different approaches to solve various electromagnetic problems [Chew, 10], [Volakis, 109]. To name a few of the most popular[3], these would probably be the finite difference time domain (FDTD) technique, finite elements method (FEM), and the method of moments (MoM) [Davidson, 13]. Based on the differences in formulation and applicability to the problem that needs to be solved, one of the methods would be able to provide the solution with required accuracy faster than others.

The *finite difference time domain* (FDTD) method [Taflove, 106] considers the volume of a structure, and applies a volumetric grid. A low order approximation of the differential form of Maxwell's equations is used to calculate the electrical and magnetic fields on the grid. A successful meshing scheme introduced by Yee [Yee, 112] uses two grids, one for the electrical field and one for the magnetic field. These grids are displaced from one another. By alternating the calculation of the electrical and magnetic fields on the grids, and thus incrementally stepping/propagating in time, the problem is solved in the time domain, meaning that the solution is a function of time. The solution is obtained in-place, at the points of the grid, without building a separate matrix equation. Although this method is both very simple and flexible, it best serves the problems where the volume is small. For radiation problems, the minimum volume is restricted by the need to space the radiation boundary condition (absorbing outgoing waves) to at least about a quarter of a wavelength, to permit formation of the wave-front. Under these conditions, the memory and computational requirements quickly become very high. In this sense, the radiation problems where the distances and sizes

[3] Some updates on the advances in the most popular methods can be found for instance in [Volakis, 109], [Davidson, 12], [Chew, 10].

are often large compared to wavelength, are not well suited. Otherwise this is an exceptionally simple and powerful approach.

The *finite elements method* (FEM) [Silvester and Ferrari, 101], [Awadhiya, 3], [Itoh et al., 33] is also based on the differential form of Maxwell's equations, transformed to a form referred to as a vector wave equation. The method is mostly used in the frequency domain. A so-called weak form of that equation, obtained by either minimisation of a functional or by application of the Rayleigh-Ritz method, is applied to the field and used to do the actual computations. The matrix of linear equations is sparse. This method relies on the meshing of a volume. Although application of variational techniques softens the requirements on the mesh density compared to the FDTD, this method still requires filling the volume contained by the object under study. In addition, like in the FDTD, the boundary conditions must be applied at the boundaries of the volume. For radiation problems, this again leads to high requirements on processing power and memory. However, for not too wide bands of frequencies, FEM provides one of the most powerful formulations for electromagnetic modelling for antennas containing dielectric material, particularly if the material is inhomogeneous or anisotropic. Although this method may also be used for antennas made of solid conducting material, the method of moments shows superior performance in that domain [Volakis, 109].

The *method of moments* (MoM) is often referred to as the *moment method* and *method of weighted residuals*. It is the general method of converting integral equations into a system of simultaneous linear algebraic equations [Harrington, 27], [Harrington, 28], [Peterson, 85]. The method originated from mechanics and mathematics and received its name in association with the *n*-th moment of a function. First, the unknown in the integral equations is expressed as a linear combination of known functions (referred to as *basis functions*, or otherwise *expansion functions*). Then the testing procedure is applied, where the equations are convoluted with another set of known functions. This step converts a single equation with multiple unknowns into a system of equations. Where the number of equations matches the number of unknowns, this system may be inverted to obtain a solution. If the number of equations exceeds the number of

unknowns, the system is over-determined, but can still be solved by the *least square* procedure [Kolundzija, 46].

There exist several variants of the MoM. The equations may be formulated to apply to surfaces or volume, resulting in surface integral equations (SIE) or volume integral equations (VIE), respectively. The SIE formulation is best suited for radiation problems where the radiation is produced by the currents flowing on surfaces of wires, plates or dielectrics[4]. The VIE MoM has many similarities with FEM and is often compared with it. As FEM, VIE MoM works most efficiently where the geometrical structure is complex and the problem is closed (i.e. applies to a finite volume). VIE is also capable of a straightforward solution in the situation where very thin layers are present. When a layer of dielectric is thin, the currents on its large sides are nearly parallel and have nearly equal amplitudes. In SIE formulation, these currents are treated as independent, whilst in reality they are closely coupled, making the resulting linear system ill-conditioned. There are mechanisms to treat this type of irregularity within the SIE formulation of MoM. They are outside of the scope of this text, and shall not be discussed. In terms of performance, the difference between the dense matrices generated by the VIE MoM and sparse matrixes produced by FEM often give the FEM a significant advantage.

This work has its origins in an analysis of radiation problems with electrically large sparsely filled volumes. The method of moments is the best method to address this type of problems.

1.3 On Computational Complexity of Solutions by Different Methods

The requirements for the volumetric and surface formulations in terms of quantity of required variables may be readily illustrated and compared by enclosing the volume of a problem with a cube with side L. The total area of its six sides is $6L^2$. The volume taken by a cube equals L^3. Considering that the mesh density on the cube of $n=N/L$, where the

[4] Although physically the currents do not flow on the surface of dielectrics, the equivalence principle [Balanis, 4] permits replacing the volumetric currents and fields with an equivalent surface formulation.

integer N is greater than 0, is sufficient to approximate the fields/currents in/on the cube correctly, the cube may be divided into $L^3/(L/N)^3=N^3$ equal sub-cubes. In the surface formulation, the total number of square patches would be $6L^2/(L/N)^2=6N^2$. The volumetric quantities have 3 dimensions and will require at least 3 projecting variables. The unknown on a surface may be represented with 2 unknowns. Thus volumetric formulation for a cube requires $3N^3$ variables, whilst the surface formulation requires $6N^2$ variables. The number of unknowns between the two approaches is equal when N=2. This simplified approach assumes no objects inside the cube. It is asymptotically valid where the cube is nearly empty, and the space is filled with simple shapes.

If the volume contains a complex structure, then the surface formulation will require to add the surfaces of the sub-cubes, making the number of unknowns due to SIE exceed the number of unknowns required by VIE formulation. In terms of the example above, taking into account all inner surfaces will increase the number of variables to $6N^2(N+1)= 6N^3+6N^2$. This number exceeds the respective value from the volumetric formulation, $3N^3$.

In the case of dense matrices produced by the MoM, the difference in the number of unknowns affects the resources required. The matrix requires an $O(N^2)$ amount of storage. In order to solve the system of linear simultaneous algebraic equation, the number of required floating point operations, such as addition or multiplication, is on the order of $O(N^3)$.

Thus, in the context of the MoM, increasing the density or size of the mesh by a factor of two will require 4 times more memory, and will take 8 times longer to solve. The same action applied to the FDTD method will require 8 times more memory, since the number of variables is directly related to the volumetric density of variables.

Problems involving electromagnetic radiation are usually open problems. Out of the above mentioned methods, the surface formulation of MoM indicates the best potential to address such scenarios, as it does not require additional mesh nodes to describe the volume to permit formation of the radiated field.

A more advanced analysis comparing SIE MoM, VIE MoM and FEM may be found in [Kolundzija and Sarkar, 49], and [Kolundzija et al., 46]).

An additional aspect should be mentioned, considering the present trend towards multi-core processors and multi-processor configurations. It is the ability of a numerical method to be parallelised (i.e. solved using the multiple processors working in parallel). For example, FDTD offers excellent (and probably, the best) options in parallelisation. The possibilities offered by MoM are much more limited in this regard. However, this option was not considered in this work.

1.4 Origins of this work and Motivations, or Looking for an Invention

Following the previous research [Lysko, 58], [Lysko and Aas, 54], the author's initial intention was to advance the numerical electromagnetic methods for modelling plainly stratified medium and applying these methods to the design and analysis of antennas for ground penetrating radars (GPR) [Daniels, 14]. However, as the depth of a stack of papers surveyed grew, this direction was found to be under an exhaustive investigation - most of the ideas that the author was nourishing were found already implemented in a plurality of ways.

At the time, the author was also offered to participate in a project for redesigning an antenna measurement system in an anechoic chamber. This work resulted in a fully automated system for antenna and radar cross section measurements in three dimensions [Lysko and Eide, 57], [Lysko, 55-56]. Recently the system was upgraded to support a frequency range up to 50 GHz. Some of the work done, including a characterisation of the mechanical components of the system using microwave techniques, is still on the way to be published.

Whilst working with that system, the author's research in antennas for GPR became more focused on spiral antennas [Nakano, 80], a class of frequency independent antennas [Rumsey, 98], [Mushiake, 79]. A simple model behind the radiation produced by spiral antennas is often associated with the so-called *active region*. It corresponds to a concentric region of the spiral, whose circumference equals one wavelength[5]. The idea under pursue was to combine spiral antennas into a co-axial array, whilst keeping the

[5] There are also higher *modes*, where the circumference equals a multiple of the wavelength.

distance between the respective active regions constant in terms of wavelength. This may be depicted with a set of cones with dissimilar opening angles, whose axes are aligned and on the same axis. This array satisfies the angle-independence and geometrical scaling principles, and was thus expected to provide a theoretically unlimited bandwidth.

Studying this type of antennas requires covering a wide frequency band. In addition, an arrayed structure is dimensionally larger and more complex than a single spiral antenna. This created the first obstacle. The ability to simulate this type of antenna was found to be very limited. At first, the program "High Frequency Structure Simulator" [HFSS, 29] sold at that time by the Hewlett Packard[6] was applied to the problem. The HFSS is based on FEM, and thus required at least a quarter wavelength spacing from the antenna to radiation boundary. Therefore, the model of a relatively small spiral antenna, which was considered at the frequency range ratio of only 2:1, quickly reached the limits of the memory in a PC, required swapping between memory and disk, took a very long time to simulate. A number of tricks to improve the efficiency of simulation were learned in the process (e.g. dummy mesh layers). Yet, an acceptable accuracy could not be achieved.

Next, a MoM based tool, WIPL-D [Kolundzija, 47], was utilised. The modelling became much easier and faster, and also provided better accuracy. However, the author regretfully found that the coupling between the antennas in the array was too strong to find the antenna practical. In addition, the axial length of the structure had to grow exponentially with the increase in the number of the antennas in the array, also making it impractical.

By that time, the author already wrote a number of Matlab [Matlab, 69] subroutines for working with WIPL-D. Also, WIPL-D had proved to be a highly efficient tool for modelling a variety of antenna types. However, as a "Lite" version of the full-featured commercial program, it had a tough restriction on the maximum number of variables that could be used. The spiral antennas were modelled using a constant angular step around the spiral's generatrix, so that the elements of the high-frequency part of the spiral antenna (near the feed point) were geometrically finer than the elements near the

[6] See http://en.wikipedia.org/wiki/HFSS .

low frequency end (i.e. the wide end, termination). This approach minimises the number of unknowns and also follows the angle-independence principle [Rumsey, 98], [Mushiake, 79]. However, the number of unknowns was too limited for modelling arrays made of antennas with finely meshed curvatures. Modelling of arrays made of plates rather than wires was not possible at all.

One of the limiting factors in modelling the spirals was that the geometrical accuracy of a stepped (i.e. piecewise linear) approximation for the smoothly curved spirals had to be made low, especially concerning the arrays. Making the angular steps high created an additional artefact – the frequency range of the numerical model was slightly shifted in frequency with respect to an ideally smooth model. These were the first silent calls for wishing to unite the several electrically small segments into larger ones, whilst working at one frequency.

1.5 On Work done, Originality, and Novelty

The number of unknowns in the version of WIPL-D available with the book [Kolundzija, 47] is limited. Both accuracy and speed of the program were however superior [Stamm and Breakall, 102], [Djordjevic and Notaros, 19] to several other codes, including the freely available NEC [Burke, 7]. Looking for an unlimited number of variables and accuracy provided by the WIPL-D, the author decided to take the road of writing his own MoM code based on the same theory as WIPL-D.

This proved to be a difficult but a fruitful learning and understanding journey. The program was written in Matlab [Matlab, 69] and the code is entirely original. The current capabilities and features of the code are (for more information on the developed Matlab program, please refer to Appendix C):

- Flexible programmable variable- and Matlab- based user interface;
- Works with arbitrary three dimensional configuration of wires;
- Supports arbitrary quantity and combination of multiple generators, as well as of plurality of lumped and distributed load types;
- Minimises the number of variables by using piecewise linear (PWL) basis functions derived to incorporate and automatically satisfy Kirchhoff's current law;

- Supports perfect electric conductor (PEC) and perfect magnetic conductor (PMC) symmetry planes with arbitrary combination of *XY*, *YZ* and/or *XZ* planes;
- Displays the geometry of the structure under investigation graphically, denoting nodes, wires, positions of generations etc.;
- Computes currents, as well as network parameters (admittance, impedance, and scattering matrixes *Y*, *Z*, *S*, respectively) in one of two modes: exciting one port at a time or all ports simultaneously;
- Estimates solution errors through usage of condition number;
- Computes far field patterns, gain, and radiated power;
- Uses novel composite chain basis functions, enabling higher efficiency in modelling curved and low-frequency structures;
- Within the framework of the multiple domain basis functions (MDBF) and chains, supports both PWL and also piecewise sinusoidal (PWS) interpolating MDBFs.

Additional functionality to utilise the capabilities of WIPL-D:

- Imports and exports of WIPL-D compatible files defining geometry and definitions (.IWP, ,.SMB), current on wires and plates (.CU1), containing network parameters (.AD1), far field radiation patterns (.RA1) and near field (.NF1);
- Enables direct conversion between PCAAD and WIPL-D file formats for geometry files;
- Offers an option of executing WIPL-D software to process a project;
- Generates parameterised geometries for several types of antennas, such as dipole, monopole, corrugated monopole, meandered monopole, loop, Archimedean and equiangular spiral antennas.

The origin for the variation of the method of moments used in the text is predominantly based on the works published by Professor Branko M. Kolundzija, Serbia and his colleagues, although publications by many authors from other research groups were also used. The references to the relevant sources are provided in the text *ad hoc*, and, where considered necessary, the theory for these methods is described.

Some aspects of the theoretical grounding and also many algorithms had to be re-invented, since the producers of commercial software advertise the features and their benefits but rarely publish the actual algorithms. Examples of these are the algorithms for automatic assignment of basis functions to an arbitrary combination/configuration of wires, identification of incorrect configurations etc.

There are a **number of novel concepts and techniques that has been developed, implemented, and tested**. These include:

- Section 3.1: A possibility to reduce the condition number with only very little overhead was identified and the relevant investigation has been made, based on multiple numerical models.
- Section 3.2.7 mentions a novel memoization-based technique, which was successfully applied to the process of filling in the impedance matrix [Lysko, 61, 62]. In Matlab environment, this technique has shown a speed up in filling in the impedance matrix by a factor of up to five.
- Section 3.10 and Appendix B: A fast and efficient technique for computing a radiation pattern with higher-order polynomial basis functions was developed [Lysko, 66].
- Chapter 4: Novel composite basis functions defined on multiple domains were introduced. Due to their nature, for they cover wires connected in series, these basis functions were termed *chain basis functions*. For a more general case, these functions are also termed as *multiple domain basis functions* (MDBF).
    - Sections 4.1 - 4.1.3.4 and 4.2.2 - 4.7.5 introduce the original concepts and provide the necessary theoretical and practical basis for a successful implementation. Several algorithms for meshing into and from chains were developed and tested. They include identification of chains, optimal and sub-optimal segmentation of chains, assignment of chain basis functions to chains, and inter-linking of the chain basis functions with the original basis functions [Lysko, 59].

- Sections 4.8 to 4.13 extend the theory even further. The type of basis functions that may be applied to chains were expanded from piecewise linear functions (PWL) onto arbitrary shaped linearly interpolated functions. The piecewise sinusoidal (PWS) profile was tested [Lysko, 60]. A theoretical foundation was also made for application of higher order basis functions within the framework of chains [Lysko, 63]. An estimation of computational complexity for the concept has also been made.
- Chapter 5 provides examples of applications for the MDBFs [Lysko, 59-65] and relevant discussions.

- Appendix A introduces an original approach for relating the resonance frequency accuracy for modelling of a loop antenna to the required number of straight segments in a regular polygon.

1.6 Towards Concept of Chains

The work on multiple domain basis functions is considered to have a potential impact on the application of the method of moments to curved structures. The background surrounding this work may therefore warrant a special note.

Whilst working with combining the piecewise linear (PWL) functions into doublet basis function (i.e. two PWLs defined over a pair of connected wires), it was noted that the impedance matrix elements may be represented by four terms corresponding to the four possible ways in which two pairs of wires could interact. It was then identified that the same decomposition could be applied to an arbitrary number of wires interconnected in series (thus the name *chain*). Such an approach could be expected to (a) reduce the number of variables required when modelling large smoothly bent objects, and (b) help to extend the applicability of the thin wire approximation, where one of the conditions is to have the length of a wire segment much greater than its radius.

Hereinafter, an aggregated set of such wires is referred to as a *chain* in this text. Following this notation, the wires that belong to a chain are called *chained wires* etc.

Once the idea was identified and thought through, a search began for prior art, i.e. papers that could have already described a realisation and results on the technique. It

took many iterations to trace two papers, co-authored by Shawn D. Rogers and Chalmers M. Butler [Rogers and Butler, 97], [Rogers and Butler, 96], that discussed an approach based on the same principles. Their research called for *composite basis functions* applied to curved wire structures approximated with straight linear segments. The composite basis functions were made up by a weighted sum of piecewise linear and piecewise constant basis functions. Their main goal was to uncouple the number of variables from the number of straight segments used to approximate the structure, and thus reduce the rank of the resulting matrix.

The work by Rogers and Butler [Rogers, 96-97] incited the author's own work into systemizing the author's approach. Originally, the author was working with a realisation that requires implementation at the level of the core of the MoM. This means that the integrals over the interconnected wires were computed following the sequence of interconnected wires. That sequence is associated with the sum of basis function in a doublet, as mentioned earlier. Despite saving memory in terms of the impedance matrix, this made identification and utilisation of repetitions and symmetries more difficult. The advantage of the matrix approach used by Rogers and Butler is in unification of the procedure, as well as in making the implementation of this technique more independent from the original impedance matrix. Considering these advantages, the author's initial code was modified to work with the matrix approach. The Section 4.2.1 reflects on this.

It must also be noted that the papers by Rogers et al. [Rogers and Butler, 96-97] are based on an implementation of MoM where the basis functions are piecewise linear (PWL) and the testing functions are pulse functions. Following the results of research done by a number of authors, for example, [Harrington, 28], [Butler, 8], [Miller, 73], [Medgyesi-Mitschang, 71], and [Kolundzija, 45], that combination of basis functions is less robust than the Galerkin's procedure [Petrov, 86], [Harrington, 27] (where both basis and testing functions are the same). The Galerkin procedure is presented in this thesis.

Following the historical order of developments in the work, the author's research has also shown that the approach of chaining individual segments enables implementing arbitrary-shaped linearly-interpolated basis functions. The basis functions combined in a chain are weighted to obtain the final profile of a composite basis function. By varying

the weights, it is possible to approximate basis functions of any shape. For example, a profile close to the shape of a piecewise sinusoidal (PWS) basis function [Richmond, 95] may be generated by appropriately weighting a series of piecewise linear functions. The term *linearly interpolated* is used to highlight that the permitted shape is limited by the ability to approximate it with a weighted linear combination of the actual basis functions.

The above-mentioned work was then followed by the development of a theoretical framework for applying the approach of chains to the higher-order polynomial basis functions. The computational complexity of the technique has also been estimated.

1.7 Overview of Chapters

This chapter (Chapter 1) provides an overview of the historical background of, and some alternatives to the method of moments (MoM) and inter-compares the alternatives. It also introduces the prior art and some advancements in the field, to be discussed in more depth throughout the rest of the text.

Chapter 2 reviews the foundations of the moment method applied to thin wires. It includes derivations of the necessary equations, as well as discussions and derivations related to the basis functions.

Chapter 3 introduces several original techniques, and adds to the review of the framework of MoM. A new method for reducing the condition number of the impedance matrix starts the chapter. In the next sections, some considerations are given for the treatment of the impedance matrix integrals, excitations, lumped and distributed loading, and symmetry planes. This is followed with a detailed example. A novel solution to the problem of computing the radiation pattern for higher order polynomial basis functions is then introduced in Section 3.10; a copy of the paper with details is provided in Appendix B.

Chapter 4 introduces novel composite multiple domain basis functions and chains of wires, and establishes the respective mathematical basis. Several algorithms and techniques developed for implementing the concepts are discussed. The proposed approach is then extended from the piecewise linear basis functions onto arbitrary

piecewise-linearly-interpolated shapes, including piecewise-linearly-interpolated piecewise sinusoidal functions. The chapter is ended with derivations and discussions for extending the technique from the linear basis functions to higher order polynomials. The computational complexity of the devised method is estimated. It is also shown how to apply multiple-domain basis functions to quadrilaterals, with virtually no additional programming code.

Chapter 5 focuses on the application of the matrix compression technique. Both piecewise linear and piecewise sinusoidal basis functions are considered, together with all three chain splitting algorithms *A*, *B*, and *C*, on several examples. The compression technique's ability to reduce the number of unknowns without sacrificing accuracy is demonstrated on an object that includes curved structures.

Chapter 6 concludes the work and gives suggestions for the further research and development.

Appendix A gives an original derivation for an equivalent radius of curvature for a regular polygon which may be used in approximating a loop antenna. This is used to develop a simple relationship linking the error in the resonant frequency of a loop antenna to the number of sides of the polygon. Appendix B provides a copy of the paper on a novel method to calculate radiation patterns. Appendix C describes the engineered software code and its functionality. It also provides an example for code validation. Appendix D provides a flowchart to show the modifications required to support the compression technique for a standard MoM program. Finally, Appendix E describes the main steps in a procedure used to extract data from plots in scanned papers.

Chapter 2. Core of the Method of Moments

This chapter prepares the groundwork for applying the concept of chains to the Galerkin formulation of the method of moments, introduced in the chapters to follow. The equations of the method of moments (MoM) are obtained in the thin wire approximation. The restriction on the basis functions to satisfy Kirchhoff's current law at the free ends of wires and at the junctions with many wires attached, are stated, and then applied to hierarchical polynomials. The resulting polynomial basis functions are used in conjunction with Kirchhoff's law and current expansion on a junction to derive a new, large-domain set of basis functions. These basis functions are then used in the MoM to build a system of linear equations.

2.1 On Method of Moments for Generalised Wire Antennas

The wire antennas are one of the oldest types of antennas, used since the time of Marconi [Kraus, 52]. Although the interest in techniques for modelling wire structures has probably passed its peak, the usefulness of the concept cannot be underestimated. Besides being an excellent example for explaining the principles of MoM, and so used in many of the well-regarded textbooks [Balanis, 5], [Kraus, 52], [Stutzman, 104], it has many practical applications, and often plays a role of the accelerating factor in optimisation. Since thin wire modelling is very efficient computationally, the optimisation of the antennas is often significantly accelerated, when a simplified wire model of a real structure is optimised first.

Another goal pursued by utilisation of the thin wire theory was to simplify the programming, code debugging, algorithm verification and performance tuning. These are easier to do with more compact expressions and lesser dependencies, featured with the thin wire code.

Last but not least, it must also be mentioned that the wire structures can indeed be modelled with flat stripes or other flat elements. This avoids a dedicated analytical work and programming code for treatment of wires. There are two approaches for such modelling. One is in approximating (covering) the wire surface with patches. This gives accurate results but is very costly computationally. The other approach uses the

equivalence between a wire of radius a and an equal length flat strip of width 4*a*. The latter approach was successfully utilised by Makarov in his textbook on the MoM [Makarov, 67] utilising RWG basis functions [Rao, 94]. The drawback of this technique compared with pure thin wire approximation is in doubling the number of unknowns[7], which for large objects may result in an order of magnitude longer calculation time.

In the following sections, the Galerkin procedure is applied in the context of MoM to the *electric field integral equation* (EFIE) for *thin* wires (wires whose radii are much smaller than their length, and are also much smaller then the wavelength) to obtain a system of linear algebraic simultaneous equations. The elements of the resulting square impedance matrix are then presented as a sum of partial impedances, where each of the partial impedances is a sum of several integrals related to vector and scalar potentials. The large/entire domain basis functions [Kolundzija, 46] are used for the approximation of currents along wire surfaces. These basis functions are a special form of polynomial basis functions that automatically satisfies the current continuity law (in a quasi-static sense) at the wire free ends and at junctions with multiple wires.

2.2 Introduction into the Method of Moments

Many of the electromagnetic problems, including wire antennas and scatterers, can be described in the form of a linear operator $L(\vec{r}')$ acting on an unknown function $f(\vec{r})$ in presence of a source function $e(\vec{r}')$:

$$L(\vec{r}')\left[f(\vec{r})\right] = e(\vec{r}'), \tag{2.1}$$

where $\vec{r}$ and $\vec{r}'$ are vector coordinates of the source and observation/field points, respectively. The linear operator L acts from the space of the coordinates $\vec{r}$ of a point, and results in a function dependent on a primed coordinates $\vec{r}'$, denoted explicitly with the notation $L(\vec{r}')$.

[7] A surface current has to be decomposed into a minimum of two projections as compared with one-dimensional current in the thin wire approximation. Under a piecewise linear current approximation, a long and narrow structure like a wire requires up to a double in the number of unknowns when modelling with plates..

An algorithm for the MoM may be described in several steps. First, the unknown function is approximated by a series based on a set of known linearly independent functions $f_p(\vec{r})$ referred to as *basis functions*[8].

$$f(\vec{r}) \cong \sum_{p=1}^{N} a_p f_p(\vec{r}), \tag{2.2}$$

where $\left[a_p\right]_{p=1,2,..,N}$ are the unknown weight coefficients to be determined and N is the number of expansion functions used. The accuracy of approximation thus depends on the type of basis functions, as well as on their quantity *N*.

The following equation is an approximation of the original equation (2.1) based on the expansion (2.2):

$$\sum_{p=1}^{N} a_p L(\vec{r}')\left[f_p(\vec{r})\right] = e(\vec{r}') \tag{2.3}$$

At this step, it is already possible to convert this into a system of linear equations for determination of the unknown coefficients. It can be done by requesting that the equation (2.3) is to be satisfied at N specified points:

$$\sum_{p=1}^{N} a_p L(\vec{r}_j')\left[f_p(\vec{r})\right] = e(\vec{r}_j'), \quad j = 1, 2, \ldots, N \tag{2.4}$$

Here, $\vec{r}_j'$ are the coordinates of these points and referred to as *matching points*. Hence, this method is known as the *point-matching method* or the *collocation method.*

However, this method is shown [Harrington, 28] to be inferior to more advanced approaches for solving such linear operator equations. One of the main issues in the collocation method is the need to have a large number of sampling/matching points, which leads to a great number of unknowns, and therefore very large matrixes.

Following the MoM outline, next a so-called *test procedure* is applied, where each side of equation (2.3) is multiplied by *j*-th *testing function,* $w_j(\vec{r}'), \quad j = 1, 2, \ldots, M$ (this set

[8] Also referred to as *expansion functions*.

of functions is also referred to as *weighting functions*) and integrated over the domain where the j^{th} weighting function is defined:

$$\sum_{p=1}^{N} a_p \int_{S_j} w_j(\vec{r}\,') L\left[f_p(\vec{r})\right] dS' = \int_{S_j} w_j(\vec{r}\,') e(\vec{r}\,') dS'_j, \quad j = 1,2,\ldots,M \tag{2.5}$$

The integration[9] is with respect to the primed co-ordinates denoted with dS'_j.

Thus, a system of linear equations $\mathbf{ZI} = \mathbf{V}$ is obtained:

$$\begin{pmatrix} Z_{11} & \cdots & Z_{1N} \\ \vdots & \ddots & \vdots \\ Z_{M1} & \cdots & Z_{MN} \end{pmatrix} \begin{pmatrix} a_1 \\ \vdots \\ a_N \end{pmatrix} = \begin{pmatrix} V_1 \\ \vdots \\ V_M \end{pmatrix}, \tag{2.6}$$

where the impedance matrix **Z** is described by its elements

$$Z_{jp} = \int_{S_j} w_j(\vec{r}\,') L(\vec{r}') \left[f_p(\vec{r})\right] dS'_j, \quad p = 1,2,\ldots,N, \quad j = 1,2,\ldots,M \tag{2.7}$$

and the excitation vector **V** has elements

$$V_j = \int_{S_j} w_j(\vec{r}\,') e(\vec{r}') dS'_j, \quad j = 1,2,\ldots,M\,.$$

In electromagnetics, the linear operator L is often associated with the electrical field (e.g. when electrical field integral equation is used). At the same time, the testing functions may be the same as the basis functions (Galerkin's procedure) and represent current (for wires) or current density (for plates). Then the matrix elements Z_{jp} may be written as the inner product of the electrical field and current $Z_{jp} = \int_{S_j} I_j E_p dS'_j$, with indexes $p = 1,2,\ldots,N, \quad j = 1,2,\ldots,M$. The result has not the units of resistance, Ohm, but the matrix is nevertheless referred to as the impedance matrix.

[9] Typically this is a surface or volumetric integral, depending on whether the method is based on the surface integral equations (SIE) or volume integral equations (VIE). This work deals with thin wire antennas. The integration thus reduces to a line integral, as will be shown later in the text.

The obtained system of linear equations can be solved by one of the standard methods available [Golub, 24], [Press, 92], [Råde, 93].

There is a particular kind of the general method of moments called the *Galerkin method* [Petrov, 86], [Harrington, 27] that has proven [Harrington, 28], [Butler, 8], [Miller, 73], [Medgyesi-Mitschang, 71], and [Kolundzija, 45] to give accurate and more robust results for an equal or smaller number of unknowns needed, compared with many other variations of the MoM (collocations, weighted point matching, least square etc.). In the Galerkin's procedure, the weighting functions are the same as the basis functions. This method is utilised in the dissertation and will be further detailed in the sections to follow.

In a practical implementation, the following steps of the MoM algorithm are often applied at each frequency of interest:

1. apply a grid to the object under study;
2. assign N basis functions to the geometrical elements identified by the grid;
3. calculate elements of the $N \times N$ impedance matrix, $[Z_{jp}]$;
4. calculate excitation vector
5. solve the system of linear equations to obtain unknown coefficients (currents)
6. the current distribution is obtained by insertion of found coefficients into the basis function expansion, and may be used to determine any other parameters of interest, such as antenna input impedance, radiated fields, radar cross sections etc.

The variation of the MoM described in this chapter has adopted many of its theoretical elements from [Kolundzija et al., 45-47, 48] and [Djordjevic et al., 18].

2.3 Generalised Wires

The right truncated cones (termed *generalised wires*) are chosen for approximation of wires. Such cones can approximate cylindrical and conical wires, electrically small disks and wire ends of various shapes [Kolundzija, 47].

The cone surface (excluding the top and bottom disks) may be described with the following parametric equation:

$$\vec{r}(s,\varphi) = \vec{r_a}(s) + a(s)\vec{u_\rho}(\varphi) \tag{2.8}$$

where φ is the local circumferential coordinate, $\vec{u_\rho}(\varphi)$ is a radial unit vector in the local coordinate system[10], and $\vec{r_a}(s)$ and $a(s)$ are defined by the parametric equations of the cone axis and its local radius. The two latter equations are

$$\vec{r_a}(s) = \vec{r_1} + (s - s_1)\frac{\vec{r_2} - \vec{r_1}}{s_2 - s_1} = \vec{r_1} + \vec{u_z}(s - s_1)\cos\alpha \ , \ s_1 \le s \le s_2 \tag{2.9}$$

$$a(s) = a_1 + (s - s_1)\frac{a_2 - a_1}{s_2 - s_1} = a_1 + (s - s_1)\sin\alpha \ , \ s_1 \le s \le s_2 \tag{2.10}$$

There equations assume the following notations. Here, s is a local coordinate along the cone reference generatrix[11], $\vec{u}_z$ is the cone axis unit vector (condition to the choice of s_1 and s_2 as minus and plus half-length of the cone), α is the angle between the cone axis and its generatrix. The subscript indexes 1 and 2 refer to the *beginning* and *end* of the cone, respectively. Then the $\vec{r}_1$ and $\vec{r}_2$ are the position vectors of the beginning and the end of the cone, s_1 and s_2 are s-coordinates of the beginning and the end of the cone reference generatrix, and a_1 and a_2 are the radii at the beginning and the end of the cone, respectively. This is illustrated in Figure 2-1, where O is the origin of the global coordinate system and P is the field (observation) point.

---

[10] The reference direction of φ, corresponding to the orientation of $\vec{u}_\rho(0) = \vec{u}_x$, may be chosen arbitrarily.

[11] The *generatrix* is a point, *line*, or surface whose motion generates a line, *surface*, or solid [Merriam-Webster Dictionary, 72]. As per [Encyclopaedia Britannica, 21], the generatrix of a cone is assumed to be infinite in length, extending in both directions from the vertex. The cone so generated, therefore, has two parts that extend infinitely. A finite cone has a finite base, the surface enclosed by the directrix, and a finite length of generatrix.

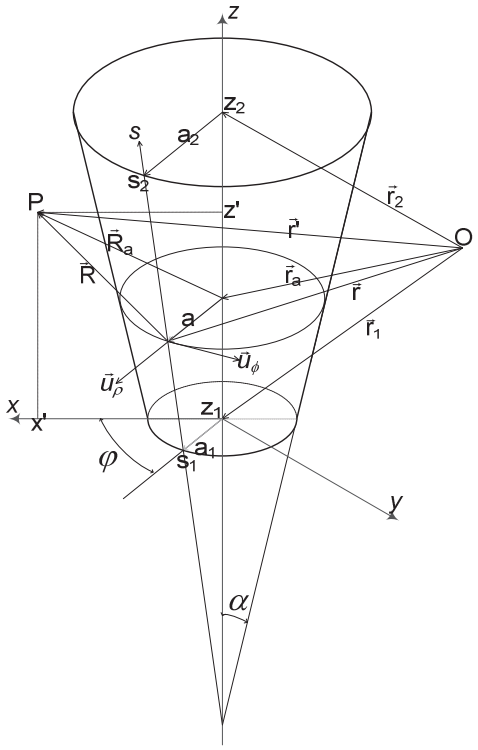

Figure 2-1. Coordinates for a generalised wire. The origin is denoted with *O*, and field point *P*.

Further, the coordinates of the ends of the cone generatrix are chosen to be $s_2 = -s_1 = L$, where L is the half-length (half-height) of the cone along the s-coordinate.

The equations (2.9) and (2.10) may also be described with the equations utilising potential symmetry of the wires with respect to their centres. The following relationships are obtained by shifting the variable s to have the origin at the centre of the wire, namely $s \to s - \frac{1}{2}(s_1 + s_2)$:

$$\begin{aligned} \vec{r}_a(s) &= \vec{r}_c + \vec{u}_z s\cos\alpha \\ a(s) &= a_c + s\sin\alpha \end{aligned}, \qquad (2.11)$$

where $\vec{r}_c = (\vec{r}_1 + \vec{r}_2)/2$ and $a_c = (a_1 + a_2)/2$.

One of the advantages of this presentation is a small reduction in the number of arithmetical operations required for computing functions $\vec{r_a}(s)$ and $a(s)$, and, subsequently, a decrease in the time required to compute integrands due to the impedance matrix elements. The other advantage, reflecting usage of symmetry, may come handy when dealing with the integrals due to the electrical potential and shall be discussed later.

2.4 Thin Wire Approximation Requirements

From electromagnetic modelling point of view, objects may belong to the class of thin wires, if these restrictions are satisfied:

- The current is only on the surface of the object, so the perfect conductor approximation is applicable;
- The current is along the main axis;
- The current distribution does not depend on the circumferential coordinate of the object.

These lead [Balanis, 4] to the requirement on the radius of wire to be much smaller than the length of the wire, and much smaller than the wavelength.

2.5 On the Boundary Condition

The electric field integral equation (EFIE) for the current distribution is derived from the boundary condition for the tangential component of the total electric field at the conductor surface. The boundary condition (2.12) is used on the surface of a hollow cone:

$$(\vec{E} + \vec{E}^{inc})\Big|_{\tan} = 0 \qquad (2.12)$$

where vector $\vec{E}^{inc}$ [V/m] is the incident electric field, and $\vec{E}$ [V/m] is the electric field due to induced surface currents and charges, with densities $\vec{J}_s$ [A/m^1] and ρ_s [C/m^2], respectively.

Assuming the opening angle of a cone α [rad] being small, this boundary condition may be written as a first order approximation (with error of $O(\alpha^2)$):

$$E_z + E_z^{inc} = 0\,, \tag{2.13}$$

where E_z and E_z^{inc} are the components of the electric field due to the currents and charges, and of the incident field, respectively, along the truncated cone's axis. The expression is used along the axis of a solid cone. In [Popovic et al, 89], this condition is referred to as the *extended boundary condition*.

2.6 Retarded Potentials A and V

The electric field vector $\vec{E}$ [V/m] due to induced surface currents and charges with angular frequency ω [rad/s], with densities $\vec{J}_s$ [A/m] and ρ_s [C/m^2], in vacuum, can be expressed in terms of the electric scalar potential V [V] and the magnetic vector potential $\vec{A}$ [V/(m/s)] as

$$\vec{E}(\vec{r}') = -j\omega\vec{A} - \text{grad}'V\,, \tag{2.14}$$

$$V(\vec{r}') = \frac{1}{\varepsilon_0}\int_S \rho_s\, g(R)\, dS, \quad \vec{A}(\vec{r}') = \mu_0 \int_S \vec{J}_s\, g(R)\, dS\,, \tag{2.15}$$

$$g(R) = \frac{e^{-jkR}}{4\pi R}, \quad k = \omega\sqrt{\varepsilon_0\mu_0}\,, \quad R \equiv R\left(\vec{r}', \vec{r}\right) = \left|\vec{r}' - \vec{r}(s,\phi)\right|, \tag{2.16}$$

where ω [rad/s] is the angular frequency, the gradient operator *grad* is taken with respect to the primed co-ordinate, $\vec{r}'$ [m] is the position vector of the observation/field point and $\vec{r}(s,\phi)$ [m] is the position vector of the source point or the coordinate of the truncated cone surface given by equation (2.8), k [rad/m] is the phase constant (wavenumber), and $g(R)$ is the Green's function for free space. The constants $\varepsilon_0 = 8.8542\cdot 10^{-12}$ F/m and $\mu_0 = 4\pi\cdot 10^{-7}$ H/m are the permittivity and permeability of vacuum, respectively.

Thus, with the aid of the continuity equation $\text{div}\,\vec{J}_s = -j\omega\rho_s$ and expressions (2.15)-(2.16), the electrical field (2.14) due to the current in a conical wire is then

$$\vec{E}(\vec{r}') = -j\omega\mu_0\left(\int_S \vec{J}_s(\vec{r})g(R)dS + \frac{1}{k^2}\int_S \mathrm{div}\,\vec{J}_s(\vec{r})\vec{u}_R\frac{dg(R)}{dR}dS\right) \tag{2.17}$$

where the unit vector $\vec{u}_R = \vec{R}/R$.

2.7 Current Continuity Equation for Thin Conical Wires

Assuming that the current is directed along the wire coordinate s only, the surface current density $\overrightarrow{J_s}$ may be written as

$$\overrightarrow{J_s}(s,\varphi) = J_s(s)\overrightarrow{u_s}(\varphi), \text{ with } s_1 \le s \le s_2 \text{ and } -\pi < \varphi \le \pi \tag{2.18}$$

where $\overrightarrow{u_s}$ is the unit vector along the generatrix of the cone.

The expressions for surface current density J_s and charge per unit length Q_s' are

$$J_s(s) = \frac{I(s)}{2\pi a(s)}, \qquad \text{and} \qquad Q_s'(s) \equiv \frac{dQ}{ds} = \frac{d}{ds}\left(\frac{-j\omega Q}{-j\omega}\right) = \frac{1}{-j\omega}\frac{d}{ds}\left(-j\omega Q\right) = \frac{1}{-j\omega}\frac{dI(s)}{ds}. \tag{2.19}$$

The surface charge density for truncated cones may then be written as

$$\rho_s = \frac{Q_s'(s)}{2\pi a(s)} = \frac{1}{-j\omega}\frac{1}{a(s)}\frac{d}{ds}\left(a(s)J_s(s)\right). \tag{2.20}$$

This expression may be interpreted as the current continuity equation for thin conical wires.

2.8 Formulation of the Electric Field Integral Equation

With the help of Figure 2-2, the area element dS [m^2] can be expressed as

$$dS = a(s)\,ds\,d\varphi, \text{ with } s_1 \le s \le s_2 \text{ and } -\pi < \varphi \le \pi \tag{2.21}$$

It is convenient to adopt the direction $\varphi = 0$ such that $R(\varphi = 0) = R_{\min}$, i.e. that the field point P is in the plane xOz of the local coordinate system shown in Figure 2-1. Then $R(\varphi) = R(-\varphi)$, as to reduce the integration over φ from the interval $[-\pi,\pi]$ to $[0,\pi]$.

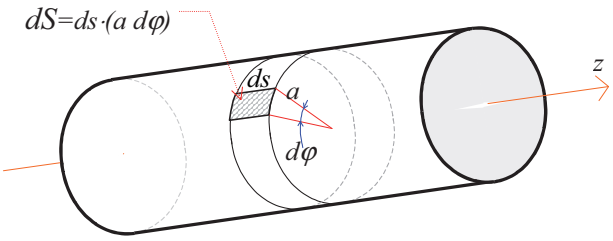

Figure 2-2. Definition of the surface area element *dS* on a nearly cylindrical wire, where *dS* composed of the longitudinal side *ds* and circumferential side *a*(*s*)*dφ*.

Thus, with the aid of Figure 2-1, the formulas for the potentials come to the form of

$$V(\vec{r}') = \frac{j}{\omega\varepsilon_0}\frac{1}{\pi}\int_0^{\pi}\int_{s_1}^{s_2}\frac{dI(s)}{ds}\,g(R)\,ds\,d\varphi \tag{2.22}$$

and

$$\vec{A}(\vec{r}') = \frac{\mu_0}{2\pi}\int_0^{\pi}\int_{s_1}^{s_2} I(s)\left(\vec{u}_s(\varphi)+\vec{u}_s(-\varphi)\right)g(R)\,ds\,d\varphi \tag{2.23}$$

with

$$R = \left|\vec{R}_a(s) - a(s)\vec{u}_\rho(\varphi)\right|, \text{ and } \vec{R}_a(s) = \vec{r}' - \vec{r}_a(s)\,. \tag{2.24}$$

In the case, when the field point is on the cone axis, the Green's function is independent of the φ coordinate. When the field point is far away from the cone axis, the Green's function is only weakly dependent on this coordinate. Therefore, for these cases, it is sufficient to integrate over φ in an approximate way, by using the midpoint rule, i.e. substitute the value of the integral over φ by the integrand at $\varphi = \pi/2$ multiplied by the integration interval, π.

This gives[12] the reduced kernel in the integrand and the approximate formulas for the potentials

$$V(\vec{r}') = \frac{j}{\omega\varepsilon_0}\int_{s_1}^{s_2}\frac{dI(s)}{ds}g(R_e)ds \text{ , and} \tag{2.25}$$

$$\vec{A}(\vec{r}') = \vec{u}_z\mu_0\cos\alpha\int_{s_1}^{s_2}I(s)\,g(R_e)\,ds\,, \tag{2.26}$$

where
$$R_e = \sqrt{R_a(s)^2 + a(s)^2} \tag{2.27}$$

The reduced expressions for potentials (2.25)-(2.26) grant the following expression for the electric field due to an equivalent filamentary line-source current located on the surface of the wire (a truncated cone):

$$\vec{E}(\vec{r}') = -j\omega\mu_0\left(\vec{u}_z\cos\alpha\int_{s_1}^{s_2}I(s)g(R_e)ds + \frac{1}{k^2}\int_{s_1}^{s_2}\frac{dI(s)}{ds}\,\mathrm{grad}'\,g(R_e)\,ds\right) \tag{2.28}$$

The expressions (2.25)-(2.28) were derived under the assumptions of the thin wire approximation stated in Section 2.4. In practice, where the distance between wires is not large, the smallness of the wire radius may become of an additional importance. This is also due to the approximate way of integrating when calculating the potentials existing between the points of the wires.

The integrand in the second term of (2.28) contains the factor $\mathrm{grad}'\,g(R_e) = \mathrm{grad}'(R_e)\dfrac{dg(R_e)}{dR_e}$. This factor may be further expanded as

$$\mathrm{grad}'\,g(R_e) \equiv \nabla'\frac{e^{-jkR_e}}{4\pi R_e} = -\frac{e^{-jkR_e}}{4\pi}\left(\frac{jk}{R_e}+\frac{1}{R_e^{\,2}}\right)\frac{\vec{R}_e}{R_e} = -g(R_e)\left(jk+\frac{1}{R_e}\right)\vec{u}_R\,. \tag{2.29}$$

---

[12] The following relationships have also been used: $\vec{u}_s(\alpha,\varphi) = \vec{u}_z\cos\alpha + \vec{u}_\rho(\varphi)\sin\alpha = \vec{u}_z\cos\alpha + \vec{u}_x\sin\alpha\cos\varphi + \vec{u}_y\sin\alpha\sin\varphi$;

$\frac{1}{2}\left(\vec{u}_s(\varphi)+\vec{u}_s(-\varphi)\right) = \vec{u}_z\cos\alpha + \vec{u}_x\sin\alpha\cos\varphi$, and the second term is being integrated with respect to φ over the interval 0 to π, which eliminates it.

The form of the electric field integral equation (EFIE) based on (2.28) may be compared with Pocklington's integral equation given in [Balanis, 5]. The degree of singularity of the integrand in the present equation is by three orders of R lower, making it easier to compute the integrals numerically. Thus, it is expected that this form of the equation is better suited for numerical treatment. In addition, it is also clear that the degrees of singularities of the different terms in (2.28) are different. Thus, considering the limitations of numerical accuracy, it is expected that it may be numerically more advantageous to perform the integration for these terms separately.

2.9 Generalisation of EFIE to Support Multiple Wires

The total electrical field $\vec{E}(\vec{r}')$ produced by the currents and charges in M_w wires may be written as a superposition of electrical fields due to all individual wires:

$$\vec{E}(\vec{r}') = \sum_{m=1}^{M_w} \vec{E}^{(m)}(\vec{r}') = \sum_{m=1}^{M_w} \left(-j\omega \vec{A}^{(m)}(\vec{r}') - \nabla' V^{(m)}(\vec{r}') \right), \tag{2.30}$$

where $\vec{E}^{(m)}$ is the electrical field, $V^{(m)}$ and $\vec{A}^{(m)}$ are the electric scalar potential and the magnetic vector potential, all due to the currents and charges on m-th wire.

After taking into account (2.25)-(2.30), the expanded expression for the total electric field due to the currents and charges on m-th wire may be written as:

$$\vec{E}^{(m)}(\vec{r}') = -j\omega\mu_0 \left(\begin{array}{l} \vec{u}_z^{(m)} \cos\alpha^{(m)} \int_{s_1^{(m)}}^{s_2^{(m)}} I^{(m)}(s^{(m)}) g(R_e) ds^{(m)} \\ -\frac{1}{k^2} \int_{s_1^{(m)}}^{s_2^{(m)}} \frac{dI^{(m)}(s^{(m)})}{ds^{(m)}} g(R_e) \left(jk + \frac{1}{R_e} \right) \vec{u}_R \, ds^{(m)} \end{array} \right). \tag{2.31}$$

The expression inside the brackets includes 3 terms. The first term is due to the vector potential and produces the strongest effect in far field at high frequencies. The second and third terms are both due to the scalar potential. At close distances, and especially at low frequencies, the last term has the most pronounced effect due to its factor $1/k^2 R_e$.

In accordance with the MoM scheme, the current *in each wire* may be expanded into basis functions as shown by the expression (2.2). The number of basis functions per wire may vary. Let $n_b^{(m)}$ denote the number of basis functions assigned to represent the current distribution on the m^{th} wire. Thus, the potentials will be represented by their expansions, which may be written as

$$\vec{A}^{(m)}(\vec{r}') = \sum_{i=1}^{n_b^{(m)}} \vec{A}_i^{(m)}(\vec{r}'), \quad V^{(m)}(\vec{r}') = \sum_{i=1}^{n_b^{(m)}} V_i^{(m)}(\vec{r}'). \tag{2.32}$$

The bracketed superscript stands for the wire number (in a linear list of all wires), whilst the subscript stands for the local number of the basis function within this particular wire.

Note:

The index p used in (2.2) refers to the global linear indexing of all the basis functions for a system including $M_w \geq 1$ wires, and with multiple basis functions assigned to each wire. The index i used in the last expression above refers to a local numbering of basis functions within a single, m^{th} wire.

The expression (2.30) may then be rewritten as

$$\begin{aligned} \vec{E}(\vec{r}') &= \sum_{m=1}^{M_w} \sum_{i=1}^{n_b^{(m)}} \vec{E}_i^{(m)}(\vec{r}') \\ &= \sum_{m=1}^{M_w} \sum_{i=1}^{n_b^{(m)}} \left(-j\omega \vec{A}_i^{(m)}(\vec{r}') - \nabla' V_i^{(m)}(\vec{r}') \right) \end{aligned}, \tag{2.33}$$

where $\vec{E}_i^{(m)}$ is the electrical field, $V_i^{(m)}$ and $\vec{A}_i^{(m)}$ are the electric scalar potential and the magnetic vector potential, all due to the partial currents and charges on *m*-th wire carried (expressed) by its *i*-th basis function (index *i* is local to this wire).

Although this may go a bit ahead of the general line of the derivations, the form of the partial electric field produced by the i^{th} basis function of the m^{th} wire may already be obtained. Once the current is expressed through the basis functions, as per (2.2), the partial electric field may be written as

$$\vec{E}_i^{(m)} = a_i^{(m)}(-j\omega\mu_0)\begin{pmatrix} \vec{u}_z^{(m)}\cos\alpha^m \int_{s_1^{(m)}}^{s_2^{(m)}} f_i\ (s^{(m)})g(R_e)ds^{(m)} \\ -\frac{1}{k^2}\int_{s_1^{(m)}}^{s_2^{(m)}} \frac{df_i(s^{(m)})}{ds^{(m)}} g(R_e)\left(jk+\frac{1}{R_e}\right)\vec{u}_R\, ds^{(m)} \end{pmatrix}. \qquad (2.34)$$

This expression does not change its presentation in comparison with (2.31) except for the additional factor – a constant unknown coefficient $a_i^{(m)}$.

The electrical field integral equation (EFIE) is obtained by substituting the expressions (2.33) and (2.34) into the boundary condition (2.13) on each of the domains defined by basis functions and respective wires. The resulting electrical field integral equation may then be written as

$$\vec{u}_z^{(q)} \cdot \sum_{m=1}^{M_w}\sum_{i=1}^{n_b^{(m)}} a_i^{(m)}\, j\omega\mu_0 \begin{pmatrix} \vec{u}_z^{(m)}\cos\alpha^m \int_{s_1^{(m)}}^{s_2^{(m)}} f_i\ (s^{(m)})g(R_e)ds^{(m)} \\ -\frac{1}{k^2}\int_{s_1^{(m)}}^{s_2^{(m)}} \frac{df_i(s^{(m)})}{ds^{(m)}} g(R_e)\left(jk+\frac{1}{R_e}\right)\vec{u}_R\, ds^{(m)} \end{pmatrix} = \vec{u}_z^{(q)} \cdot \vec{E}^{inc}, \qquad (2.35)$$

where $q = 1, 2, \ldots, M_w$ is the index of the wire segment for which the boundary condition is impressed, and $\vec{E}^{inc}$ is the incident field due to a source. The notation for the incident field may include multiple individual sources: $\vec{E}^{inc} = \sum_k \vec{E}_k^{inc}$.

The double summation in equation (2.35) includes all the basis functions and respective coefficients. At this moment, the expression (2.35) is ready for the testing (weighting) procedure.

2.10 On Basis Functions

For simplicity and without loosing generality, it is assumed that there is only one, m^{th} wire present. Thus, the superscripts denoting the wire numbers will not be used, unless shown otherwise.

The current distribution $I(s)$ in the expression (2.31) is unknown. As has been mentioned in the previous section, this unknown current is expanded into a series of

known, pre-defined functions $f_i(s)$ referred to as *basis functions*[13], with yet unknown coefficients a_i:

$$I(s) = \sum_{i=1}^{n_b} a_i f_i(s), \quad s \in [s_1, s_2] \tag{2.36}$$

where a_i are the unknown coefficients to be determined, n_b is the number of expansion functions used, s_1 and s_2 are the coordinates of the beginning and the end of the cone generatrix (setting the domain of definition for the basis function).

The number of basis functions n_b directly contributes to the achievable accuracy. An increase in the number of linearly independent basis functions per wire segment usually brings a higher accuracy although it is at the expense of longer computations.

The choice of the basis functions depends on a number of criteria, such as the geometry of the problem, the required accuracy etc. Typically, the closer the basis functions describe the physical current behaviour, the better accuracy is achieved for the same amount of computations.

It must also be noted that, as a result of limited numerical accuracy, the type of basis functions plays an important role in the ability to improve accuracy by increasing the number of basis functions per wire.

2.10.1 Satisfaction of the Continuity Equation

Current is defined by the movement of charges. At free ends of wires, the charge has nowhere to flow, and there is no current. In mathematical terms, this translates into a boundary condition of zero current and constant charge distribution at a free end. At a junction of two or more wires, the amount of charge, and thus current, flowing into a junction must be compensated by the same quantity flowing out of the junction. At the quasi-static frequencies, also applicable to the ends of very thin wires, these relationships are expressed by the *Kirchhoff's current law* [Balanis, 4].

[13] Also referred to as *expansion functions*.

A straightforward method of incorporating the Kirchhoff's current law (KCL) at the free wire ends and at the junctions of several wires (nodes), is to add the equations expressing the law to the set of linear equations, e.g.

$$\sum_{k=1}^{m} I_1^{(k)} = 0 \tag{2.37}$$

where, $I_1^{(k)}$ is the current at the beginning of the wire number k joining a node with m wires[14]. It is assumed, without losing generality that the wires join the node with their beginnings.

This approach is easy to implement. However, it may significantly increase the number of equations, and it forces to use the sub-domain testing functions or/and to apply a point-matching procedure, as the number of unknowns and number of linear equations would not match otherwise.

Another possibility to satisfy the current continuity condition is to restrict the basis functions to automatically comply with the KCL [Kolundzija and Popovic, 45]. In that technique, an arbitrary set of basis functions $\{f_i(s)\}_{i=1,2,\ldots,n_b}$ is forced to satisfy the KCL at the ends of the wires, leading to a new set of basis functions that now automatically satisfy KCL. Only one of the new basis functions may then have a non-zero value at an end. This approach does not have the above-mentioned drawbacks and simply utilises the flexibility provided by the MoM.

The notations used in this approach are illustrated in Figure 2-3, which shows a wire, a local co-ordinate system associated with this wire, and the current distribution $I(s)$ on that wire (defined arbitrary at this stage).

The current at the beginning and the end of a wire is then expressed in terms of unknown coefficients I_1 and I_2:

$$I(s_1) = I_1 \quad I(s_2) = I_2 \,. \tag{2.38}$$

[14] The usage of symbol m here (number of wires at a junction) is different to the meaning given to m in the previous sections (wire number/index). Hopefully, this should not create confusion.

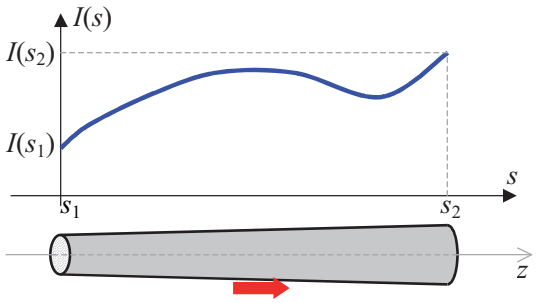

Figure 2-3. Example of current distribution on a wire, also illustrating the notations for the current intensity at the ends of the wire. The beginning and end of wire are denoted with s_1 and s_2, respectively. The positive direction of current, defined by the beginning and end, is shown with an arrow.

Each of the two equations in (2.38) may be substituted into (2.36). This gives a system of linear equations (2.39) with respect to the coefficients a_1 and a_2:

$$\begin{cases} I_1 = a_1 f_1(s_1) + a_2 f_2(s_1) + \sum_{i=3}^{n_b} a_i f_i(s_1) \\ I_2 = a_1 f_1(s_2) + a_2 f_2(s_2) + \sum_{i=3}^{n_b} a_i f_i(s_2) \end{cases}. \tag{2.39}$$

The coefficients a_1 and a_2 may be expressed through the current amplitudes I_1 and I_2 and other terms of (2.39). The resulting expressions may be substituted back into (2.36). After simplifications, it is then possible to come to a new set of basis functions for the expansion of the current [Kolundzija and Popovic, 45], as shown in (2.40):

$$I(s) = I_1 N_2(s) - I_2 N_1(s) + \sum_{i=3}^{n_b} a_i S_i(s), \quad s \in [s_1, s_2]. \tag{2.40}$$

Here, the *node basis functions* $N_1(s)$ and $N_2(s)$ are defined as (2.41)

$$N_i(s) = \frac{f_2(s_i)}{Q_{1,2}} f_1(s) + \frac{f_1(s_i)}{Q_{2,1}} f_2(s), \quad i = 1 \text{ and } 2, \tag{2.41}$$

and the *segment basis functions* $S_i(s)$ are defined as (2.42)

$$S_i(s) = f_i(s) + \frac{Q_{2,i}}{Q_{1,2}} f_1(s) + \frac{Q_{1,i}}{Q_{2,1}} f_2(s), \quad i = 3, 4, \ldots, n, \tag{2.42}$$

and the intermediate quantities $Q_{i,j}$ are expressed as (2.43):

$$Q_{i,j} = f_i(s_1) f_j(s_2) - f_i(s_2) f_j(s_1). \tag{2.43}$$

The new current expansion (2.40) has a new set of unknown coefficients: I_1, I_2 and $a_i, \quad i = 3,4,\ldots,n_b$. The new basis functions in this expansion are equal to zero at wire ends, except for the node basis functions which are zero at one end only: $N_1(s)\big|_{s=s_2} = -1$ and $N_2(s)\big|_{s=s_1} = 1$.

The negative sign in the second term in (2.40) reflects the initial assumption of currents flowing *into* a junction. The first term is attributed to the current at the beginning of the wire, and the respective current is thus defined as "positive". The second term is due to the current at the end of the wire. Since the end of the wire represents another junction (compared to the beginning), this current flows into that other junction. This current is thus flowing into the end of wire. In the sense of direction, it is equivalent to flowing out of the beginning of the wire, making the sign negative.

The procedure (2.38)-(2.40) separates the functions into two groups. The segment basis functions (SBF) automatically satisfy the KCL at the free wire ends (not connected to other wires) and approximate current within a single wire segment. As such, they are referred to as *singletons*. A singleton is zero at the ends of the interval of its definition, as illustrated with Figure 2-4.

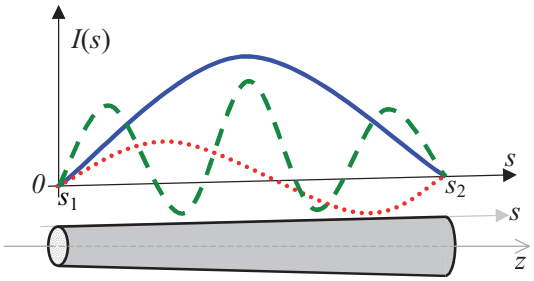

Figure 2-4. Examples of singletons defined on a wire segment.

In order to satisfy to the continuity equation at the junctions of several wire segments, the node basis functions are utilised. The current distribution profile over a junction with two attached wires may be considered. This leads to the formulation of a new basis function referred to as *doublet*. Formation of a doublet is shown in Figure 2-5, where two linear functions corresponding to the current intensity profiles in the respective wires form a two piecewise linear function shaped as a roof-top. For these reasons, some authors refer to this type of function as a *piecewise-linear* basis function, as well as a *roof-top* basis function.

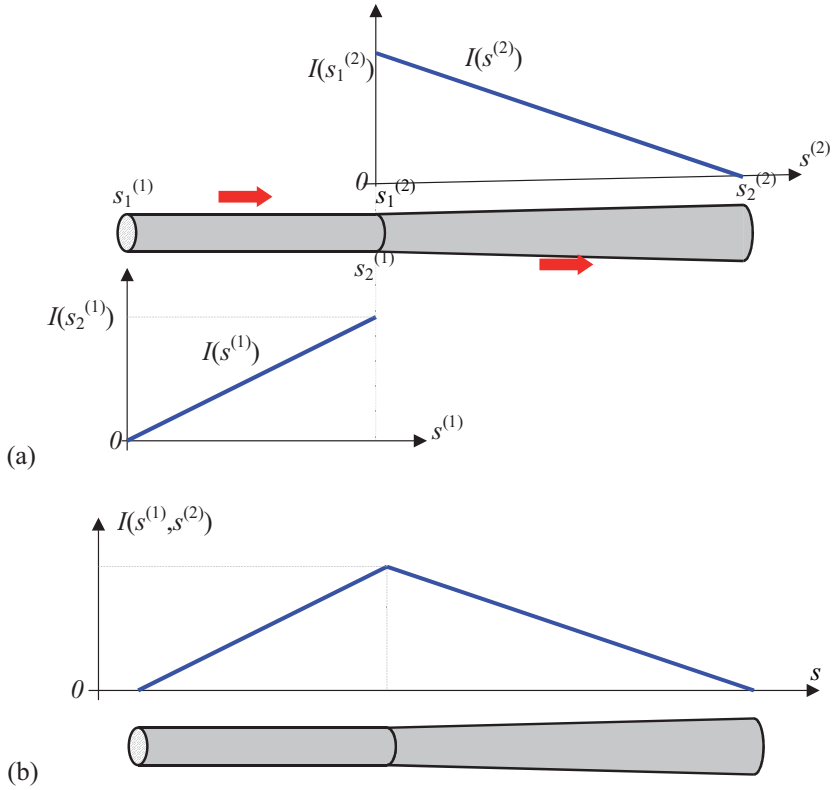

Figure 2-5. Doublet basis function for a junction of two wires. (a) Individual piecewise linear current profiles on the wires 1 and 2. All variables and parameters related to wire number *i* are denoted with the superscript $^{(i)}$, where *i*=1,2. (b) The profile of the resulting doublet (roof-top) basis function defined on the domain composed of the domain of wire 1 and domain of wire 2.

A doublet may immediately be used in modelling linear wire antennas. However, a node may have more than 2 wires attached to it. The current through such a junction may be expressed using several doublets. In [Kolundzija et al., 46], a composite basis function based on several doublets defined over such a junction is referred to as a *multiplet* basis function.

This is illustrated with Figure 2-6 (within a piecewise linear approximation). The current distribution on the wires that belong to this junction is shown Figure 2-6a. This distribution may be readily modelled with only 2 doublets. One of the possibilities is shown Figure 2-6b, where wire 1 is used as the common (or "reference") wire. It is also possible to choose wire 2 or wire 3 as the common domain for the 2 doublets.

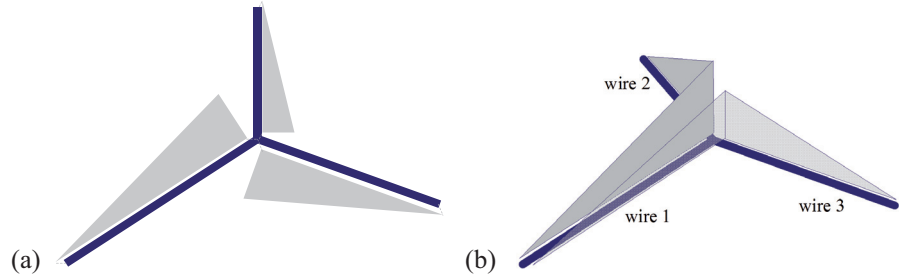

Figure 2-6. Examples of a junction with 3 wires attached. (a) The current profiles on individual wires. (b) Two doublets assigned to the junction. The wires are shown with thick solid lines. The current distribution shown in this figure is modelled with piecewise linear functions displayed with grey triangles.

A multiplet basis function may be derived as follows.

The connected wire segments can be considered as an interconnection of m wires, which join the joint node by either their beginnings ($s = s_1$) or ends ($s = s_2$). In the domain defined by these wires connected to the node, the following current expansion I_{jun} due to the currents at the junction may be written:

$$\begin{aligned} I_{jun}(s^{(1)}, s^{(2)}, \ldots, s^{(m)}) &= \sum_{k=1}^{m} d_0^{(k)} I_{d_1^{(k)}}^{(k)} \cdot d_0^{(k)} N_{d_2^{(k)}}^{(k)}(s^{(k)}) \\ &= I_{d_1^{(1)}}^{(1)} N_{d_2^{(1)}}^{(1)}(s^{(1)}) + \sum_{k=2}^{m} I_{d_1^{(k)}}^{(k)} N_{d_2^{(k)}}^{(k)}(s^{(k)}) \end{aligned}, \qquad (2.44)$$

where the current $I^{(k)}_{d_1^{(k)}}$ through the k^{th} wire is now modelled by the node basis functions with indexing functions $d_l^{(k)}, \quad k=1,2,\ldots,m, \quad l=0,1,2$, which are defined with Table 2-1. The products $d_0^{(k)} I^{(k)}_{d_1^{(k)}}$ and $d_0^{(k)} N^{(k)}_{d_2^{(k)}}$ include the factor $d_0^{(k)}$ to explicitly specify the direction of the current, and to compensate for the minus in the definition (2.40) of the function N_2, respectively.

Table 2-1 Junction current expansion indexing functions. The function d_0 is effectively a sign function, whilst the functions d_1 and d_2 enable manipulations between the indexes 1 and 2 for the beginning and end of a wire, respectively.

Which part of the wire is at the junction	$d_0^{(k)}$	$d_1^{(k)}$	$d_2^{(k)}$
the beginning of wire k is at the junction	+1	1	2
the end of wire k is at the junction	−1	2	1

In a manner similar to (2.44), the KCL equation (2.37) may be rewritten to automatically include the direction of current. This is again done by usage of the indexing sign function $d_0^{(k)}$ defined in Table 2-1. One of the unknowns is to become a dependent variable and must be expressed through the other unknowns chosen to be the independent variables. In this derivation, the current intensity through the 1st wire, $I^{(1)}$, is taken as the dependant variable:

$$d_0^{(1)} I^{(1)}_{d_1^{(1)}} = -\sum_{k=2}^{m} d_0^{(k)} I^{(k)}_{d_1^{(k)}}, \tag{2.45}$$

The expression (2.45) is substituted into the junction current expansion (2.44), which brings the latter to the form[15]

$$I_{jun}(s^{(1)}, s^{(2)}, \ldots, s^{(m)}) = \sum_{k=2}^{m} I^{(k)}_{d_1^{(k)}} \left(N^{(k)}_{d_2^{(k)}}(s^{(k)}) - d_0^{(k)} d_0^{(1)} N^{(1)}_{d_2^{(1)}}(s^{(1)}) \right) \tag{2.46}$$

[15] Note that $d_0^{(k)} = 1/d_0^{(k)}$.

This defines the new *doublet basis functions* $D^{(i,j)}$ composed of two node basis functions

$$D^{(i,k)}(s^{(i)},s^{(k)}) = N^{(k)}_{d_2^{(k)}}(s^{(k)}) - d_0^{(k)} d_0^{(i)} N^{(i)}_{d_2^{(i)}}(s^{(i)}) \tag{2.47}$$

These doublets provide the current flow between the i^{th} and k^{th} wires and automatically satisfy the continuity of the current at the junctions. All the $m-1$ doublets overlap along the i^{th} wire in the junction.

Note:

In expressions (2.44)-(2.46), the common wire (where the basis functions overlap) is referred to as number 1. This should not create confusion since the choice of numbering the wires attached to a junction is arbitrary.

Thus, the current on a set of wire segments is represented by the doublets defined on the wires attached to the corresponding junctions, and singletons defined on the single wire segments.

It may be noted that the doublets are composed of piecewise linear functions, and also closely related to the *roof-top* basis functions [Balanis, 5]. The property of continuity of the current over a junction is also found in a very popular RWG basis function [Rao, 94].

2.10.2 Example: Doublet for a Junction of Two Wires

Consider a junction of two wire segments, a dipole. If the size of the dipole is sufficiently small and the arms are of the same length, the profile of the magnitude of current distribution on the dipole resembles an equilateral triangle, as shown in Figure 2-7.

The current distribution may then be written as $I(s) = -I_2^{(1)} N_1^{(1)}(s^{(1)}) + I_1^{(2)} N_2^{(2)}(s^{(2)})$. According to the Kirchhoff's current law, the sum of currents entering a node must be equal to the sum of currents leaving this node. Thus, at the junction point, it is possible to write that $I_2^{(1)} = I_1^{(2)}$. Then the expression for the current distribution can be rewritten

as $I(s) = I_2^{(1)}\left(-N_1^{(1)}(s^{(1)}) + N_2^{(2)}(s^{(2)})\right)$ or, equivalently, as $I(s) = I_1^{(2)}\left(N_2^{(2)}(s^{(2)}) - N_1^{(1)}(s^{(1)})\right)$, depending on the choice of reference current.

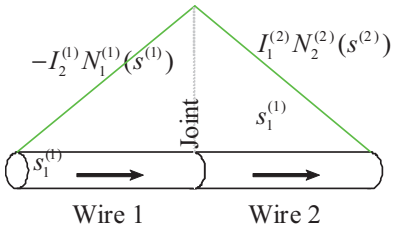

Figure 2-7. Current distribution on an electrically small dipole, modelled with two nodal basis functions.

Table 2-2. Expressions for doublet current expansions on a dipole.

Current Direction	$I^{(2)}$ towards the joint	$I^{(2)}$ outwards the joint
$I^{(1)}$ towards the joint	$I_2^{(2)}(-1)\left(N_1^{(2)} - N_1^{(1)}\right)$ $= I_2^{(2)}\left(-N_1^{(2)} + N_1^{(1)}\right)$ $= I_2^{(1)}\left(-N_1^{(1)} + N_1^{(2)}\right)$	$I_2^{(1)}\left(-N_1^{(1)} + N_2^{(2)}\right)$ $I_1^{(2)}(+1)\left(N_2^{(2)} - N_1^{(1)}\right)$
$I^{(1)}$ outwards the joint	$I_2^{(2)}(-1)\left(N_1^{(2)} - N_2^{(1)}\right)$ $I_2^{(2)}\left(-N_1^{(2)} + N_2^{(1)}\right)$ $= I_1^{(1)}\left(N_2^{(1)} - N_1^{(2)}\right)$	$I_1^{(1)}\left(N_2^{(1)} - N_2^{(2)}\right)$ $I_1^{(2)}(+1)\left(N_2^{(2)} - N_2^{(1)}\right)$

The general case of the current expansion profile for a doublet applied to a dipole can be considered in a similar manner. Figure 2-8 illustrates the definitions for the geometry.

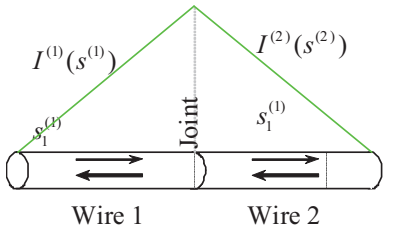

Figure 2-8. Current distribution on an electrically small dipole, modelled with a doublet.

A summary of the resulting expansions for various definitions of the current directions on the wires composing the dipole is given in Table 2-2.

2.10.3 Converting the Kirchhoff's Current Law into a Matrix Form

The equation (2.45) describing the transformation of *m* currents to *m-1* independent currents may be expressed in a matrix form $\mathbf{I}^{all} = \mathbf{K}\cdot\mathbf{I}^{indep}$. Here $\mathbf{I}^{all}$ denotes a vector column for the set of *m* original currents flowing through a junction, $\mathbf{I}^{indep}$ is a vector column for the set of *m-1* currents that are chosen to play the role of independent currents, and **K** is the $m \times m\text{-}1$ matrix performing the transformation. In this matrix, each of *m* rows describes the transformation from old set of currents to the new set. All of *m-1* rows corresponding to the independent currents have only one none-zero element. That element equals $d_0^{(k)}$ (i.e. +1 or –1, depending on whether the current flows into the junction or out of it), and is at the position (column) k , corresponding to the number of the respective independent variable. The remaining row corresponding to the selected dependent variable is filled with products $-d_0^{(k)}d_0^{(1)}, \quad k = 2,3\ldots m$, due to the match or mismatch in the defined direction of currents on the respective pair of wires number *k* and number *1*. It should be noted that in this explanation, the current through wire number 1 was chosen as the dependent variable.

With these in mind, the transformation may be written in an expanded matrix form (2.48):

$$\underbrace{\begin{bmatrix} I^{(1)}_{d_1^{(1)}} \\ I^{(2)}_{d_1^{(2)}} \\ I^{(2)}_{d_1^{(2)}} \\ \vdots \\ I^{(m)}_{d_1^{(m)}} \end{bmatrix}}_{\mathbf{I}^{all}} = \underbrace{\begin{bmatrix} -d_0^{(2)}d_0^{(k)} & -d_0^{(3)}d_0^{(1)} & \cdots & -d_0^{(m)}d_0^{(1)} \\ 1 & 0 & \cdots & 0 \\ 0 & 1 & \cdots & 0 \\ \vdots & \vdots & \ddots & \vdots \\ 0 & 0 & \cdots & 1 \end{bmatrix}}_{\mathbf{K}} \underbrace{\begin{bmatrix} I^{(2)}_{d_1^{(2)}} \\ I^{(3)}_{d_1^{(3)}} \\ \vdots \\ I^{(m)}_{d_1^{(m)}} \end{bmatrix}}_{\mathbf{I}^{indep}} \tag{2.48}$$

The top row describes the dependency of the dependent variable $I^{(1)}_{d_1^{(1)}}$ on the remaining, independent variables at the junction. The combination of the remaining rows forms a square identity matrix.

For a number of separate junctions, the resulting matrix may have a form of a block matrix [Råde, 93], where each block is a footprint of the matrix **K** for the respective junction. Otherwise, this block matrix may also be transformed into the form of (2.48), where top rows describe the dependencies of dependent variables and form a block-diagonal matrix. The number of top rows equals the number of junctions with more than two wires attached. The remaining rows will also form a square identity matrix.

This linear transformation may be readily applied to a MoM code that does not take advantage of the Kirchhoff's current law, and will help to improve the stability of the resulting new linear system of equations, and the accuracy of the solution (please refer to Section 3.8). The application of this transformation may be done in the few following mathematical steps.

- the column vector of currents $\mathbf{I}^{all}$ in the original system $\mathbf{Z}^{all}\,\mathbf{I}^{all} = \mathbf{V}^{all}$ is replaced with new column vector of currents $\mathbf{I}^{indep}$ obtained through the transformation $\mathbf{I}^{all} = \mathbf{K}\cdot\mathbf{I}^{indep}$.
- The resulting system $\mathbf{Z}^{all}\,\mathbf{K}\,\mathbf{I}^{indep} = \mathbf{V}^{all}$ is multiplied from the left-hand side by the transposed matrix **K**: $\mathbf{K}^{\mathrm{T}}\cdot\mathbf{Z}^{all}\cdot\mathbf{K}\cdot\mathbf{I}^{indep} = \mathbf{K}^{\mathrm{T}}\cdot\mathbf{V}^{all}$.
- The product $\mathbf{K}^{\mathrm{T}}\cdot\mathbf{Z}^{all}\cdot\mathbf{K}$ is identified as the new impedance matrix $\mathbf{Z}^{new}$, and the product $\mathbf{K}^{\mathrm{T}}\cdot\mathbf{V}^{all}$ is identified as the new excitation vector $\mathbf{V}^{new}$. These lead to a new linear system $\mathbf{Z}^{new}\cdot\mathbf{I}^{indep} = \mathbf{V}^{new}$, where matrix $\mathbf{Z}^{new}$ has its rank reduced in comparison with the original matrix $\mathbf{Z}^{all}$.
- This new system can now be inverted to obtain the solution $\mathbf{I}^{indep}$.
- The original currents $\mathbf{I}^{all}$ may be readily computed by the matrix multiplication $\mathbf{I}^{all} = \mathbf{K}\cdot\mathbf{I}^{indep}$.

Note:

This matrix technique may also be used to re-number the variables but a simpler approach was used in this work instead.

2.10.4 Polynomial Basis Functions

The basis functions should preferably closely resemble the physical models of current distribution (e.g. PWS basis functions) and propagation (i.e. include an oscillating exponentially decaying term). Such an expansion should provide accurate results with minimum number of terms. It is however difficult to apply for an inhomogeneous medium as the effective propagation constant depends on the position in a manner that is difficult to prognose for a general situation. In addition, overly complicated basis functions may slow the computations substantially down due to the large amount of calculations.

Polynomials, on the other hand, are well known and relatively easy to work with, with respect to the symbolic manipulations as well as to calculations. The works of [Popovic and Djordjevic, 88], [Kolundzija, 40] have shown that both the accuracy and speed are easily achievable with these functions. The polynomials belong to the class of hierarchical expansions[16].

The polynomial current expansion of degree $n_b - 1$, with respect to the normalised variable s/L, and with the unknown coefficients a_i, takes shape described by the expression (2.49):

$$I(s) = \sum_{i=1}^{n_b} a_i \left(\frac{s}{L} \right)^{i-1}, \; s_1 = -L \le s \le s_2 = L . \tag{2.49}$$

The obtained dimension of the unknown coefficients is thus the same as for the current intensity.

Transformation of the basis functions to satisfy the current continuity law gives an expansion in the form of (2.40):

$$I(s) = I_1 N_2(s) - I_2 N_1(s) + I_s(s) , \tag{2.50}$$

[16] Hierarchical expansions are those where the order of expansion is increased by adding a new, higher-order, term to an existing expansion without changing the existing functions.

where the current due to the singleton basis functions $I_s(s)$ is

$$I_s(s)=\sum_{i=3}^{n_b} a_i\left(\left(\frac{s}{L}\right)^{i-1}-\left(\frac{s}{L}\right)\frac{1}{2}\left(1-(-1)^{i-1}\right)-\frac{1}{2}\left(1-(-1)^{i-2}\right)\right). \tag{2.51}$$

A piecewise linear approximation (PWL) is a particular case of the expansion (2.50), when n_b is chosen to be equal to 2, so that the summation (2.51) includes no terms.

Separating the odd and even indexes, as in [Kolundzija and Popovic, 45] the same expression may be written in a clearer form:

$$I_s(s)=\sum_{i=3}^{n_b} a_i\left\{\begin{array}{ll}\left(s/L\right)^{i-1}-1, & i\ is\ odd\\ \left(s/L\right)^{i-1}-\left(s/L\right), & i\ is\ even\end{array}\right\} \tag{2.52}$$

Note:

A computationally more efficient way of summation, particularly useful for accelerating the far and near field calculations, may be done by rewriting (2.52) as

$$I_s(s)=\sum_{i=3,5,\ldots}^{n_b} a_i\left(\left(\frac{s}{L}\right)^{i-1}-1\right)+\frac{s}{L}\sum_{i=3,5,\ldots}^{n_b-1} a_{i+1}\left(\left(\frac{s}{L}\right)^{i-1}-1\right) \tag{2.53}$$

Here, the bracketed terms in the second sum repeat the terms from the first summation and can be reused. Furthermore, the form (2.53) may be brought to an even more computationally - efficient presentation:

$$I_s(s)=\sum_{i=3,5,\ldots}^{n_b-1}\left(a_i+\frac{s}{L}a_{i+1}\right)\left(\left(\frac{s}{L}\right)^{i-1}-1\right)+a_{n_b}\left(\left(\frac{s}{L}\right)^{n_b-1}-1\right).$$

The last term in the second sum in (2.53) and the last expression may need to be omitted, depending on the value of n_b.

It should also be noted that to increase the efficiency of computations further, the above forms of polynomials may be computed using the Horner's scheme [Råde, 93].

The node basis functions are

$$N_1(s) = -\frac{1}{2}\left(1+\frac{s}{L}\right)$$
$$N_2(s) = +\frac{1}{2}\left(1-\frac{s}{L}\right) \tag{2.54}$$

It should be noted that the definition of the node basis function given in [Kolundzija, 46] has positive sign for N_1, so that both functions are positive for the interval $-L \le s \le L$.

The summary of the basis functions and their derivatives with respect to s, which shall be utilised later, is given in Table 2-3.

Table 2-3 Polynomial-based basis functions satisfying Kirchhoff's current continuity law (KCL), and their first derivatives.

Global name of basis function	Function used for $f_i(s)$	Derivative of the function, $\frac{df_i(s)}{ds}$
$f_1(s)$	$N_2(s) = \frac{1}{2}\left(1-\frac{s}{L}\right)$	$+\frac{dN_2(s)}{ds} = -\frac{1}{2L}$
$f_2(s)$	$-N_1(s) = \frac{1}{2}\left(1+\frac{s}{L}\right)$	$-\frac{dN_1(s)}{ds} = +\frac{1}{2L}$
$f_i(s), i = 3,5,\ldots,n_b$	$S_i(s) = \left(s/L\right)^{i-1} - 1$	$\frac{dS_i(s)}{ds} = \frac{i-1}{L}\left(s/L\right)^{i-2}$
$f_i(s), i = 4,6,\ldots,n_b$	$S_i(s) = \left(s/L\right)^{i-1} - \left(s/L\right)$	$\frac{dS_i(s)}{ds} = \frac{i-1}{L}\left(s/L\right)^{i-2} - \frac{1}{L}$

Note:

It must also be noted that the singletons may belong to a wider class of functions than ones stated in Table 2-3. The only real restriction on the applicable functions is the requirement of them being zero at the ends of the interval, i.e. at the positions s_1 and s_2.

This opens doors to usage of orthogonal sets of functions [Abramowitz et al., 2]. Keeping to the class of polynomials, the Chebishev, spherical and many other types of orthogonal sets may be applicable (although a complete set may not be used, since the node basis functions will have to remain the first two functions in a set).

2.10.5 Note On the Degree of Orthogonality of Hierarchical Polynomial Basis Functions

The relationship describing the orthogonality for a set of functions $\{f_i(x)\}$ on an interval $[a,b]$ may be expressed as the weighted inner product of any two representatives of the set, $f_i(x)$ and $f_j(x)$:

$$\int_a^b w(x)\, f_i(x)\, f_j(x)\, dx = \begin{cases} \neq 0, & i = j \\ = 0, & i \neq j \end{cases}, \tag{2.55}$$

where $w(x)$ is a weight function, specific to the type of functions. If the functions are also *orthonormal*, then the inner product is also normalised and will produce either unity (for $i=j$) or 0 (for $i \neq j$).

These properties are usually very useful in providing a discrete version of a physical system (in a form of a matrix equation) with good numerical properties, including low condition number. The advantage of having a low condition number is in reduced requirements on the accuracy of the elements of the linear system. This translates into a more numerically stable and accurate (within the accuracy of the elements of the linear system, refer to Section 3.8) solution.

The integral (2.55) was calculated for the first 50 of the functions $\{f_i(x)\}$ and the results are shown in Figure 2-9.

The inner product of an orthogonal set, displayed as a matrix, should produce a pattern reflecting the presence of the main diagonal ($i=j$) only. Figure 2-9 shows a check-mate board pattern, and thus indicates that the hierarchical polynomials do not possess the orthogonality, although are partially orthogonal (in the sense of orthogonality between the functions with odd and even indexes only).

It should be possible to enhance the numerical properties of the system by utilising a polynomial set of basis functions that have better orthogonality [Abramowitz et al., 2]. Following the requirement on continuity of the current at the junctions and free ends, the node basis functions (2.54) will have to remain the first two functions in such a set. Thus, a complete set of orthogonal functions may not be used. However, the higher order terms (starting with the second term) may still be used. Thus, a higher order

polynomial set of basis functions may be devised, that substantially enhances the numerical properties of the linear system for large objects. The paper [Djordjevic and Notaros, 19] gives an excellent example of such approach.

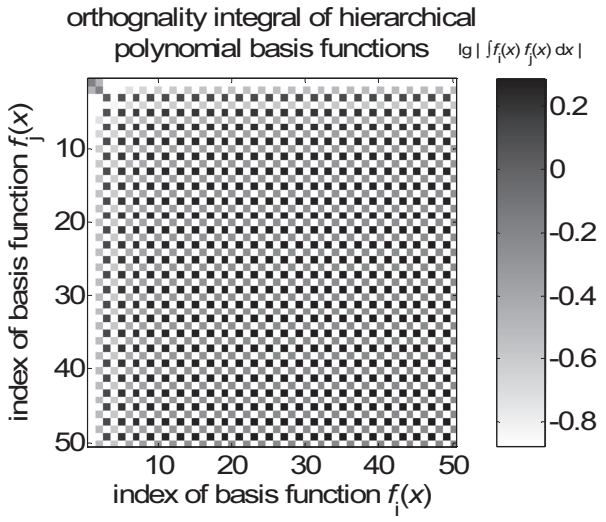

Figure 2-9. Logarithm of the inner product of hierarchical polynomial basis functions. Dark squares reflect non-zero result. White squares are zeros.

2.10.6 Note on the Basis Functions Based On a Quasi-Electrostatic Restriction

The accuracy of analysis can be further enhanced by inclusion of the quasi-static behaviour of charges due to discontinuities at wire ends and junctions into basis functions [Kyle, 53], [Miller and Deadrick, 74], [Kolundzija, 41]. These electrically small discontinuities can be approximately taken into account by including quasi-static relationships into the basis functions [Kolundzija, 46] in a way similar to the inclusion of the continuity equation done earlier. Effectively, this translates into matching the derivative of the current over a junction.

The resulting basis functions do improve convergence rate and accuracy [Kolundzija, 46, Ch.6.1]. This is at the expense of requiring at least 1 unknown more per wire than the previously described basis functions. These functions are the most efficient when applied to electrically long structures.

This opens a new opportunity for research looking into application of these basis functions on the composite chain basis functions (discussed later in the text). Presently, however, this combination is not considered in the thesis. Partially this was due to the greater restrictions applied to the polynomials and inability to apply the orthogonal sets instead of singletons.

2.11 On the Number of Variables and Re-Indexing of the Unknowns

To be able to practically realise the expansion obtained, it is necessary to build a connection between the numbering scheme utilised in the previous sections and a linear style of numbering usual for programming languages.

Starting with a presentation of the current distribution (2.46) generalised for a set of M_w thin wires with local coordinates $s^{(m)}$, $m=1,2,\ldots,M_w$, and applying the expansion (2.40) it is possible to write the current distribution on these wires as

$$\begin{aligned} I(s^{(1)},s^{(2)},\ldots,s^{(M_w)}) &= \sum_{m=1}^{M_w}\sum_{i=1}^{n_b^{(m)}} a_i^{(m)} f_i(s^{(m)}) \\ &= \sum_{m=1}^{M_w}\sum_{i=1}^{2} I_{d_1^{(m)}}^{(m)} (-1)^{i-1} N_{d_2^{(m)}}(s^{(m)}) + \sum_{m=1}^{M_w}\sum_{i=3}^{n_b^{(m)}} a_i^{(m)} S_i(s^{(m)}) \end{aligned}, \quad (2.56)$$

where the superscript $^{(m)}$ refers to the m^{th} wire. The factor $(-1)^{i-1}$ is equivalent to the current direction function d_0. So far, the KCL has not been applied and the total number of unknown coefficients is $N=\sum_{m=1}^{M_w} n_b^{(m)}$.

Taking into account M_w^1 wires with free (open) second end (while the first end is connected to another wire), M_w^2 wires with free (open) first end, and $M_w^{1,2}$ wires with the both ends connected to other wires, the expansion can be written as

$$\begin{aligned} I(s^{(1)},s^{(2)},\ldots,s^{(M_w)}) &= \sum_{m=1}^{M_w^1} I_1^{(m)} N_2(s^{(m)}) - \sum_{m=1}^{M_w^2} I_2^{(m)} N_1(s^{(m)}) \\ &+ \sum_{m=1}^{M_w^{1,2}}\sum_{i=1}^{2} I_{d_1^{(m)}}^{(m)} (-1)^{i-1} N_{d_2^{(m)}}(s^{(m)}) + \sum_{m=1}^{M_w}\sum_{i=3}^{n_b^{(m)}} a_i^{(m)} S_i(s^{(m)}) \end{aligned} \quad (2.57)$$

The number of unknowns $N = M_w^1 + M_w^2 + 2M_w^{1,2} + \sum_{m=1}^{M_w}\left(n_b^{(m)} - 2\right)$ now is smaller by $M_w - M_w^1 - M_w^2 - M_w^{1,2}$ due to excluded free ends.

It is important to note that a wire with both ends free should be divided into at least two wires, if no singleton is to be used on it.

Taking into account the KCL at the junctions of several wires, it is possible to further reduce the number of unknowns:

$$\begin{aligned} I(s^{(1)}, s^{(2)}, \ldots, s^{(M_w)}) &= \sum_{n=1}^{M_{jun}} I_{jun}^{(n)}(s^{(jn,w1)}, s^{(jn,w2)}, \ldots, s^{(jn,wn_w^{(n)})}) + \sum_{m=1}^{M_w}\sum_{i=3}^{n_b^{(m)}} a_i^{(m)} S_i(s^{(m)}) \\ &= \sum_{n=1}^{M_{jun}}\sum_{k=2}^{n_w^{(n)}} I_{a_1^{(k)}}^{(jn,wk)} D^{(1,k)}(s^{(jn,w1)}, s^{(jn,wk)}) + \sum_{m=1}^{M_w}\sum_{i=3}^{n_b^{(m)}} a_i^{(m)} S_i(s^{(m)}) \end{aligned} \tag{2.58}$$

The superscript $^{(jn,wk)}$ stands for the wire number k at the junction n, where the numbering of the wires is localised to each individual junction. The first summation is over the currents defined by the doublets, and the second sum is over the currents defined by the singletons. The numbering under summation for the doublets is localised for the $n_w^{(n)}$ wires joining the n^{th} junction; e.g. the index k here corresponds to a localised numbering of wires at a junction[17].

Note:

Figure 2-10 shows the backward transformation that can be used in the programming code to obtain the parameters of the integration domain and the basis function.

The values of the dependent unknown currents excluded in (2.58) can be obtained by the KCL (2.45).

[17] In the realised programming code written in Matlab, the wires may be found using the structure like `junctions(n).wires(k)`.

To simplify expressions and to come closer to the programming of the MoM, it is convenient to map/re-index the unknowns and the respective basis functions with the aim of introducing a linear indexing scheme, and thus rewriting the current expansion as

$$I(s^{(1)},s^{(2)},\ldots,s^{(M_w)}) = \sum_{p=1}^{N_D} \tilde{a}_p^D \tilde{D}_p + \sum_{q=1}^{N_S} \tilde{a}_q^S \tilde{S}_q \,, \tag{2.59}$$

where the mapping/equivalency is as follows: the doublet-related new unknown current coefficient $\tilde{a}_q^D \leftrightarrow I_{d_1^{(k)}}^{(n)(k)}$, basis function $\tilde{D}_p \leftrightarrow D^{(n)(1,k)}(s^{(n)(1)},s^{(n)(k)})$, singleton-related new unknown coefficient $\tilde{a}_q^S \leftrightarrow a_i^{(m)}$ and basis function $\tilde{S}_q \leftrightarrow S_i(s^{(m)})$. The indexes p and q are thus the substitutions for the double indexes (n,k) and (m,i), respectively (where n is the junction number, k is the wire number local to this n^{th} junction, m is the wire number and i is the singleton number on this m^{th} wire).

The total number of unknowns N_b, the number of unknowns due to doublets N_D and the number of unknowns due to singletons N_S are

$$N_b = N_D + N_S, \quad N_D = \sum\nolimits_{n=1}^{M_{jun}} \left(n_w^{(n)} - 1\right), \quad N_S = \sum\nolimits_{m=1}^{M_w} \left(n_b^{(m)} - 2\right) \tag{2.60}$$

The new set of unknowns $\tilde{a}_i, \quad i = 1,2,\ldots,N_b$ consists of subsets $\tilde{a}^D$ and $\tilde{a}^S$, and the new set of expansion functions $\tilde{f}_i, \quad i = 1,2,\ldots,N_b$ consists of subsets $\tilde{D}$ and $\tilde{S}$:

$$\begin{aligned} \{\tilde{a}_i\}_{i=1}^{N_b} &= \left\{\tilde{a}_1^D,\tilde{a}_2^D,\ldots,\tilde{a}_{N_D}^D,\tilde{a}_1^S,\tilde{a}_2^S,\ldots,\tilde{a}_{N_S}^S\right\} \\ \left\{\tilde{f}_i\right\}_{i=1}^{N_b} &= \left\{\tilde{D}_1,\tilde{D}_2,\ldots,\tilde{D}_{N_D},\tilde{S}_1,\tilde{S}_2,\ldots,\tilde{S}_{N_s}\right\} \end{aligned} \tag{2.61}$$

Thus, the new, shorter form of the current expansion (directly associated with the general MoM expansion (2.2)) can be written as

$$I(s^{(1)},s^{(2)},\ldots,s^{(M_w)}) = \sum_{i=1}^{N_b} \tilde{a}_i \tilde{f}_i \tag{2.62}$$

The indexing scheme in Figure 2-10 describes the following information flow for computation related to the doublets. Singletons may be processed in a similar, but simpler sequence because (a) they do not need to be associated with any junction, and

(b) they are always attributed to one wire, and so require only one branch out of the two shown in Figure 2-10.

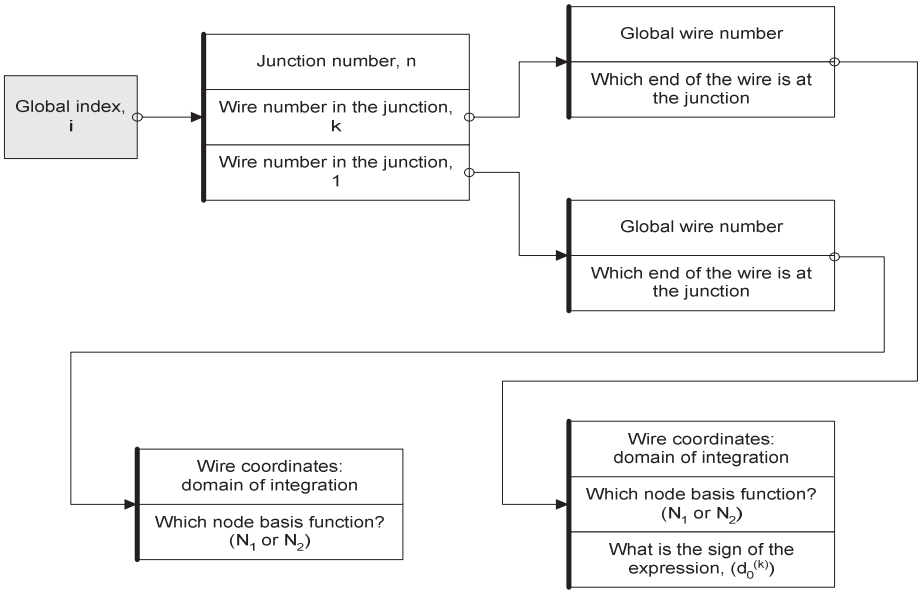

Figure 2-10. The flowchart showing translation of a global linear index *i* for the global linear basis function number/index into the respective numbers/indexes for wires, doublets, and node basis functions.

2.12 On Geometrical Modelling

Traditionally, during the process of geometrical modelling, the basis functions are assigned to the geometrical structure. Depending on the complexity of the realisation of the MoM, this process may also be advanced by the following steps:

- Dividing electrically long wires into shorter segments of permitted maximum length.

  The low order current approximations due to piecewise constant and piecewise linear basis functions cannot represent fast variations in the current unless the length of each interval (where such approximation is applied) is sufficiently short. Higher order basis functions are more flexible in this regard and permit longer segments, but are still restricted by the limited numerical accuracy. A higher-order polynomial

basis function permits the length of a wire segment of about one-two wavelengths (when single precision number representation is used for storage and calculations) [Kolundzija, 46].

- Sub-dividing the parts of wires in vicinity of the free wire ends.

  The function of charge distribution near free ends (not attached to anything else) experiences a sharp change (here – growth). This is also reflected by the sharper decay in the current density, coming to zero at the end of the wire. Application of a finer non-equidistant mesh near the wire ends improves the accuracy and convergence of the results [Kolundzija, 46].

- Sub-dividing the wires in vicinity of the junctions, where the wires join at a sharp angle.

  The same applies as for the wires in vicinity of the free wire ends.

- Sub-dividing the wires that are in vicinity of other wires and may thus be affected by strong coupling.

  The same comments apply here as for the wires in vicinity of the free wire ends. Advantages are discussed in [Kolundzija, 41].

- Replacing free wire ends with wire caps having zero radius at the free end.

  By forcing zero radius at the free ends of the wires and at the point where a wire is attached to a the delta-gap generator, the continuity equation is satisfied better, which results in a more numerically stable system, and may produce more accurate results [Kolundzija, 46], [Kolundzija, 41].

- Selecting the reference wire for the doublets assigned to a junction of more than two wires.

  The correct choice may help to improve the numerical properties of the linear system. This is discussed in detail in Section 3.1, later in the text.

The above steps aid to make the numerical model satisfy the physical laws better, less approximately. This usually results in a more stable and accurate numerical model.

Note:

The current programming realisation described later, in the text, does not as yet support these features. Nevertheless, such functionality is of high importance in a user-friendly program [Kolundzija, 46*], and therefore the mentioning has been included in the present work.*

2.13 Building a System of Linear Equations

The next step is to build a system of linear algebraic simultaneous equations, also referred to as a matrix equation.

In a fashion similar to (2.56)-(2.59), the current distribution on a system of wires may be written as

$$I = \sum_n I_{jun}^{(n)} + \sum_m I_s^{(m)}, \tag{2.63}$$

where the first summation is over all currents approximated by doublets, and the second summation is over the currents approximated with singleton basis functions.

Since the expression for the electric field (2.31) is linear with respect to the current, it may be presented in the same form as (2.63):

$$\vec{E} = \sum_n \vec{E}_{jun}^{(n)} + \sum_m \vec{E}_s^{(m)} \tag{2.64}$$

The boundary condition (2.13) may be applied to the expression (2.64) at the domains of each basis function, similarly to how it was done to obtain (2.35) in Section 2.9.

This is followed by the test procedure outlined in (2.5), and utilising the set of weighting functions (2.62). These weighting functions are the same as the expansion/basis functions, since the Galerkin procedure is being followed. Keeping in mind the order of unknowns and respective basis functions specified by (2.61), the following set of $N_D + N_S$ linear equations results:

$$\begin{cases} \sum_{p=1}^{N_D} \tilde{a}_p^D \int_{s^{(j)}} \vec{\tilde{D}}_j \vec{E}_p^D ds'^{(j)} + \sum_{q=1}^{N_S} \tilde{a}_q^S \int_{s^{(j)}} \vec{\tilde{D}}_j \vec{E}_q^S ds'^{(j)} = -\int_{s^{(j)}} \vec{\tilde{D}}_j \vec{E}^{inc} ds'^{(j)}, \quad j = 1,2,\ldots,N_D \\ \sum_{p=1}^{N_D} \tilde{a}_p^D \int_{s^{(j)}} \vec{\tilde{S}}_j \vec{E}_p^D ds'^{(j)} + \sum_{q=1}^{N_S} \tilde{a}_q^S \int_{s^{(j)}} \vec{\tilde{S}}_j \vec{E}_q^S ds'^{(j)} = -\int_{s^{(j)}} \vec{\tilde{S}}_j \vec{E}^{inc} ds'^{(j)}, \quad j = 1,2,\ldots,N_S \end{cases} . \tag{2.65}$$

In this set of equations, the notations use vector basis functions for the sake of minimising the space. The meaning of these notations, related to (2.61), is:

$$\vec{\tilde{D}}_j \equiv \vec{u}_s^{(j)}(s'^{(j)})\tilde{D}_j, \quad \vec{\tilde{S}}_j \equiv \vec{u}_s^{(j)}(s'^{(j)})\tilde{S}_j \tag{2.66}$$

It must also be noted that the integration domains for doublets consist of two wires, whilst the domain for singletons consist of single wires ($s'^{(j)} \in \left[s_1'^{(j)}, s_2'^{(j)} \right]$).

Expanding any of the integrands, e.g. $\vec{\tilde{D}}_j \vec{E}_p^D = \vec{u}_s^{(j)}(s'^{(j)})\tilde{D}_j \vec{E}_p^D$, it is possible to give the following interpretation to the factor $\vec{u}_s^{(j)}(s'^{(j)})\vec{E}_p^D$. It is the component of the electrical field vector due to the p^{th} basis function in the direction of the generatrix of the wire/truncated cone on which the j^{th} basis function is defined.

The matrix equation (2.65) can also be written in a reduced form as

$$\left[Z_{jp} \right]\left[a_p \right] = \left[U_j^{src} \right], \quad j, p = 1, 2, \ldots, N \tag{2.67}$$

or, more explicitly, as

$$\sum_{p=1}^{N} Z_{jp} a_p = U_j^{src}, \quad j = 1, 2, \ldots, N . \tag{2.68}$$

2.14 Components of the Matrix Equation

It is easy to notice that the matrix resulting from (2.65) may be presented by four sub-matrixes Z^{DD}, Z^{DS}, Z^{SD} and Z^{SS}. The right-hand side, the excitation column vector is also made up of two sub-vectors, U^D and U^S. Keeping the order in which the unknowns and basis functions are sorted, (2.61), the matrix equation may be written as

$$\begin{pmatrix} Z^{DD} & Z^{DS} \\ Z^{SD} & Z^{SS} \end{pmatrix} \begin{pmatrix} \tilde{a}^D \\ \tilde{a}^S \end{pmatrix} = \begin{pmatrix} U^D \\ U^S \end{pmatrix}, \tag{2.69}$$

where the $N_D \times N_D$ sub-matrix Z^{DD} is associated with the interaction between the low-order basis functions (doublets), sub-matrix Z^{SD} and sub-matrix Z^{DS} with sizes $N_S \times N_D$ and $N_D \times N_S$, respectively, are associated with the interaction between

doublets and singletons. The $N_D \times N_D$ sub-matrix Z^{SS} describes the interaction between the higher-order modes, the singletons.

The excitation column vector on the right hand side is also composed of two sub-vectors U^D and U^S, associated the inner products of the electrical fields due to excitations, and the doublet (superscript ^{D}) and singleton (superscript ^{S}) basis functions, respectively.

Expressions for each of the components are written down separately.

Expressions for the "doublet -doublet" partial impedances $\boldsymbol{Z}^{\mathrm{DD}}$

Each "doublet-doublet" impedance matrix element Z_{jp}^{DD} can be decomposed into two components corresponding to the vector and scalar potentials

$$Z_{jp}^{DD} = Z_{jp}^{DDA} + Z_{jp}^{DDV} \tag{2.70}$$

For doublets, each basis function consists of two node basis functions. Therefore the double integral can be represented by four double integrals due to expanding the product of two doublets:

$$\begin{aligned} Z_{jp}^{DDA} &= \left(-j\omega\mu_0\right)\begin{pmatrix} Z^{N_j^k N_p^k A} + d_0^{(j)(k)} d_0^{(j)(1)} d_0^{(p)(k)} d_0^{(p)(1)} Z^{N_j^1 N_p^1 A} \cdots \\ - d_0^{(p)(k)} d_0^{(p)(1)} Z^{N_j^k N_p^1 A} - d_0^{(j)(k)} d_0^{(j)(1)} Z^{N_j^1 N_p^k A} \end{pmatrix} \\ Z_{jp}^{DDV} &= \frac{1}{-j\omega\varepsilon_0}\begin{pmatrix} Z^{N_j^k N_p^k V} + d_0^{(j)(k)} d_0^{(j)(1)} d_0^{(p)(k)} d_0^{(p)(1)} Z^{N_j^1 N_p^1 V} \cdots \\ - d_0^{(p)(k)} d_0^{(p)(1)} Z^{N_j^k N_p^1 V} - d_0^{(j)(k)} d_0^{(j)(1)} Z^{N_j^1 N_p^k V} \end{pmatrix} \end{aligned}, \tag{2.71}$$

where the partial sub-impedances $Z^{N_j^k N_p^m A}$ due to the vector magnetic potential $\vec{A}$ are

$$Z^{N_j^k N_p^m A} = \left(\vec{u}_z^{(j)(k)} \cdot \vec{u}_z^{(p)(m)}\right)\cos\alpha^{(p)(m)} \int_{s_1^{(j)(k)}}^{s_2^{(j)(k)}} N_{d_2^{(j)(k)}}(s') \int_{s_1^{(p)(m)}}^{s_2^{(p)(m)}} N_{d_2^{(p)(m)}}(s)\, g(R_e)\, ds\, ds' \tag{2.72}$$

and the partial sub-impedances due to the scalar electric potential V are

$$Z^{N_j^k N_p^m V} = \int_{s_1^{(j)(k)}}^{s_2^{(j)(k)}} N_{d_2^{(j)(k)}}(s') \int_{s_1^{(p)(m)}}^{s_2^{(p)(m)}} \frac{dN_{d_2^{(p)(m)}}(s)}{ds} g(R_e)\left(jk + \frac{1}{R_e}\right)\left(\vec{u}_z^{(j)(k)} \cdot \vec{u}_R^{(p)(m)}\right) ds\, ds' . \tag{2.73}$$

Here, as well as in the following expressions, whenever the double indexing (*j*)(*k*) or (*j*)(*1*), e.g. N_j^k and N_j^1, is used, it refers to the k^{th} and to the 1^{st} wires (and respective basis functions) addressed by the global linear index *j*. See Figure 2-10 for more details.

Expressions for the "singleton-doublet" partial impedances $\mathbf{Z}^{\text{SD}}$ and $\mathbf{Z}^{\text{DS}}$

The impedance matrix elements Z_{jp}^{SD} and Z_{jp}^{DS} are also decomposed into two components corresponding to the vector and scalar potentials. On the example of Z_{jp}^{SD}, they are

$$Z_{jp}^{SD} = Z_{jp}^{SDA} + Z_{jp}^{SDV} \tag{2.74}$$

For doublets, each basis function consists of two node basis functions. Therefore the double integral can be represented by two double integrals due to expanding the product of a singleton and a doublet:

$$\begin{aligned} Z_{jp}^{SDA} &= \left(-j\omega\mu_0\right)\left(Z^{S_j^k N_p^k A} - d_0^{(p)(k)} d_0^{(p)(1)} Z^{S_j^k N_p^1 A}\right) \\ Z_{jp}^{SDV} &= \left(\tfrac{j}{\omega\varepsilon_0}\right)\left(Z^{S_j^k N_p^k V} - d_0^{(p)(k)} d_0^{(p)(1)} Z^{S_j^k N_p^1 V}\right) \end{aligned}, \tag{2.75}$$

where the partial sub-impedances $Z^{N_j^k N_p^m A}$ due to the vector magnetic potential $\boldsymbol{A}$ are

$$Z^{S_j^k N_p^m A} = \left(\vec{u}_z^{(j)(k)} \cdot \vec{u}_z^{(p)(m)}\right)\cos\alpha^{(p)(m)} \int_{s_1^{(j)(k)}}^{s_2^{(j)(k)}} S^{(j)(k)}(s') \int_{s_1^{(p)(m)}}^{s_2^{(p)(m)}} N_{d_2^{(p)(m)}}(s)\, g(R_e)\, ds\, ds' \tag{2.76}$$

and the partial sub-impedances due to the scalar electric potential V are

$$Z^{S_j^k N_p^m V} = \int_{s_1^{(j)(k)}}^{s_2^{(j)(k)}} S^{(j)(k)}(s') \int_{s_1^{(p)(m)}}^{s_2^{(p)(m)}} \frac{dN_{d_2^{(p)(m)}}(s)}{ds} g(R_e)\left(jk + \frac{1}{R_e}\right)\left(\vec{u}_z^{(j)(k)} \cdot \vec{u}_R^{(p)(m)}\right) ds\, ds' \tag{2.77}$$

The expressions for Z_{jp}^{DS} may be written in a similar manner.

Expressions for the "singleton-singleton" partial impedances Z^{SS}

The expressions for the singletons are the simplest, as may be seen from (2.78):

$$\begin{aligned} &Z_{jp}^{SS} = Z_{jp}^{SSA} + Z_{jp}^{SSV}, \quad \text{where} \\ &Z_{jp}^{SSA} = \left(-j\omega\mu_0\right)\left(Z^{S_j^k S_p^k A}\right), \quad \text{and} \quad Z_{jp}^{SSV} = \left(\tfrac{j}{\omega\varepsilon_0}\right)\left(Z^{S_j^k S_p^k V}\right), \end{aligned} \tag{2.78}$$

where the partial sub-impedances due to the magnetic and electric potential are

$$\begin{aligned} Z^{S_j^k S_p^m A} &= \left(\vec{u}_z^{(j)(k)} \cdot \vec{u}_z^{(p)(m)}\right) \cos\alpha^{(p)(m)} \int_{s_1^{(j)(k)}}^{s_2^{(j)(k)}} S^{(j)(k)}(s') \int_{s_1^{(p)(m)}}^{s_2^{(p)(m)}} S^{(p)(m)}(s)\, g(R_e)\, ds\, ds' \\ Z^{S_j^k S_p^m V} &= \int_{s_1^{(j)(k)}}^{s_2^{(j)(k)}} S^{(j)(k)}(s') \int_{s_1^{(p)(m)}}^{s_2^{(p)(m)}} \frac{dS^{(p)(m)}(s)}{ds} g(R_e) \left(jk + \frac{1}{R_e}\right) \left(\vec{u}_z^{(j)(k)} \cdot \vec{u}_R^{(p)(m)}\right) ds\, ds' \end{aligned} \tag{2.79}$$

Expressions for the excitation vector element $\mathbf{U}^{\mathrm{D}}$ and $\mathbf{U}^{\mathrm{S}}$

For doublets, the element U_j^D is composed of two sub-excitations due to the inner products with the two node basis functions N_j^k and N_j^1, respectively:

$$U_j^D = U_j^{N_j^k} + U_j^{N_j^1} \tag{2.80}$$

Each one may be written as

$$U_j^{N_j^k} = -\int_{s_1^{(j)(k)}}^{s_2^{(j)(k)}} N_{d_2^{(j)(k)}}(s') \left(\vec{u}_z^{(j)(k)} \cdot \vec{E}^{inc}(\vec{r}')\right) ds' \tag{2.81}$$

The details of calculating these integrals are discussed in the next chapter.

2.15 Summary

The chapter reviews and discusses the essentials of Galerkin's formulation of the method of moments, used throughout the following chapters.

The chapter starts with a brief historic overview and an introduction to the main steps of the method of moments (MoM). This is followed by a description of the generalized conical wire, which is the model used to represent actual wires. Starting with the retarded potentials, the thin wire approximation in combination with the conical wire approximation is then used to establish the electrical field integral equation (EFIE). Next, the higher order hierarchical polynomial basis functions satisfying the Kirchhoff's current law (KCL) are described and discussed in detail. The KCL identifies the relationships for current at the free wire ends and at the junctions with multiple wires. In

applying the KCL to these, the initial set of hierarchical polynomials is converted to a new set composed of doublet and singleton basis functions. The satisfaction of the KCL is ensured by the doublets. At the junctions with more than two wires, a multiplet basis function is defined, based on the same principles.

Subsequently, the Galerkin's method is applied to the integral equation to build a system of linear algebraic equations. On the left-hand side, the system has a product of the so-called impedance matrix and the vector of unknowns. The right hand side is an excitation vector. The elements of the impedance matrix indicate the strength of electromagnetic coupling between respective wire segments. The numbering scheme for the unknowns in the linear system is defined by the numbering of the basis functions. In the proposed realization, if the singletons are used, the matrix is shown to be composed of four block sub-matrices. The chapter ends with stating the four respective types of expressions for the impedance matrix elements. These result from the possible combinations of the doublet and singleton basis functions.

Chapter 3. Details of Implementation for MoM

This chapter discusses the performance-related aspects of the method of moments (MoM). These aspects include a new method of reducing the condition number by selection of the reference wire, calculation of integrals that appear in the impedance matrix elements, considerations of matrix symmetry, and novel technique for re-usage of repeating elements. In addition, this chapter discusses the treatment of excitation and loading, support of symmetry planes, calculation of network parameters Y, Z and S, and also numerical estimation of the uncertainties in the solution. This is followed by an example. The chapter is ended with an introduction into a new method of radiation pattern estimation. This method is compared in terms of accuracy and speed against analytical formulas and commercial software.

3.1 Reducing Condition Number by Selection of the Reference Wire in a Multiplet

This section discusses a numerical investigation in connection with the dependency of the condition number of the impedance on the selection of the reference wire in the decomposition of current on a junction with attached wires (multiplet). A reduction in the condition number is expected to improve the stability of the linear system and accuracy of the result, the topic discussed in more details in Section 3.8.

In this section, it is shown that it is possible to minimise the condition number by an appropriate selection of the reference wire. The selection criteria were found to be based on the electrical length. An empirical rule for selecting the reference wire is developed. An order of magnitude reduction in the condition number of the impedance matrix is observed.

3.1.1 Problem formulation

A complex system of interconnected wires may be decomposed into junctions. A junction, as discussed in Section 2.10.1, may have an arbitrary number of wires attached to it. This junction with the attached wires may be considered as an isolated three-

dimensional object or sub-system with associated impedance sub-matrix. It is expected that minimising the condition number[18] of the impedance sub-matrixes for each individual sub-system should lead to a lower condition number for the system, and thus to a more numerically stable solution. This consideration makes treatment of junctions a prime target in this section.

The equations (2.44) and (2.46) describe the current distribution over a junction with several individual wires attached. This current distribution, referred to as a *multiplet*, is approximated with doublet basis functions (discussed in Section 2.10). It states that the wire number 1 is selected as the reference wire (also referred to in this text as a *common* wire). The term *reference* is used to highlight that an unknown current amplitude on this wire is defined as a variable that is dependent on the current amplitudes of the other wires attached to the same node. However, the enumeration of the wires attached to this node/junction may be done in an arbitrary manner, as long as the assigned numbers are unique. Thus, any wire may be selected as the reference wire.

This discussion may be illustrated with an example. In a simple structure shown in Figure 3-1, there are 3 wires attached to the same node. It may be readily observed that there are 6 possible ways to refer to the wires using indexes 1, 2 and 3.

The situation discussed in this example was met during a stage of re-programming the code related to the assignment of basis functions. It was noted that the condition number of the resultant impedance matrix depends on the choice of a reference wire (more precisely, on the electrical length of the reference wire).

A literature search did not result in any references on the subject. Therefore, this question was investigated numerically. A number of numerical models with various degrees of complexity were tested. The geometry and also the numbering (labelling) of the elements (wires) were varied to evaluate their effect on the condition number of the impedance matrix. The main criterion for the evaluations was the dependence of the condition number on the length of the reference wire.

[18] The condition number of impedance matrix and its relation to the moment method's solutions is discussed later in the text, in Section 3.8 starting from page 109.

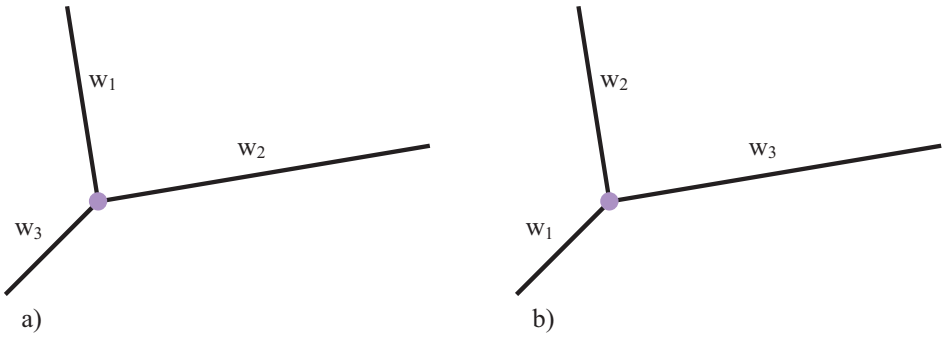

Figure 3-1. Numbering of wires attached to a node/junction. Two out of six possible combinations are shown in (a) and (b). Each wire is denoted with the symbol *w* and a unique number.

In all tests, the wires were forced to have polynomial of 1st degree (piecewise linear function) for a basis function. Enabling higher order basis functions may alter the results and requires a thorough additional investigation.

3.1.2 Quasi-Static Scenario

In this set of numerical experiments, the total length of wires was kept much shorter than the wavelength, as to ensure the quasi-static condition The frequency of modelling was in most cases set to 0.1 MHz (which corresponds to the wavelength of 3000 m). The length of any individual wire was, at the same time, kept strictly much larger than the wire's radius, so as to satisfy the thin wire approximation (refer to Section 2.4). All wires were set to have the radius of 1 mm. This value was used in all other simulations described in the subsections to follow, unless mentioned otherwise.

Several combinations of wires were tested using *doublet* (otherwise referred to as *roof-top* or *piecewise linear*) basis functions (discussed in Section 2.10.1).

3.1.2.1 Simplest Case – a Junction with Two Wires Forming a Dipole

For a junction of only two wires, there is only one doublet. Thus, there is no common wire. The number of unknowns here is 1. Thus the impedance matrix rank is 1, so that the condition number is also 1, regardless of the lengths of the wires, angle between

them, or any other parameters associated with a truncated cone approximation for a straight wire.

This example is provided here to contrast with more complex scenarios that follow.

3.1.2.2 A Junction with Three Wires

Nodes in this project were defined as in Table 3-1. The wires had their beginning at the node number 1 and ended at the other nodes (in various combinations). In total, six different combinations were tested.

An example of the wires defined via nodes is given in Table 3-2. This example may be illustrated with Figure 3-2.

Table 3-1 . A junction with 3 wires: Definitions for node coordinates.

Node no.	X, m	Y, m	Z, m	Comment
1	0	0	0	Common node for all wires
2	1	0	0	The shortest distance to node 1
3	0	10	0	
4	0	0	100	The longest distance to node 1

Table 3-2. A junction with 3 wires: An Example of defining the wires.

Wire no.	Nodes defining the wire (beginning, end)
w1	1,2
w2	1,3
w3	1,4

This geometry requires 2 unknowns and 2 doublet basis functions. The algorithm used in the program automatically generated (assigned) the following definition for 2 doublet basis functions to this structure:

$$N_2^{(2)} - N_2^{(1)} \text{ and } N_2^{(3)} - N_2^{(1)},$$

where the nodal functions $N_{1,2}$ are defined on page 34 (Section 2.10).

The both doublets set the wire number 1 as the reference wire, i.e. common for these two basis functions. Therefore, the condition number of the impedance matrix was considered as a function of the length of the wire number 1 (further referred to as w1).

Table 3-3 summarises the results of this investigation. The results show that selecting the longest wire as the reference wire helps to minimise the condition number of the resultant impedance matrix, at least under quasi-static conditions.

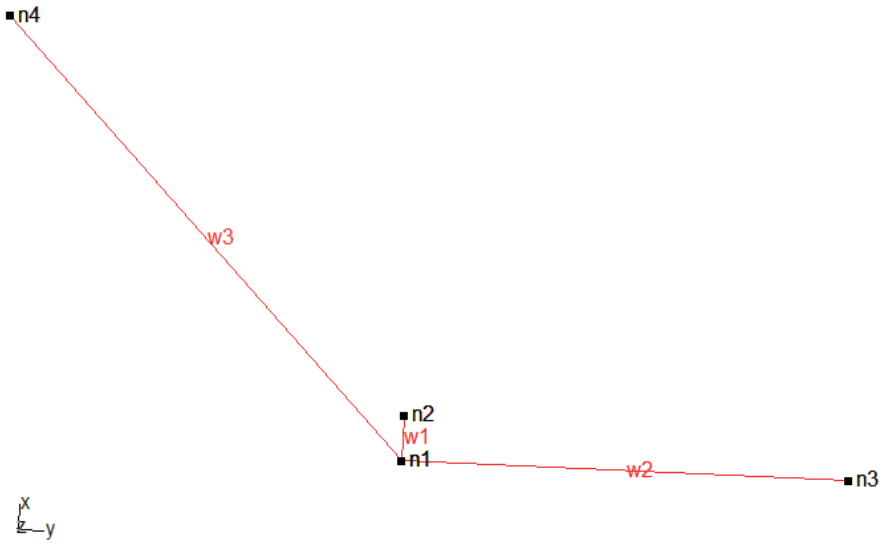

Figure 3-2. Sample structure used for investigation of the dependence of the condition number on the choice of the reference wire. Model: "A Junctions with Three Wires" (3 wires; each one is at a right angle to each of the other two wires; lengths of wires 1m, 10m, and 100m). Note on the perspective: the *z*- axis on this figure is close to but not perpendicular to the page (not easy to see as the angle is about 8 degrees off), and so the *x*- and *y*- axes are not exactly parallel to the page.

Table 3-3 . One Junction with 3 Wires: Condition Number of Impedance Matrix for Various Assignments of Wires to Nodes.

Config. No.	Nodes of wires w1, w2, and w3: as (beginning, end)	Condition number	Comment
A	(1,2) (1,3) (1,4)	**27.84**	Shortest wire is the common one
B	(1,3) (1,2) (1,4)	8.136	Middle is the common one
C	(1,2) (1,4) (1,3)	27.84	Shortest wire is the common one
D	(1,4) (1,2) (1,3)	**7.019**	Longest wire is the common one
E	(1,4) (1,3) (1,2)	**7.019**	Longest wire is the common one
F	(1,3) (1,4) (1,2)	8.136	Middle is the common one

The variation of the condition number against the accuracy of calculations was tested. The testing was done by considering two configurations of wires that produce two closest, distinct, values of the condition number, i.e. configurations E and F from Table 3-3. These chosen condition number values are then approximately 7.019 and 8.136. Each value was computed with integral accuracy levels 4 (default in the program) and 6 (higher accuracy). The obtained condition numbers were then compared. The results are shown in Table 3-4.

For the configuration corresponding to the lowest condition number, the fractional accuracy of computing the value of condition number (at integral accuracy level 4 compared to the integral accuracy level 6), may be estimated as 1.1e-6. This number is much smaller than 0.16, i.e. the relative difference between the two condition numbers for the two configurations. This indicates that the condition number estimates are stable and may be used for comparison purpose.

Table 3-4. Condition number variation in different configurations.

<table>
<tr><th>Config. No.</th><th>Accuracy level for calculating impedance matrix elements</th><th>Impedance matrix element's (Integral's) tolerance</th><th>Impedance matrix condition number</th><th>Difference of condition num-bers for each wire configuration</th><th>Difference of condition num-bers for the configurations E_4 and F_4, relative to condition number of A</th></tr>
<tr><td colspan="5">Wires defined with nodes as (1,4) (1,3) (1,2):</td><td rowspan="5">(8.136412-7.018764) / 7.018764
= 0.16</td></tr>
<tr><td>E_4</td><td>4</td><td>2.5e-6</td><td>7.018764</td><td rowspan="2">absolute=8e-6, relative=1.1e-6</td></tr>
<tr><td>E_6</td><td>6</td><td>2e-8</td><td>7.018772</td></tr>
<tr><td colspan="5">Wires defined with nodes as (1,3) (1,4) (1,2):</td></tr>
<tr><td>F_4</td><td>4</td><td>2.5e-6</td><td>8.136412</td><td rowspan="2">absolute=-3.6e-5, relative=4.4e-6</td></tr>
<tr><td>F_6</td><td>6</td><td>2e-8</td><td>8.136376</td><td></td></tr>
</table>

3.1.2.3 Considering a System of Sub-Systems, where Each Sub-System Is the Junction with Three Wires

It was stated in Section 3.1 on page 60 that a complex system composed of sub-systems should gain better (lower) system condition number by optimizing (minimizing) the

condition number for each individual sub-system. In this section, this assumption is tested.

The single junction with 3 wires already considered in the previous subsection is used as a building block (sub-system) for a larger structure. Figure 3-3 shows several systems of different size. The simplest case is in Figure 3-3a, where three wires are joined at a node/junction. There, a system consists of one subsystem only. This structure was then copied to form a system composed of two equal independent subsystems. The result is displayed in Figure 3-3b. In the numerical experiments, the number of subsystems was varied from 1 to 20. The most complex system with twenty subsystems is shown in Figure 3-3c.

Notes:

1. Program WIPL-D [Kolundzija, 46*] was used to generate the geometry of the models. The actual calculations of impedance matrices and respective condition numbers were done using author's Matlab code.*

2. To address a wider spectrum of applications, the investigation in this subsection goes beyond the quasi-static frequencies.

In each scenario with a fixed number of subsystems, the impedance matrix was computed for three different basis function assignments. In one configuration, the shortest wires, i.e. wires no 1, 4, 7, …, were used to define the common domains for halves of the roof-top basis functions (as the reference/common wires for the respective junctions). In the next tested configuration, wires with intermediate length, i.e. wires no 2, 5, 8, …, were used as the reference/common. In the 3rd assignment, the longest wires, i.e. wires no 3, 6, 9, …, were used as the reference/common.

The results of simulations are shown in Figure 3-4.

All plots in Figure 3-4 have a common feature. The condition number saturates as the size of the system increases. The only exception is observed at the frequency of 2.46 MHz. Around this frequency, a resonance is observed in each individual sub-system. The trend towards saturation is still present there, but is much less pronounced. The value of the condition number near the resonance is much higher than far outside of the resonance frequency.

This observation may help to explain the saturation of the condition number with linear growth of the system: When the second subsystem is added to the original one, these two subsystems start to interact, affecting current distribution in each other. As more subsystems are added, the new additions are spaced further apart from the original subsystem, and thus have less interaction with the original subsystem. In addition, the subsystems standing in-between may act as a screen. Thus, continuing to add new subsystems does not increase the complexity of interactions proportionally, resulting in saturation.

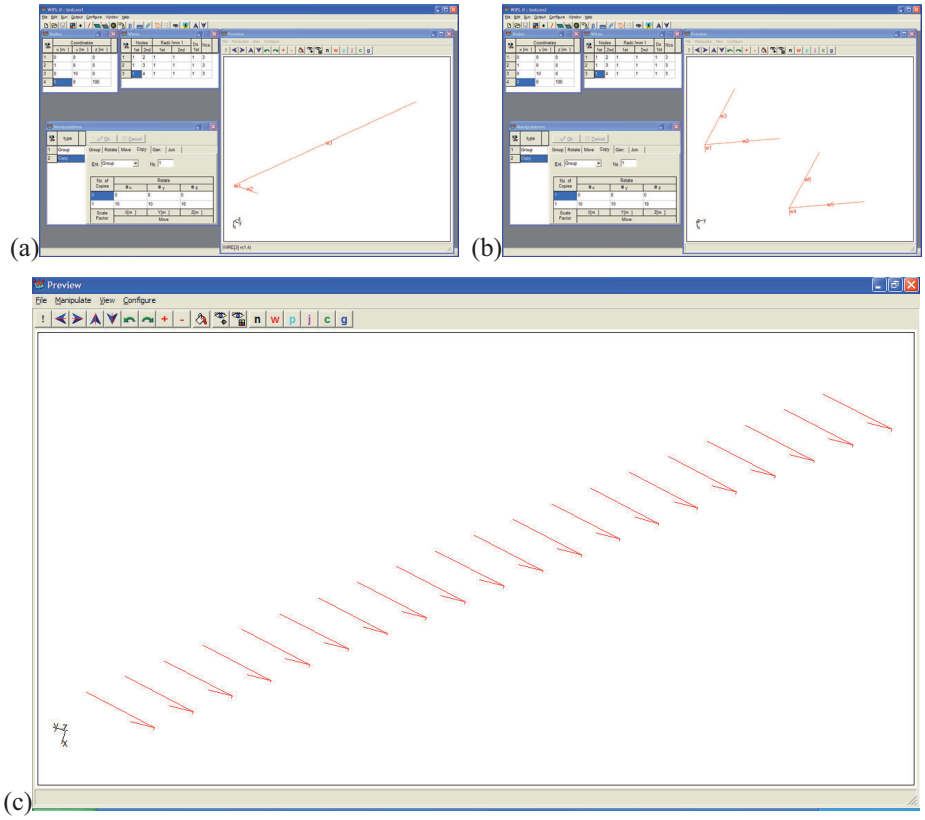

Figure 3-3. Stages of making a larger system out of a single junction with 3 wires. The print-screen in (a) shows the basic element – a junction with 3 wires attached (lengths 1 m, 10 m, and 100 m, all perpendicular to each other). Print-screens (b) and (c) show how the complexity was increased. There is one subsystem in (a), two subsystems in (b), and twenty subsystems in (c). The spacing between the subsystems is equidistant and equals (10 m, 10 m, 10 m) for the coordinates (x,y,z), respectively.

However, when resonance conditions occur (e.g. around the frequency 2.46 MHz), the interactions become more intense. In the system under consideration, most of coupling between subsystems is due to the longest wires that are parallel to each other. The distance between the wires is approximately $(10^2+10^2)^{1/2}$=14.1 m. This is close to one eighth of the wavelength λ, i.e. λ/8= 15.2 m, providing conditions to have strong interactions through long-distance couplings. It is assumed that the result is a tightly coupled large system with a high condition number, as illustrated in Figure 3-4b.

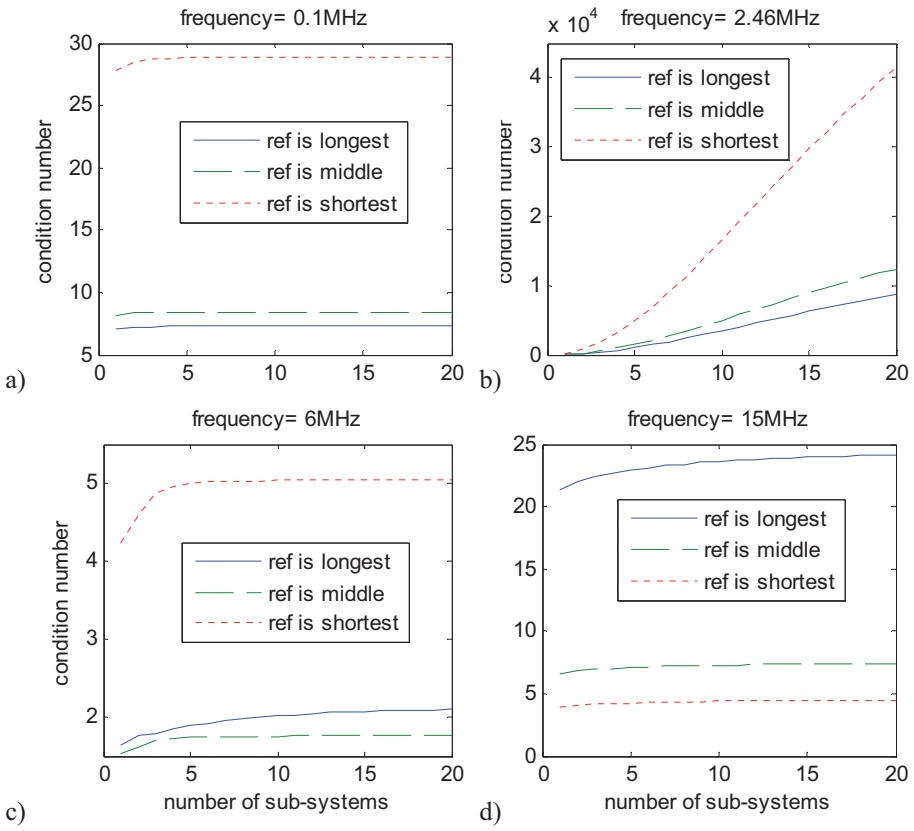

Figure 3-4. Condition number versus complexity of system, computed for different assignments of reference/common wires at respective junctions. The four plots display graphs for four different frequencies (from quasi-static to very high).

With regards to lowering the condition number, the results plotted in subplots of Figure 3-4 confirm the conclusions made in the previous sections: selecting the longest wire for the reference wire minimises the condition number at low frequencies. In a similar

manner, selecting the shortest wire as the common wire minimises the condition number at higher frequencies.

3.1.2.4 A Junction with Three Wires of Various Lengths

The geometry of the setup and the nature of investigation are similar to the one described in subsection 3.1.2.2, with the difference that the node assignment was fixed, and the lengths of wires were varied instead.

Many combinations of various lengths of wires were tried. The minimum length used was 0.01 m and the maximum length used was 100 m. Analysis of the condition number values confirmed the conclusion of the previous section. Under the quasi-static conditions, selecting the longest wire as the common wire should lead to the lowest condition number.

3.1.2.5 Three Wires Connected in Series, in a straight line

Project: *tstcond4*

This project was created to expand the case study to include a wider range of applications, where basis functions cover interconnected subsystems. The purpose was to confirm whether the same observations can be made as those mentioned in previous sub-sections (3.1.2.2-3.1.2.4).

Three wires were connected in series, as shown in Figure 3-5, and their lengths were varied.

Figure 3-5. Three Wires Connected in Series.

The results are shown in Table 3-5. The comparison of the condition number for different wire lengths confirms that, under quasi-static conditions, the longest wire should be selected as the common wire.

Table 3-5. Three Wires Connected in Series: Condition Number of Impedance Matrix for Various Lengths of Wires.

No.	Length of w1	Length of w2 (common)	Length of w3	Total length	Condition Number
1	50 m	50 m	50 m	150	2.854
2	50 m	100 m	50 m	200	**1.956**
3	100 m	50 m	100 m	250	4.704
4	100 m	100 m	100 m	300	2.936
5	50 m	100 m	200 m	350	3.371
6	100 m	200 m	100 m	400	**2.037**
7	200 m	100 m	200 m	500	5.101

In addition to the main conclusion, it is possible to make an additional observation. A comparison of experiments number 2 and 6, where the ratio of the lengths of the common wire to the side wires is the same, indicates that the condition number may grow with the total length of the structure. This is possibly due to the total length of the structure becoming closer to a resonance length.

3.1.2.6 Four Wires Connected in Series, in a straight line

In this test, a combination of three overlapping basis functions was modelled. The total length of wires is fixed to 200 m (that corresponds to the first resonance frequency of about 0.75 MHz). This permitted a direct comparison of the results in terms of the condition number.

The results are shown in Table 3-6. They generally confirm the conclusions made in Sections 3.1.2.2-3.1.2.5. However, it was also noted that when the ratios of wire lengths are very high or very low, those conclusions might become invalid as the condition number may become very large.

Note:

The current distribution on an electrically small dipole is of a triangular shape [Balanis, 5]. *Thus, a single rooftop basis function should be sufficient to model such a current distribution. In this example, three rooftop basis functions were used instead of one*.

When the ratio of the lengths of the elements becomes exceedingly large or small (e.g. 1:99 or 95:5), as may be seen in the marked rows in Table 3-6 (nrs. 7, 8, and 10), the

condition number grows. It becomes especially large when the two middle wires are very short (nrs. 7, 8). This is probably due to a high degree of similarity between the behaviour of current described by the respective basis functions. When the two middle wires are very short, these two basis functions become close to being linearly dependent on each other.

Note:

The distribution with short wires in the middle of a dipole (99,1,1,99) was also modelled with the usage of a symmetry plane (discussed later, in Section 3.5). This reduced the structure down to two wires with lengths of 1 m and 99 m. It was found that the condition number for this compact formulation, taking advantage of a perfect ground plane, is much smaller. For a resultant monopole, the condition number was equal to 56.3, as compared to 254 for a complete dipole.

Table 3-6. Four Wires Connected in Series: Condition Number of Impedance Matrix for Various Lengths of Wires. The total length of wires is 200 m. The best (lowest) and worst (highest) values of the condition number are shown in bold.

No.	Length of w_1	Length of w_2 (common #1)	Length of w_3 (common #2)	Length of w_4	Condition Number
1	50 m	50 m	50 m	50 m	5.379
2	25 m	75 m	75 m	25 m	**3.454**
3	75 m	25 m	25 m	75 m	12.61
4	75 m	25 m	75 m	25 m	7.676
5	25 m	100 m	25 m	50 m	6.628
6	50 m	100 m	25 m	25 m	5.754
7*	95 m	5 m	5 m	95 m	62.28
8*	99 m	1 m	1 m	99 m	**254.3**
9	5 m	95 m	95 m	5 m	8.395
10*	1 m	99 m	99 m	1 m	32.2

3.1.2.7 For various meshing of the wire

The tests that were run in this section address the influence of meshing (in the sense of positioning of nodes on a dipole's arm) on the condition number of the impedance matrix.

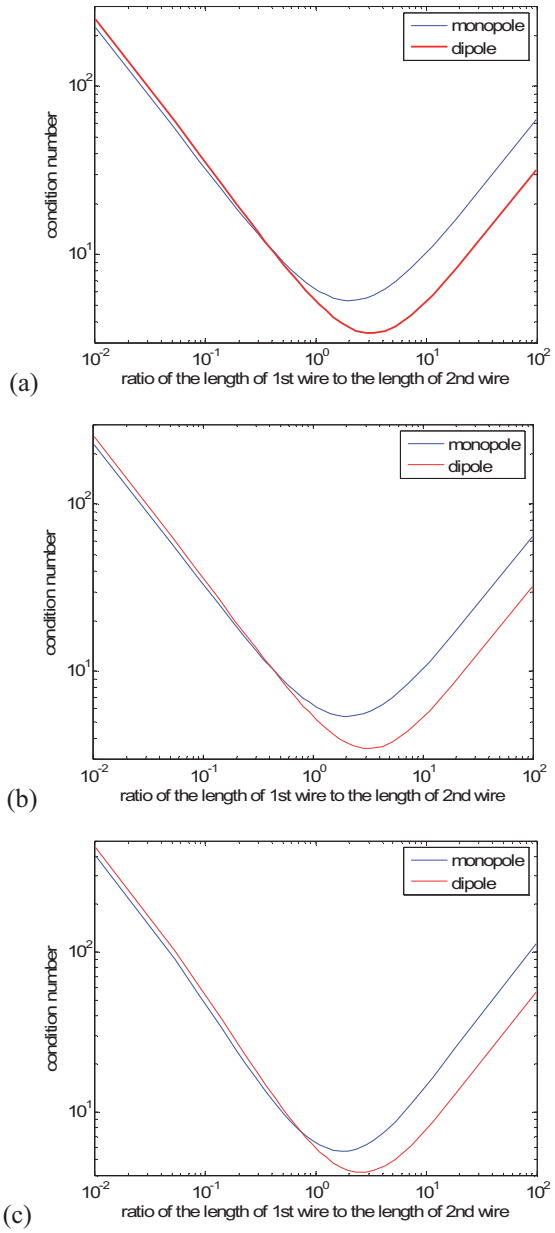

Figure 3-6. Four Wires Connected in Series: condition number versus ratio of length of wires. Two configurations: monopole and dipole. Frequency is below the first resonance (which is at around 0.75 MHz): (a) 0.01 MHz, (b) 0.1 MHz, and (c) just above the first resonance, 1 MHz.

A dipole with total length of 200 m was modelled with 4 wires (2 wires per dipole's arm) placed symmetrically with respect to the centre of the dipole. The ratio of the lengths of wires composing the dipole's arm was varied.

After that, a monopole with total length 100 m, placed on and perpendicular to a perfectly conducting ground plane was modelled. The ratio of the lengths of the 2 wires composing the monopole was varied.

The results of varying the ratio for these two models are depicted in Figure 3-6.

By analysing the plots, the following observations may be made:

a) There exist a minimum in the condition number with respect to the ratio of lengths of wires;

   Considering Figure 3-6a, in the case of a dipole, the minimum occurs when the wire attached to the generator is about 3 times longer than the wire with one end free. In the case of a monopole, this minimum is observed when the ratio is smaller, about 2 times. A similar situation is observed in Figure 3-6b,c.

b) The condition number at its minimum is higher for a monopole;

   Considering the picture Figure 3-6a, the value of the condition number around the minimum is about 3.5 for the dipole, and about 6 for the monopole. This difference is probably due to a higher chance of cancellation of terms in the impedance matrix of a monopole, where each element includes sub-impedances due to the direct waves and the waves reflected off the symmetry plane waves (refer to Section 3.5).

c) The position of the minimum changes with the frequency. It shifts towards a slightly lower ratio for a higher frequency;

d) The value of the condition number at the minimum shows a slight increase with an increase in the frequency;

   This effect may be attributed to the growth of the condition number around resonances.

e) Asymptotically, for very low and very high ratios of wire length, the condition number shows the same rate of growth for both dipole and monopole.

It may be added that more investigations are required to improve on completeness of the general picture. These investigations should include:

i) Higher ratios of wire lengths;

ii) Higher frequencies of analysis.

3.1.2.8 Conclusion

Following the results of investigation shown in Sections 3.1.2.1-3.1.2.7, it is observed that, under quasi-static conditions, there exist a minimum in the condition number (as a function of the ratio of wire lengths). Outside the vicinity of this minimum, the condition number grows.

Note:

In order to reduce the possibility of an unnecessarily high condition number, it should be possible to sub-divide the long wires into shorter ones, or to unite the short and long segments into longer equivalent wires (termed chains, as discussed later, in Chapter 4).

3.1.3 A Junction of Six Orthogonal Wires - On Frequency Dependence

The geometry of the project is shown in Figure 3-7[19]. The structure is composed of 6 wires that were chosen to be aligned with the axes of the Cartesian coordinate system. Presence of many wires makes the radiator more complex, but also gives more degrees of freedom to explore. In particular, this subsection deals with the frequency dependence of the choice minimising the condition number. As it will be shown in the

[19] The figure displays the structure with WIPL-D. It may need to be highlighted that the WIPL-D was used to merely display the geometrical dataset and also to validate the currents produced by the Matlab code. Unfortunately, WIPL-D could not be used to calculate the condition number directly.

below, the six wires define five distinct frequency regions. Each frequency region has its own optimum choice of the reference wire, minimising the condition number.

3.1.3.1 Preparatory Work

In the first step, the frequency range to be considered for investigating this system is studied to identify the boundaries of applicability of the resonance effects. The 6 wires may be considered in pairs. Approximating the complete complex system with a set of independent dipoles will bring about a set of resonance frequencies for the respective dipoles. Under an assumption of a weak coupling between the dipoles, the resonance frequencies from the set of independent dipoles should not differ much from the true natural frequencies.

With the binomial coefficient [Råde, 93], it is possible to compute that there are $\frac{6!}{2!(6-2)!}=15$ unique combinations, where each combination includes 2 wires. Each pair may be considered as a dipole. This gives a list of 15 resonance frequencies, from 30 MHz (due to the longest combination: 3m+2m=5m => wavelength λ=10m, and frequency 30 MHz) to 257.16 MHz (due to the shortest combination: 0.25m+0.3333m => wavelength λ=1.167m, and frequency 257.16 MHz). The combinations of the six arm lengths (3m, 2m, 1m, 0.5m, 0.3333m, 0.25m) form the list of 15 unique resonant frequencies shown in Table 3-7.

Table 3-7. List of values of resonant frequencies (in MHz) obtained with a simplified model considering isolated pairs and disregarding coupling.

30, 37.5, 42.9, 45, 46.15, 50, 60, 64.3, 66.7, 100, 112.5, 120, 180, 200, 257.2

When inspecting the frequencies listed in Table 3-7, one should keep in mind that these estimates were obtained with disregard for coupling and thus should be used as indicators of the frequency range rather than exact values for the resonance frequencies.

In the next step, the system shown in Figure 3-7 was simulated using the MoM code. Figure 3-8 shows the susceptance at each port[20] as a function of frequency. It is possible to see that the actual resonance frequencies[21] are not the same as the values shown in Table 3-7 (where a simplified approach assuming an absence of coupling was used) and shown in Figure 3-8 with dots. The actual values, where *Im*(Y)=0, are slightly different. This effect may be explained by considering a pair of wires as a dipole, whilst the remaining wires are then considered as an equivalent load. Depending on the electrical dimensions of the load (i.e. electrical lengths of attached wires), it may have an inductive or capacitate nature, and also add radiation losses. This introduces respective positive or negative shift in the imaginary part of admittance, and thus in the resonance frequency. For example, the admittance Y_{11} in Figure 3-8 has a positive shift at low frequencies and a negative shift at high frequencies.

It may also be noted in Figure 3-8 that there is resonance-like behaviour in the curves but the susceptance does not really cross zero. This is attributed to the non-zero capacitance at the positions of the delta-gap generators (since the wire radius there is a finite value of 1 mm).

In general, as shown in Figure 3-8, the resonance behaviour for self-impedances is concentrated in the frequency range of about 20 to 300 MHz.

Note:

It is also possible to see that there are a finite number of resonances reflected in the results of simulations. This is attributed to the restrictions imposed by using the doublet basis functions (i.e. piecewise linear basis functions), an approximation that is only suitable at low frequencies.

[20] The admittance is calculated when the rest of the ports are shortened (as per definition of the network admittance matrix parameters [Pozar, 90]). The location and definition of ports may be found in sub-window *Generators* in Figure 3-7.

[21] A *resonance frequency* is defined here as per the condition of crossing the zero reactance line, i.e. *Im*(Y)=0.

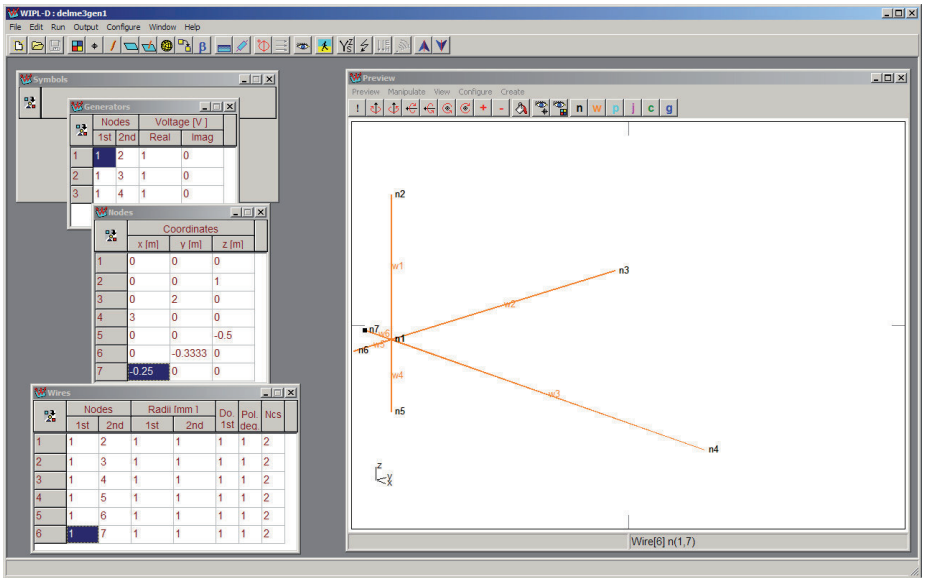

Figure 3-7. Geometry of the project. The details of the geometry, such as definitions for nodes, wires and generators, may be read off this print-screen. The geometry definition is shown with WIPL-D for 2 reasons: (a) WIPL-D was used to validate the solutions (complex current amplitudes) obtained, and (b) this presentation permitted saving paper by displaying all the relevant geometry-defining information on one screen.

3.1.3.2 On Condition Number

In order to expand the numerical analysis from quasi-static frequencies (Section 3.1.2) onto a more general situation, the structure shown in Figure 3-7 was simulated at a sufficiently wide range of frequencies. The range of discrete frequencies was chosen to include all the resonances found in the previous subsection. All wires were tested to serve as the reference/common wire at each of the discrete frequencies. A sample of the results is shown in Table 3-8.

At each frequency, one particular choice of the reference wire provides an optimal (minimal) value of the condition number. In Table 3-8, these values are shown in bold.

It is easy to see from the table that the optimal choice of a reference wire is frequency-dependent.

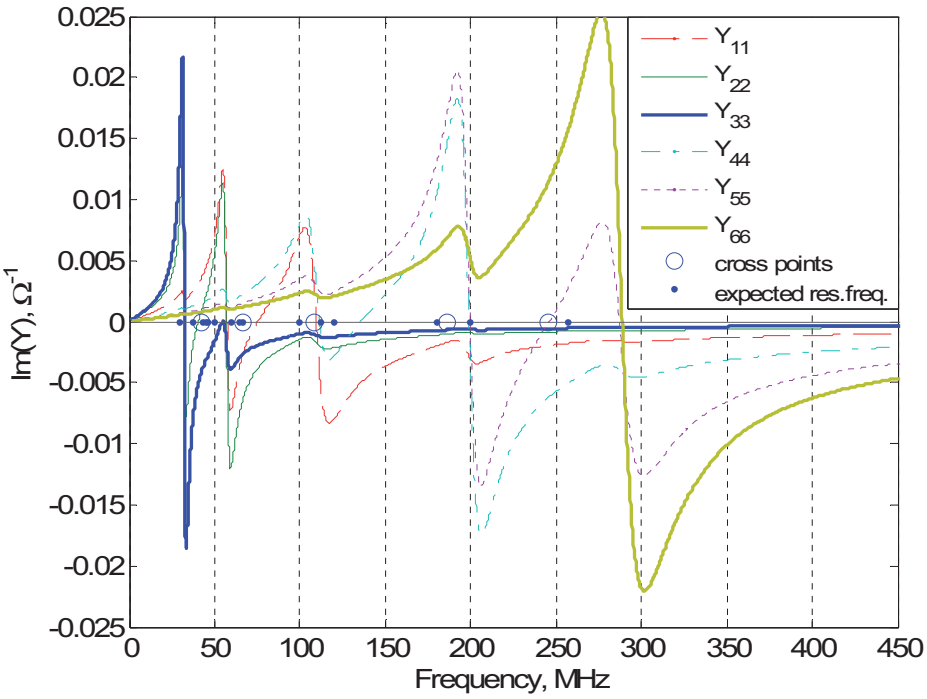

Figure 3-8. Susceptance plot for the geometry defined in Figure 3-7. Six susceptances are shown, as well as the expected positions of the resonances (denoted with dots), and the cross-over frequencies (related to the condition number and optimum selection of wire; see the definition on page 80; in this figure they are denoted with circles).

At any individual frequency, it is possible to introduce the ratio of a maximum found value of the condition number, denoted as *max*(*cond*) in Table 3-8, to its lowest found value, denoted in Table 3-8 as *min*(*cond*). This ratio may be considered as reflecting either (a) an improvement in accuracy of the obtained solution or (b) a permissible relaxation in the tolerance required when computing impedance matrix integrals. In either case, the ratio may be referred to as the *condition number gain*.

In Table 3-8, the best available condition number gain, resulting from the optimum selection of the reference wire, is denoted with "max(cond)/min(cond)". In the example under consideration, the best available condition number gain ranges from 5.1 to 12.4. This is equivalent to an order of magnitude of improvement when modelling the system shown in Figure 3-7.

Table 3-8. Condition number of impedance matrix versus frequency and reference wire number. Values shown in bold indicate the minimum condition number per selected frequency (per column). The two bottom rows are intended to trace the potential gain from avoiding circumstances leading to a high condition number. The *cond* there stands for the condition number of the impedance matrix. It gets different values depending on which wire was chosen to be the reference wire.

Frequency, MHz	1	10	30	50	100	150	345	500	1500
λ, m Ref. wire no.	300	30	10	6	3	2	0.87	0.6	0.2
#3 (3m)	**7.16**	**7.24**	**19.8**	14.1	70.6	54.3	199	88.5	58.7
#2 (2m)	9.11	9.67	42.1	**8.14**	43	36.3	138	61.9	41
#1 (1m)	14.9	16.3	90.9	16	**9.13**	17	77.4	35.3	23.8
#4 (0.5m)	22.2	24.4	145	45.1	13.1	**5.92**	47.4	22.5	15.6
#5 (0.3333m)	29.4	32.4	196	64.0	31.7	**6.68**	30.5	15.5	11.4
#6 (0.25m)	36.6	40.3	246	81.8	45.2	11.1	**17.1**	**10.7**	**8.96**
max(cond)/min(cond)	5.1	5.6	12.4	10.0	7.7	9.2	11.6	8.3	6.6
max(cond)/$cond_{1m}$	2.5	2.5	2.7	5.1	7.7	3.2	2.6	2.5	2.5

Note:

A criterion for selecting the reference wire that would provide an optimal choice may be computationally too costly to realise. This is because it may require a simulation for each junction with wires as many times as there are wires at that junction.

The goal of this investigation is to find a way to take sufficient advantage of the ability to select any wire as the common domain for the doublets on a junction. It is assumed that the most important is to prohibit the condition number to grow too large (i.e. minimizing the maximum condition number). This is instead of trying to find the true optimum (lowest possible value of condition number). For instance, a sub-optimum choice may be based on selecting the reference wire whose length is the closest to an

average[22] *length of all wires. In this example, it is wire #1, whose length is 1 m. In Table 3-8, the row denoted with "max(cond)/cond$_{1m}$" shows the resulting respective condition number gain. Although it is mostly lower than the best available condition number gain, it is clear that this very much simplified and computationally inexpensive approach still provides a substantial advantage over a random selection of the reference wire.*

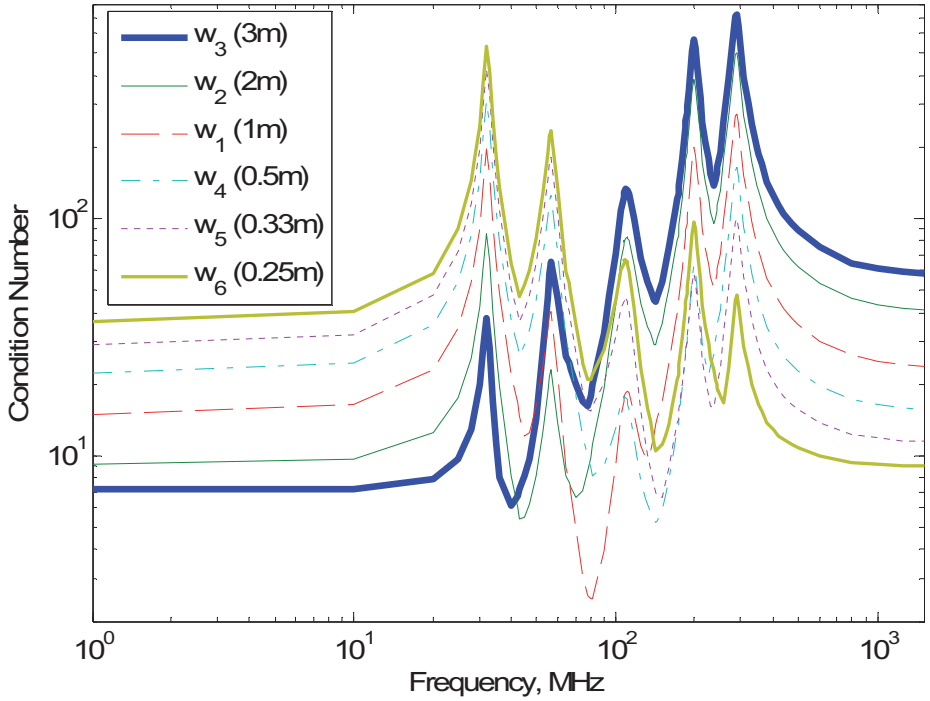

Figure 3-9. Condition number versus Frequency for various choices of reference wire (shown in legend) in project "A Junction of Six Orthogonal Wires".

The preliminary results shown in the discussion above provide a valuable insight into some of the possibilities opened by a systematic selection of the reference wire. In the

[22] The choice of averaging is a separate topic for an investigation. In this example, the arithmetic and geometric averages [Råde, 93] were considered, where the arithmetic average of lengths of all wires is 1.18 m, and the geometric average of the same is 0.79 m. Thus both these averages lead to the same choice of reference wire.

expectation of finding more about the behaviour of the condition number, a more detailed investigation (with more frequency points) was made. The description follows.

Some of the results are shown in Figure 3-9. Also, a comparison of Figure 3-9 against Figure 3-8 indicates that the condition number grows around resonances.

In Figure 3-9, one may observe that there exists a lower bound on the condition number. At low frequencies, this bound corresponds to the wire number 3 (the longest wire) chosen as the reference wire. Then, between approximately 41.5 MHz and 66.5 MHz, selecting the wire number 2 as the common wire gives the lowest possible condition number. This is followed by the range 66.5 MHz to 107.5 MHz, where wire number 1, if selected as the reference wire, gives the lowest value of the condition number. This sequence of selecting the different wires for different frequency ranges may be continued.

Table 3-9. Frequencies at which the common wire has to be changed to minimise the condition number. The arrows in the last column refer to sweeping the frequency from lower toward higher frequencies.

Frequency, MHz	Wavelength, m	Minimum Condition number (with respect to different wires).	Length of the wire attributed to the min condition number
42	7.14	6	3 m $\rightarrow$ 2 m
67	4.48	6.82	2 m $\rightarrow$ 1 m
108	2.78	17.7	1 m $\rightarrow$ 0.5 m
186	1.61	28.03	0.5 m $\rightarrow$ 0.3333 m
245	1.22	19.2	0.3333 m $\rightarrow$ 0.25 m

The values of frequencies where the reference wire should be changed to keep the condition number minimal are shown in Table 3-9. Hereinafter, these values are referred to as *cross-over frequencies*.

Note:

As an observation, it is possible to note from the admittance plot in Figure 3-8 that the positions of the cross-over points are at the frequencies where all curves follow the

same trend (e.g. all have positive slope). An explanation to this has not been found, as yet.

Figure 3-10a shows where in the frequency domain each wire is to be selected to minimise the condition number. This selection provides the highest condition number gain, as may be seen in Figure 3-10b. Analysis of this curve tells that a proper selection of the reference wire may reduce the condition number in this example by a factor of up to 5 to 20. Such reduction in the condition number may help to relax the required accuracy for computing the impedance matrix elements by an order of magnitude.

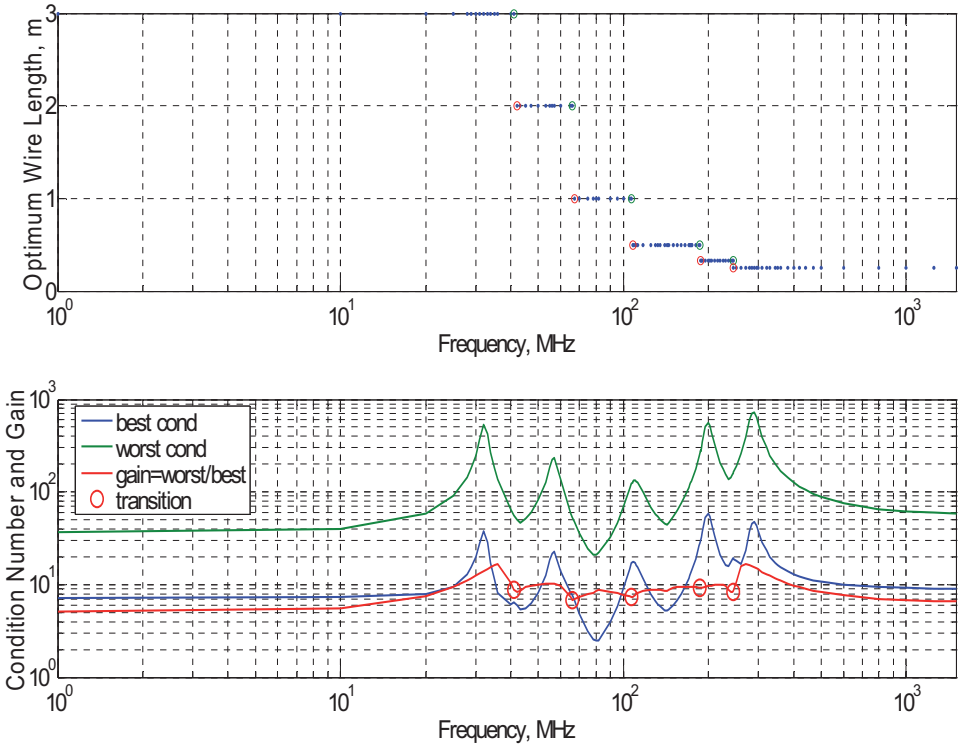

Figure 3-10. (a) Optimum wire length and (b) Condition number and condition number gain versus frequency for the model "A Junction of Six Orthogonal Wires". Plot (a) displays the selection of reference wire length leading to a minimal value of the condition number. Plot (b) shows the respective lowest (*best cond*) and highest (*worst cond*) values of condition number, as well as an inverse of their ratio, referred to as the condition number gain (*gain*). The circles (*transition*) on the gain curve indicate the points where the choice of reference wire is not unique, i.e. one of two wires may be selected to give the same condition number.

The transition points in Figure 3-10 are all in the vicinity of the local minimums of the condition number gain curve. This is probably because at a cross-point no wire is optimal in the sense of the condition number reduction.

An additional insight may be gained by considering the distribution of the impedance matrix condition number as a function of frequency (wavelength) and wire lengths, shown in Figure 3-11. At some frequencies (see, for example, the wavelength of 2 m), the choice of the reference wire does not play a significant role in the value of the condition number, except, perhaps, for the border (maximum or minimum) wire lengths. On the other hand, it is possible to see that, at some other frequencies, the value of condition number is especially high except for the choice of one "optimal" reference wire. An example to this may be seen around the wavelength of 10 m.

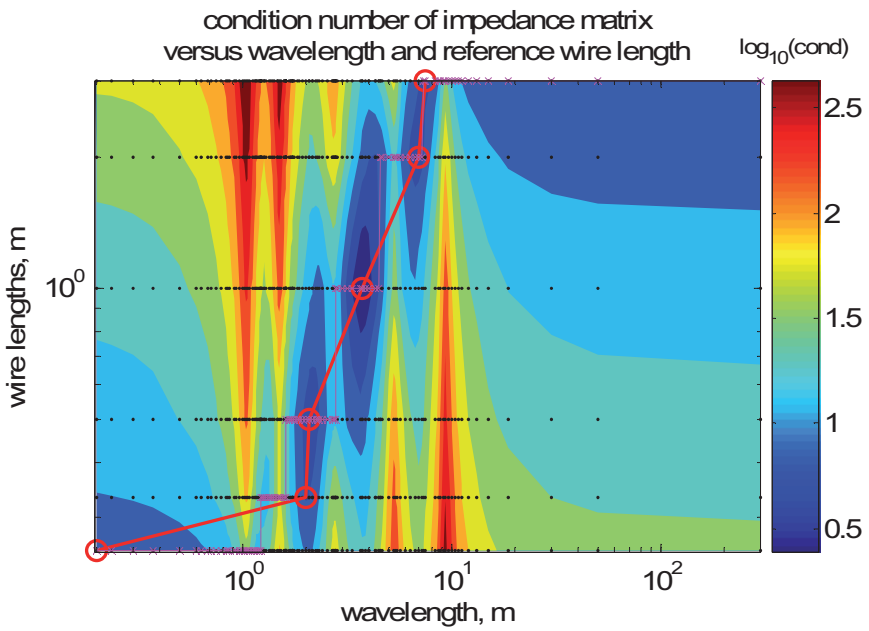

Figure 3-11. Distribution of the condition number of impedance matrix against wavelength and the length of common/reference wire. Dots indicate the discrete positions at which a model was run. Circles ○ joined with a red line show at which wavelength (frequency) the condition number is minimal for each wire. Crosses × joined with a magenta line show the selection of the reference wire that minimises the condition number, at each wavelength (frequency). Project: "A Junction of Six Orthogonal Wires".

It is thus possible that an empirical sub-optimal criterion for selecting a reference wire is to, rather, minimise the condition number at around those frequencies where the condition number is particularly high.

With this in mind, a set of points was collected from the data represented in Figure 3-11. These points are listed in Table 3-10.

Table 3-10. Approximate values for points corresponding to the lowest condition number at the frequencies (wavelengths) with the highest average condition number. Model: "A Junction of Six Orthogonal Wires".

Point No.	Wavelength, m	Optimal wire length, m
1	5.26	**2**
2	2.8	0.75
3	1.5	0.33

A linear fit through these points gives the equation to calculate the desired length of reference wire L_{opt} as a function of wavelength λ:

$$L_{opt}(\lambda) = 0.45 \cdot \lambda - 0.41. \quad (3.1)$$

3.1.4 Practical Notes

1. The ratio of the length of this wire to the length of the shortest wire must not be too high (as per Section 3.1.2.6).

2. It is also possible to select a wire whose length is the next higher value to the average length of the wires attached to the node. This choice is not optimal, but still avoids the highest values of the condition number.

3. This section does not deal with the angle at which the selected reference wire is against the other wires. A numerical modelling has shown that this may affect the e in section 3.1selection criteria. However, this requires a significant investment of additional effort since this adds a series of degrees of freedom in terms of a numerical approach, and is left for another stage of research.

4. Another model was made, where the long wires were made longer, and the short wires were made shorter. The range of wire lengths in the structure (i.e the ratio of maximum length to minimum length) was increased from 4 to 100. The distribution and

geometrical mean of all the wire lengths remained approximately the same. This model resulted in the linear-fit equation

$$L_{opt}(\lambda) = 0.5 \cdot \lambda - 0.47. \quad (3.2)$$

Comparing this equation with the equation (3.1) obtained earlier, it is possible to observe that coefficients, i.e. slope and intercept, are very close.

It should however be noted that more studies are required to see whether this equation would hold for the scenarios where the distribution of wire lengths is centred near shorter or longer lengths, and the angles between wires is not straight.

5. It is also possible to make a compromise solution, where the equation (3.2) is used to identify two or three possible test configurations for each junction. These configurations may then be tested and the best configuration selected. The elements of the impedance matrices computed for each individual junction may be reused in filling in the impedance matrix for the complete system.

3.2 Impedance Matrix Evaluation

This section deals with calculation of impedance matrix elements, i.e. the integrals derived in the previous chapter, and ways to improve accuracy and to speed this process up. This includes enhancing the performance by extraction of singularities in the integrand of the impedance matrix element, and by consideration of symmetries and repetitions.

3.2.1 Introduction

Calculation of impedance matrix elements[23] is an important topic that has received attention since the origins of the method of moments. As shown in Section 3.8, the accuracy of these calculations affects the accuracy of the final result, the currents. The required calculations involve integration of a product of complex Green's function and

[23] The expressions for these elements, specific to the implemented realisation of the MoM, may be found in Section 2.14.

basis functions. Under general conditions, an exact analytical evaluation is not possible due to the complexity of the integrand. A numerical quadrature, enhanced with analytical manipulations, is usually used instead. The need in preparing the integrand is due to singularity of the integrand. The denominator of the Green's function, proportional to the distance between the source and field points, may become very small, on the order of wire's radius. This phenomenon always occurs when the so-called self-impedance terms[24] of the impedance matrix are computed.

In order to produce accurate results efficiently, a numerical quadrature requires a smooth integrand. The described near-singular behaviour of the Green's function forces to use a very high number of integration points around the singularity. This leads to an excessively high number of calculations involving the complex Green's function, rendering the numerical quadratures in their direct/pure form inefficient.

In order to improve the computational efficiency, a number of methods may be used. These include polar coordinate transformation [Schwab and Wendland, 100], Duffy's method [Duffy, 20], and singularity extraction method (sometimes also called singularity subtraction) [Wilton D.R., et al., 111], [Caorsi et al., 9], [Järvenpää et al., 34], [Kolundzija, 51].

In this work, a simple variation of the singularity subtraction technique partially based on [Kolundzija, 51] is realised. The impedance matrix elements are calculated in accordance with the results of derivations from Section 2.14. The integrals due to electric potential V and vector potential $\mathbf{A}$ are treated separately, in accordance to the different degree of singularity they pose. The integral due to the scalar electric potential is decomposed into several terms, as shown in subsection 3.2.3. The terms involving integration are then treated using a singularity subtraction technique.

[24] This refers to the terms on the main diagonal of the impedance matrix. The effect may also take place when calculating impedance matrix elements that reflect coupling between joined wires.

3.2.2 Integrals Due to Vector Potential **A**

The impedance matrix elements' integrals due to the vector potential **A** are calculated directly, using a low-order adaptive Simpson quadrature [Matlab, 69], [Press et al.,92]. The adaptive lower-order Simpson quadrature was found to be more efficient in treating the singular behaviour of the Green's function, as compared to a higher-order adaptive Gauss-Lobatto quadrature. This is due to the oscillatory behaviour of and singularity in the integrand, making a less sophisticated Simpson quadrature more efficient than the Gauss-Lobatto procedure.

3.2.3 Integrals Due to Electric Potential V

The decomposition discussed through the formulas (3.3)-(3-5) follows the paper [Kolundzija, ???].

It is possible to recall that the partial sub-impedances due to the scalar electric potential in (2.73), (2.77) and (2.79) may be expressed with (2.14) as

$$Z_{jp}^{V} = \int_{s_1^{(j)}}^{s_2^{(j)}} f_j(s') \left(\vec{u}_z^{(j)} \cdot \mathrm{grad}' V_p \right) ds', \tag{3.3}$$

where the inner integrals have been replaced by the gradient of the electric scalar potential along the generatrix of the conical wire, $V_p(s)$. The gradient in the integrand increases the order of singularity and makes the application of a numerical quadrature highly inefficient. This integral may however be integrated by parts. The resulting expression is

$$Z_{jp}^{V} = -\frac{1}{\cos\alpha^{(p)}} \left(f_j V_p \Big|_{s_1^{(j)}}^{s_2^{(j)}} - \int_{s_1^{(j)}}^{s_2^{(j)}} \frac{df_j(s')}{ds'} V_p(s') ds' \right), \tag{3.4}$$

One of the two terms $f_j V_p$ is zero, as the node basis function is zero at one of the ends.

For singletons, the function f_j is zero at the both ends, so the expression may be simplified further:

$$Z_{jp}^{V} = +\frac{1}{\cos\alpha^{(p)}} \int_{s_1^{(j)}}^{s_2^{(j)}} \frac{df_j(s')}{ds'} V_p(s') ds' \tag{3-5}$$

Note:

It is also possible to note that the derivative of the basis function is a constant for a piecewise linear basis function. This constant can be taken outside of the integration sign, saving on additional multiplications.

3.2.4 On Singularity Subtraction

The integrands in those elements of the impedance matrix for wire problems that require a double integration over the same element and also those that require integration of adjacent elements, may display a near-singular behaviour. The singularity of the integrand may be removed or reduced, as shown below, softening the requirements on the number of points required by a quadrature. The so-called singularity subtraction technique may be described as follows.

The complex exponent in the numerator of the Green's function **(2.16)** may be considered as having two terms: $\frac{\mathrm{e}^{-jkR}}{R} = \frac{\cos(kR)}{R} + j\frac{\sin(kR)}{R}$. The second term is a smooth function, and does not require a specialised treatment besides a Maclaurin expansion in the vicinity of R=0. The first term has a non-removable singularity at R=0 and has near-singular behaviour in the vicinity of this point.

The core of the singularity subtraction method is in subtracting the first N_t+1 terms of the Taylor expansion of the exponential function from the numerator of the Green's function, and working with them separately. This is shown in the following expansion:

$$\frac{e^{-jkR}}{R} = \frac{e^{-jkR} - P_e^{N_t}(jkR) + P_e^{N_t}(jkR)}{R} = \frac{e^{-jkR} - P_e^{N_t}(jkR)}{R} + \frac{P_e^{N_t}(jkR)}{R} \tag{3.6}$$

where $P_e^{N_t}(jkR) = 1 + jkR + \frac{1}{2!}(jkR)^2 + \frac{1}{3!}(jkR)^3 + \ldots + \frac{1}{N_t!}(jkR)^{N_t}$ is a series expansion of the exponential function in the numerator of the Green's function, truncated to N_t+1 terms.

The integral may then be split into two integrals, corresponding to the two terms in the expression (3.6). The first integral is computed using an adaptive quadrature, whilst the second integral is computed analytically using the technique developed in [Kolundzija, 51]. It must however be noted that the above-mentioned analytical techniques [Kolundzija, 51] apply only to the wires of constant radius.

Through numerical experiments, it was noticed that N_s=3 smoothes the integrand sufficiently to apply a numerical quadrature efficiently.

3.2.5 Impedance Matrix Symmetry Considerations

The impedance matrix filling time can be reduced by taking into account the symmetry of the matrix (*condition to all the wires, i.e. cones, to have the same opening angle*). For the doublets, as per notations of Section 2.14, this symmetry can be expressed as

$$Z_{jp}^{DD} = Z_{pj}^{DD} \tag{3-7}$$

This results is saving on filling of nearly a half of the matrix (for a large number of unknowns N). The new number of elements to be calculated is $N(N+1)/2 \cong N^2/2$, $N \to \infty$. This new number of unknowns is twice smaller in comparison to the original total number of matrix elements, N^2.

3.2.6 Repeating Elements

Junctions of multiple wires (with more than two wires joining such a junction) give a possibility to save on computation of the "reference" elements $Z_{jp}^{N_j^1 N_p^1}$, as these are common for all the doublet basis functions at that junction.

Compared with the symmetry discussed in 3.2.5, for most practical situations (when there are not many junctions with multiple wires), this feature will not provide a significant advantage. However, this kind of optimisation is nevertheless applicable for arbitrary wire structures. In a few situations where many wires are joined at a single point (e.g. to form an approximation for a finite size ground plane), it may give a noticeable time saving. This is especially so if the domain of reference wire is related to

a self-impedance term[25]. For these reasons, this approach has not been implemented in the program.

3.2.7 Usage of Memoization for accelerated Filling in the Impedance Matrix

A special technique based on the memoization [Lysko, 61, 62] was invented in order to accelerate the process of filling in the impedance matrix, when the geometrical structure is regular in terms of its element. This speeded the process by a factor of up to 5 (although a further optimization of the code is planned, which shall permit to increase the speed even more). The technique is restricted to structures having multiple repeating geometrical elements.

The references [Lysko, 61, 62] give a general overview of the method devised.

3.3 Source Model: Delta-Function Generator

This section deals with the treatment of the sources and formation of the excitation vector.

A delta-function generator is an infinitesimal ideal voltage generator [Balanis, 5] and is perhaps the simplest and most frequently used model available for an excitation.

A delta-generator source is placed between two wires, as shown in Figure 3-12. It is assumed that the field due to this generator is uniformly distributed between the ends of the two wires. It is furthermore assumed that the excitation voltage V is at the feed terminals only, and zero elsewhere. Since both the distance and voltage between the terminals are constant, the electric field between them is constant as well. This

[25] As it has been mentioned earlier, the self-coupling terms ($Z^{N_j^k N_p^m}\Big|_{j=p,\,k=m}$) of impedance matrix elements are numerically difficult (time-consuming) to compute due to rapid variation in the free-space Green's function, as the source point approaches the field point. This variation usually makes the numerical integration inefficient. The common term in doublets due to a junction has $k = m = 1$.

approximation works best where the physical gap between the physical wires is small [Balanis, 4].

A delta-function generator may be characterised by a generator complex voltage V, its geometrical position $\vec{r}_0$ (relative to the field point $\vec{r}$), and by its direction specified with the unit vector $\vec{u}^{inc}$:

$$\vec{E}^{inc}(\vec{r}) = \vec{u}^{inc}\, V\, \delta(\vec{r} - \vec{r}_0) \tag{3-8}$$

In a local coordinate system, the look of the formula is simplified:

$$\vec{E}^{inc}(s) = \vec{u}^{inc}\, V\, \delta(s - s_0) \tag{3-9}$$

Consider the case when the delta-generator is placed at a junction node of two wires, shown in Figure 3-12. The junction is assumed to have an infinitesimally small gap between the wire ends (caps).

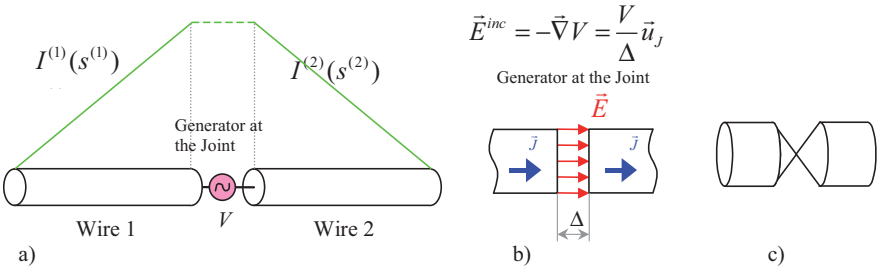

Figure 3-12 Delta-generator at a junction of two wires. (a) Its positioning, and example of current distribution on the arms of a dipole. (b) Electric field produced. Red thin arrows show direction of the electric field in the gap. Thick blue arrows show the direction of the current in the wires. The vertical dimension, i.e. the width of the conductor at the gap is enlarged for clarity of the view. (c) Configuration minimising the gap capacitance with zero-width gap.

Note:

An important note for practical usage of such a model is that bringing two wire ends of finite area Figure 3-12b so close forces the capacitance between them to be exceedingly large. This creates a large imaginary component of current and leads to numerical problems and a large reactive value of the input impedance. A fine mesh near the gap permits more current fluctuations [Popovic et al., 89] and thus may worsen the problem. A better model of applying the delta generator [Kolundzija, 46, Sec.7.2.1]

includes conical ends for the wire ends attached to the joint (shown in Figure 3-12c), as to eliminate the large gap capacitance. This also suggests an especially rough meshing near the delta gap generator. Otherwise, only low-order basis functions must be used there.

Applying the testing procedure with doublet basis function $D^{(i,k)}$ in the form (2.47) brings out the following integral

$$U_j^{src} = -\left(\int_{s_1^{(j)(k)}}^{s_2^{(j)(k)}} \vec{u}^{(j)(k)} N_{d_2^{(j)(k)}} \vec{E}^{inc}\, ds - d_0^{(k)} d_0^{(i)} \int_{s_1^{(j)(i)}}^{s_2^{(j)(i)}} \vec{u}^{(j)(i)} N_{d_2^{(j)(i)}} \vec{E}^{inc}\, ds \right) \qquad (3\text{-}10)$$

To simplify the integration, the delta-function may be considered as a limiting case of a rectangular window function defined by

$$\delta(x) = \begin{cases} \lim_{\Delta \to 0} \frac{1}{\Delta}, & -\frac{1}{2}\Delta \le x \le \frac{1}{2}\Delta \\ 0, & otherwise \end{cases} \qquad (3\text{-}11)$$

Performing the test procedure integration (illustrated by Figure 3-13) separates each of the integrals in (3-10) into two (with one of them vanishing). The integral over a wire attached to the joint by its end reduces[26] to

[26] Notations used in this section: (a) the multiplication of the vectors is in the sense of the dot product; (b) the functions N_1 and N_2 in the brackets show two possible singlet functions used to approximate current, and only one of them is used per integral. The other approach may be based on a consideration of a monopole antenna on a ground plane. Then the generator should rather be specified as inserted between one specified wire and the joint connecting the other wires (here, ground plane). Such a set-up has a clear physical interpretation and should still be equivalent to the set-up discussed previously, as the generator is still defined at a point, in a quasi-static sense. Mathematically this translates into shifting the delta-function's centre off the joint point. Now, an edge of the rectangle describing the asymptotically defined delta-function (3-11) is at the junction. This is shown in Figure 3-14.

$$\int_{s_1}^{s_2} \vec{u} \begin{pmatrix} -N_1 \\ +N_2 \end{pmatrix} \vec{E}^{inc}\, ds = \lim_{\Delta \to 0} \left(\cancel{\int_{s_1}^{s_2 - \Delta/2} \vec{u} \begin{pmatrix} -N_1 \\ +N_2 \end{pmatrix} \vec{E}^{inc}\, ds} + \int_{s_2 - \Delta/2}^{s_2} \vec{u} \begin{pmatrix} -N_1 \\ +N_2 \end{pmatrix} \vec{E}^{inc}\, ds \right) = \begin{pmatrix} \vec{u}\vec{u}^{inc} V/2 \\ 0 \end{pmatrix},$$

and the integral over a wire attached to the joint by the beginning gives a similar answer

$$\int_{s_1}^{s_2} \vec{u} \begin{pmatrix} -N_1 \\ +N_2 \end{pmatrix} \vec{E}^{inc}\, ds = \lim_{\Delta \to 0} \left(\int_{s_1}^{s_1 + \Delta/2} \vec{u} \begin{pmatrix} -N_1 \\ +N_2 \end{pmatrix} \vec{E}^{inc}\, ds + \cancel{\int_{s_1 + \Delta/2}^{s_2} \vec{u} \begin{pmatrix} -N_1 \\ +N_2 \end{pmatrix} \vec{E}^{inc}\, ds} \right) = \begin{pmatrix} 0 \\ \vec{u}\vec{u}^{inc} V/2 \end{pmatrix}$$

Zeros in the answers are due to basis functions N_{d_2} approaching zero at the respective ends. In the formulas above, the minus sign in front of the function N_1 was taken, since it originates from the expansion (2.40).

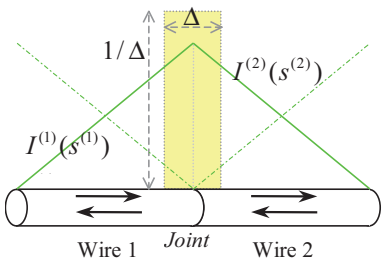

Figure 3-13. Delta-function integration at a junction of two wires. The unit area taken by the delta-function is greyed out. The nodal basis functions giving a finite value after integration are profiled with solid green lines, while the ones vanishing are dash-dot green lines. Not shown: the beginning of each wire can be denoted with s_1, and the end is denoted with s_2. The superscript refers to the wire number.

Combining the results gives the following expression for the voltage column-vector element corresponding to the doublet basis function for the junction with generator:

$$U_j^{src} = -\left(\frac{\mathrm{V}}{2} \vec{u}^{inc} \cdot \vec{u}^{(j)(k)} - d_0^{(j)(k)} d_0^{(j)(1)} \frac{\mathrm{V}}{2} \vec{u}^{inc} \cdot \vec{u}^{(j)(1)} \right) \qquad (3\text{-}12)$$

The other doublet basis functions will give zeros, as they "touch" the generator junction by the vanishing ends of their node basis functions. When applied to the singleton basis functions, this method also gives zeros, as the singletons equal zero at the wire ends. Therefore, all the other elements of the voltage vector are zero.

The formula (3-12) may be interpreted as splitting the generator between the two wires that a doublet basis function is based upon. It has a straightforward interpretation for a junction of two aligned wires. However, if the wires are not on the same axis (e.g. angle between them is 90 degrees), the definition of the excitation unit vector $\vec{u}^{inc}$ must be refined; otherwise the generator will not be able to function as an ideal voltage generator supplying full voltage V between the two terminals (wires).

In an artificial attempt to remedy this problem, this unit vector should then be split into two vectors, the first, $\vec{u}^{inc_k}$, to be used on one side of the joint, while the second, $\vec{u}^{inc_l}$, to be used on the other side of the joint. Then expression (3-12) can then be rewritten as

$$U_j^{src} = -\left(\frac{\mathrm{V}}{2} \vec{u}^{inc_k} \cdot \vec{u}^{(j)(k)} - d_0^{(j)(k)} d_0^{(j)(1)} \frac{\mathrm{V}}{2} \vec{u}^{inc_l} \cdot \vec{u}^{(j)(1)} \right), \tag{3-13}$$

where the unit vectors $\vec{u}^{inc_k}$ and $\vec{u}^{inc_l}$ lie along the axes corresponding the wire unit vectors $\vec{u}^{(j)(k)}$ and $\vec{u}^{(j)(1)}$, respectively, with the directions of the former pair defined by going from the beginning of the original unit vector $\vec{u}^{inc}$ towards the joint, and then to the end of $\vec{u}^{inc}$.

It is possible to simplify the formula (3-13) by substituting the dot products in it by equivalent products of function d_0 defined by Table 2-1 (the dot products in (3-13) result in either +1 or -1). For the case when the generator is specified to be directed from wire (*j*)(*k*) towards wire (*j*)(*1*), this leads to

$$U_j^{src} = -\frac{V}{2}\left(-d_0^{(j)(k)} - d_0^{(j)(k)} d_0^{(j)(1)} \, d_0^{(j)(1)} \right) = +V \, d_0^{(j)(k)}. \tag{3-14}$$

For the opposite direction, it is

$$U_j^{src} = -\frac{V}{2}\left(+d_0^{(j)(k)} - d_0^{(j)(k)} d_0^{(j)(1)} \left(-d_0^{(j)(1)} \right) \right) = -V \, d_0^{(j)(k)}. \tag{3-15}$$

In obtaining the solutions (3-14) and (3-15), the identity $(d_0)^2=1$ was used.

Unfortunately, this formulation of the delta generator still gives a unique interpretation for a junction of only two arbitrarily directed wires. When there are more than 2 wires joined at one point, another approach is required.

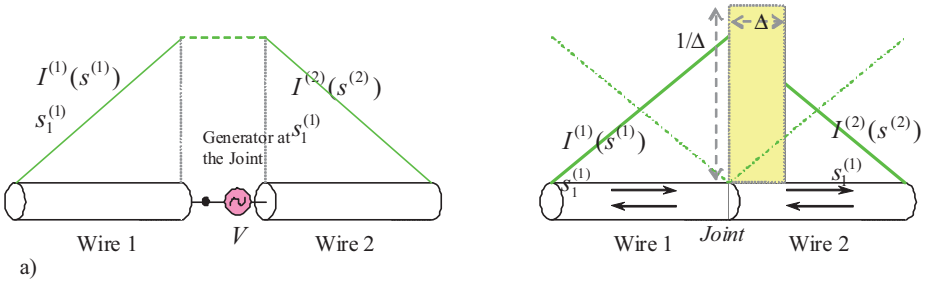

Figure 3-14 Attachment of a delta generator to one wire. (a) Introduction of a reference node separating two wires. (b) Shifted delta-function integration at a junction of two wires. Generator is attached to wire 2 only. The unit area taken by the delta-function is greyed out. The node basis functions giving a finite value after integration are profiled with solid green lines, while the ones vanishing are dash-dot green lines.

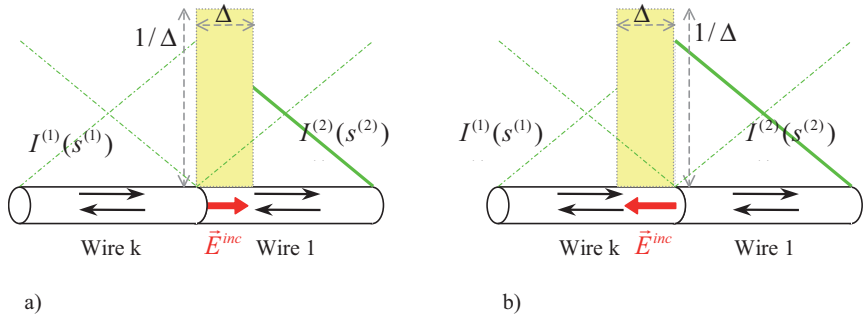

Figure 3-15 Delta-function generator is defined on one wire only: (a) defined on the 1st (common) wire, (b) defined on the *k*th wire. Red arrows specify the origin and direction of the excitation $\vec{E}^{inc}$ and are considered in the sense of them being infinitesimally small. On the integration of the shifted delta-function for a junction of two wires (on a doublet): the unit area taken by the delta-function is greyed out. The node basis functions giving a finite value after integration are profiled with solid green lines, while the ones vanishing are dash-dot green lines.

Starting with (3-10), with aid of Figure 3-15, it is easy to follow steps similar to ones done earlier in this section. In doing so, the product of signs introduced by the basis function N_{d_2}, the product of unit vectors $\vec{u}^{inc_n} \cdot \vec{u}^{(j)(n)}$, the direction of integration and, the functions $-d_0^{(j)(k)} d_0^{(j)(1)}$ (applicable to the reference node basis function) must be

considered. It is then easy to show that the test procedure results in the excitation vector element U_j^{src} shown in (3-16):

$$U_j^{src} = \begin{cases} -V\left(\vec{u}^{inc_k} \cdot \vec{u}^{(j)(k)}\right) = -V\, d_0^{(j)(k)}, & s_0 \in s^{(j)(k)} \\ -V\left(-d_0^{(j)(k)} d_0^{(j)(1)}\right)\left(\vec{u}^{inc_1} \cdot \vec{u}^{(j)(1)}\right) = +V\, d_0^{(j)(k)}, & s_0 \in s^{(j)(1)} \end{cases} \tag{3-16}$$

As expected, the answer for the considered situation of two wires is the same as the one derived from the intermediate (3-14)-(3-15) interpretation of the delta generator.

Note:

In the process of debugging the Matlab code, a number of situations were simulated, and the results were compared with the expected results, as well as with the results produced by WIPL-D of edition [Kolundzija, 47]. An inconsistency between the results was seen for the scenario of several generators connected at one point. This was reported to the software manufacturer, WIPL-D d.o.o. Newer versions of WIPL-D address this scenario.

3.4 Antenna Loading

This section discussed the effects of loading antennas and scatterers, and the required changes to the impedance matrix elements.

Modelling of antenna/scattering including the effects of loading helps to achieve a more accurate modelling of the real structures by inclusion of losses due to finite conductivity of metal and/or losses in dielectric, and be able to forecast the resulting performance.

Traditionally, there are two approximations available to model antenna loading. Losses are modelled as either distributed or lumped (concentrated). The former model covers the losses due to finite conductivity of conductors and the high-frequency skin-effect [Kolundzija, 46]. The latter approximation is simpler and best suited for electrically small resistive and reactive elements inserted at wire joints, as well as for modelling source or load impedances (e.g. 50 Ohms for a generator or receiver).

These approximate methods of taking the losses into account originate from the corrections due to the non-zero right-hand part of the boundary condition in equations (2.12) and (2.13). The equations describe the total tangential electrical field at the

boundary of two media (that are denoted with indexes 1 and 2). Where losses are present, the right-hand part is not zero. Instead, it equals $\vec{J}/\sigma$, where $\vec{J}$ is the electrical current density and σ is the effective conductivity defined [Kolundzija, 46] as $\sigma = \sigma_2 - \sigma_1 + j\omega(\varepsilon_2 - \varepsilon_1)$. In the last expression, σ_k and ε_k are the conductivity and permittivity of the k^{th} medium (here, index k=2 corresponds to a metal, and k=1 to vacuum).

With these in mind, the boundary condition (2.12) on the surface of a conductor with finite conductivity may be written as

$$(\vec{E} + \Delta\vec{E} + \vec{E}^{inc})\Big|_{\tan} = 0 \tag{3.17}$$

where vector $\vec{E}^{inc}$ [V/m] is the incident electric field with angular frequency ω [rad/s], and $\vec{E}$ [V/m] is the electric field due to induced surface currents and charges with densities[27] $\vec{J}_s$ [A/m] and ρ_s [C/m^2] respectively, in a perfect conductor/in absence of load. The term $\Delta\vec{E}$ is the change in the electric field due to loading/imperfect conductivity:

$$\Delta\vec{E} = -\frac{\vec{J}}{\sigma}, \tag{3.18}$$

where the effective conductivity σ [S] is described earlier in this section.

The simplified boundary condition (2.13) may also be rewritten in a form similar to (3.17), except that the projection on the cone's axis must be taken in all terms.

In the applications enabled by the equations (3.17) and (3.18), and discussed further in the text of this thesis, it is assumed that a conical wire approximation is used, and the current density $\vec{J}$ may be described in the form utilised in the Section 2.7.

[27] A hollow tube is assumed.

3.4.1 Distributed Loading

The distributed loading is used to emulate the effects of finite conductivity and dielectric coating on continuous surfaces, such as the surface of a wire. In the derivation given below, only the circumferential surface of a conical wire is considered. Following the thin wire approximation (Section 2.4), the surfaces of the top and bottom disks of a wire are not considered.

The total electrical field in the left-hand side of (2.12) is corrected through (3.17) by adding the term $\Delta\vec{E} = \Delta\vec{E}^{distr}$:

$$\Delta\vec{E}^{distr} = -\frac{\vec{J}}{\sigma} = -\vec{u}_s^{wire} I(s)\, Z', \tag{3.19}$$

where $\vec{u}_s^{wire}$ is the unit vector for the current direction defined on the wire to which this load is attributed, and $I(s)$ is the current intensity through the wire at the position $s \in [s_1, s_2]$, and Z' is an equivalent distributed impedance. This impedance expresses how the surface of the wire is loaded. The value of the impedance Z' depends on the type of effect being modelled. A summary of the three most frequently used types of distributed loadings is given Table 3-11.

The unit vector $\vec{u}_s^{wire}$ in (3.19) may be replaced with $\vec{u}_z^{wire}$, under the same conditions that were used to transform (2.23) into (2.26).

Following the Galerkin procedure of the general MoM approach described in Section 2.2, the integral equation is considered in the context of the boundary condition (3.17) on each individual set of wires corresponding to the basis functions (2 wires per doublet, 1 wire per singleton). After that, a test procedure is applied.

In order to simplify the derivations, and without losing the generality, the boundary condition will be applied to each wire individually, so that the results per wire are later combined into results per basis function. Then the electrical field correction term (3.19) for the wire (*j*)(*i*) may be written as

$$\Delta\vec{E}^{distr} = -\vec{u}_s^{(j)(i)} I^{(j)(i)}(s)\, Z'^{(j)(i)}, \tag{3.20}$$

where the notation (*j*)(*i*) addresses the wire number *i* (local to a junction) through the global variable index *j*. This method of addressing/writing up the terms was discussed earlier in Sections 2.9 and 2.11.

Table 3-11 Summary of distributed loading types along wire of radius a. Courtesy of [Kolundzija, 46]. σ_m is the conductivity of metal, a is the wire radius, f is the frequency, μ_0 is the permeability of vacuum, $\varepsilon_{1,2}$ are dielectric permittivity of media.

	Resistive layer of thickness δ	Skin-effect	Dielectric rod[28]
Per-unit-length impedance Z'	$\frac{1}{2\pi a\delta\sigma_m}$	$\frac{1}{2\pi a}\sqrt{\frac{\pi\mu_0 f}{\sigma_m}}$	$\frac{1}{j2\pi f\left(\varepsilon_2-\varepsilon_1\right)\pi a^2}$

Once the boundary condition and the test procedure are applied, the correction term to an element of the impedance matrix $Z_{jj}^{(j)(i)}$ takes the form

$$\Delta Z^{distr} = -\int_{s_1^{(j)(i)}}^{s_2^{(j)(i)}} \vec{u}_z^{(j)(i)} f_j(s')\,\vec{u}_s^{(j)(i)} I^{(j)(i)}(s')\,Z'\,ds'. \tag{3-21}$$

It should be noted that a wire (*j*)(*i*) that is a part of the domain of a doublet basis function **(2.47)** should require special treatment. If this wire corresponds to a singleton or to the independent variable $I_{d_2^{(j)(k)}}^{(j)(k)}$ in a doublet, the integral may be calculated in a straightforward manner. However, where the wire happens to be attributed to a dependent variable $I_{d_2^{(j)(1)}}^{(j)(1)}$ of a doublet, Kirchhoff's law may be applied (2.45), resulting in the sum

$$\Delta Z^{distr} = -\int_{s_1^{(j)(1)}}^{s_2^{(j)(1)}} f_j(s')\left(-\sum_{k=2}^{m} d_0^{(j)(k)} d_0^{(j)(1)}\, I_{d_1^{(k)}}^{(j)(1)}(s')\right) Z'\,ds', \tag{3.22}$$

[28] It should be noted that a dielectric rod must still satisfy the thin wire approximation requirements stipulated in Section 2.4. This may be more restrictive for a rod where the dielectric permittivity of the material is high. The same applies to a dielectric coating applied to a wire.

where $I_{d_1^{(k)}}^{(j)(k)}(s)$ stands for the profile of the current distribution defined by a respective basis function. In this expression, it is also taken into account that the dot product $\left(\vec{u}_z^{(j)(i)} \cdot \vec{u}_s^{(j)(i)}\right)$ degenerates into a unity.

In the expressions (3-21) and (3.22), the current intensities $I_{d_1^{(k)}}^{(j)(k)}(s')$ and $I_{d_1^{(k)}}^{(j)(1)}(s')$ (respectively to the two expressions) are the same as the basis functions $f_j(s')$.

Note:

In this work, it is assumed that the impedance Z' is constant along the wire. Then, under the condition that the basis functions are polynomials, the integrals (3-21) *and* (3.22) *can be readily calculated analytically.*

Moreover, it is still possible to perform the integration analytically, if the behaviour of the impedance Z' is approximated with a polynomial or another function that may be factored with a polynomial to be integrated analytically [Råde, 93]. This higher-order extension of the distributed loading is, however, not considered in this thesis.

3.4.2 Lumped Loading

It is presumed that the size of a *lumped* (or, in other words, *concentrated*) load is very small compared to wavelength (ideally, infinitesimal). A lumped load is inserted between wires, at the joint point of a wire junction.

The derivations for lumped loading are similar to ones done for distributed loadings in previous subsection. The difference/simplification is that a lumped impedance changes the electrical field expressed with (2.14) by the value expressed with a delta function [Råde, 93] localising the placement of load to one point (wire end s_0):

$$\Delta\vec{E} = -\frac{\vec{J}}{\sigma} = -\vec{u}_z^{wire} I_{load}(s_0) Z_{load} \delta(s - s_0) \tag{3.23}$$

where $\vec{u}_z^{wire}$ is the unit vector for the current direction defined on the wire to which this load is attributed, and I_{load} is the total current through the wire at its end s_0. The position s_0 of the end of this wire is the position where the load is attached (and through

the load to the junction) and can be either s_1 or s_2. It thus may be noted that the concentrated loading does not change the impedance matrix elements tested with singletons.

In a structure based on thin wires, consider a lumped impedance Z_{load} inserted at a junction of two wires. These two wires, referred to[29] with $(p)(k)$ and $(p)(1)$, define the domain for a doublet basis function. There may be more wires attached to the junction, with possibly more lumped loads. Therefore, to clarify the physical interpretation, the lumped impedance Z_{load} may be considered in the same way as it was discussed in Section 3.3 "Source Model: Delta-Function Generator". It is considered as inserted between the junction itself and the wire to which this load is attributed.

The load can be attributed to either wire $(p)(k)$ or wire $(p)(1)$. Applying the testing procedure of MoM, i.e. multiplying by a basis function and integrating over the domain of this basis function results in the two terms of a doublet:

$$\Delta Z_{jp} = \int_{s_1^{(j)(k)}}^{s_2^{(j)(k)}} \vec{u}_z^{(j)(k)} N_{d_2^{(j)(k)}} \Delta\vec{E}_p \, ds' - d_0^{(j)(k)} d_0^{(j)(1)} \int_{s_1^{(j)(1)}}^{s_2^{(j)(1)}} \vec{u}_z^{(j)(1)} N_{d_2^{(j)(1)}} \Delta\vec{E}_p \, ds' \qquad (3\text{-}24)$$

If the load generating $\Delta\vec{E}_p$ is attributed to the wire end corresponding to an independent variable j (effectively meaning that the first integral in (3-24) is non-zero), so $\vec{u}_z^{wire} I_{load} = \vec{u}_z^{(j)(k)} I_j$. Thus the value of the corresponding diagonal element of the impedance matrix is changed from Z_{pp} to $Z_{pp} - Z_{load}$, where p denotes the index of the unknown current for this doublet.

Where the load is defined on a wire $(p)(k)$, the second integral in (3-24) is zero, and the remaining integral may be readily converted to a closed form.

If the load is defined on wire $(p)(1)$, the first integral in (3-24) is zero. The expression (3-24) with the remaining second integral may be rewritten as

[29] In accordance with the notations introduced for doublets in Section 2.10.1.

$$\Delta Z_{jp} = -d_0^{(j)(k)} d_0^{(j)(1)} \int_{s_1^{(j)(1)}}^{s_2^{(j)(1)}} \vec{u}_z^{(j)(1)} N_{d_2^{(j)(1)}} \left(-\vec{u}_z^{wire} I_{load} Z_{load} \delta(s - s_0) \right) ds' \qquad (3.25)$$

In the integrand, the unit vectors are the same: $\vec{u}_z^{wire} = \vec{u}_z^{(j)(1)}$. In addition, when the current I_{load} is associated with a dependent variable, then this current has to be represented by the independent currents $I_{d_1^{(k)}}^{(p)(k)}$ via the KCL **(2.45)**:

$$\Delta Z_{jp} = d_0^{(j)(k)} d_0^{(j)(1)} Z_{load} \left(-\sum_{k=2}^{m} d_0^{(p)(k)} d_0^{(p)(1)} I_{d_1^{(k)}}^{(p)(k)} \right) \qquad (3.26)$$

Effectively, this changes *those elements* of the impedance matrix that are *attributed to this junction*:

$$Z_{jp} = Z_{jp} - d_0^{(j)(k)} d_0^{(j)(1)} d_0^{(p)(k)} d_0^{(p)(1)} Z_{load}, \; \underline{k = 2,3,\ldots,m}, \qquad (3.27)$$

where m is the number of wires attached to the junction. This represents a change in a square sub-matrix of the part of the impedance matrix attributed to doublet-doublet interactions, $\left[Z^{DD} \right]$.

The effect of changes being made in a number of elements (including the elements off the main diagonal) rather than in a single element on the main diagonal is in contrast with a simpler definition of PWL and PWS basis functions used more frequently [Nakano, 80], [Burke, 7], [Balanis, 4], [Balanis, 5].

It should also be mentioned that, just as in consideration of the delta-generator, the singletons do not produce any contribution due to lumped loading.

Note:

The practical implementations of the derivations given in this section were tested against reference examples modelled with WIPL-D. A perfect match was found between the result produced by WIPL-D and author's Matlab code.

Note:

From a practical point of view, the main issue in using the concentrated model of loading is the requirement of the load to be very small in terms of wavelength. As the frequency increases, this requirement is more difficult to fulfil. In addition, the parasitic

capacitance across the lumped load increases, as in the case of the delta generator. These factors may restrict applicability of this otherwise very useful model.

3.5 Symmetry Considerations - On Implementation of an Infinite PEC or PMC Ground Plane

This section reviews considerations of symmetry planes, including a ground plane, i.e. a symmetry plane made of perfect electric conductor (PEC), and how the introduction of a symmetry plane alters the impedance matrix of the method of moments.

An infinite ground plane is a mathematically exact physical approximation, where an object and a plane of symmetry (e.g. ground plane) are considered. The object is reflected to the other side of the symmetry plane, as shown in Figure 3-16, and the reflected copy is referred to as an *image*.

The image theory [Balanis, 4, Ch. 4.7-4.8] enables modelling of antennas and scatterers placed above a ground plane, e.g. Earth. Application of this theory also helps to reduce the computational burden. The theory is mathematically exact, but is an approximation of a physical phenomenon. The accuracy of this approximation[30] depends on the flatness of the surface, its size, and conductivity.

3.5.1 Derivations

In the following, the image theory method is applied to the wires over a symmetry plane, although it may be readily extended to geometries that are more complex. An element of impedance matrix Z_{ij} is composed of four partial impedances, e.g. (2.71). Each partial impedance[31] $Z_{ij}^{(n)D}$ involves double integration, e.g. (2.72). The outer

[30] The more complex related methods that support bending and finite size of structures, such as physical optics and uniform diffraction theory, are not considered in this text.

[31] The symbol D in the partial impedance is used to denote the direct interaction, as compared to the interaction through the fields reflected off the ground plane and denoted with letter R. This usage of the symbol D has nothing to do with the doublet basis functions discussed in the previous chapter.

integration can be considered as a vector weighted averaging of the field $\mathbf{E}_j(s')$ produced by current $|\mathbf{f}_j(s)|$ in the j^{th} wire, at the observation/field points on the wire W_i.

$$Z_{ij}^{(n)D} = \int_{Wi} \boldsymbol{w}_i(s') \cdot \mathbf{E}_j^D(s')\, ds', \tag{3.28}$$

where the dot stands for a dot product, $\boldsymbol{w}_i(s')$ is the weighting function; field incident on the wire W_i is denoted with $\mathbf{E}_j^D(s')$, and the integration is done over the wire W_i. The inner integration (not shown in the expression above) computes the field $\mathbf{E}_j^D(s')$, and is over all the source points on the source wire j with a certain current distribution defined by $\mathbf{f}_j(s)$.

The field incident on wire W_i is produced by the source wire W_j and may be written as $\mathbf{E}_j^D(s') = \int_{Wj} \mathbf{f}_j(s)\, G(s,s')\, ds$, where $G(s,s')$ is the free space Green's function. This last integral may be interpreted as the total field produced by a set of infinitesimal dipoles (integration over source points due to the current distribution). Each infinitesimal dipole has length ds, current magnitude $|\mathbf{f}_j(s)|$, unit vector $\mathbf{f}_j(s)/|\mathbf{f}_j(s)|$, and produces the field

$$\mathbf{dE}_j(s') = \mathbf{f}_j(s)\, G(s,s')\, ds. \tag{3.29}$$

At this point, one can easily apply the image theory. Then the field at the observation point is composed of the original field $\mathbf{E}_j^D(s')$ and the field produced by the reflection off the symmetry plane $\mathbf{E}_j^R(s') = \int_{Ri} \mathbf{f}_j(s)\, G(s,s')\, ds$, that is the field produced by an image wire R_j of the wire W_j. Figure 3-16 illustrates the concept with an example of a ground plane made of a perfect electric conductor (PEC).

In the figure, the original source wire W_i has the current that flows from node n_1 toward node n_2, and defined with a basis function $N_2^{(Wi)}$. A perfect ground plane may be replaced with a virtual source that is positioned/imaged symmetrically, with respect to the ground plane. To satisfy the boundary condition at the surface of the ground plane, in the image each *horizontal* component of infinitesimal current must have the direction opposite to the direction in the original source. Each *vertical* component of infinitesimal current must follow the same direction as the original current. This can also be seen in the figure above. Thus, the direction of current in the image, wire R_i, is from node n_2 toward node n_1'. This effectively requires to change the sign of the field term corresponding to the image wire. Since the profile of the current distribution must be

kept intact between the equivalent points of the actual source and image, the basis function applied to the image wire is changed from $N_2^{(Wi)}$ to $N_1^{(Ri)}$.

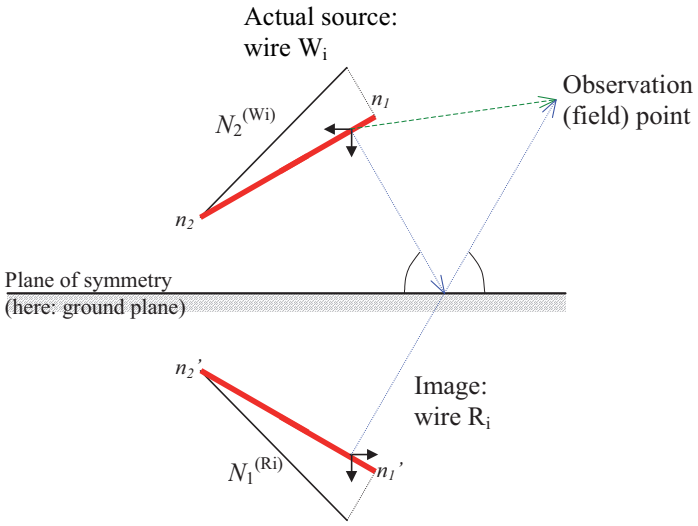

Figure 3-16 Wire W_i above infinite flat perfect electric conductor, and its associated image – wire R_i (virtual source). The direction of current flow in wire W_i is from node n_1 toward node n_2. The decomposition of the direction of current into vertical and horizontal components is shown with small arrows. The basis function $N_2^{(Wi)}$ is assigned to wire W_i.

As a result, the new partial impedance, including the influence of a ground plane, is now composed of two sub-components, corresponding to the original "direct" partial impedance $Z_{ij}^{(n)D}$ and the partial impedance due to the reflection, $Z_{ij}^{(n)R}$:

$$\begin{aligned} Z_{ij}^{(n)} &= \int_{Wi} \boldsymbol{w}_i(s') \, (\mathbf{E}_j^D(s') + \mathbf{E}_j^I(s')) \, ds' \\ &= \int_{Wi} \boldsymbol{w}_i(s') \, \mathbf{E}_j^D(s') \, ds' + \int_{Wi} \boldsymbol{w}_i(s') \, \mathbf{E}_j^I(s') \, ds' \\ &= Z_{ij}^{(n)D} + Z_{ij}^{(n)R}. \end{aligned} \tag{3.30}$$

Note:

In practical terms, this can be easily implemented by either of two approaches:

In the first approach, the reflection term is calculated immediately after the direct term, and the results are added together before starting with another matrix element. The

second option allows more flexibility through calculating a separate "image" impedance matrix and combining the two matrices just before solving the linear system.

3.5.2 On the Performance of the Technique

In terms of performance, the symmetry provided by a reflection off a plane reduces the number of unknowns by a factor of 2. This translates into 4 times fewer elements to fill in the impedance matrix. It must however be noted that according to the image theory each new element (including the influence of the image) is effectively composed of two elements (one above the plane of symmetry and the other below it), so it takes approximately twice longer to compute. Thus, the image theory reduces the time required to fill in the impedance matrix by a factor of 2.

An even more significant saving is achieved when the problem is electrically large and requires many unknowns. This is done through a reduction in the number of operations required to obtain a solution. Since the number of unknowns with usage of a symmetry plane is 2 times smaller, the time required to solve the linear system is reduced by a factor of up to 8, i.e. 2^3.

Note:

The described approach may be compared with one used in NEC2 [Burke and Poggio, 7]. In NEC2, the time to fill in the matrix is reduced. However, the resultant impedance matrix includes the matrix elements for both halves of the space around a symmetry plane.

In the approach described in this section, the time to fill in the matrix is not reduced. Instead, the benefit is gained at the stage of solving the linear system. Large models require substantially more processing power for solving a system compared to filling in of the impedance matrix. Thus, the approach introduced in this section is especially beneficial for large systems.

Note on ease of implementation:

In the subroutines for computing impedance matrix elements, the program code related to the field index i, was copied "as is". The code related to the source index, j, had to be

modified a little. In addition, the subroutines for computing far field had to be extended, and a special case of a wire attached to no other wire but to a symmetry plane had to be considered in the indexing core. Currently, the Matlab code supports perfect electric conductor (PEC) and perfect magnetic conductor (PMC) types of symmetries applied to an arbitrary combination of coordinate planes XY, YZ and XZ.

3.6 Solution of the System of Linear Equations

This section provides an introductory overview of a method for solving the system of linear algebraic equations, namely LU decomposition.

The system of linear algebraic equations in the form **ZI**=**V** results from a discretization of the electrical field integral equation (as per Chapter 2). In the program, it is set to be solved using the direct[32] LU-decomposition [Press et al., 92] based approach. Other techniques (e.g. Gaussian elimination or iterative[33] conjugate gradient method) may also be used by altering the respective settings in the program.

3.6.1 Few details on the LU decomposition

Due to its flexibility, the LU decomposition is probably the most popular method for solving general dense matrix equations. In this method, the matrix **Z** is transformed into a matrix product of two matrices **Z**=**L**·**U**, where **L** and **U** are a lower triangular, and an upper triangular matrix, respectively.

[32] The term *direct* refers to the class of methods that obtain a solution of the system of linear equations in a finite, pre-determined number of steps. The obtained solution is exact, except for round-off/truncation errors that accumulate throughout the steps of the solution. Thus these methods are ideal for solving small to intermediate sized well-conditioned problems, where the number of variables is not high and the equations are far from being linearly dependent.

[33] The main distinct advantage of the iterative solution is that it may enable obtaining of a solution that is arbitrarily close to the exact solution, although at the expense of computational time.

The LU decomposition itself is based on Crout's algorithm described elsewhere [Forsythe et al., 22], [Press et al.,92].

Once the factorisation of **Z** is done, the linear system may be rewritten as

$$\mathbf{Z}\cdot\mathbf{x}=\left(\mathbf{L}\cdot\mathbf{U}\right)\cdot\mathbf{x}=\mathbf{L}\cdot\left(\mathbf{U}\cdot\mathbf{x}\right)=\mathbf{b} \tag{3.31}$$

Effectively, this breaks the original system into two successive sets.

$$\begin{aligned}\mathbf{L}\cdot\mathbf{y}&=\mathbf{b}\\ \mathbf{U}\cdot\mathbf{x}&=\mathbf{y}\end{aligned} \tag{3.32}$$

The advantage offered by the introduction of the two systems with triangular matrices is in the simplicity of algorithms to follow, and in a reduced count of the operations required to determine all unknowns. The first equation in (3.32) is solved by forward substitution:

$$\begin{aligned}y_1&=b_1\big/L_{11}\\ y_i&=1\big/L_{ii}\left(b_i-\sum_{j=1}^{i}L_{ij}y_j\right),\quad i=2,3,\ldots,N\end{aligned}\;. \tag{3.33}$$

The second equation in (3.32) is then solved by back-substitution:

$$\begin{aligned}x_N&=y_N\big/U_{N,N}\\ x_i&=1\big/U_{i,i}\left(y_i-\sum_{j=i+1}^{N}U_{ij}x_j\right),\quad i=N-1,N-2,\ldots,1\end{aligned} \tag{3.34}$$

It may also be noted that the separation of the original system into two systems (3.32) permits re-usage of the matrices **L** and **U**, for solving a system of linear equations with various right-hand side excitation vectors. This feature is particularly useful for solving problems with multiple excitations.

Once the LU decomposition is done, it is also possible to calculate the inverse of **Z**. This may be done in a column by column order, applying the back-substitution procedure with unit vectors instead of **y**.

For N unknowns, the LU decomposition requires on the order of N^3 count of floating point operations (such as addition, multiplication) on complex numbers, and is at least

as efficient in the scenario of dense matrices produced by MoM as most of other methods [Press et al, 92].

3.7 Antenna's Network Parameters

There are several network parameters, such as impedance ***Z***, admittance ***Y*** and scattering ***S*** – network matrices [Pozar, 90] that are frequently used to characterise the matching performance of an antenna with respect to the receiver/generator's input/output impedance, or to evaluate the coupling between antenna elements. This section offers an overview of an approach to obtain these parameters.

The excitation in the discussed realisation of the MoM is considered as a set of ideal voltage generators. Therefore, it is the easiest to obtain the ***Y***-parameters from the pre-defined voltages and computed currents. The definition for the elements of the ***Y***- matrix follows [Pozar, 90] and is

$$Y_{ij}^{port} = \left. \frac{I_i^{port}}{V_j^{port}} \right|_{V_{i\neq j}=0}, \quad i,j = 1,2,\ldots,N_{YZS}, \tag{3-35}$$

where N_{YZS} is the number of ports (generators) defined. The voltage applied to the j^{th} port (in the other words, voltage due to the j^{th} generator) is denoted with V_j^{port}. This voltage results in a short-circuit current I_i^{port} observed at the i^{th} port.

In order to obtain the complete admittance matrix, the following procedure is repeated as many times as there are ports (excitations) defined. In each iteration, only one port is considered activated (set to V_j^{port}). In accordance with the definition (3-35), the other excitations are set to zero. Thus, a single iteration produces one column of the *Y*-matrix.

Note:

The above procedure may become computationally intensive if there are many ports. To improve the performance it is advantages to store either the inverse of the original impedance matrix or the LU-decomposition of the impedance matrix, computed during the first iteration. Refer to Section 3.6 for details (most of the discussions related to the impedance matrix are directly applicable to the network matrices).

After the admittance matrix is filled in, the ***Z***-matrix may be calculated by inversion of the ***Y*** matrix:

$$\left[Z_{ij}^{port}\right]=\left[Y_{ij}^{port}\right]^{-1} \tag{3-36}$$

The scattering matrix (***S*** parameters) is computed by

$$[S]=\left(\left[Y_i^{ref}\right]-\left[Y_{ij}^{port}\right]\right)\cdot\left(\left[Y_i^{ref}\right]+\left[Y_{ij}^{port}\right]\right)^{-1}, \tag{3-37}$$

where $\left[Y_i^{ref}\right]$ is a diagonal matrix with elements Y_i^{ref}, $i=1,2,\ldots,N_{YZS}$. Each Y_i^{ref} is the reference admittance for the i^{th} port (typically equals 1/50 Ω^{-1}).

Note:

However, in certain situations, calculation of the network impedance matrix and/or the network scattering matrix might not be possible, as the admittance matrix might be singular. This may, for instance, happen for a simple geometry with three straight wires connected in a T-junction with three generators, all having their references at the junction.

Under such circumstances, the other possible approaches include de-embedding based on the transmission line theory [Gamage, 23]. Usage of the transmission line theory may utilise a decomposition of the current into direct and reflected waves so that the network scattering matrix elements may then be evaluated directly. The decomposition into a sum of exponents may be done using, for example, method of Prony [Press et al., 92], or the generalised pencil of function (GPOF) method [Hua and Sarkar, 30].

3.8 Estimation of the Numerical Uncertainty in the Currents and Secondary Parameters Y, Z and S

In this section, the numerical uncertainty in the solution (currents) is expressed through the condition number of the impedance matrix and the uncertainty in calculating the impedance matrix elements. This provides a figure of merit for estimating the required accuracy in calculating and storing impedance matrix elements. The uncertainty in the network admittance matrix ***Y*** is then related to the uncertainty in obtained currents. The

uncertainty in the other network matrix parameters, $\boldsymbol{Z}$ and $\boldsymbol{S}$ – matrices, is derived in a similar manner.

3.8.1 Problem Definition

Suppose that there exists an exact system of linear algebraic equations

$$\mathbf{A}\mathbf{x} = \mathbf{b}\,. \tag{3.38}$$

In a practical realisation, the terms in such a system may include errors. The effect of these errors converts the exact system (3.38) into a perturbed system (3.39):

$$\left(\mathbf{A} + \delta\mathbf{A}\right)\mathbf{y} = \mathbf{b} + \delta\mathbf{b}\,, \tag{3.39}$$

where the symbol δ denotes the perturbation terms.

This new system produces an approximate solution **y** instead of the exact solution **x**. The main source of error is the inaccuracy in calculating the terms **A** and **b**, i.e the impedance matrix and excitation vector, respectively, in terms of the MoM. However, even when these variables are calculated accurately, the number representation used in personal computers (PC) may still introduce an additional error.

3.8.2 Note on Number Representation in PCs

Digital computers store the numbers in various formats, depending on the usage required. These formats, or the number representation in modern personal computers (PC), are governed by the standard [IEEE 754-1985, 32]. There are integer numbers that are fast to work with but are limited in the dynamic range and thus in the accuracy of values that may be represented. For example, in personal computers (PC), a byte is capable of accurately representing 2^8=256 different values (where 8 is the number of bits in a byte and 2 is the number of states into which each bit may be put). This translates into available ranges of integer numbers, such as [0,1,..,255], [-128,-127,..,127], etc.. Thus the best relative uncertainty one may expect through a linear mapping is ±0.5 / (256-1) ≈ ±0.002. Increasing the number of bits to 32 with widest integer type *integer*32* gives the range of 0 to 4294967295 ≈ $4.29\cdot10^9$, and the accuracy on the order of 10^{-10}. This might be sufficient for a number of specialised

applications including digital signal processing (DSP), where a high performance is most often the dominating factor. Unfortunately, this data representation is difficult to use for general complex scientific applications, including numerical electromagnetic modelling.

A more convenient format is the floating-point number representation, where a number X is factorised[34] into a mantissa M and exponent E as $X \approx M \cdot 2^E$. The exponential factor defines the order of magnitude of the number and thus the range of values possible to map, whilst the mantissa is a normalised representation of the number and therefore defines the accuracy of such representation.

In Matlab [Matlab, 69] on PC, the default number representation is the so-called *double precision* (called *REAL*8*, in FORTRAN). In this representation, the sign of the number is represented through 1 bit, the mantissa consumes 52 bits, and the exponent takes 11 bits. All together, there are 64 bits or 8 bytes per one real (not complex) number.

Keeping aside the underflow and overflow errors due to the limited[35] range provided by the exponent, the tolerance of this number representation can be defined as $\varepsilon_0 = 2^{-52} \approx 2.2 \cdot 10^{-16}$. Then an arbitrary exact number x_0 may be represented approximately as $x \approx x_0 \left(1 \pm \varepsilon_0\right)$.

This representation illustrates why the equation (3.38) becomes (3.39) for a general system stored digitally in a computer.

[34] For example, the number 0.25 can be represented as $0.25=2^{-2}=1\cdot 2^{-2}$. However, the numbers that cannot be represented *exactly* by a superposition of a limited number of powers of 2, have a limited precision, e.g. $7\frac{1}{3} \approx 0.916666666666667 \cdot 2^3$, $\frac{1}{11} \approx 0.727272727272727 \cdot 2^{-3}$.

[35] The range is limited but is nevertheless sufficiently wide for most electromagnetic problems related to MoM. The smallest represented number is $2.2250738585072\cdot 10^{-308}$, while the largest one is $1.79769313486232\cdot 10^{308}$.

Note:

The problems arise when two or more numbers with similar magnitude have to be subtracted from one another. The resultant has a small magnitude (due to the difference) and a large fractional error (that is the sum of two respective errors). Often this effect leads to a complete loss of accuracy and is difficult to trace numerically.

3.8.3 On the Role of the Condition Number in the Error of the Solution/Current

As mentioned earlier, there are several contributions to the inaccuracy of the unknown $\boldsymbol{x}$ in (3.38). These are the errors in calculating the impedance matrix elements and excitation vector, and also the error due to the number representation. In this subsection, the accuracy of calculating the matrix elements is linked to the accuracy of the calculated current distribution.

Following [Råde, 93] and [Golub, 24], an error estimate for a solution of a perturbed system of linear equations (3.39), relative to the solution of the exact system (3.38) may be expressed as the following inequality:

$$\frac{\|\mathbf{y}-\mathbf{x}\|}{\|\mathbf{x}\|} \le \frac{1}{1-r}\kappa(A)\left(\frac{\|\delta\mathbf{A}\|}{\|\mathbf{A}\|}+\frac{\|\delta\mathbf{b}\|}{\|\mathbf{b}\|}\right), \qquad r=\|\delta\mathbf{A}\|\cdot\|\mathbf{A}^{-1}\|<1, \tag{3.40}$$

where

$$\kappa(\mathbf{A}) \equiv \|\mathbf{A}\|\cdot\|\mathbf{A}^{-1}\| \tag{3.41}$$

is the condition number of a non-singular matrix $\mathbf{A}$, and the notation $\|\mathbf{A}\|$ denotes the norm of the matrix **A**.

Note:

The condition number $\kappa(\mathbf{A})$ *is the figure of merit for measuring the numerical instability of a linear system and so the sensitivity of the linear equation solution to the errors in input data (e.g. in the entries of matrix* **A***). Values of condition number near 1 indicate a well conditioned matrix. Large values of condition number signal an ill*

conditioned matrix. In the cases where an iterative method is used for solving a linear system, this may lead to a very slow convergence to the solution [Chew et al., 10].

In all computations done throughout the preparation of this thesis, the 2-norm condition number was used. The condition number is computed as the ratio of the largest singular value of the matrix to the smallest. For more information on the matrix norms, condition number definition and calculation, singular values etc., see, for example, references [Golub et al., 24], [Forsythe et al., 22], and [Råde, 93].

As per the expressions shown above and [Golub et al., 24], the condition number may be looked at as a factor by which the inaccuracy of the elements of matrix $\mathbf{A}$ is multiplied. Assuming that the right-hand side of the linear system, i.e. the excitation vector, is exact (which is usually the case when only the delta-gap generator is used), the solution error estimate (3.40) can be rewritten as

$$\frac{\|\mathbf{y}-\mathbf{x}\|}{\|\mathbf{x}\|} \le \frac{r}{1-r} = \kappa(\mathbf{A})\frac{\|\delta\mathbf{A}\|}{\|\mathbf{A}\|} \Bigg/ \left(1-\kappa(\mathbf{A})\frac{\|\delta\mathbf{A}\|}{\|\mathbf{A}\|}\right), \qquad \kappa(\mathbf{A})\frac{\|\delta\mathbf{A}\|}{\|\mathbf{A}\|} < 1 \tag{3.42}$$

In order to shorten notations, it is possible to specify the desired accuracy of the solution ξ_x as

$$\frac{\|\mathbf{y}-\mathbf{x}\|}{\|\mathbf{x}\|} \le \xi_x \tag{3.43}$$

The expression (3.42) may then be rewritten to relate the required accuracy of the matrix, $\|\delta\mathbf{A}\|/\|\mathbf{A}\|$, to the condition number $\kappa(\mathbf{A})$:

$$\frac{\|\delta\mathbf{A}\|}{\|\mathbf{A}\|} \le \frac{1}{\kappa(\mathbf{A})}\frac{\xi_x}{1-\xi_x}. \tag{3.44}$$

This may be interpreted as a prerequisite on the required accuracy of calculating the impedance matrix elements to be better (lower) than the desired low accuracy of the final solution divided by the condition number.

3.8.3.1 *On the size of solvable system versus the required accuracy of calculating integrals*

A rough estimate for the condition number[36] may be made by considering the effect of the accumulation of round-off errors. Then, the total uncertainty of the result is proportional to the square root of the number of floating point operations involved in solving a general system of linear equations. The latter is approximated as N^3, where N is the number of unknowns. That gives $\kappa(\mathbf{A}) \cong \kappa_N = N^{3/2}$. Therefore a very rough estimate for the required accuracy in calculating the impedance matrix elements may be expressed as $\frac{\|\delta\mathbf{A}\|}{\|\mathbf{A}\|} \le \frac{1}{N^{3/2}} \frac{\xi_x}{1-\xi_x}$.

Numerical experiments, where a complex matrix was filled with uniformly distributed random numbers, have confirmed[37] the assumption that the condition number increases with the size of the system in a manner generally resembling $\kappa_N = N^{3/2}$. An arithmetic mean of the ratio of the simulated condition number to the estimate $\kappa_N = N^{3/2}$ is approximately equal to 18. This difference is attributed to the numbers in the matrix being complex. One complex multiplication takes 6 real floating-point operations (FLOPS), and a complex division requires 11 FLOPS, thus increasing the estimated count of floating point operations.

A more accurate numerical estimate may be obtained by repeating this sort of simulation with a specific kind of matrix inversion on the actual matrices obtained by MoM.

---

[36] The reference [Chew, et al., 10] provides much more accurate (although problem-specific) estimates for the condition number.

[37] Each experiment, including generation of a new set of random numbers and solving the system, was repeated 100 times to obtain an average value of the condition number. The validity of assuming a uniformly distributed matrix is perhaps the weakest point in the estimation, as the MoM matrices tend to have a dominating main diagonal.

Having developed a model for estimating the matrix element accuracy from the size of matrix, it is possible to give an estimate for the desired level of accuracy for calculating the integrals. The starting point is the maximum size of a matrix (i.e. the number of variables) to be dealt with. The fastest solvers for systems of linear equations are usually direct[38] and they require the complete matrix to be in memory.

Table 3-12 Samples of memory and accuracy requirements for the MoM. Greyed out (marked) entries correspond to numerically unstable matrices.

Memory available	Single Precision (4 bytes per a real number, $\varepsilon_0 = 2^{-23} \approx 1.2 \cdot 10^{-7}$)		Double Precision (8 bytes per a real number, $\varepsilon_0 = 2^{-52} \approx 2.2 \cdot 10^{-16}$)	
	Maximum number of unknowns	Matrix element's accuracy required (relative accuracy of current is specified as 0.5)	Maximum number of unknowns	Matrix element's accuracy required (relative accuracy of current is specified as 0.5)
4 kB	22	$9 \cdot 10^{-3}$	16	$1 \cdot 10^{-2}$
1 MB	362	$1 \cdot 10^{-4}$	256	$2 \cdot 10^{-4}$
512 MB	8192	$1 \cdot 10^{-6}$	5792	$2 \cdot 10^{-6}$
2 GB	16384	$5 \cdot 10^{-7}$ ***	11585	$8 \cdot 10^{-7}$
32 GB	65536	$6 \cdot 10^{-8}$ ***	46341	$1 \cdot 10^{-7}$

Note:

Most of PCs are still 32-bit and therefore support up to $2^{31} = 2GB$ *of memory (one bit in a 32-bit long word is usually reserved). The commercially available 64-bit computers typically support much greater amounts of memory. Table 3-12 gives estimates for memory and accuracy requirements for PC-s. It is easy to see that comparatively simple models requiring fewer than about a thousand unknowns may be simulated relatively easily. However, complex models with a large number of unknowns require a high*

[38] Iterative solvers may also be used. They are particularly important when a matrix size exceeds the physically available memory, or an approximate solution is known so that only a few iterations are required.

degree of accuracy when calculating the matrix elements. To set a reference, it is possible to require an accuracy of better than 0.5.

In addition, the real-world MoM matrices have condition numbers which are often by one to three orders of magnitude higher than the estimate $\kappa_N = N^{3/2}$. *This means that it is necessary to reserve (add) several extra significant digits of accuracy to the estimates discussed.*

There is also an option of so-called "outcore" solution using iterative approaches. A discussion on this topic may be found for instance in [Yuan, Sarkar, and Kolundzija, 116].

3.8.4 A Straightforward Method for Estimating Numerical Uncertainty in Network Parameters *Y*, *Z* and *S*

In this variation of the MoM, the network admittance matrix ***Y*** is computed first, before ***Z*** and ***S*** matrices[39]. Each element of the admittance matrix is computed as a ratio of the current through a generator to the voltage across a generator, in accordance with (3-35). The current is obtained through solving the linear system. The estimation of uncertainty in the current is discussed earlier in this section, and in particular in subsection 3.8.3. The voltage is the respective element of the excitation vector. Thus, the accuracy of elements of the network admittance matrix ***Y*** equals the accuracy of currents.

Next, the network impedance matrix ***Z*** and network scattering matrix ***S*** are computed. Both of them are computed from the admittance matrix[40] using expressions (3-36) and (3-37), respectively. The uncertainties in the resulting matrices may be estimated using the same approach based on the condition number as was proposed in subsection 3.8.3.

[39] It is important to differentiate between the impedance matrix **Z**, and the network impedance matrix ***Z***. In this text, the latter is written in *italics*.

[40] It is also possible to compute ***Z*** and ***S*** matrices via one another but this may lead to a slightly higher error (due to error accumulation).

In this section, it is assumed that the excitation vector is computed accurately, which is the case when delta-gap generators are used for excitation. It should be possible to extend the approach to include the uncertainty in the excitation vector.

3.9 Example 1A: Building a System of Linear Equations

This example serves to demonstrate, in practice, how a system of linear algebraic equations is obtained for a given wire geometry. The example may also be used to provide a reference set of data for building one's own moment method code.

An expansion of this example, Example 1B, is considered later, in Section 4.5.

3.9.1 Project Definition

Let's consider the following geometrical configuration consisting of five wire segments interconnected in the way shown in Figure 3-17 below. The details of this geometry may be described with the following Table 3-13.

The generator is defined as a point source located at node 4, directed toward node 6, with a voltage of 1.0 Volts. The frequency of operation is set to 1 MHz.

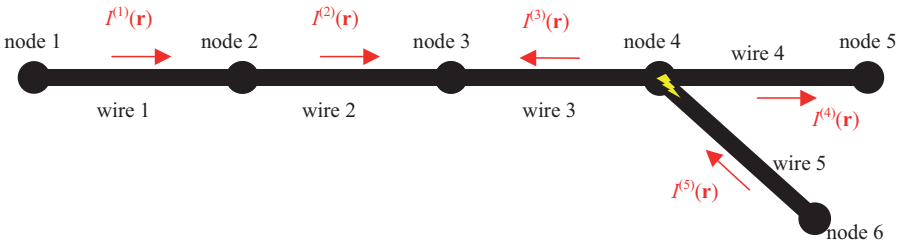

Figure 3-17. Geometry of a wire structure, and the definitions for the direction of current in the wires. Large dots denote the position of nodes. The arrows show the assumed direction of current through each wire (taken, for example, as the direction from the beginning toward the end of each particular wire). The point generator is positioned at node 4 and its electrical field is pointing toward node 6.

Table 3-13. Definitions of nodes and wires for the examples 1A and 1B.

A. Positions of nodes

Nodes			
No.	**x, [m]**	**y, [m]**	**z, [m]**
1	0	0	0
2	0	0.5	0
3	0	1	0
4	0	1.5	0
5	0	2	0
6	0.5	1.5	0

B. Definition of wires in terms of nodes.

Wires		
No.	**1st node (beginning)**	**2nd node (end)**
1	1	2
2	2	3
3	4	3
4	4	5
5	6	4

3.9.2 Discussions

As a first step, consider that the net current may be written in a piecewise manner as $I(\mathbf{r}) = \sum_{n_w=1}^{5} I^{(n_w)}(\mathbf{r})$, where the index n_w refers to the wire number and the vector $\boldsymbol{r}$ defines the position in space. It should be possible to introduce local co-ordinate systems for each of the wires as specified in [Sarkar et al., 47], so the expressions for the current in the wires may be re-written in a shorter form: $I^{(n_w)} \equiv I^{(n_w)}(s^{(n_w)}) \equiv I^{(n_w)}(s^{(n_w)}(\mathbf{r})) \equiv I^{(n_w)}(\mathbf{r})$.

In the next step, it is necessary to introduce a set of basis functions, so that the currents through the wires $I^{(n_w)}(s^{(n_w)})$ may be expressed mathematically. The currents in each wire can thus be written in the form introduced earlier:

$$I^{(n_w)}(s^{(n_w)}) = I_1^{(n_w)} N_2^{(n_w)}(s^{(n_w)}) + I_2^{(n_w)} N_1^{(n_w)}(s^{(n_w)}) + \sum_{i=3}^{n_b^{(n_w)}} a_i^{(n_w)} S_i^{(n_w)}(s^{(n_w)}), \quad n_w = 1,2,\ldots,5.$$

Since the ends of wires 1,4 and 5 at the nodes 1, 5 and 6 are free ends, Kirchhoff's law requires the current magnitude there to be zero: $I_1^{(1)}=0$, $I_2^{(4)}=0$, and $I_1^{(5)}=0$. Also, in order to keep this example simple and short, the singletons have been left out.

The profiles of these function with the wires, can be sketched as shown in Figure 3-18.

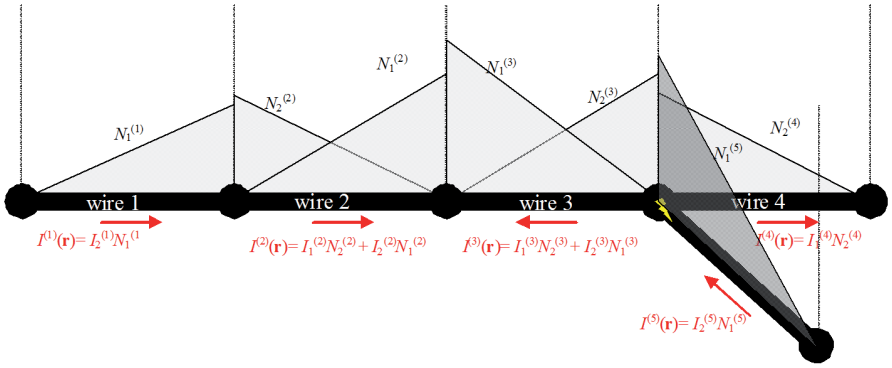

Figure 3-18. Assignment of basis functions to the wires in Example 1A.

Kirchhoff's law applied at the nodes where the wires meet gives the three equations (the most left column):

$$\begin{array}{l|l|l} I^{(1)}(s_2^{(1)}) - I^{(2)}(s_1^{(2)}) = 0, & I_2^{(1)} = I_1^{(2)}, & I_1 \equiv I_2^{(1)} \\ I^{(2)}(s_2^{(2)}) + I^{(3)}(s_2^{(3)}) = 0, & I_2^{(2)} = -I_2^{(3)}, & I_2 \equiv I_2^{(3)} \\ -I^{(3)}(s_1^{(3)}) - I^{(4)}(s_1^{(4)}) + I^{(5)}(s_2^{(5)}) = 0, & I_2^{(5)} = I_1^{(3)} + I_1^{(4)}, & I_3 \equiv I_1^{(4)}, \quad I_4 \equiv I_2^{(5)} \end{array} .$$

These equations relate currents, as shown in the middle column. Then, the four independent unknowns termed I_1, I_2, …, I_4 are *chosen* (in the most right hand side column: $I_2^{(1)}$, $I_2^{(3)}$, $I_1^{(4)}$, $I_2^{(5)}$). Once these unknowns are obtained, the rest of the current amplitudes (the dependent unknowns) could be easily found through the relationships from the middle column.

Now, putting together the current distributions on the wires and expressing $I_1^{(2)}$, $I_2^{(2)}$, and $I_1^{(3)}$ via the defined unknowns I_1-I_4, the current distribution may be written in a piecewise manner as

$$I(\mathbf{r}) = \underbrace{I_2^{(1)}}_{I_1}\underbrace{\left(N_1^{(1)} + N_2^{(2)}\right)}_{D_1^{(1,2)}} + \underbrace{I_2^{(3)}}_{I_2}\underbrace{\left(N_1^{(3)} - N_1^{(2)}\right)}_{D_2^{(3,2)}} + \underbrace{I_1^{(4)}}_{I_3}\underbrace{\left(N_2^{(4)} - N_2^{(3)}\right)}_{D_3^{(4,3)}} + \underbrace{I_2^{(5)}}_{I_4}\underbrace{\left(N_1^{(5)} + N_2^{(3)}\right)}_{D_4^{(5,3)}}$$

Here it is taken that $N_i^{(j)} \equiv N_i^{(j)}(s^{(j)})$ are the basis (expansion) functions, and that I_1 - I_4 are the unknown coefficients. This expansion may be illustrated with Figure 3-19:

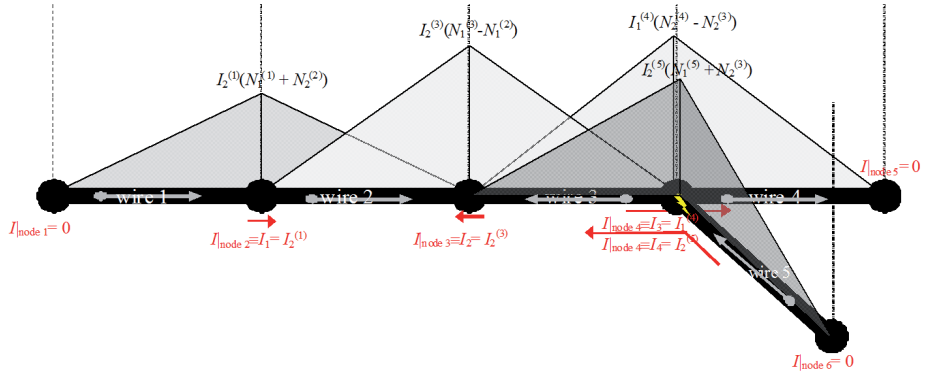

Figure 3-19. Assignment of basis functions to wires with application of the Kirchhoff's current law.

To shorten the notations, doublet functions $D_i^{(j,p)} \equiv D_i^{(j,p)}(s^{(j)}, s^{(p)})$ may also be introduced.

Recall the notations introduced in Sections 2.2 and 2.10, where $\mathbf{L}$ is the electric field operator $\mathbf{L}\,I(\mathbf{r})$ acting on current $I(\mathbf{r})$. Using this notation, the electric field produced by the set current distribution can be written[41] as

$$\begin{aligned}\mathbf{E}(\mathbf{r}) &= I_1\,\mathbf{L}\underbrace{\left(N_1^{(1)} + N_2^{(2)}\right)}_{D_1} + I_2\,\mathbf{L}\underbrace{\left(N_1^{(3)} - N_1^{(2)}\right)}_{D_2} + I_3\,\mathbf{L}\underbrace{\left(N_2^{(4)} - N_2^{(3)}\right)}_{D_3} + I_4\,\mathbf{L}\underbrace{\left(N_1^{(5)} + N_2^{(3)}\right)}_{D_4} \\ &= I_1\,\mathbf{L}D_1 + I_2\,\mathbf{L}D_2 + I_3\,\mathbf{L}D_3 + I_4\,\mathbf{L}D_4\end{aligned}$$

This is an expression with four unknowns. Following the Galerkin's procedure, to obtain four linear equations for the four unknowns, the boundary condition $\left(\mathbf{E}(\mathbf{r}) + \mathbf{E}^{inc}(\mathbf{r})\right)\Big|_{surface} = 0$ is to be satisfied individually on all the domains where the basis functions $D_1, D_2, D_3,$ and D_4 are defined. The boundary condition is multiplied by the corresponding basis function and the product is integrated over the corresponding domain. For example, for the first basis function D_1, this leads to the following

[41] To simplify write up, the superscripts have been omitted. If required, the superscripts may be identified from the previous expression for $I(\mathbf{r})$.

equation: $\int_{S^{(1,2)}} D_1^{(1,2)}\mathbf{E}(\mathbf{r})dS = -\int_{S^{(1,2)}} D_1^{(1,2)}\mathbf{E}^{inc}(\mathbf{r})dS$. Identifying that the right-hand side is zero, and expanding the left-hand side gives:

$$\underbrace{I_1 \int_{S^{(1,2)}} D_1\mathbf{L}D_1 dS}_{Z_{11}} + \underbrace{I_2 \int_{S^{(1,2)}} D_1\mathbf{L}D_2 dS}_{Z_{12}} + \underbrace{I_3 \int_{S^{(1,2)}} D_1\mathbf{L}D_3 dS}_{Z_{13}} + \underbrace{I_4 \int_{S^{(1,2)}} D_1\mathbf{L}D_4 dS}_{Z_{14}} = 0 .$$

This expression is linear with respect to the unknown coefficients and can be written in a shorter form, as $I_1 Z_{11} + I_2 Z_{12} + I_3 Z_{13} + I_4 Z_{14} = 0$.

Similar equations are written for the other domains. The 4th equation will have a unity in the right hand side, as there is a 1 Volt point source present in the domain of the basis function D_4. This may be shown with the following transformation:

$$\begin{aligned} -\int_{S^{(5,3)}} D_4\mathbf{E}^{inc}(\mathbf{r})dS &= -\left(\int_{S^{(5)}} N_1^{(5)} \underbrace{\mathbf{E}^{inc}(\mathbf{r})}_{\neq 0,\, \mathbf{r}\in S^{(5)}} dS + \int_{S^{(3)}} N_2^{(3)} \underbrace{\mathbf{E}^{inc}(\mathbf{r})}_{\equiv 0,\, \mathbf{r}\in S^{(3)}} dS \right) \\ &= -\int_{s_1^{(5)}}^{s_2^{(5)}} N_1^{(5)}(s)\left(-\delta(s-s_2^{(5)})\right) ds = 1 \end{aligned}$$

This last equation can also be written explicitly as $I_1 Z_{41} + I_2 Z_{42} + I_3 Z_{43} + I_4 Z_{44} = 1$.

The equations may be put together and make up a system of four equations for four unknowns:

$$\begin{pmatrix} Z_{11} & Z_{12} & \cdots & Z_{14} \\ Z_{21} & & & \\ \vdots & & \ddots & \\ Z_{41} & & & Z_{44} \end{pmatrix} \begin{pmatrix} I_1 \\ I_2 \\ I_3 \\ I_4 \end{pmatrix} = \begin{pmatrix} 0 \\ 0 \\ 0 \\ 1 \end{pmatrix}, \text{ which can be written as } \mathbf{ZI} = \mathbf{V} .$$

The elements of the impedance matrix **Z** may be calculated. Their values are as follows:

```
-0.0021948 +59704i,   0.0021947 +27391i,   -0.0021947 - 1939i,    0.0010974 + 1752i
 0.0021947 +27391i,  -0.0021948 +59704i,    0.0021947 +27391i,   -0.0010974 -26661i
-0.0021947 - 1939i,   0.0021947 +27391i,   -0.0021948 +59704i,    0.0010974 -29852i
 0.0010974 + 1752i,  -0.0010974 -26661i,    0.0010974 -29852i,   -0.0010974 +57558i
```

The condition number of this impedance matrix is 6.3767. The eigenvalues are:

```
-0.0005884     + 118420i

-6.58e-005     +  70914i

-0.0064778     +  18571i

-0.0005496     +  28760i
```

The excitation vector, as per the discussions made earlier, may be written as

$$\mathbf{V}= [0, 0, 0, 1]^{T}.$$

The system $\mathbf{ZI} = \mathbf{V}$ can be solved and the current amplitudes of independent unknowns obtained. The remaining dependent unknowns may be easily found via the Kirchhoff's law as discussed earlier. Solving the system, i.e. finding $\mathbf{I}=\mathbf{Z}^{-1}\cdot\mathbf{V}$, gives the independent unknown currents (in Amperes) as

```
 2.3324e-12 + 5.3718e-6i

-3.1993e-12 - 10.588e-6i

 1.6349e-12 - 8.3558e-6i

-1.3604e-12 - 26.775e-6i
```

These values can be readily identified in the print-out made by the program and shown in the below.

Simulation Results (for a simplified task without the singleton):

Gen 1 is attached to the end 2 of wire 5
doublet# 1: $N_1^{(1)} + N_2^{(2)}$
doublet# 2: $N_1^{(3)} - N_1^{(2)}$
doublet# 3: $N_2^{(4)} - N_2^{(3)}$
doublet# 4: $N_1^{(5)} + N_2^{(3)}$
$I_2^{(w1)}$ = 2.33e-9 +0.00537j mA = 2.33e-6 +5.37j uA
$I_2^{(w3)}$ = -3.2e-9 -0.0106j mA = -3.2e-6 -10.6j uA
$I_1^{(w4)}$ = 1.63e-9 -0.00836j mA = 1.63e-6 -8.36j uA
$I_2^{(w5)}$ = -1.36e-9 -0.0268j mA = -1.36e-6 -26.8j uA
Wire # 1: s=-1.000, I=+0 +0, |I|=0 mA, arg(I)=0deg
Wire # 1: s=+0.000, I=+1.17e-009 +0.00269, |I|=0.00269 mA, arg(I)=90deg
Wire # 1: s=+1.000, I=+2.33e-009 +0.00537, |I|=0.00537 mA, arg(I)=90deg
Wire # 2: s=-1.000, I=+2.33e-009 +0.00537, |I|=0.00537 mA, arg(I)=90deg
Wire # 2: s=+0.000, I=+2.77e-009 +0.00798, |I|=0.00798 mA, arg(I)=90deg
Wire # 2: s=+1.000, I=+3.2e-009 +0.0106, |I|=0.0106 mA, arg(I)=90deg
Wire # 3: s=-1.000, I=-3e-009 -0.0184, |I|=0.0184 mA, arg(I)=-90deg
Wire # 3: s=+0.000, I=-3.1e-009 -0.0145, |I|=0.0145 mA, arg(I)=-90deg
Wire # 3: s=+1.000, I=-3.2e-009 -0.0106, |I|=0.0106 mA, arg(I)=-90deg
Wire # 4: s=-1.000, I=+1.63e-009 -0.00836, |I|=0.00836 mA, arg(I)=-90deg
Wire # 4: s=+0.000, I=+8.17e-010 -0.00418, |I|=0.00418 mA, arg(I)=-90deg

Wire # 4: s=+1.000, I=+0 +0, |I|=0 mA, arg(I)=0deg
Wire # 5: s=-1.000, I=+0 +0, |I|=0 mA, arg(I)=0deg
Wire # 5: s=+0.000, I=-6.8e-010 -0.0134, |I|=0.0134 mA, arg(I)=-90deg
Wire # 5: s=+1.000, I=-1.36e-009 -0.0268, |I|=0.0268 mA, arg(I)=-90deg

3.10 Far-Field Radiation Pattern Estimation

This section introduces a novel method for estimating the radiation pattern, the method based on a combination of two analytical techniques. This section should be considered together with a copy of the relevant paper provided in Appendix B.

The far-field region (otherwise referred to as the *Fraunhofer region*) is the region where the electromagnetic field distribution is essentially independent of the distance from the antenna [IEEE Standard, 31]. This requires that the electrical distance to an observer is large: $kR>>1$, where k [m^{-1}] is the propagation constant of the medium, and R [m] is the distance from the antenna to the observer.

Note:

In practice, the antennas have a finite, not infinitesimal size, produce a complex near field phase distribution, and so an additional size-related requirement becomes necessary. This requirement is frequently formulated [Stutzman and Thiele, 104] for a maximum phase error of π/8 radian as $R \geq 2D^2/\lambda$, *where* D *is the maximum dimension of the antenna and* λ *is the wavelength.*

The radiation pattern for an antenna in free space is normally calculated with an assumption of an infinite distance between the antenna and observation point.

With reference to [Balanis, 4], the electrical field in the Fraunhofer region may be expressed as a function of only magnetic vector potential[42]: $\vec{E} = -j\omega\vec{A}$. The electrical field in the far field zone due to a straight wire along z axis, with current distribution $I(s)$ may then be approximated with (2.26) alone:

[42] This relation is only valid for the transversal field components. The vector **A** often has a longitudinal component that does not result in any field component.

$$\vec{E}(\vec{r}\,') \approx -\vec{u}_\theta\, j\omega\mu_0 \cos\alpha \int_{s_1}^{s_2} I(s) g(R_e)\, ds\,, \tag{3.45}$$

where $\vec{u}_\theta \equiv (\vec{u}_z \cdot \vec{u}_r)$ is the dot product of the wire and observation point unit vectors.

In practice, the wire segments whose direction is different from *z* axis simply needs to use their own unit vectors instead of the $\vec{u}_z$. This comment also applies to other references to the unit vector $\vec{u}_z$ in this chapter.

At large distances from the source, the denominator of the Green's function (2.16) in (3.45) changes slowly. This may be taken advantage of by asymptotically expanding (2.27) into a series with respect to a large $|\vec{r}\,'|$. The dependence on the integration co-ordinate *s* becomes linear:

$$R_e \;\approx\; |\vec{r}\,'| - \vec{u}_{r'} \vec{r}_a(s) \;=\; |\vec{r}\,'| - \vec{u}_{r'} \vec{r}_c - \vec{u}_{r'} \vec{u}_z\, s \cos\alpha, \quad |\vec{r}\,'| \to \infty\,, \tag{3.46}$$

where $\vec{u}_{r'} = \dfrac{\vec{r}\,'}{|\vec{r}\,'|}$ is the unit vector towards the observer, $\vec{r}_c$ is the vector to the middle point of the wire, $\vec{u}_z$ is the unit vector of the wire, $s \in [s_1, s_2]$ is the local co-ordinate on the wire, and α is the opening angle of the cone (in terms of the truncated cone approximation for generalised wires discussed in Section 2.3 and illustrated with Figure 2-1 and Figure 3-20).

The current distribution *I*(*s*) in (3.45), approximated with polynomial (2.49), may be conveniently rewritten as

$$I(s) = \sum_{i=0}^{n_b-1} \hat{a}_i s^i\,, \tag{3.47}$$

where $\hat{a}_i = a_i / L^i$.

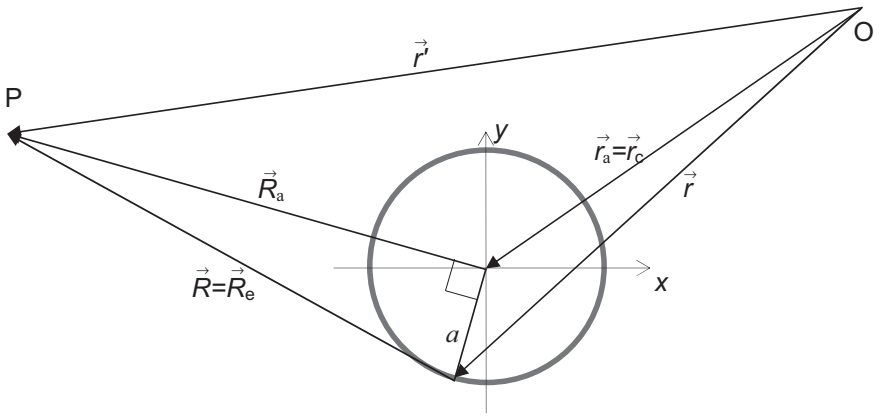

Figure 3-20. Mutual disposition of vectors for a central cross-section (shown with a circle) of a conical wire. The crossing of *x* and *y* is at the centre of the wire's axis. The unit vector $\vec{u}_z$ originates from the same crossing and points out of the page. The points O and P denote source and observation points, respectively.

The expressions (3.46) and (3.47) may be substituted into (3.45), and, without losing generality, an *i*-th term of the result may be considered. This permits to write down the partial electric field $\vec{E}^i$ due to the i^{th} term of the current approximation (3.47) on a single wire segment in the form of (3.48):

$$\begin{aligned}\vec{E}^i(\vec{r}') &= -\vec{u}_\theta\, j\omega\mu_0\, \hat{a}_i \cos\alpha \int_{s_1}^{s_2} s^i \frac{e^{-jkR_e}}{4\pi R_e} ds \\ &= -\vec{u}_\theta\, j\omega\mu_0\, \hat{a}_i \cos\alpha \frac{e^{-jk|\vec{r}'|}}{4\pi|\vec{r}'|} e^{+jk(\vec{u}_{r'}\cdot\vec{r}_c)} \int_{s_1}^{s_2} s^i e^{+jk(\vec{u}_{r'}\cdot\vec{u}_z)s\cos\alpha}\, ds \qquad (3.48) \\ i &= 0,1,2,\ldots \quad \text{and} \quad k|\vec{r}'| >> 1\end{aligned}$$

where $r' \equiv |\vec{r}'|$ is the distance from the centre point of the wire to the observation point, $(\vec{u}_{r'}\cdot\vec{r})$ and $(\vec{u}_{r'}\cdot\vec{r}_c)$ are the dot products of the vectors already mentioned in the description for (3.46).

To simplify further manipulations, with introduction of the notation $\xi = jk(\vec{u}_{r'}\cdot\vec{u}_z)\cos\alpha$, the integral is denoted as $F_i^u(\xi) = \int_{z_1}^{z_2} z^i e^{\xi z} dz$. **The details related to the computation**

of this function are published in [Lysko, 66]. For convenience, the full text of this reference is provided in Appendix B.

The total far-field electrical field $\vec{E}^{(wn)}$ due to a single straight wire segment may then be written as a sum of the partial fields $\vec{E}^{i}$ due to MoM basis functions/modes s^{i}, i=0,1,…n_b-1:

$$\vec{E}^{(wn)} \approx -\vec{u}_\theta j\omega\mu_0 \cos\alpha \frac{e^{-jkr'}}{4\pi r'} e^{+jk(\vec{u}_{r'}\cdot\vec{r}_c)} \sum_{i=0}^{n_b-1} \hat{a}_i F_i^u \left(jk(\vec{u}_{r'}\cdot\vec{u}_z)\cos\alpha\right). \qquad (3.49)$$

An antenna is a system, which usually includes a plurality of wires. The total electrical field $\vec{E}^{total}$ is the sum of the partial fields produced by the individual wires. This may be written as

$$\begin{aligned}\vec{E}^{total} &\approx \frac{e^{-jkr'}}{r'} \frac{-j\omega\mu_0}{4\pi} \sum_{l=1}^{n_w} \vec{u}_\theta^{(l)} \cos\alpha^{(l)} e^{jk\left(\vec{u}_{r'}\cdot\vec{r}_c^{(l)}\right)} \sum_{i=0}^{n_b^{(l)}-1} \hat{a}_i^{(l)} F_i^u \left(jk\left(\vec{u}_{r'}\cdot\vec{u}_z^{(l)}\right)\cos\alpha^{(l)}\right) \\ &= \vec{\mathrm{E}}(\theta,\phi)\frac{e^{-jkr'}}{r'}\end{aligned}, \qquad (3.50)$$

where the quantities with the superscript $^{(l)}$ refer to the wire number l.

The normalising factor $\frac{e^{-jkr'}}{r'}$ in the expression (3.50) signifies an outgoing spherical wave. It includes the total phase delay kr' introduced by the propagation from the antenna to the observer, as well as attenuation. This normalisation factor preserves the phase characteristics in $\vec{\mathrm{E}}(\theta,\phi)$ and removes an infinite attenuation for the assumed infinite distance.

If needed, the magnetic field may then be readily [Balanis, 5, Ch. 4] computed using a cross product of the total electric field $\vec{E}^{total}$ and the unit vector towards the observer $\vec{u}_{r'}$:

$$\vec{H}^{total} = \frac{1}{\eta}\left[\vec{u}_{r'}\times\vec{E}^{total}\right] = \frac{1}{\eta}\left[\vec{u}_{r'}\times\vec{\mathrm{E}}(\theta,\phi)\right]\frac{e^{-jkr'}}{r'} \equiv \vec{\mathrm{H}}(\theta,\phi)\frac{e^{-jkr'}}{r'}. \qquad (3.51)$$

Note:

The Matlab program developed calculates the radiation pattern quantities $\vec{\mathrm{E}}(\theta,\phi)$ *and* $\vec{\mathrm{H}}(\theta,\phi)$ *at a uniformly distributed discrete set of angles* θ *and* φ.

A list of most frequently encountered radiation parameters calculated by the Matlab program developed, and their definitions are based in the famous textbook [Balanis, 5, Ch.2].

3.11 Summary

This chapter contains a collection of the originally developed as well as of known methods, which addresses the speed and/or accuracy of the implementation of the method of moments (MoM). Parts of the chapter contain novel materials, for example a method to reduce the condition number of the impedance matrix and a practical technique for computing radiation pattern efficiently. Several other sections of the chapter review previously know approaches included due to their relevance. Many of these derivations and formulae could not be found in literature and were done originally.

The chapter can be structured into two subsequent parts. The issues affecting the system of linear equations itself, in particular the impedance matrix and excitation vector, are discussed in the first part of the chapter. The second part of the chapter begins with a method for solving the linear system and continues on computation of parameters which can be derived from the solution (current).

The first part of the chapter starts with a new and original study directed to reduce or limit the condition number of the impedance matrix. The condition number indicates the numerical stability of the linear system. If an iterative method of solving the linear system is required, the high condition number also tells about a possibly slow speed of convergence towards a solution. The study presented focuses on the junctions of more than two wires. It was found that the condition number could usually be reduced by an appropriate, wavelength-dependent choice of the reference wire, i.e. the wire that defines the common domain for the multiplet. A ten-fold reduction in the value of condition number was observed in the tests performed, illustrating the improvement due

to the technique proposed. The section also provides a set of guidelines as well as an empirical expression for selecting the reference wire.

Next, the chapter proceeds to discuss several techniques used to speed up the computation of the impedance matrix elements. These techniques include the singularity subtraction, symmetry and repeating elements considerations. The singularity subtraction technique reduces the degree of singularity of the integrand in a quadrature by treating the subtracted singularity analytically. This permits computing the remaining part of the integrand efficiently using simple numerical quadratures. A new technique for improving the efficiency of filling-in the impedance matrix is also mentioned here.

The chapter then continues with the treatments of the excitation source, loadings and symmetry plane. The excitation source used in this thesis is the delta-gap generator. The discussion and expressions for the delta-gap generator are presented. In particular, the singular behaviour often introduced by this quasi-static source and possible remedies are discussed. This is followed by derivations for the distributed and lumped loadings. After that, the symmetry plan implementation is examined from both coding and performance points of view.

The above-mentioned topics concern the formation of the impedance matrix and excitation vector, and the steps prior to solving the system of linear equations.

The following part of the chapter starts with a short review of the LU decomposition, a *de-facto* standard method for obtaining solutions of the system of linear equations efficiently in the presence of multiple generators. This is continued with a discussion on obtaining the network parameters, such as network impedance and network scattering matrices.

Next, an original discussion follows on the numerical uncertainty in the solution and its relation to the condition number of the impedance matrix and the accuracy of matrix elements. Using a simple empirical expression, it is shown that the ability to solve a problem may be limited by the accuracy of the impedance matrix elements and ultimately by the number representation. It is also proposed that the accuracy of the calculated network parameters may be estimated in a similar manner.

This is followed with a detailed numerical example of applying the method developed, to a structure composed of five wires and including a junction of three wires

The chapter also introduces a new and efficient method of computing a radiation pattern. The electrical field expressions are derived valid for polynomial basis functions in the far field zone. It is found that neither traditional numerical quadrature nor purely analytical integration can offer a solution that is both accurate and an efficient simultaneously. Instead, it is proposed to evaluate the integrals in one of two ways, depending on the electrical length of the wire segment. If the wire segment is short, Taylor's expansion is used. Otherwise, an analytical recursive integration method is applied. The results indicate that the efficiency of the proposed approach matches or exceeds the efficiency of the numerical quadrature routines used in commercial software.

Chapter 4. Multiple-Domain Basis Functions for Chains

This chapter focuses on establishing the understanding, mathematical basis, relationships, and basic algorithms for application of novel composite basis functions.

Each of these functions is defined on a domain composed of several geometrical segments connected in series, and is referred to as multiple domain or chain basis function.

The chapter begins with a discussion on the need for this extension of MoM, compared to the traditional approach of attributing a basis function per each geometrical element.

This is followed by an overview of the proposed method, and its application to a sequence of wires interconnected in series, herein referred to as a chain of wires.

Several original algorithms for the generation and the sub-division of chains are introduced and discussed. An original algorithm for the generation of a matrix **M***, the matrix that transforms and compresses the impedance matrix, is introduced for piecewise linear composite multiple domain basis functions. An example is then discussed in detail and used to highlight some perspective extensions of the approach.*

It is then shown that the techniques applied to accommodate piecewise linear basis functions may be immediately extended to the piecewise sinusoidal basis functions, as well as to any other piecewise-defined basis functions that are zero on one end. This extension uses a piecewise linear interpolation of a given function profile.

Finally, the technique devised is extended from the piecewise linear and sinusoidal basis functions to higher order polynomials. The computational complexity is estimated and compared to traditional MoM. It is also shown how to apply the multiple-domain basis functions to surface quadrilaterals, with virtually no new programming code.

4.1 Motivation

The previous chapters outline the Method of Moments (MoM) formulation where the basis functions rely on a piecewise linear *geometrical* approximation for the geometry

of arbitrary wire structures. The piecewise linear approximation simplifies evaluation of some of the integrals and is efficient in a computational sense. However, it also has drawbacks, including poor efficiency in modelling curvatures and limitations on the accuracy of modelling electrically small objects using the thin wire approximation.

4.1.1 On Accuracy and Computational Cost of Piecewise Linear Geometrical Approximation of Curvature

A piecewise linear geometrical approximation is inefficient for modelling smoothly curved geometries present in loops, helixes, spirals, parabolic reflectors, spheres and many other structures. For instance, a loop antenna modelled with a polygon instead of a perfect circle may have a shifted resonance frequency[43]. This is discussed qualitatively in Appendix A. A model of a parabolic reflector antenna, relying on *flat* quadrilateral or triangular elements, may produce inaccurate phase in the reflected fields and thus lead to an incorrect focus of the antenna's beam.

In both cases, a mesh of discrete points interconnected with straight segments defines the closeness of the geometry in a numerical model to the physically smooth original. In order to improve the accuracy of geometrical representation, the density of a piecewise linear mesh needs to be high enough (although the current on this mesh often varies slowly). This is especially important in automated[44] processing of mechanical CAD based designs, which often include small elements not essential to the accurate results but consuming resources through adding to the total count of unknowns.

[43] Hereinafter, the assumed condition for a resonance is to have the imaginary part of the input impedance being zero at the resonance frequency.

[44] In a manual preparation of a model, a skilled person should be able to offset many of the links between the geometrical accuracy and current representation accuracy. For example, by tuning the effective/equivalent radius of the loop in a numerical model, as shown in Appendix A, it is possible to reduce keep the number of required unknowns low.

A thin wire circular loop antenna may be considered as a simple example of a curved structure. Appendix A quantifies the relationship between the mesh density and accuracy of calculating the resonance frequency for this structure.

Example (refer to Appendix A for formulas):

In a single turn loop antenna, in order to achieve the resonance frequency estimate with a relative error of 10^{-3}, one needs 82 straight segments, translating into at least 82 unknowns in spite of the very simple current distribution pattern along the loop. An array of such antennas may thus require very substantial resources.

The expression (A.8) says that, if the resonance frequency accuracy requirement is made stricter by a factor of N_ε, the number of segments and unknowns must be increased by a factor of $\sqrt{N_\varepsilon}$. For example, in order to obtain an additional significant digit of accuracy (i.e. by 10 times) in the resonance frequency, the number of variables must be increased by a factor of $\sqrt{10} \approx 3.2$.

The inefficiency in such modelling is caused by the need to increase the number of straight segments when a higher accuracy in the *geometrical* modelling is required. In the traditional approach, the number of unknowns is directly linked to the number of segments.

It is possible to estimate the computational overhead created by this inefficiency. A direct solution of a linear system requires $O(N^3)$ floating-point operations (FLOPs), where N is the number of unknowns. Therefore, achieving the N_ε times better accuracy in calculating the resonance frequency of a loop antenna will require $O(N_\varepsilon^{3/2})$ times more time. The memory usage is also affected – it is directly proportional to the desired improvement in accuracy of resonance frequency.

It may also be mentioned that a simple uniform increase in the mesh density may also result in a more ill-conditioned system[45].

It is evident that refining a mesh can increase the geometrical approximation accuracy. However, this introduces more unknowns and often worsens the numerical stability of the resulting linear system. Thus, refining a mesh to accommodate curvatures is not an efficient method to model many types of antennas and scatterers that rely on curved geometry. In particular, this applies to the cases where the curvature radius is comparable to or smaller than the wavelength.

4.1.2 On a Limitation of the Thin Wire Approximation for Electrically Short Wires

Many practical structures, such as coils and helical antennas [Nakano, 80], in their physical realisation are often made of a wire. A tight winding found in radio frequency (RF) coils requires a high degree of curvature. Under these circumstances, the restrictions of the thin wire approximation (defined in Section 2.4) quickly become difficult to fulfil within a traditional, e.g. following [Harrington, 28], formulation. This is because the length of a single wire segment may become of the same order of magnitude or even smaller than the wire's radius. This limits the range of applications of the otherwise computationally-efficient thin wire approximation.

4.1.3 A Solution Proposed

In many cases, the problems stated in the previous sections may be easily addressed using an approach described in detail in the Sections to follow. In brief, the solution

[45] This is because the current amplitude variation profile (especially the nearly flat regions) might not require the exceedingly high mesh density. It rather introduces nearly cancelling values in the matrix. The result of subtractions between these values usually produces substantially higher error in the result than the errors present in the values themselves. In addition, an increase in the total number of round-off effects may also add a slight negative impact.

proposed is to extend the domain of a basis function from only one or two straight interconnected segments to an arbitrarily large number of interconnected segments. Thus, several interconnected segments may be covered by a single basis function. For certain structures, like helixes and spirals, this may dramatically decrease the number of unknowns needed, thus reducing the computational efforts.

Application of the higher-order basis functions on top of the aggregation of the domains may further improve the computational efficiency of this approach.

Such aggregation of multiple domains also helps to satisfy the current continuity better. This effect is achievable when the new composite basis function and its derivatives are continuous over the domains on which this basis function is defined. The improvement stems from the reduction in the number of points where the current continuity condition is satisfied poorly. Such points may be found, for instance, at the junctions of piecewise linear basis functions, where the function continuity is satisfied but not the derivative continuity.

Note:

The number of unknowns (and so the size of the impedance matrix) may be reduced with this technique. It may however be noted that the aggregation of interconnected straight segments does not reduce the amount of integration to be carried out in order to fill in the impedance matrix. In the process of domain aggregation, the multiple definite integrals are then simply joined at their respective limits into fewer integrals over larger segments, where the new limits include/cover all of the original integration segments. In this sense, the original impedance matrix elements are therein redistributed among the impedance matrix elements of a new, smaller, impedance matrix.

4.1.3.1 Example with Several Possibilities for Aggregation

A sample of structure, where the domain aggregation may be applied, is shown in Figure 4-1a. The figure shows a structure with 3 arms, composed of 6 straight wire segments. One of the arms is composed of 4 segments. They may be considered as

either four, or three, or two, or just one wire. Some of these configurations are shown in Figure 4-1b,c

The first (and the simplest) option is to apply piecewise linear (root-top/triangular) basis functions directly, as shown in Figure 4-1a. This is the way it is done in all commercial and freely available MoM codes known to the author. This is a simple and robust technique. It is robust in the sense that the ill-conditioning of the impedance matrix may, to a certain degree, be compensated for by improving the accuracy of evaluation of the impedance matrix integrals, as mentioned in Section 3.8. This approach does however require spending computational resources two times. Firstly, a larger number of variables is required for a finer mesh. Secondly, a higher accuracy in computing impedance matrix elements may be required to compensate for a larger and usually less stable impedance matrix.

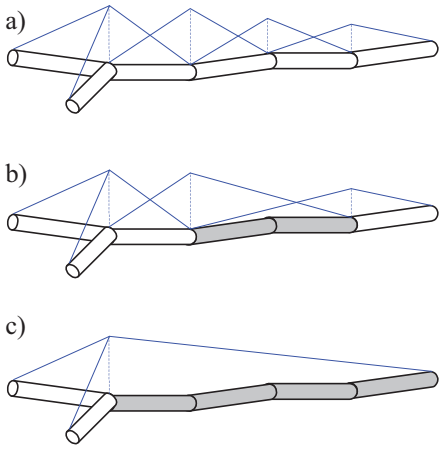

Figure 4-1 Examples of grouping 6 straight wire segments: a) piecewise linear basis functions applied to all of the wires, requiring 5 unknowns; b) 2 greyed wires are grouped, which reduces the number of unknowns to 4; c) piecewise linear basis function applied to a group of 4 segments, needing only 2 unknowns. Other combinations are not shown.

Figure 4-1b shows an intermediate option in reducing the computational requirements. In this scenario, the two middle wires in the right hand side arm (shown in grey) are considered as a logically single wire. In this figure, there are two piecewise linear

functions that are assigned to this logically single wire (with a bend). The resulting function for current distribution is now continuous within the domain of the two greyed wire segments. This may be compared with the same wire segments in Figure 4-1a, where four piece-wise linear functions (parts of two roof-top basis functions) are assigned to these very two wire segments.

This option is not optimal for an electrically very small structure, for it still requires more unknowns compared, for instance, to the grouping shown in Figure 4-1c. However, as the electrical size of the structure increases, the ability to model a current profile more complex than linear may become an advantage.

Figure 4-1c illustrates the aggregation scheme optimal for very low frequencies. The arm composed of 4 segments is considered as a single wire (with bends). The current distribution is approximated with a roof-top basis function (triangle current distribution). This scheme maximises the coverage (covers the largest number of individual wire segments with a single basis function), and thus minimises the number of unknowns. If this wide coverage is to be applied at higher frequencies, the higher-order basis functions should be used on this arm instead of a simple piecewise linear basis function.

4.1.3.2 Note on the Condition Number

The effects of the aggregation of domains may be given another, parallel, interpretation. It seems reasonable to assume that a better satisfaction of the continuity equation should enable a more stable and accurate modelling of structures. When the current over several geometrical segments is described with a single continuous (within these segments) function, the current over such an interval is a continuous function with continuous derivatives. As discussed earlier (incl. Section 3.8), this should, on average, provide a general improvement in the numerical stability of the linear system. The condition number depends on a plurality of factors. One of these factors is the degree of uniformity of the mesh. From the author's practical experience, when the mesh has some elements very small or large compared to the average size, this may lead to a substantially increased condition number, and thus a less stable linear system, giving less accurate results. This observation is also substantiated by the spectral theory

applied to the estimation of condition number [Chew et al., 10, Section 1.3.1, and Chapter 6].

4.1.3.3 Note on the Advantage of the Higher-Order Basis Functions

It is intuitively clear that, for large smoothly curved objects, the higher order basis functions should be able to take a greater advantage of this approach, as compared with the lower order basis functions (such as piece-wise linear functions). This is due to the fact that the higher order basis functions require a lower density of unknowns per wavelength (or per square wavelength for a surface formulation) to achieve the same accuracy, compared to linear basis functions [Chew, 10], [Kolundzija, 46]. Aggregating shorter segments into equivalent longer/larger structures should permit better utilisation of the full potential of the higher order basis functions.

4.1.3.4 Summary of Expectations

Based on the preliminary discussions stated above, the following may be expected from uniting several single segments into an aggregated structure described with a single basis function and defined on a domain composed of the domains of the original single segments:

- It should permit a better geometrical approximation accuracy for the piecewise linear geometrical modelling of curved structures by allowing to increase the density of mesh on them without a necessary increase in the total number of required unknowns. It is expected that this is possible without sacrificing performance in terms of either speed or accuracy;
- It should extend the applicability of the thin wire approximation by improving the ratio of the length of a wire to its radius. The ratio is improved by grouping several short interconnected wire segments into an equivalent longer wire;
- It should decrease the condition number for the resulting reduced rank impedance matrix;

- It may substantially reduce the memory (as $O(K^2)$) and processing power (as $O(K^3)$) requirements without affecting the accuracy. Here, K is the ratio of the number of the original basis functions to the number of the new, aggregated basis functions.

4.2 Aggregation of the Domains of the Basis Functions

Originally, the idea of aggregating the domains of the basis functions came about by analysing the structure of an impedance matrix element.

An impedance matrix element Z_{jp} due to a doublet is a sum of couplings between individual wire segments, as indicated by (2.71). The wire segments define the basis function's domain and thus the integration interval. The domain of integration $S^{(j)}$ for a j^{th} doublet consists of two sub-domains on the two wires making up this domain:

$$S^{(j)} = S_1^{(j)} + S_2^{(j)} \tag{4.1}$$

A single integral over the domain $S^{(j)}$ can thus be considered as a sum of two separate integrals over the two respective wire segments. Then the impedance matrix element, in a Galerkin realisation of the MoM, e.g. (2.71), may be written as

$$\begin{aligned} Z_{jp} &= \int_{S^{(j)}} f_j \int_{S^{(p)}} Lf_p \, dS^{(p)} dS^{(j)} = \int_{S_1^{(j)}+S_2^{(j)}} f_j \int_{S_1^{(p)}+S_2^{(p)}} Lf_p \, dS^{(p)} dS^{(j)} \\ &= \sum_{k=1}^{2}\sum_{l=1}^{2} \int_{S_k^{(j)}} f_j \int_{S_l^{(p)}} Lf_p \, dS^{(p)} dS^{(j)} = \sum_{k=1}^{2}\sum_{l=1}^{2} Z_{j_k p_l} \end{aligned} \tag{4.2}$$

The last part of this expression may be interpreted as grouping, aggregating or combining the impedances $Z_{j_k p_l}$ due to the coupling between individual wire segments (mathematically, through the corresponding basis functions) into a composite impedance, Z_{jp}. The domains of two wire segments are united to obtain an effective single basis function, the doublet, as shown in Figure 4-2. *It then should also be possible to aggregate more than two wire segments* to define a domain for a *single*, *composite* basis function.

On the other hand, reversing the situation, a single wire may be cut into several segments. As long as these segments are still electrically connected in series and

match/follow the geometry of the original wire, these segments and the original wire should have the same physical (electrical) properties, leading to the same current distribution.

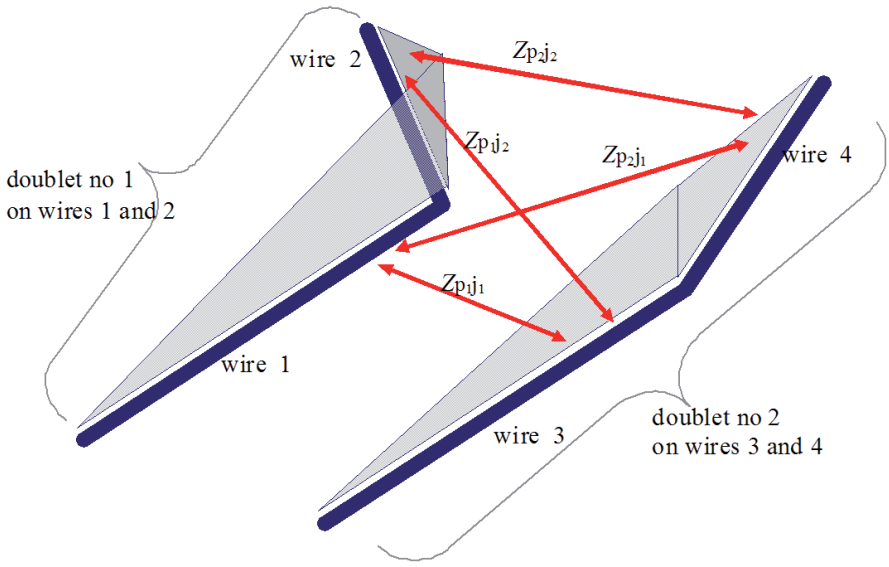

Figure 4-2. Decomposition of an element of the impedance matrix, Z_{jp}, into mutual couplings between individual elements of the two doublets used in this matrix element: $Z_{jp} = \sum_{k=1}^{2}\sum_{l=1}^{2} Z_{j_k p_l}$. Each doublet basis function is defined on a pair of wire segments (through respective associated piecewise linear functions shown with grey triangles). The four individual couplings (i.e. $Z_{j_k p_l}$) are shown with double-headed arrows. The assignment (numbering) of these couplings is only exemplary.

Therefore, a set of individual wire segments connected in series could also be aggregated *logically*, and considered as a single equivalent wire that has bends. The single basis function may then be defined on a respective domain described in a piecewise manner.

The original approach attempted by the author followed the ideas described in the above exactly. The impedance matrix elements were computed/integrated following the united domains of the wire segments. This approach had its drawback – many integrals were computed several times, since there was no simple mechanism to establish and reuse the redundant calculation of the same integral.

4.2.1 Reformulation in the form of a Matrix Approach

After two publications on a similar topic were found, namely by papers Shawn D. Rogers and Chalmers M. Butler [Rogers and Butler, 97], [Rogers and Butler, 96], the method was reformulated in terms of matrices following the approach in the cited papers.

The papers described essentially the same ideas, but applied in a different, non-Galerkin formulation of the MoM. In these two references, the expansion functions were piecewise linear and the testing functions were piecewise constant functions. The paper [Rogers and Butler, 96] introduced a formalisation of the approach in terms of matrix operations. This immediately solved the dilemma of avoiding redundant calculations.

The approach of [Rogers and Butler, 96] was adapted to the Galerkin technique used in this text (introduced in Section 2.2). Mathematically, an adaptation of this matrix approach to the Galerkin procedure may be expressed in a few simple steps:

It is assumed that it is possible to express the relationship between the vector of original (old) unknowns $\mathbf{I}$ and the vector with new unknowns $\tilde{\mathbf{I}}$ in a matrix form, as $\mathbf{I} = \mathbf{M}\tilde{\mathbf{I}}$. Herein, $\mathbf{M}$ is the basis functions' grouping/aggregating matrix $\mathbf{M}$, whose elements define how . The expression relating the old unknowns to the new ones is substituted into the original system of linear equations $\mathbf{ZI} = \mathbf{V}$. The resultant system $\mathbf{ZM}\tilde{\mathbf{I}} = \mathbf{V}$ is then left-multiplied by the transposed transformation matrix $\mathbf{M}$ to obtain the new system of linear equations: $\underbrace{\mathbf{M}^T\mathbf{ZM}}_{\tilde{\mathbf{Z}}}\tilde{\mathbf{I}} = \underbrace{\mathbf{M}^T\mathbf{V}}_{\tilde{\mathbf{V}}}$. This system may be rewritten in a short form as $\tilde{\mathbf{Z}}\tilde{\mathbf{I}} = \tilde{\mathbf{V}}$. Once this new system is solved and new unknowns $\tilde{\mathbf{I}}$ obtained, the original unknowns may be computed from $\mathbf{I} = \mathbf{M}\tilde{\mathbf{I}}$.

4.2.2 On Computational Complexity of Integration

It may also be noticed from the expression (4.2) for Z_{pj}, given above, that, for a fixed geometry, the amount of integration[46] required for filling in the impedance matrix (i.e. calculation of all the matrix elements) depends on the electrical size of the structure but not on the fineness of the mesh. Therefore, the technique cannot reduce the matrix fill time. However, for large matrices (systems with over about a thousand unknowns), the total time to obtain the solution is usually dominated by the time required to solve the system of linear equations [Kolundzija, 46]. This dominant part can be reduced through a reduction in the number of variables when applying the above-described techniques to modelling of large and smooth antennas and scatterers.

4.3 Defining and Identifying Chains

In order to set up rules and algorithms for uniting multiple individual wire segments into singled logically aggregated structures, it is necessary to give a sufficiently clear definition to the type of structures that may be united.

The ideas related to the aggregation of wire segments may be applied to a rather general class of wire structures. In this work, the aggregation is limited to structures where the current is considered as a function of only one variable, position along a wire. This follows the simplifications due to the thin wire approximation (Section 2.4). Herein, such structures are referred to as *chains*. Generalisation of the technique onto wire grids and solid surfaces is possible (as illustrated by Sections 4.13 and 4.12, respectively) but was left outside the main scope of this text.

A *chain* is identified as a number of wire segments electrically connected in series, so that for each inner node within a chain there are only 2 wires connected to this node. Other elements, such as free ends of wires, junctions with more than 2 wire segments,

[46] The phrase "amount of integration" here stands for the number of floating point operations (FLOP-s) required to calculate the integrals over the function of current (defined on a geometrical structure) with a given fixed accuracy.

generators, and lumped loads are herein considered as breaking the chains. Therefore, these points may only correspond to either the beginning or end of a chain.

The algorithm for identifying chains in a wire structure may be based on stepping through nodes, wires or junctions of wires. As an example, in the following algorithm, the chains are identified by sequentially stepping through all wires available.

4.3.1 Chain Generation Algorithm

1 It is assumed that there are N_w wires[47].

2 Each wire is assigned a flag indicating whether it has been processed. Initially, all flags are cleared. Number of chains N_c is set to zero.

3 For each wire, i=1,2, …, N_w, if this wire has not been processed, the following two step procedure is used to identify the beginning and end of a chain to which this wire belongs or should belong.

3.1 Forward search. The i-th wire (under consideration) is set as the current wire (in the sense of counting wire segments, not in the sense of movement of charges). The direction of search is set to be from the beginning of the current wire to its end – the starting point is the beginning of the current wire.

3.2 The wire(s) connected to the opposite end of the current wire are identified from the geometrical data (e.g. by finding all the wires attached to the respective node).

3.3 If there is only one wire attached to the end of the current wire and this wire has not been processed as yet, then the current wire is marked as belonging to a chain, and the attached wire is set as the new current wire. The forward search is continued from 3.2.

3.4 Otherwise, if there is no wire attached (free end), or if there is more than one wire attached to the end of the current wire, then the current, i-th, wire is considered as the last wire in the chain. Go to step 4.

4 Backward search. The i-th wire (under consideration from 3) is set as the current wire (again, in the sense of counting the wires or time, and not in the sense of movement of charges). The direction of search is set to be from the end of the current wire to its beginning – the starting point is the end of the current wire.

4.1 The wire(s) connected to the opposite end of the current wire are identified.

4.2 If there is only one wire attached to the end of the current wire and this wire has not been processed as yet, then the current wire is marked as belonging to a chain,

[47] To shorten the notations, the term “wire” in the text of the algorithm stands for a “wire segment”.

and the attached wire is set as the new current wire. The backward search is continued from 4.1.

4.3 Otherwise, if there is no wire attached (free end), or if there is more than one wire attached to the end of the current wire, then the current wire is considered as the last wire in the chain. Go to step 5.

5 Number of chains counter N_c is incremented by one. The record of the wires continuously/uninterruptedly connected in series as identified through the forward and backward searches is added to the record of chains.

6 If the i-th wire from 3 is not the last wire, then take the next available, (i+1)-th wire and go to 3. Otherwise, stop.

Note:

It is possible to use any other algorithm for chain generation or, later, for chain division or processing. In order to unify the approach, any remaining individual wire segments may be considered as / converted to chains (one wire segment per chain).

However, it will be shown later, in Section 4.11, that such a unification may affect the performance, and therefore need to be considered carefully.

Once the chains have been identified and recorded, some of the chains may be found exceedingly long. The restriction on the length of a chain may arise from a number factors: It may be the type of basis functions used (for example, the piecewise linear functions should not be used on the intervals larger than a quarter of wavelength). The integration subroutine may influence the length limits as well, since the accuracy of a quadrature depends on the length of the integration interval.

Thus, it might be necessary to limit the maximum length of a chain, and sub-divide the long chains into shorter ones. This process is considered in the next section, and is referred to as *meshing*.

4.4 Chain Meshing – Division of a Chain into Sub-Chains

A chain may be electrically very long, e.g. when modelling helical or spiral antennas. This may easily exceed the electrically small sizes of wire segments (up to, at most, a quarter of wavelength) supported by the piecewise linear basis functions. Even the hierarchical polynomials used as basis functions are incapable of accurate reproduction of the exact current variations when the wires become too long, and so the number of oscillations is high. The increase in the order of the approximating polynomial does not

provide an adequate increase in the accuracy of the approximation and may lead to an instability of the resulting linear system. Using floating point numbers with double precision[48], the maximum length of a wire should be limited to about twice the wavelength, and the maximum degree of polynomial to 9-10 [Kolundzija, 46]. This section addresses the need to divide electrically long chains, and introduces original solutions and discussions to this practical problem.

The same restrictions apply to chains. At the same time, in order to reduce the number of unknowns thus achieving the maximum efficiency, it is still desirable to keep the length of chains to a maximum.

There is a plurality of ways in which a chain may be divided into shorter chains, herein termed *sub-chains*. These ideas can be formulated into respective algorithms.

4.4.1 On an Optimum Sub-Division

A chain may need to be split into sub-chains that are shorter. Each new chain (sub-chain) is composed of some of the wire segments from the original chain. It is possible to split a chain into shorter sub-chains optimally. The term *optimal* herein may have a number of meanings. The meaning should reflect the criteria of optimality, such as enhancing efficiency, allowing to minimise the condition number etc. Some of these criteria are summarised below:

- Minimising the number of sub-chains;
- Minimising the span of lengths for the sub-chains: $\min\{ \max_i(l) - \min_i(l) \}$;
- Maximising the minimum length of a sub-chain: $\max\{ \min_i(l) \}$;
- Minimising the deviation from an average sub-chain length: $\min\{ \mathrm{std}(\Delta l_{ij}) \}$,

where Δl_{ij} is the difference between the lengths of two sub-chains.

Once a criterion or a weighted combination of criteria is selected, it is possible to find a solution (i.e. such a subdivision of a chain into a set of shorter sub-chains) that would be

[48] A double precision floating point number representation [IEEE 754-1985, 32] uses 51 bit for the mantissa. This gives the relative (fractional) uncertainty of $2^{-53} \approx 1.1 \cdot 10^{-16}$.

optimum in terms of this criterion. The search for optimum may be done iteratively, by testing all possible combinations of sub-divisions.

However, trying to find an optimum solution may take 2^{N-1} iterations. This is because N wires connected in series have N-1 inner junctions. There are two possible states for each junction between any two interconnected wire segments: these two segments are either considered as combined/grouped, or individual/separate. Thus, the two possible states at each of the N-1 junctions give a total of 2^{N-1} states.

This can also be illustrated (and possibly proven using induction), considering the following:

- chain has only 1 wire → only 1 combination possible:
  - (w_1)
- chain has 2 wires → 2 combinations possible:
  - (w_1) , (w_2)
  - (w_1 , w_2)
- chain has 3 wires → 4 combinations:
  - (w_1) , (w_2) , (w_3)
  - (w_1 , w_2) , (w_3)
  - (w_1) , (w_2 , w_3)
  - (w_1 , w_2 , w_3)
- chain has 4 wires → gives 8 combinations:
  - (w_1 , w_2 , w_3 , w_4)
  - (w_1 , w_2 , w_3) , (w_4)
  - (w_1 , w_2) , (w_3) , (w_4)
  - (w_1 , w_2) , (w_3 , w_4)
  - (w_1) , (w_2 , w_3 , w_4)
  - (w_1) , (w_2 , w_3) , (w_4)
  - (w_1) , (w_2) , (w_3 , w_4)
  - (w_1) , (w_2) , (w_3) , (w_4)
- and so on …

A Matlab script was written to look closer at the opportunities offered by this type of optimisation. Unfortunately, the numerical tests only confirmed the feasibility limitations related to the high number of iterations required by the optimisation. Nevertheless, it was possible to compare the results of the optimal solutions against the results produced by other algorithms, and this provided valuable reference information. Some of the results are discussed in the Sections 4.4.2 and 4.4.7.

4.4.2 An Example of Optimal Solutions in Sub-Dividing a Chain

The optimal sub-division of a chain may be illustrated on the following example. A chain is composed of 8 wire segments with (electrical[49]) lengths listed below:

2, 1, 2, 2, 2, 1, 1, and 1 (rad).

This sequence was selected out of several randomly generated sequences, as an illustration giving a useful insight into a comparison between the optimal approach and its sub-optimal alternatives (discussed later, in Sections 4.4.4-4.4.7). The sequence may originate from a variety of geometries, with a few samples displayed in Figure 4-3.

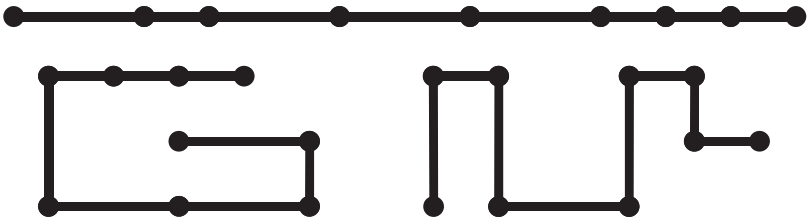

Figure 4-3. Three examples of sequences of wires whose electrical lengths make up the sequence {2, 1, 2, 2, 2, 1, 1, 1} (rad).

The parameter restricting the maximum permitted electrical length of a sub-chain was set to 4 rad.

[49] It may be noted that the units of length are irrelevant for this investigation, for it deals with rearranging of the fixed length segments (i.e. a set of numbers) in accordance with a pre-defined limit which has the same units.

Criterion no. 1 (“Max-Min”)

First, an optimum algorithm minimising the difference between the longest and the shortest sub-chains (denoted with “Max-Min”) was run. A complete listing for the optimisation process is shown:

```
SplitIntoSubChains( el_lengths, max_kx, 'o:Max-Min', Logs );
maxKL=4, maxEl=8, maxLen=12, Method=o:Max-Min

 0) m="O1" n=1 b=0000000 SubChain(s)=  2  1  2  2  2  1  1  1 weight=1
 1) m="O1" n=2 b=0000001 SubChain(s)=  2  1  2  2  2  1  2 weight=1
 2) m="O1" n=3 b=0000010 SubChain(s)=  2  1  2  2  2  2  1 weight=1
 3) m="O1" n=4 b=0000011 SubChain(s)=  2  1  2  2  2  3 weight=2
 4) m="O1" n=5 b=0000100 SubChain(s)=  2  1  2  2  3  1  1 weight=2
 5) m="O1" n=6 b=0000101 SubChain(s)=  2  1  2  2  3  2 weight=2
 6) m="O1" n=7 b=0000110 SubChain(s)=  2  1  2  2  4  1 weight=3
 7) m="O1" n=8 b=0000111 SubChain(s)=  2  1  2  2  5 ... not permitted (too long)
 8) m="O1" n=9 b=0001000 SubChain(s)=  2  1  2  4  1  1  1 weight=3
 9) m="O1" n=10 b=0001001 SubChain(s)=  2  1  2  4  1  2 weight=3
10) m="O1" n=11 b=0001010 SubChain(s)=  2  1  2  4  2  1 weight=3
11) m="O1" n=12 b=0001011 SubChain(s)=  2  1  2  4  3 weight=3
12) m="O1" n=13 b=0001100 SubChain(s)=  2  1  2  5  1  1 ... not permitted (too long)
13) m="O1" n=14 b=0001101 SubChain(s)=  2  1  2  5  2 ... not permitted (too long)
14) m="O1" n=15 b=0001110 SubChain(s)=  2  1  2  6  1 ... not permitted (too long)
15) m="O1" n=16 b=0001111 SubChain(s)=  2  1  2  7 ... not permitted (too long)
16) m="O1" n=17 b=0010000 SubChain(s)=  2  1  4  2  1  1  1 weight=3
17) m="O1" n=18 b=0010001 SubChain(s)=  2  1  4  2  1  2 weight=3
18) m="O1" n=19 b=0010010 SubChain(s)=  2  1  4  2  2  1 weight=3
19) m="O1" n=20 b=0010011 SubChain(s)=  2  1  4  2  3 weight=3
20) m="O1" n=21 b=0010100 SubChain(s)=  2  1  4  3  1  1 weight=3
21) m="O1" n=22 b=0010101 SubChain(s)=  2  1  4  3  2 weight=3
22) m="O1" n=23 b=0010110 SubChain(s)=  2  1  4  4  1 weight=3
23) m="O1" n=24 b=0010111 SubChain(s)=  2  1  4  5 ... not permitted (too long)
24) m="O1" n=25 b=0011000 SubChain(s)=  2  1  6  1  1  1 ... not permitted (too long)
25) m="O1" n=26 b=0011001 SubChain(s)=  2  1  6  1  2 ... not permitted (too long)
26) m="O1" n=27 b=0011010 SubChain(s)=  2  1  6  2  1 ... not permitted (too long)
27) m="O1" n=28 b=0011011 SubChain(s)=  2  1  6  3 ... not permitted (too long)
28) m="O1" n=29 b=0011100 SubChain(s)=  2  1  7  1  1 ... not permitted (too long)
29) m="O1" n=30 b=0011101 SubChain(s)=  2  1  7  2 ... not permitted (too long)
30) m="O1" n=31 b=0011110 SubChain(s)=  2  1  8  1 ... not permitted (too long)
31) m="O1" n=32 b=0011111 SubChain(s)=  2  1  9 ... not permitted (too long)
32) m="O1" n=33 b=0100000 SubChain(s)=  2  3  2  2  1  1  1 weight=2
33) m="O1" n=34 b=0100001 SubChain(s)=  2  3  2  2  1  2 weight=2
34) m="O1" n=35 b=0100010 SubChain(s)=  2  3  2  2  2  1 weight=2
35) m="O1" n=36 b=0100011 SubChain(s)=  2  3  2  2  3 weight=1
36) m="O1" n=37 b=0100100 SubChain(s)=  2  3  2  3  1  1 weight=2
37) m="O1" n=38 b=0100101 SubChain(s)=  2  3  2  3  2 weight=1
38) m="O1" n=39 b=0100110 SubChain(s)=  2  3  2  4  1 weight=3
39) m="O1" n=40 b=0100111 SubChain(s)=  2  3  2  5 ... not permitted (too long)
40) m="O1" n=41 b=0101000 SubChain(s)=  2  3  4  1  1  1 weight=3
41) m="O1" n=42 b=0101001 SubChain(s)=  2  3  4  1  2 weight=3
42) m="O1" n=43 b=0101010 SubChain(s)=  2  3  4  2  1 weight=3
43) m="O1" n=44 b=0101011 SubChain(s)=  2  3  4  3 weight=2
44) m="O1" n=45 b=0101100 SubChain(s)=  2  3  5  1  1 ... not permitted (too long)
45) m="O1" n=46 b=0101101 SubChain(s)=  2  3  5  2 ... not permitted (too long)
46) m="O1" n=47 b=0101110 SubChain(s)=  2  3  6  1 ... not permitted (too long)
47) m="O1" n=48 b=0101111 SubChain(s)=  2  3  7 ... not permitted (too long)
48) m="O1" n=49 b=0110000 SubChain(s)=  2  5  2  1  1  1 ... not permitted (too long)
49) m="O1" n=50 b=0110001 SubChain(s)=  2  5  2  1  2 ... not permitted (too long)
50) m="O1" n=51 b=0110010 SubChain(s)=  2  5  2  2  1 ... not permitted (too long)
```

51) m="O1" n=52 b=0110011 SubChain(s)= 2 5 2 3 ... not permitted (too long)
52) m="O1" n=53 b=0110100 SubChain(s)= 2 5 3 1 1 ... not permitted (too long)
53) m="O1" n=54 b=0110101 SubChain(s)= 2 5 3 2 ... not permitted (too long)
54) m="O1" n=55 b=0110110 SubChain(s)= 2 5 4 1 ... not permitted (too long)
55) m="O1" n=56 b=0110111 SubChain(s)= 2 5 5 ... not permitted (too long)
56) m="O1" n=57 b=0111000 SubChain(s)= 2 7 1 1 1 ... not permitted (too long)
57) m="O1" n=58 b=0111001 SubChain(s)= 2 7 1 2 ... not permitted (too long)
58) m="O1" n=59 b=0111010 SubChain(s)= 2 7 2 1 ... not permitted (too long)
59) m="O1" n=60 b=0111011 SubChain(s)= 2 7 3 ... not permitted (too long)
60) m="O1" n=61 b=0111100 SubChain(s)= 2 8 1 1 ... not permitted (too long)
61) m="O1" n=62 b=0111101 SubChain(s)= 2 8 2 ... not permitted (too long)
62) m="O1" n=63 b=0111110 SubChain(s)= 2 9 1 ... not permitted (too long)
63) m="O1" n=64 b=0111111 SubChain(s)= 2 10 ... not permitted (too long)
64) m="O1" n=65 b=1000000 SubChain(s)= 3 2 2 2 1 1 1 weight=2
65) m="O1" n=66 b=1000001 SubChain(s)= 3 2 2 2 1 2 weight=2
66) m="O1" n=67 b=1000010 SubChain(s)= 3 2 2 2 2 1 weight=2
67) m="O1" n=68 b=1000011 SubChain(s)= 3 2 2 2 3 weight=1
68) m="O1" n=69 b=1000100 SubChain(s)= 3 2 2 3 1 1 weight=2
69) m="O1" n=70 b=1000101 SubChain(s)= 3 2 2 3 2 weight=1
70) m="O1" n=71 b=1000110 SubChain(s)= 3 2 2 4 1 weight=3
71) m="O1" n=72 b=1000111 SubChain(s)= 3 2 2 5 ... not permitted (too long)
72) m="O1" n=73 b=1001000 SubChain(s)= 3 2 4 1 1 1 weight=3
73) m="O1" n=74 b=1001001 SubChain(s)= 3 2 4 1 2 weight=3
74) m="O1" n=75 b=1001010 SubChain(s)= 3 2 4 2 1 weight=3
75) m="O1" n=76 b=1001011 SubChain(s)= 3 2 4 3 weight=2
76) m="O1" n=77 b=1001100 SubChain(s)= 3 2 5 1 1 ... not permitted (too long)
77) m="O1" n=78 b=1001101 SubChain(s)= 3 2 5 2 ... not permitted (too long)
78) m="O1" n=79 b=1001110 SubChain(s)= 3 2 6 1 ... not permitted (too long)
79) m="O1" n=80 b=1001111 SubChain(s)= 3 2 7 ... not permitted (too long)
80) m="O1" n=81 b=1010000 SubChain(s)= 3 4 2 1 1 1 weight=3
81) m="O1" n=82 b=1010001 SubChain(s)= 3 4 2 1 2 weight=3
82) m="O1" n=83 b=1010010 SubChain(s)= 3 4 2 2 1 weight=3
83) m="O1" n=84 b=1010011 SubChain(s)= 3 4 2 3 weight=2
84) m="O1" n=85 b=1010100 SubChain(s)= 3 4 3 1 1 weight=3
85) m="O1" n=86 b=1010101 SubChain(s)= 3 4 3 2 weight=2
86) m="O1" n=87 b=1010110 SubChain(s)= 3 4 4 1 weight=3
87) m="O1" n=88 b=1010111 SubChain(s)= 3 4 5 ... not permitted (too long)
88) m="O1" n=89 b=1011000 SubChain(s)= 3 6 1 1 1 ... not permitted (too long)
89) m="O1" n=90 b=1011001 SubChain(s)= 3 6 1 2 ... not permitted (too long)
90) m="O1" n=91 b=1011010 SubChain(s)= 3 6 2 1 ... not permitted (too long)
91) m="O1" n=92 b=1011011 SubChain(s)= 3 6 3 ... not permitted (too long)
92) m="O1" n=93 b=1011100 SubChain(s)= 3 7 1 1 ... not permitted (too long)
93) m="O1" n=94 b=1011101 SubChain(s)= 3 7 2 ... not permitted (too long)
94) m="O1" n=95 b=1011110 SubChain(s)= 3 8 1 ... not permitted (too long)
95) m="O1" n=96 b=1011111 SubChain(s)= 3 9 ... not permitted (too long)
96) m="O1" n=97 b=1100000 SubChain(s)= 5 2 2 1 1 1 ... not permitted (too long)
97) m="O1" n=98 b=1100001 SubChain(s)= 5 2 2 1 2 ... not permitted (too long)
98) m="O1" n=99 b=1100010 SubChain(s)= 5 2 2 2 1 ... not permitted (too long)
99) m="O1" n=100 b=1100011 SubChain(s)= 5 2 2 3 ... not permitted (too long)
100) m="O1" n=101 b=1100100 SubChain(s)= 5 2 3 1 1 ... not permitted (too long)
101) m="O1" n=102 b=1100101 SubChain(s)= 5 2 3 2 ... not permitted (too long)
102) m="O1" n=103 b=1100110 SubChain(s)= 5 2 4 1 ... not permitted (too long)
103) m="O1" n=104 b=1100111 SubChain(s)= 5 2 5 ... not permitted (too long)
104) m="O1" n=105 b=1101000 SubChain(s)= 5 4 1 1 1 ... not permitted (too long)
105) m="O1" n=106 b=1101001 SubChain(s)= 5 4 1 2 ... not permitted (too long)
106) m="O1" n=107 b=1101010 SubChain(s)= 5 4 2 1 ... not permitted (too long)
107) m="O1" n=108 b=1101011 SubChain(s)= 5 4 3 ... not permitted (too long)
108) m="O1" n=109 b=1101100 SubChain(s)= 5 5 1 1 ... not permitted (too long)
109) m="O1" n=110 b=1101101 SubChain(s)= 5 5 2 ... not permitted (too long)
110) m="O1" n=111 b=1101110 SubChain(s)= 5 6 1 ... not permitted (too long)
111) m="O1" n=112 b=1101111 SubChain(s)= 5 7 ... not permitted (too long)
112) m="O1" n=113 b=1110000 SubChain(s)= 7 2 1 1 1 ... not permitted (too long)
113) m="O1" n=114 b=1110001 SubChain(s)= 7 2 1 2 ... not permitted (too long)

```
114) m="O1" n=115 b=1110010 SubChain(s)=  7  2  2  1 ... not permitted (too long)
115) m="O1" n=116 b=1110011 SubChain(s)=  7  2  3 ... not permitted (too long)
116) m="O1" n=117 b=1110100 SubChain(s)=  7  3  1  1 ... not permitted (too long)
117) m="O1" n=118 b=1110101 SubChain(s)=  7  3  2 ... not permitted (too long)
118) m="O1" n=119 b=1110110 SubChain(s)=  7  4  1 ... not permitted (too long)
119) m="O1" n=120 b=1110111 SubChain(s)=  7  5 ... not permitted (too long)
120) m="O1" n=121 b=1111000 SubChain(s)=  9  1  1  1 ... not permitted (too long)
121) m="O1" n=122 b=1111001 SubChain(s)=  9  1  2 ... not permitted (too long)
122) m="O1" n=123 b=1111010 SubChain(s)=  9  2  1 ... not permitted (too long)
123) m="O1" n=124 b=1111011 SubChain(s)=  9  3 ... not permitted (too long)
124) m="O1" n=125 b=1111100 SubChain(s)= 10  1  1 ... not permitted (too long)
125) m="O1" n=126 b=1111101 SubChain(s)= 10  2 ... not permitted (too long)
126) m="O1" n=127 b=1111110 SubChain(s)= 11  1 ... not permitted (too long)
127) m="O1" n=128 b=1111111 SubChain(s)= 12 ... not permitted (too long)
 Best solution(s) with "Max-Min" is(are) #  0  1  2 35 37 67 69 with weight = 1
 1) solution# 0  (bits=0000000): ( w1) ; ( w2) ; ( w3) ; ( w4) ; ( w5) ; ( w6) ; ( w7) ; ( w8) ;
 2) solution# 1  (bits=0000001): ( w1) ; ( w2) ; ( w3) ; ( w4) ; ( w5) ; ( w6) ; ( w7 w8) ;
 3) solution# 2  (bits=0000010): ( w1) ; ( w2) ; ( w3) ; ( w4) ; ( w5) ; ( w6 w7) ; ( w8) ;
 4) solution#35  (bits=0100011): ( w1) ; ( w2 w3) ; ( w4) ; ( w5) ; ( w6 w7 w8) ;
 5) solution#37  (bits=0100101): ( w1) ; ( w2 w3) ; ( w4) ; ( w5 w6) ; ( w7 w8) ;
 6) solution#67  (bits=1000011): ( w1 w2) ; ( w3) ; ( w4) ; ( w5) ; ( w6 w7 w8) ;
 7) solution#69  (bits=1000101): ( w1 w2) ; ( w3) ; ( w4) ; ( w5 w6) ; ( w7 w8) ;
List of 7 best solution(s) using method "o:Max-Min":
 1) solution: ( w1 ) ; ( w2 ) ; ( w3 ) ; ( w4 ) ; ( w5 ) ; ( w6 ) ; ( w7 ) ; ( w8 ).  Sum(Len)=12
 2) solution: ( w1 ) ; ( w2 ) ; ( w3 ) ; ( w4 ) ; ( w5 ) ; ( w6 ) ; ( w7 w8 ).  Sum(Len)=12
 3) solution: ( w1 ) ; ( w2 ) ; ( w3 ) ; ( w4 ) ; ( w5 ) ; ( w6 w7 ) ; ( w8 ).  Sum(Len)=12
 4) solution: ( w1 ) ; ( w2 w3 ) ; ( w4 ) ; ( w5 ) ; ( w6 w7 w8 ).  Sum(Len)=12
 5) solution: ( w1 ) ; ( w2 w3 ) ; ( w4 ) ; ( w5 w6 ) ; ( w7 w8 ).  Sum(Len)=12
 6) solution: ( w1 w2 ) ; ( w3 ) ; ( w4 ) ; ( w5 ) ; ( w6 w7 w8 ).  Sum(Len)=12
 7) solution: ( w1 w2 ) ; ( w3 ) ; ( w4 ) ; ( w5 w6 ) ; ( w7 w8 ).  Sum(Len)=12
>>
```

This copy of the solution trace shows that it took 128 iterations to check all the necessary combinations for just 8 wires.

In this process, some of the tests were discarded (e.g. #7, #12, etc. show “not permitted”) since some of the sub-chains were too long (i.e. exceeded the maximum permitted length). Otherwise, the total weight is calculated as the difference between the maximum length of a sub-chain and the minimum length of a sub-chain. The lowest weight is considered as the criterion for the “Best Solutions”.

The optimisation algorithm produced 7 solutions of equal significance (with regards to the optimisation criterion).

Note:

Out of these 7 solutions, it is then possible to select the last 4 solutions, since they result in the smallest number of sub-chains (5), and are thus expected to be the most efficient computationally.

These four solutions have different distributions of the length for the sub-chains (2,3,2,2,3; 2,3,2,3,2; 3,2,2,2,3; and 3,2,2,3,2). Probably, the solutions that have the greatest difference (most change) in the length of the neighbouring elements should be discarded, but the correct answer to the optimality in this sense requires a separate investigation.

Criterion no. 2 ("MinL")

Next, the optimisation criterion was changed to a maximisation of the minimal length of a sub-chain, denoted with "MinL". A reduced/summarised solution trace is shown:

```
maxKL=4, maxEl=8, maxLen=12, Method=o:MinL

Best solution(s) with "MinL" is(are) # 35 37 43 67 69 75 83 85 with weight = 0.5
List of 8 best solution(s) using method "o:MinL":
 1) solution: ( w1 ) ; ( w2 w3 ) ; ( w4 ) ; ( w5 ) ; ( w6 w7 w8 ).  Sum(Len)=12
 2) solution: ( w1 ) ; ( w2 w3 ) ; ( w4 ) ; ( w5 w6 ) ; ( w7 w8 ).  Sum(Len)=12
 3) solution: ( w1 ) ; ( w2 w3 ) ; ( w4 w5 ) ; ( w6 w7 w8 ).  Sum(Len)=12
 4) solution: ( w1 w2 ) ; ( w3 ) ; ( w4 ) ; ( w5 ) ; ( w6 w7 w8 ).  Sum(Len)=12
 5) solution: ( w1 w2 ) ; ( w3 ) ; ( w4 ) ; ( w5 w6 ) ; ( w7 w8 ).  Sum(Len)=12
 6) solution: ( w1 w2 ) ; ( w3 ) ; ( w4 w5 ) ; ( w6 w7 w8 ).  Sum(Len)=12
 7) solution: ( w1 w2 ) ; ( w3 w4 ) ; ( w5 ) ; ( w6 w7 w8 ).  Sum(Len)=12
 8) solution: ( w1 w2 ) ; ( w3 w4 ) ; ( w5 w6 ) ; ( w7 w8 ).  Sum(Len)=12
>>
```

There were 8 solutions found. The last few solutions require only 4 sub-chains. It is then possible to continue a discussion on the most promising out of the optimal solutions, like it was done for the results of the previous optimisation criterion.

Criterion no. 3 ("std")

Finally, the optimisation criterion was changed to a minimisation of the standard deviation of the lengths of the sub-chains:

```
maxKL=4, maxEl=8, maxLen=12, Method=o:std

Best solution(s) with "std" is(are) #  1  2 with weight = 0.48795
List of 2 best solution(s) using method "o:std":
 1) solution: ( w1 ) ; ( w2 ) ; ( w3 ) ; ( w4 ) ; ( w5 ) ; ( w6 ) ; ( w7 w8 ).  Sum(Len)=12
 2) solution: ( w1 ) ; ( w2 ) ; ( w3 ) ; ( w4 ) ; ( w5 ) ; ( w6 w7 ) ; ( w8 ).  Sum(Len)=12
>>
```

There were 2 solutions found. These solutions are very different compared to the results of the 2 previous optimisation criteria. The minimisation of the standard deviation produced the greatest number of sub-chains (7). This makes this criterion the least efficient, computationally. Also, the computation of the weight requires usage of floating point numbers (which could be avoided in the previously discussed criteria).

4.4.3 Computational Complexity of Finding Optimal Solutions for the Sub-Division of a Chain

The optimization process described above can give a true geometrically optimal solution for any structure. However, for a complex structure, this approach immediately leads to a prohibitively large number of states to be considered and tested.

In structures having thousands of wires, combined in a plurality of chains, it may take a considerable time to examine this, exponentially high, number of possible combinations. The asymptotical behaviour of the exponential function 2^{N-1} for a large N, produces numbers that are much larger than the number of operations required to solve the system of linear equations, i.e. $O(N^3)$. For example, with only 12 wires, i.e. N=12, the number of required search iterations equals 2^{N-1} =2048. This value is already greater than the number of operations to solve the system, that is less than N^3=1728.

This makes finding an optimum solution a computationally unfeasible choice for most practical situations. A different approach is required.

4.4.4 Algorithm *A* – a Simple Algorithm

A very simple, computationally efficient method was devised for splitting a chain into shorter sub-chains under a restriction on the maximum permitted electrical length of any sub-chain. The algorithm is as follows.

Assume that all the information about chains is kept in a structured array *chains*(j), j=1,2, …, N_c. Each element of such array, *chains*(j), stores the information about all wires that belong to this chain (e.g. wire numbers and sequence in which they are connected).

For each chain *chains*(j), j=1,2, …, N_c, in the list of N_c chains "*chains*", repeat the following:

1. Take the current i^{th} chain, *chains*(i).
2. Prepare an empty list of chains, *temp_chains*.
3. While the total electrical length of the wires in the current chain is greater than a predefined maximum, repeat the following step (3.1):

3.1. Find the continuous portion of the current chain (one to several wires connected in series), whose total length is within the predefined maximum, remove it from the current chain, and add it to the list of chains *temp_chains*.

4. If the list of chains is not empty, (a) adjust the current chain record, and (b) add the chains from this list *temp_chains* to the end of the original list of chains.

This is a simple algorithm and it also requires a very small number of operations. However, practice has showed several key drawbacks of this approach. It is possible to see that, regardless of how many wires were present in the original chain, the last new sub-chain may happen to consist of only one wire segment. The length of this chain may be as small as the length of that wire segment. Then the situation is possible where some chains are much shorter than others, which may in turn lead to poor numerical properties of the impedance matrix.

An attempt to compensate for this drawback was made in the next version of the chain-splitting algorithm.

4.4.5 Algorithm *B* – a "2 Last Wires" Algorithm

This algorithm tries to look one step ahead, and to equalise the lengths of the two last sub-chains (if possible). The algorithm is more complex, and includes the following steps:

1. Summate through the lengths of wires, l_m, composing the chain cumulatively into an array $A=\{a_i\}$, where $a_i = \sum_{m=1,2,\ldots,i} (l_m)$, $i=1,2, \ldots, N$.
2. Set starting index $k=1$. Set new chain index $n=0$.
3. Search A starting from k, and find all $\{a_i\}$, $i=1,2, \ldots, j$, elements of A, such that each one is the closest to but it is not greater than the maximum allowed length L_{max}.
4. Take the elements $\{a_1 \ldots a_j\}$ as the 1st sub-chain, C_1: $C_1=\{c^1_i\}$, where $c_i = a_i$, $i=1,2,\ldots,j$.
5. If the index j has not reached the end of A, proceed to following step. Otherwise, go to step 11.
6. Take the elements $\{a_{j+1} \ldots a_N\}$ with a_j subtracted from each one, as the 2nd sub-chain, C_2: $C_2=\{c^2_i\}$, where $c^2_i = a_{i+j} - a_i$, $i=1,2, \ldots, N-j$.
7. Calculate the absolute difference between total lengths of these chains, $d_{12}=|c^2_j - c^1_i|$.
8. Initialise the variable d_{12p} (variable to store the value of d_{12} from the previous iteration), setting it to a large number, e.g. infinity: $d_{12p}=+\infty$.

9. Look for the optimum division in two parts - While $c_j < L_{max}$, and C_1 has more than 2 elements, and $d_{12} < d_{12p}$, do iterations:
   a. Decrease the index j by one: $j = j - 1$.
   b. Set the 1st sub-chain, C_1 and the 2nd sub-chain, C_2 as were done in steps 4 and 6.
   c. Save the value of d_{12} into a temporary variable t. Set $d_{12p} = d_{12}$, and $d_{12p}=t$.
   d. Loop back to step 9.
10. If the previous iteration of step 8 has had a smaller difference of total lengths, $d_{12p} < d_{12}$, then roll the value of index j one iteration back: $j=j-1$. Then set the 1st sub-chain, C_1 and the 2nd sub-chain, C_2 as were done in steps 4 and 6.
11. Increase new chain index n: $n=n+1$, and add chain C_1 to the list. Then take the elements of C_1 out of A, and adjust the starting index: $k=k+j$.
12. If d_{12p} has been used (d_{12p} is not equal infinity), and C_2 is not empty, and sum of lengths kept in C_2 is less than the permitted threshold L_{max}, then add the chain C_2 to the list, and do adjustments like with C_1 in the pervious step.
13. If k is greater than the length of the array, stop the algorithm. Otherwise, jump to step 3.

This algorithm version *B* has shown some improvement when compared to the Algorithm *A*. However, it still has a good chance of failure when the wire segments composing a chain are very short, and when there are many of them.

The problem in both algorithms is related to the localisation of the segment processing. In the next step, another approach was tested. That approach is based on a "globalisation" of the sub-division from considering one or two individual segments to a set of all segments in the chain.

4.4.6 Algorithm *C* – a Pseudo-Optimal Solution

Where conditions permit, it is desirable to have a well-grouped (narrow) distribution of chain lengths. The following algorithm was designed to provide a nearly optimum solution, grouping the segment lengths to minimise the difference between the lengths of the resulting sub-chains. In each iteration, it tries to split the remaining part of the chain into equal sub-chains (unlike the first algorithm that targeted maximisation of the lengths). The algorithm is nearly as fast as the previous algorithm.

This algorithm may be written in terms of the Matlab like code:

Start with the 1st wire.
```
ind0 = 1;
```
While the currently processed wire is not the last wire in the chain, repeat the steps:
```
while ind0<=length(el_lengths), %length(el_lengths(ind0:end))>0
```
Calculate a cumulative sum of the wire lengths
```
    cs = cumsum(el_lengths(ind0:end));
```
Estimate the number of parts N_{parts} that the chain should be divided into as the ratio of the electrical chain length to the maximum permitted electrical length of a wire/chain
```
    Nparts = cs(end)/max_kx;     dLNparts = cs(end)/Nparts;
```
Calculate the same ratio as rounded towards plus infinity and set to N_{ceil}
```
    Nceil = ceil( Nparts );      dLNceil = cs(end)/Nceil;
```
Use the cumulative sum to find the set of wires ind1 whose total electrical length is within the maximum permitted electrical length
```
    ind1 = find( cs <= dLNparts );
    if isempty(ind1), error('Wires are too long (electrically)!!!');
end;
```
Use the cumulative sum of wires from the set ind1 to find the set of wires ind2 whose total electrical length is greater than or equal to the total length divided by N_{ceil}
```
    ind2 = find( cs(ind1) >= dLNceil );
    if ~isempty(ind2),
```
If the set ind2 is not empty, take the combination from the set, giving the smallest total length
```
        ind3 = ind2(1); % take the smallest one
    else
```
Otherwise, take the combination of wires from the set ind1, giving the largest total length
```
        % well, well, well ... no x, such that dLNceil <= x <=
dLNparts
        % things are smaller here!!! BAD!
        % unfortunately, can do nothing about it.
        % take the largest available ...
        ind3 = ind1(end);   % NB! This
    end;
```
The combination of wires is attributed to a new sub-chain
```
% ADD the SUB-CHAIN TO a LIST HERE ...
```
Remove/forget the attributed wires from the original long chain
```
% now, perpaps, let's look at the remaining part "freshly"
    % like it is a brand new chain that requires sub-division
    ind0 = ind0 + ind3;
end
```

In the tests, this algorithm produced sub-chains that did not have defects attributed to the previous versions (*A* and *B*). This may be illustrated with an example based on the same data set as was used in Section 4.4.2.

4.4.7 Algorithms *A*, *B* and *C* compared

The non-optimal algorithms (described in Sections 4.4.4 - 4.4.6) were executed using the same input data set. The results were compared against each other and also against the results obtained by the generic optimization algorithm with respect to various criteria (discussed in Sections 4.4.1 - 4.4.3).

The algorithm *A* produced the following results:

```
maxKL=4, maxEl=8, maxLen=12, Method=A
 1)m="A"  2 segments from  1- 2: Len=3
 2)m="A"  2 segments from  3- 4: Len=4
 3)m="A"  3 segments from  5- 7: Len=4
 4)m="A"  1 segments from  8- 8: Len=1
List of 1 best solution(s) using method "A":
 1)    solution: ( w1 w2 ) ; ( w3 w4 ) ; ( w5 w6 w7 ) ; ( w8 ).  Sum(Len)=12
```

The last sub-chain in the solution contains the wire segment number 8 only and has length of 1. On the other hand, the sub-chain before the last is composed of wires 5, 6 and 7, and has a length of 4. This illustrates the problem attributed to this overly simple algorithm – it does not care about the length of the last sub-chain, which may lead to an unnecessarily high condition number.

The results of a run with the algorithm *B* follow:

```
maxKL=4, maxEl=8, maxLen=12, Method=B
 1)m="B"  2 el. from  1- 2: Len=3
 2)m="B"  2 el. from  3- 4: Len=4
 3)m="B"  1 el. from  5- 5: Len=2
*4)m="B"  3 el. from  6- 8: Len=3
List of 1 best solution(s) using method "B":
 1) solution: ( w1 w2 ) ; ( w3 w4 ) ; ( w5 ) ; ( w6 w7 w8 ).  Sum(Len)=12
>>
```

The solution produced by this algorithm is the same as the 7th solution of the optimisation “minL” discussed earlier (see Section 4.4.2). This indicates that results of the algorithm *B* may lead to an optimal solution. The only undesired feature in this solution is that the distribution of the length of sub-chains (3,4,2,3) has a jump in the lengths of the two middle sub-chains (from 4 to 2) that could have been avoided.

The algorithm *C* was also applied to the same data set:

```
maxKL=4, maxEl=8, maxLen=12, Method=C
 1)m="C"  2 el. from  1- 2: Len=3
 2)m="C"  2 el. from  3- 4: Len=4
 3)m="C"  2 el. from  5- 6: Len=3
```

```
 4)m="C"  2 el. from  7- 8: Len=2
List of 1 best solution(s) using method "C":
 1) solution: ( w1 w2 ) ; ( w3 w4 ) ; ( w5 w6 ) ; ( w7 w8 ).  Sum(Len)=12
>>
```

Its solution is also the last (8^{th}) solution of the generic optimisation with respect to minimal sub-chain length ("minL" in Section 4.4.2). This indicates that the algorithm *C* is also capable of producing results that are optimal for a certain criterion. Compared to the algorithm *B*, the distribution of the lengths of the sub-chains (3,4,3,2) is closer to uniform and is expected to result in a more stable solution.

Note 1 On Optimal Geometrical Modelling – Condition Number

It is also possible to improve the results produced by the algorithms by exploiting the knowledge of the length of the wire segments adjacent to the ends of the chain. This may help to improve the condition number further, but requires an additional development and investigation.

Note 2 On Optimal Geometrical Modelling – Symmetry and Asymmetry

Splitting/sub-dividing chains which correspond to symmetrical wire structures may create asymmetrical current profiles. This may happen, for example, when a sub-division algorithm processes one arm of a dipole starting from the generator, whilst the other arm is processed starting from the free end. Then the distribution of the sub-chains on the arms may be somewhat different, leading to an asymmetry in the current intensity profile.

This can be best avoided by usage of symmetry planes. Some of temporary measures could also be:

- *an appropriate re-numbering of nodes/wires, which would force the algorithm to start with different wires/nodes that would effectively change the order of processing;*
- *splitting a chain into most equal sub-chains, or optimal splitting of long chains into shorter chains. This may reduce the negative effects (although not eliminating the problem completely);*
- *setting the algorithm to go away from a generator (if there is any);*

- *assigning numbers to the sub-chains (that would tell which initial chain they originated from and the order in which they were created). It would then be possible to sub-divide chains linked to the same point outwards from that point.*

Unfortunately, none of these temporary measures is able to solve the issue in a general manner. Unless a symmetry plane is enforced, it is difficult to implement an algorithm that would be able to tackle an arbitrary situation correctly/optimally.

4.5 Example 1B: Building a Compressed System of Linear Equations Using Chains

This section is concerned with application of the concept of chains to the structure already discussed in Example 1A in Section 3.9.

Continuing with the wire model discussed in Example 1A, assume that the total length of wire 1 to 3 is not large, so that a polynomial of 1st or at most 2nd degree can describe the electrical current variation sufficiently well.

Looking at the geometry of the wire model discussed in Example 1A, it is clear that the wires 1, 2 and 3 can be *replaced* with a single equivalent wire having the same total length. Then these three wires can be *considered* as a single wire, which will be referred to as a *chain*. A complete description should also include the order in which the wire segments are to be counted in a chain, and the definition for the chain's beginning and end. It is *chosen* such that the chain's first wire segment is the wire number 3. The next segment is then the wire 2, and the last wire segment, ending the chain, is the wire number 1.

The direction of current through the chain is *chosen* to match the direction of current through the first wire segment in the chain, wire no. 3.

To describe the current variation throughout the *chain* mathematically, the same set of basis functions can be used as were used for the *wires*. The difference comes in defining the domains of these functions. Giving the domain composed by the wires 3, 2 and 1 the name *chain 1*, or, shortly, *c1*, the following can be written (keeping in mind that the

terms/functions are defined[50] within the respective domain denoted with a superscript, and are zero elsewhere):

$$I^{(c1)}(\mathbf{r}) = I_1^{(c1)} N_2^{(c1)} + a_3^{(c1)} S_3^{(c1)}, \quad N_2^{(c1)} \equiv N_2^{(c1)}(s^{(3)}, s^{(2)}, s^{(1)})$$

Observation:

S*ingletons can be assigned to any wire segment within a chain – it is not necessary to start at the beginning and end at the end of a chain. It may perhaps be used for modelling localised coupling effects, and for modelling end effects. NB This feature is not discussed in the text*.

The above expression for current may be illustrated with Figure 4-4, showing the profiles of the basis functions on the newly defined chain, as well as on the rest of wires. The same notations can already be used to obtain a linear system in a manner similar to the one described in Example 1A. Later in this text, the new solution will be combined with the one for wires, from Example 1A, so that the transformation between the basis functions for the wires and chains becomes clearer.

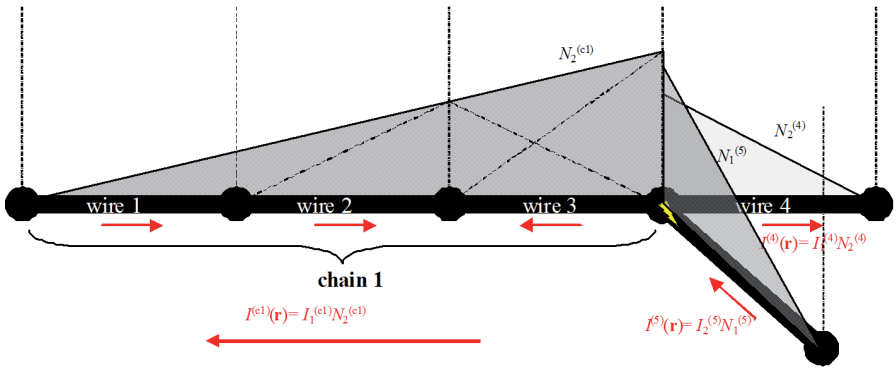

Figure 4-4. Assignment of chain basis functions to the wires in Example 1B.

The ideas for obtaining a linear system on chains are the same as were for wires. In order to apply the Kirchhoff's current law (KCL), the direction of currents is to be defined. The direction of current in wires 4 and 5 will be kept the same as before, i.e. from the beginning of a wire (1st node) towards its end (2nd node). The direction of

[50] This notation was first introduced in Section 2.9.

current through chain 1 is *chosen* to be defined by the direction of the current through wire 3. By this, it is meant that the current in the chain is assumed to flow from the first node in the chain, node 4 (the beginning of wire 3), toward the last node in the chain, node 1 (the beginning of wire 1). The direction of the current in wires 4 and 5 will be assumed to be the same as in the Example 1A.

Having defined the direction of currents, the currents around node 4 may be written mathematically (keeping in mind the piece-wise way of separating the domains of applicability of functions):

$$I(\mathbf{r}) = I^{(c1)}(\mathbf{r}) + I^{(4)}(\mathbf{r}) + I^{(5)}(\mathbf{r}) = I_1^{(c1)} N_2^{(c1)} + I_1^{(4)} N_2^{(4)} + I_2^{(5)} N_1^{(5)}.$$

There are 3 wires (with 3 unknown current amplitudes) at the joint. Only two of these current amplitudes can be taken as independent, for the 3rd can be readily expressed through Kirchhoff's current law: $I_1^{(c1)} + I_1^{(4)} - I_2^{(5)} = 0$. *Choosing* $I_1^{(4)}$ and $I_2^{(5)}$ to be the independent variables, and substituting $I_1^{(c1)} = I_2^{(5)} - I_1^{(4)}$ into the expression for the current, one may write

$$I(\mathbf{r}) = I_1^{(4)} \underbrace{\left(N_2^{(4)} - N_2^{(c1)} \right)}_{\tilde{f}_1 \equiv \tilde{D}_1^{(4,c1)}(s^{(4)}, s^{(c1)})} + I_2^{(5)} \underbrace{\left(N_1^{(5)} + N_2^{(c1)} \right)}_{\tilde{f}_2 \equiv \tilde{D}_2^{(5,c1)}(s^{(5)}, s^{(c1)})}$$

This form includes the expressions for the basis functions $\tilde{f}_1 \equiv \tilde{D}_1^{(4,c1)}(s^{(4)}, s^{(c1)}) \equiv N_2^{(4)} - N_2^{(c1)}$, and $\tilde{f}_2 \equiv \tilde{D}_2^{(5,c1)}(s^{(5)}, s^{(c1)}) \equiv N_1^{(5)} + N_2^{(c1)}$. It also includes the constant coefficients $\tilde{I}_1 \equiv I_1^{(4)}$, $\tilde{I}_2 \equiv I_2^{(5)}$ that needs to be determined. The form may be illustrated with Figure 4-5, which shows the assignment of the basis functions with the above notations to the wires.

Now, having the current expressed as $I(\mathbf{r}) = \tilde{I}_1 \tilde{f}_1 + \tilde{I}_2 \tilde{f}_2$, and with the help of the electrical field operator **L**, the electrical field may be written as

$$\mathbf{E}(\mathbf{r}) = \mathbf{L}I(\mathbf{r}) = \tilde{I}_1 \mathbf{L}\tilde{f}_1 + \tilde{I}_2 \mathbf{L}\tilde{f}_2.$$

Then, repeating the MoM procedure, a system of linear equations $\tilde{\mathbf{Z}}\tilde{\mathbf{I}} = \tilde{\mathbf{V}}$ is obtained[51]:

[51] The generator is defined as a point source located at node 4, directed toward node 6.

$$I_1^{(4)}\int \tilde{D}_1^{(4,c1)}\mathbf{L}\tilde{D}_1^{(4,c1)}dS \quad +I_2^{(5)}\int \tilde{D}_1^{(4,c1)}\mathbf{L}\tilde{D}_2^{(5,c1)}dS \quad =-\int \tilde{D}_1^{(4,c1)}\mathbf{E}^{inc}dS=0$$

$$I_1^{(4)}\int \tilde{D}_2^{(5,c1)}\mathbf{L}\tilde{D}_1^{(4,c1)}dS \quad +I_2^{(5)}\int \tilde{D}_2^{(5,c1)}\mathbf{L}\tilde{D}_2^{(5,c1)}dS \quad =-\int \tilde{D}_2^{(5,c1)}\mathbf{E}^{inc}dS$$

This system can then be solved and the new currents obtained with $\tilde{\mathbf{I}}=\tilde{\mathbf{Z}}^{-1}\tilde{\mathbf{V}}$.

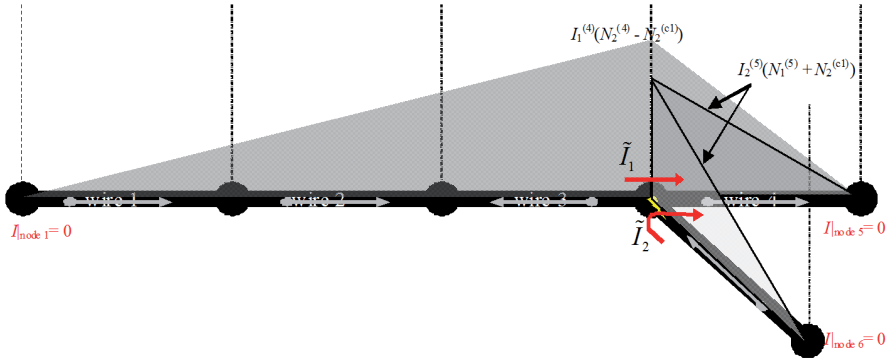

Figure 4-5. Assignment of chain basis functions after application of Kirchhoff's current law, to the wires. Example 1B.

4.6 Algorithm for Creating a Basis Function Grouping Matrix with Piecewise Linear Basis Functions

This original algorithm is used to generate an $N\times n$ matrix $\mathbf{M}$, linking the old and new unknowns.

This matrix expresses the old/original set of unknown current amplitudes described with the $N\times 1$ column vector $\mathbf{I}$, through the new set of n unknown current amplitudes $\tilde{\mathbf{I}}$. As per the Section 4.2.1, the relationship between the old and new unknowns may be written as $\mathbf{I}=\mathbf{M}\tilde{\mathbf{I}}$.

Note:

It is assumed that it is possible to transform the original system of linear equations $\mathbf{ZI} = \mathbf{V}$ *to a new lossy*[52] *compressed form* $\tilde{\mathbf{Z}}\tilde{\mathbf{I}} = \tilde{\mathbf{V}}$ *by introducing the basis function grouping/aggregating matrix* $\mathbf{M}$.

Consider the following scenario. There is a junction with a number of chains and individual wires attached to it. It is assumed that this junction has already been considered at a previous processing level (the one for assigning basis functions to wire segments, which works with wires only, and where the unknowns are assigned to the junctions, as discussed[53] in Chapter 2 and detailed in Section 2.11). The new unknowns are expected to be related to the old ones in a linear manner, as illustrated in Figure 4-6. This figure depicts three original basis functions, namely two roof-top (triangular) basis functions (each composed of two piecewise linear functions), and one piecewise linear basis function (the most right position). The figure also shows the profile of a new piecewise linear basis function.

It is clear from the picture that each of the original unknowns may be written as a linear function of the new unknown.

The algorithm for creating a basis function grouping matrix with piecewise linear basis functions was coded by the author in the Matlab and includes many lines of code. This will may make it time consuming and complex for most readers to go through Instead, the ideas behind the algorithm may be explained in terms of Example 1B discussed in Section 4.5.

There is a set of unknown current amplitudes *chosen* to be the independent variables (here, $I_2^{(1)}$, $I_2^{(3)}$, $I_1^{(4)}$ and $I_2^{(5)}$) and one unknown amplitude that can be calculated through the use of Kirchhoff's current law.

[52] The term lossy was used to highlight that the reduction in matrix size is generally not reversible.

[53] A partially relevant investigation is also discussed in Section 3.1.

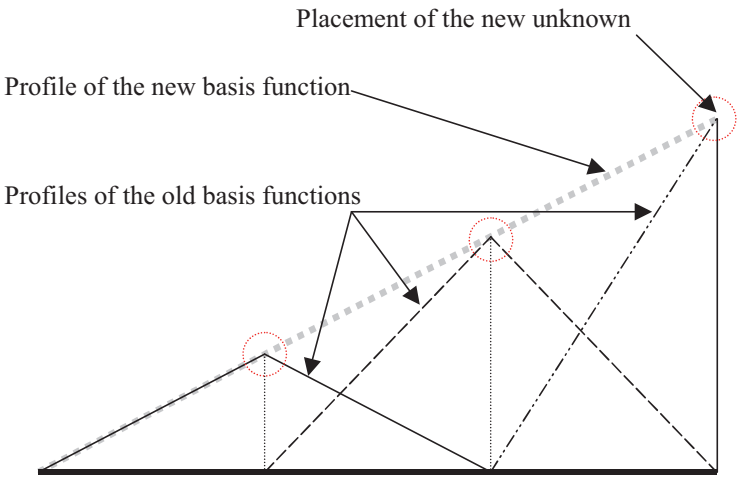

Figure 4-6. The linear relationship between the new piecewise linear basis function and the old/original piecewise linear basis functions, following from the principle of similar/equiangular triangles. Thus, the original unknown's amplitudes may be readily expressed via the new unknown amplitude using the ratios and the same principle. Positions of the original independent and/or dependent unknowns are denoted with circles.

In order to obtain a solution, the following steps need to be taken:

1) Define new independent variables at the junction. Say, $I_1^{(4)}$ and $I_2^{(5)}$ are selected to be the independent variables and the third current amplitude, $I_1^{(c1)} \equiv I_1^{(3)}$, can then be expressed using Kirchhoff's current law as $I_1^{(3)} = I_2^{(5)} - I_1^{(4)}$.

2) Now, for each chain, the following steps need to be repeated (shown here using the terms of Example 1B):

   2.1) Find all old independent variables that belong to the chain. These will be the current amplitudes $I_2^{(1)}$ and $I_2^{(3)}$.

   2.2) Now express them through the new variable(s) for the chain with yet undefined proportionality factors (weights) α and β: $\begin{pmatrix} I_2^{(1)} \\ I_2^{(3)} \end{pmatrix} = \begin{pmatrix} -\alpha \\ +\beta \end{pmatrix} \left(I_1^{(3)} \right)$. The signs reflect the matching or opposite direction between new and old currents.

3) Express (using Kirchhoff's current law) the new variable(s) through the old ones (that are now new independent variables):

   The expression $I_1^{(3)} = I_2^{(5)} - I_1^{(4)}$, put in a matrix form, will become

   $$\left(I_1^{(3)}\right) = \left(-1 \mid +1\right)\begin{pmatrix} I_1^{(4)} \\ I_2^{(5)} \end{pmatrix}.$$

4) Multiply the matrices from steps 1 and 2 to obtain the transformation matrix for the junction:

   $$\begin{pmatrix} I_2^{(1)} \\ I_2^{(3)} \end{pmatrix} = \begin{pmatrix} -\alpha \\ +\beta \end{pmatrix}\left(I_1^{(3)}\right) = \begin{pmatrix} -\alpha \\ +\beta \end{pmatrix}\left(-1 \mid +1\right)\begin{pmatrix} I_1^{(4)} \\ I_2^{(5)} \end{pmatrix} = \left(\begin{array}{c|c} +\alpha & -\alpha \\ \hline -\beta & +\beta \end{array}\right)\begin{pmatrix} I_1^{(4)} \\ I_2^{(5)} \end{pmatrix}$$

5) Combine the results with identity for the new independent variables $\begin{pmatrix} I_1^{(4)} \\ I_2^{(5)} \end{pmatrix} = \begin{pmatrix} 1 & 0 \\ 0 & 1 \end{pmatrix}\begin{pmatrix} I_1^{(4)} \\ I_2^{(5)} \end{pmatrix}$ to get to the part of matrix **M**: $\begin{pmatrix} I_2^{(1)} \\ I_2^{(3)} \\ I_1^{(4)} \\ I_2^{(5)} \end{pmatrix} = \begin{pmatrix} +\alpha & -\alpha \\ -\beta & +\beta \\ 1 & 0 \\ 0 & 1 \end{pmatrix}\begin{pmatrix} I_1^{(4)} \\ I_2^{(5)} \end{pmatrix}$,

   which gives $\mathbf{M} = \begin{pmatrix} +\alpha & -\alpha \\ -\beta & +\beta \\ 1 & 0 \\ 0 & 1 \end{pmatrix}$.

6) If the system has more junctions, this matrix **M** should be considered as part of a larger matrix $\tilde{\mathbf{M}}$ with elements $\left\{\mathrm{M}_{ij}\right\}$, $i = 1,2,\ldots N$, $j = 1,2,\ldots n$, where N and n are the numbers of independent variables in the original and compressed systems, respectively. Therefore, this matrix **M** should be added to the corresponding portion of the final transformation matrix.

This procedure should be applied to every junction, thus adding to and completing the transformation matrix.

4.7 Example 1B Continued

In Section 4.5, Example 1B discussed how the current distribution for the structure of Example 1A in Section **3.9** may be obtained using the chains rather than the traditional basis functions. The question of generating the transformation matrix **M** was then discussed in Section 4.6. This section continues the discussions and provides a detailed derivation for obtaining the elements of the transformation matrix.

The transformation matrix may be considered as a compressing matrix, as the rank of the new, compressed impedance matrix is normally smaller or equal to the rank of the original impedance matrix. This poses the question: how close can the solution of the compressed system be made to the original non-compressed solution obtained by the traditional MoM by tuning the transformation matrix elements. This question may be followed by another query – can the properties of the transformation matrix and the impedance matrix be combined and used to enhance the accuracy of the solution. The ending subsections address these two questions with simple numerical examples.

4.7.1 Inter-Relation between the Old and New Systems

It is possible to consider the relationship between the original and new systems. The expression for the current distribution may be written as

$$I(\mathbf{r}) = I_1^{(c1)} N_2^{(c1)} + I_1^{(4)} N_2^{(4)} + I_2^{(5)} N_1^{(5)} \ ,$$

and, after taking Kirchhoff's current law into account, as

$$I(\mathbf{r}) = I_1^{(4)} \left(N_2^{(4)} - N_2^{(c1)} \right) + I_2^{(5)} \left(N_1^{(5)} + N_2^{(c1)} \right).$$

Figure 4-7a shows the application of these functions to the wire structure.

It is possible to write $N_2^{(c1)}$ as $N_2^{(c1)} = -\alpha D_1^{(1,2)} + \beta D_2^{(3,2)} + N_2^{(3)}$, where α and β are constants (with the signs reflecting the direction of the new current coefficient with respect to the old one). Substituting this form into the current $I(\mathbf{r})$ permits to express the current through the "old" basis functions:

$$I(\mathbf{r}) = I_1^{(4)} \left(D_3^{(4,3)} - \beta D_2^{(3,2)} + \alpha D_1^{(1,2)} \right) + I_2^{(5)} \left(D_4^{(5,3)} + \beta D_2^{(3,2)} - \alpha D_1^{(1,2)} \right).$$

In the original form, the current may then be expressed as:

$$I(\mathbf{r}) = I_1 \underbrace{\left(N_1^{(1)} + N_2^{(2)}\right)}_{D_1^{(1,2)}} + I_2 \underbrace{\left(N_1^{(3)} - N_1^{(2)}\right)}_{D_2^{(3,2)}} + I_3 \underbrace{\left(N_2^{(4)} - N_2^{(3)}\right)}_{D_3^{(4,3)}} + I_4 \underbrace{\left(N_1^{(5)} + N_2^{(3)}\right)}_{D_4^{(5,3)}}$$
$$= I_2^{(1)}\left(N_1^{(1)} + N_2^{(2)}\right) + I_2^{(3)}\left(N_1^{(3)} - N_1^{(2)}\right) + I_1^{(4)}\left(N_2^{(4)} - N_2^{(3)}\right) + I_2^{(5)}\left(N_1^{(5)} + N_2^{(3)}\right)$$

The graphical overview of application of these expressions to the actual geometry is illustrated with Figure 4-7b. One can use the above expansion to obtain the expression for a new Z_{11} in terms of the old matrix elements:

$$\tilde{Z}_{11} = \iint D_1^{(4,c1)} \mathbf{L} D_1^{(4,c1)} = \iint \left(N_2^{(4)} - N_2^{(c1)}\right) \mathbf{L} \left(N_2^{(4)} - N_2^{(c1)}\right)$$
$$= \iint \left(N_2^{(4)} - (-\alpha D_1^{(1,2)} + \beta D_2^{(3,2)} + N_2^{(3)})\right) \mathbf{L} \left(N_2^{(4)} - (-\alpha D_1^{(1,2)} + \beta D_2^{(3,2)} + N_2^{(3)})\right)$$
$$= \iint \left\{ D_3 \mathbf{L} D_3 + \alpha\left(D_3 \mathbf{L} D_1 + D_1 \mathbf{L} D_3\right) - \beta\left(D_2 \mathbf{L} D_3 + D_3 \mathbf{L} D_2\right) + \left(-\alpha D_1 + \beta D_2\right) \mathbf{L} \left(-\alpha D_1 + \beta D_2\right) \right\}$$
$$= Z_{33} + \alpha\left(Z_{31} + Z_{13}\right) - \beta\left(Z_{23} + Z_{32}\right) + \alpha^2 Z_{11} + \beta^2 Z_{22} - \alpha\beta\left(Z_{12} + Z_{21}\right)$$

In a similar manner, it is possible to express Z_{12},

$$\tilde{Z}_{12} = \iint D_1^{(4,c1)} \mathbf{L} D_2^{(5,c1)} = \iint \left(N_2^{(4)} - N_2^{(c1)}\right) \mathbf{L} \left(N_1^{(5)} + N_2^{(c1)}\right)$$
$$= \iint \left(N_2^{(4)} - (-\alpha D_1^{(1,2)} + \beta D_2^{(3,2)} + N_2^{(3)})\right) \mathbf{L} \left(N_1^{(5)} + (-\alpha D_1^{(1,2)} + \beta D_2^{(3,2)} + N_2^{(3)})\right),$$
$$= Z_{34} - \alpha\left(Z_{31} - Z_{14}\right) + \beta\left(Z_{32} - Z_{24}\right) - \alpha^2 Z_{11} - \beta^2 Z_{22} + \alpha\beta\left(Z_{12} + Z_{21}\right)$$

and other elements of the new impedance matrix.

The resulting new 2×2 impedance matrix will have the following analytical form:

$$\mathbf{M}^T(\mathbf{ZM}) = \left(\begin{array}{c|c} \alpha^2 Z_{11} + \beta^2 Z_{22} - \alpha\beta(Z_{12} + Z_{21}) & -\alpha^2 Z_{11} - \beta^2 Z_{22} + \alpha\beta(Z_{12} + Z_{21}) \\ +\alpha(Z_{13} + Z_{31}) - \beta(Z_{23} + Z_{32}) + Z_{33} & +\alpha(Z_{14} - Z_{31}) - \beta(Z_{24} - Z_{32}) + Z_{34} \\ \hline -\alpha^2 Z_{11} - \beta^2 Z_{22} + \alpha\beta(Z_{12} + Z_{21}) & \alpha^2 Z_{11} + \beta^2 Z_{22} - \alpha\beta(Z_{12} + Z_{21}) \\ -\alpha(Z_{13} - Z_{41}) + \beta(Z_{23} - Z_{42}) + Z_{43} & -\alpha(Z_{14} + Z_{41}) + \beta(Z_{24} + Z_{42}) + Z_{44} \end{array}\right)$$

This result can also be obtained using matrix forms, leading to a more systematic approach.

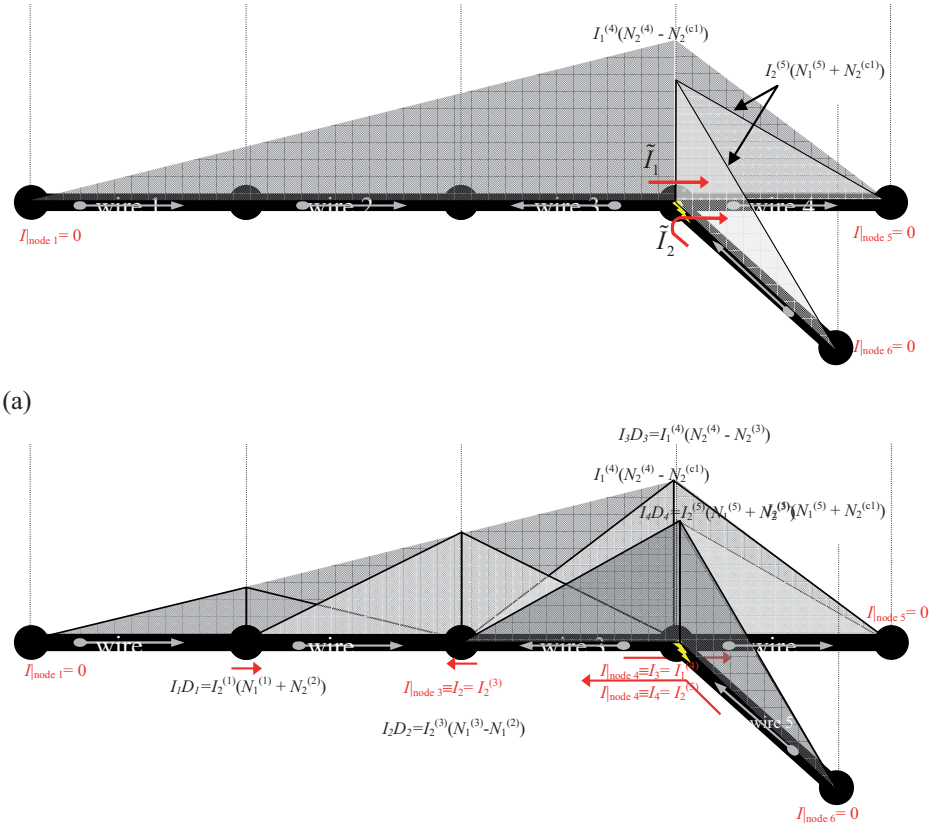

(a)

(b)

Figure 4-7. (a) New chain basis functions obeying Kirchhoff's current law assigned to the geometrical structure. (b) Relation between these new basis functions (for chains) and the basis functions for wires (from Example 1A). Note the difference in the definitions of the direction of current at the main junction between (a) and (b).

Obtaining the Same Inter-Relations in a Matrix Form

Applying the algorithm for creating a transformation (basis function-grouping) matrix **M** to the current example will lead to the following matrix manipulations.

First, the transformation between the column vector of old unknowns **I** and the column vector of new unknowns $\tilde{\mathbf{I}}$ is written as $\mathbf{I} = \mathbf{M}\tilde{\mathbf{I}}$. This may be expanded as

$$\begin{pmatrix} I_2^{(1)} \\ I_2^{(3)} \\ I_1^{(4)} \\ I_2^{(5)} \end{pmatrix} = \begin{pmatrix} & \\ & \\ 1 & 0 \\ 0 & 1 \end{pmatrix} \begin{pmatrix} I_1^{(4)} \\ I_2^{(5)} \end{pmatrix},$$

where the ones and zeros show the direct relationships between some of the original independent and new independent variables. These variables were chosen to represent current amplitude at the same ends of the wires. The empty space in the above matrix is for the four, yet unknown, matrix coefficients.

Taking into consideration the linear dependence between the old and new variables, the empty part of matrix $\mathbf{M}$ can be written as follows: $I_2^{(1)} = (+\alpha) I_1^{(4)} + (-\alpha) I_2^{(5)}$, $I_2^{(3)} = (-\beta) I_1^{(4)} + (+\beta) I_2^{(5)}$. The signs of the coefficients are determined by match/mismatch of the direction of the respective currents in the old and the new configurations. The sign is positive, if the direction of the current in the wire matches the direction of the current defined on a chain that this wires belongs to. Otherwise, the sign is negative. Let

$$\mathbf{M} = \begin{pmatrix} +\alpha & -\alpha \\ -\beta & +\beta \\ 1 & 0 \\ 0 & 1 \end{pmatrix}.$$

The new impedance matrix is computed as $\tilde{\mathbf{Z}} = \mathbf{M}^T \mathbf{Z} \mathbf{M}$. In an expanded form, this may be written down step by step as

$$\begin{aligned} \mathbf{ZM} &= \begin{pmatrix} Z_{11} & Z_{12} & Z_{13} & Z_{14} \\ Z_{21} & Z_{22} & Z_{23} & Z_{24} \\ Z_{31} & Z_{32} & Z_{33} & Z_{34} \\ Z_{41} & Z_{42} & Z_{43} & Z_{44} \end{pmatrix} \begin{pmatrix} +\alpha & -\alpha \\ -\beta & +\beta \\ 1 & 0 \\ 0 & 1 \end{pmatrix} \\ &= \begin{pmatrix} \alpha Z_{11} - \beta Z_{12} + Z_{13} & -\alpha Z_{11} + \beta Z_{12} + Z_{14} \\ \alpha Z_{21} - \beta Z_{22} + Z_{23} & -\alpha Z_{21} + \beta Z_{22} + Z_{24} \\ \alpha Z_{31} - \beta Z_{32} + Z_{33} & -\alpha Z_{31} + \beta Z_{32} + Z_{34} \\ \alpha Z_{41} - \beta Z_{42} + Z_{43} & -\alpha Z_{41} + \beta Z_{42} + Z_{44} \end{pmatrix}, \end{aligned}$$

$$\mathbf{M}^T(\mathbf{ZM}) = \begin{pmatrix} +\alpha & -\beta & 1 & 0 \\ -\alpha & +\beta & 0 & 1 \end{pmatrix} \begin{pmatrix} \alpha Z_{11} - \beta Z_{12} + Z_{13} & -\alpha Z_{11} + \beta Z_{12} + Z_{14} \\ \alpha Z_{21} - \beta Z_{22} + Z_{23} & -\alpha Z_{21} + \beta Z_{22} + Z_{24} \\ \alpha Z_{31} - \beta Z_{32} + Z_{33} & -\alpha Z_{31} + \beta Z_{32} + Z_{34} \\ \alpha Z_{41} - \beta Z_{42} + Z_{43} & -\alpha Z_{41} + \beta Z_{42} + Z_{44} \end{pmatrix}$$

$$= \left(\begin{array}{c|c} \alpha^2 Z_{11} + \beta^2 Z_{22} - \alpha\beta(Z_{12} + Z_{21}) & -\alpha^2 Z_{11} - \beta^2 Z_{22} + \alpha\beta(Z_{12} + Z_{21}) \\ +\alpha(Z_{13} + Z_{31}) - \beta(Z_{23} + Z_{32}) + Z_{33} & +\alpha(Z_{14} - Z_{31}) - \beta(Z_{24} - Z_{32}) + Z_{34} \\ \hline -\alpha^2 Z_{11} - \beta^2 Z_{22} + \alpha\beta(Z_{12} + Z_{21}) & \alpha^2 Z_{11} + \beta^2 Z_{22} - \alpha\beta(Z_{12} + Z_{21}) \\ -\alpha(Z_{13} - Z_{41}) + \beta(Z_{23} - Z_{42}) + Z_{43} & -\alpha(Z_{14} + Z_{41}) + \beta(Z_{24} + Z_{42}) + Z_{44} \end{array}\right).$$

The above expanded expression is the same as the one derived by the expansion of the doublets defined on chains into doublets defined on wires, derived earlier in this section.

On Calculation of Coefficients α and β

To complete the example, the coefficients α and β are calculated and the results discussed. Let L be the sum of the lengths of the wires w1, w2 and w3. The lengths of wires are defined in Example 1A in Section 3.9. The summation is simple:

$$L = \Sigma(L_{w1}, L_{w2}, L_{w3}) = 0.5+0.5+0.5 = 1.5.$$

Then the coefficients may be expressed as the ratio of the cumulative lengths to the total length L. That is $\alpha = L_{w1}/L = 0.5/1.5 = 1/3$ and $\beta = (L_{w1} + L_{w2})/L = (0.5+0.5)/1.5 = 2/3$.

The result of the computations may be summarised: $\mathbf{M} = \begin{bmatrix} 1/3 & -1/3 \\ -2/3 & 2/3 \\ 1 & 0 \\ 0 & 1 \end{bmatrix}$.

Thus the new, compressed impedance matrix and voltage vector are obtained:

$$\tilde{\mathbf{Z}} = \mathbf{M}^T\mathbf{ZM} = \begin{bmatrix} -0.0087789 + 42886i & 0.0065842 - 13582i \\ 0.0065842 - 13582i & -0.0054869 + 41837i \end{bmatrix}, \quad \tilde{\mathbf{V}} = \mathbf{M}^T\mathbf{V} = \begin{bmatrix} 0 \\ 1 \end{bmatrix}.$$

The condition number for the compressed impedance matrix is 1.945. This is three times lower than the condition number of the original impedance matrix. Thus, although the impedance matrix elements are computed to the same tolerance, the numerical error in currents for the new system is three times less (assuming that the new basis functions defined on chains, describe the current sufficiently accurately).

The eigenvalues of the new compressed impedance matrix are `-0.013776 + 55954i` and `-0.00049009 + 28769i`. The real parts of the eigenvalues are attributed to an exponential decay with time t progressing towards infinity, $t \to +\infty$. The imaginary part of an eigenvalue is attributed to the cyclic frequency of oscillations. Comparing eigenvalues of the new impedance matrix to the eigenvalues of the original impedance matrix shows that the new solution has slower oscillations and decays quicker. This indicates a higher stability of the new system. However, this may also imply that the new system may be incapable of handling as high frequencies as the original system can. This numerical solution thus confirms that the chain basis functions have to be applied with caution as the new basis functions define the accuracy of modelling the current, and not the original basis functions. The original basis functions attribute to the geometrical representation accuracy.

Continuing with the calculations, the new linear system may be inverted and the new unknown currents found as

$$\tilde{\mathbf{I}} = \tilde{\mathbf{Z}}^{-1}\tilde{\mathbf{V}} = \left[1.8692\cdot 10^{-12} - 8.4377\cdot 10^{-6}\mathrm{I} \qquad -1.5593\cdot 10^{-12} - 2.6642\cdot 10^{-5}\mathrm{I}\right]^{T}.$$

As the last step, the values of the old currents may be found with $\mathbf{I} = \mathbf{M}\tilde{\mathbf{I}}$. The results are listed in Table 4-1.

Table 4-1. Solutions due to the original and compressed systems. The two highlighted elements are the direct solution of the compressed matrix.

Variable	Currents produced by solving the original system	Currents obtained by solving the compressed system
$I_2^{(1)}$	2.3324e-12 +5.3718e-06j	1.1428e-12 +6.0680e-06j
$I_2^{(3)}$	-3.1993e-12 -1.0588e-05j	-2.2856e-12 -1.2136e-05j
$I_1^{(4)}$	1.6349e-12 -8.3558e-06j	1.8692e-12 -8.4377e-06j
$I_2^{(5)}$	-1.3604e-12 -2.6775e-05j	-1.5593e-12 -2.6642e-05j

The comparison of the values shows that the values of currents obtained by solving the original system and the compressed system are very close. At the terminal point, the values are close within 0.5%. This translates into the error in the input impedance between the two methods under 0.5%.

Next, the question arose whether there are options available in the method that may help to improve the accuracy.

4.7.2 Optimisation of Coefficients α and β

The linear shape of the approximating function in chain basis functions was chosen for its simplicity. The question remained: Can this approach of compressing the impedance matrix be optimised to give more accurate results, and if yes, how much closer can the results be to the results from the original non-compressed system.

4.7.3 Optimisation with Respect to the Reference Current

In this test, the error between the values of current obtained by the original MoM and new chain expansion, was considered. The error was minimised by varying the weights, i.e. the elements of the compressing matrix **M**. The optimisation gave the new values of the coefficients α=0.29164 and β=0.57481. The values for the currents calculated using these new coefficients are shown in Table 4-2.

Table 4-2. Comparison of currents produced by the original system against the currents produced by the compressed system (whose coefficients were optimised to minimise the error in currents between the compressed and original systems).

Variable	Currents produced by solving the original system	Currents obtained by multiplying the compressed system currents $\mathbf{I} = \mathbf{M}\tilde{\mathbf{I}}$ Parameters: α=0.29164 and β=0.57481
$I_2^{(1)}$	2.3324e-12 +5.3718e-06j	8.6016e-13 +5.3719e-06j
$I_2^{(3)}$	-3.1993e-12 -1.0588e-05j	-1.6953e-12 -1.0588e-05j
$I_1^{(4)}$	1.6349e-12 -8.3558e-06j	1.5889e-12 -8.3558e-06j
$I_2^{(5)}$	-1.3604e-12 -2.6775e-05j	-1.3604e-12 -2.6775e-05j

The table also lists the original currents obtained through the traditional MoM solution. The comparison between the original solution and the new solution shows that, as it could be expected, the optimized values give results that are closer to the results of the traditional MoM solution than the direct application of the chain approach. This is because the transformation matrix coefficients were especially optimized to achieve this result.

There is however some difference between the direct MoM solution and the optimized solution of a compressed system. The difference in the real parts of respective currents is attributed to the accuracy of computing the integrals in the original impedance matrix. This contributed to the error in the variable $I_2^{(1)}$, which is an element of $\tilde{\mathbf{I}}$, and this error then propagated into the solution of the compressed system with $\mathbf{I} = \mathbf{M}\tilde{\mathbf{I}}$.

The comparison further indicates that, with an optimal set of the elements of the compressing matrix, the compressed system can lead to the original solution condition.

4.7.4 Optimisation with Respect to the Condition Number

It was expected that a model that describes a physical system well should have good computational properties. For example, it should then have a well-conditioned impedance matrix, reflected by a low value of the condition number. This idea was tested.

The condition number of the compressed impedance matrix became the subject of optimization. Minimisation of this condition number by varying the values of the transformation matrix elements produced an optimum set of the coefficients: α=0.30254 and β=0.59186. The results of current calculations are tabulated in Table 4-3.

Table 4-3. List of currents found by minimising the condition number of the compressed impedance matrix, against the currents produced by the original system.Note:Error at terminal port (in $I_2^{(5)}$) is within 0.02% from the old solution.

Variable	Currents produced by solving the original system	Currents obtained by multiplying the compressed system currents $I = M\tilde{I}$ Parameters: α=0.30254 and β=0.59186
$I_2^{(1)}$	2.3324e-12 +5.3718e-06j	9.2710e-13 +5.5725e-06j
$I_2^{(3)}$	-3.1993e-12 -1.0588e-05j	-1.8137e-12 -1.0901e-05j
$I_1^{(4)}$	1.6349e-12 -8.3558e-06j	1.6559e-12 -8.3514e-06j
$I_2^{(5)}$	-1.3604e-12 -2.6775e-05j	-1.4085e-12 -2.6770e-05j

It is easy to notice that these values are closer to the values obtained by solving the original system than the values produced by compressing the matrix without any optimisation (Table 4-1). This indicates that the optimization of condition number might

be used to optimise the transformation matrix weights, i.e. the shape of the composite basis functions, without any prior knowledge about the original uncompressed solution.

4.7.5 Summary

A discussion based on Example 1B has been used to acquire an insight in several aspects related to the generation of the transformation matrix **M**. The exact analytical expressions for this relationship were derived in a step by step procedure, as well as using a more systematic matrix approach. Numerically, the input impedance due to the compressed results was within 0.5% of the original uncompressed calculation.

Next, an investigation based on the above considered two questions. In the first test, the transformation matrix elements were varied to bring the new solution as close to the original one as possible. It has been established that it was possible to take the new solution very close to the original solution. In the second test, it was questioned whether it is possible to use the knowledge of the condition number to obtain a new solution close to the true solution. In the test, the error at the port was found to be under 0.02%.

4.8 Readily Available Piecewise Linear Approximation of Arbitrary Basis Functions Applied to Chains

So far, only the piecewise linear (PWL) basis functions were discussed in the context of multiple domain basis functions (MDBF) that may be used for the chains of wires. However, besides the PWL MDBFs, piecewise linear approximations of any other types of basis functions may also be used with the chains, at no effort in either implementation or computations. In particular, the linearly-interpolated piecewise-sinusoidal (PWS) basis functions, popular for thin wire modelling [Balanis, 5] will be used to illustrate the concept.

A support for the piecewise sinusoidal (PWS) and many other basis functions may be incorporated into the concept of chains and implemented in the respective algorithms with virtually no additional computational cost, compared with piecewise linear functions. As it has been introduced in the beginning of Chapter 4, the old unknowns are related to the new ones through a product of the new unknowns and a transformation matrix with weights. By setting the weights to the profile of a PWS function instead of

the profile of a piecewise linear function, a new interpolation scheme may be achieved. The simplicity of this step may be contrasted to the intricate procedures for computing impedance matrix elements, also requiring high processing resources for the respective calculations.

4.8.1 On Piecewise Sinusoidal Basis Functions

Mathematically, a piecewise sinusoidal (PWS) basis function may be expressed as

$$f_i(x) = \begin{cases} \dfrac{\sin\left(k\left(x - x_{i-1}\right)\right)}{\sin\left(k\left(x_i - x_{i-1}\right)\right)}, & x_{i-1} \le x \le x_i \\ \dfrac{\sin\left(k\left(x_{i+1} - x\right)\right)}{\sin\left(k\left(x_{i+1} - x_i\right)\right)}, & x_i \le x \le x_{i+1} \\ 0 & \textit{otherwise} \end{cases}, \tag{4.3}$$

where x_i is the position of a mesh node (wire end), and k is the wavenumber.

The PWS function was first introduced in thin wire modelling in [Richmond, 95]. Now this function is a popular choice in thin wire modelling. There are several reasons for this. The PWS functions permits analytical evaluation of the integrals involved in calculation of the electric field [Balanis, 5]. The PWS function also requires fewer unknowns per wavelength compared with a piecewise linear (PWL) basis function. Examples of the PWS functions are shown in Figure 4-8.

Regretfully, the usability of these basis functions is limited due to their poor ability to model a current distribution with constant profile over any large interval. An example of an artefact resulting from using a $\pi/2$ long interval per PWS function is shown in Figure 4-8c.

Note:

If a program realising the method of moment permits both piecewise linear (PWL) and piecewise sinusoidal (PWS) basis functions, it is advantageous to apply the PWS basis functions at the free wire ends, where it provides a better approximation for the true current distribution.

In this regard, the concept of chains permits mixing the PWL and PWS functions without any additional computational or implementation cost, as shown in the following sub-section.

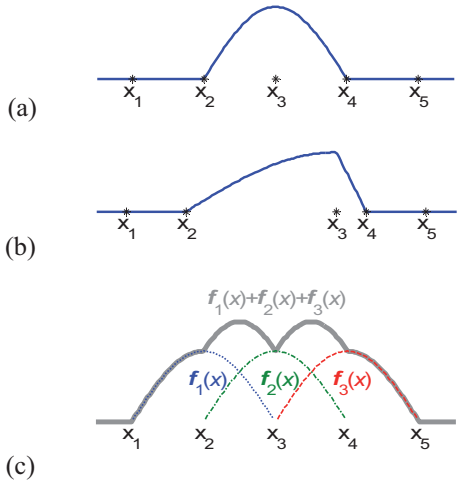

Figure 4-8. Piecewise sinusoidal (PWS) basis functions (a) on a quarter-wavelength interval x_{n+1}-x_n=π/2, (b) on a non-uniform mesh with quarter-wavelength x_3-x_2=π/2 and short x_4-x_3=π/10 intervals, and (c) the artefacts due to the sum of PWS functions when modelling a constant current distribution with quarter-wavelength intervals.

4.8.2 Application of Piecewise Sinusoidal Basis Functions to Chains

The flexibility provided by the mechanism of chains described in Section 4.6 gives an opportunity in applying the piecewise sinusoidal (PWS) basis functions within the same level of complexity as for the piecewise linear (PWL) basis functions.

The application is illustrated with Figure 4-6. The weights of the old basis functions to form a piecewise linear approximation may be easily computed by translating the centres of the original triangular basis functions into the co-ordinate system of the new basis function, and computing the PWS function (4.3) at these points. This is essentially the same procedure as required by piecewise linear functions applied to chains. This

may be seen from a comparison of Figure 4-6 and Figure 4-9. The only difference between the two is the shape (profile) of the interpolating function. In Figure 4-6 it is a linear function, whilst in Figure 4-9 it is a sinusoidal function. The rest of the details (e.g. calculation for the positions of the old unknowns) is exactly the same.

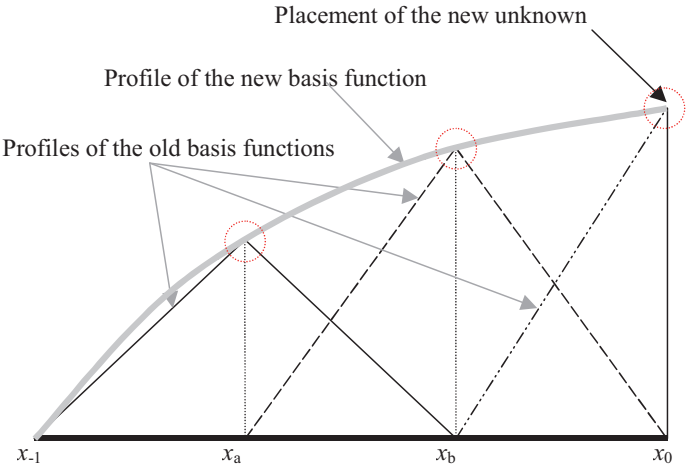

Figure 4-9. The relationship between the new piecewise sinusoidal (PWS) basis function and the old/original piecewise linear (PWL) basis functions. The original unknown amplitudes may be readily expressed using a product of the new unknown and the weights at the positions of the original unknowns (x_a, x_b, x_0), denoted with circles.

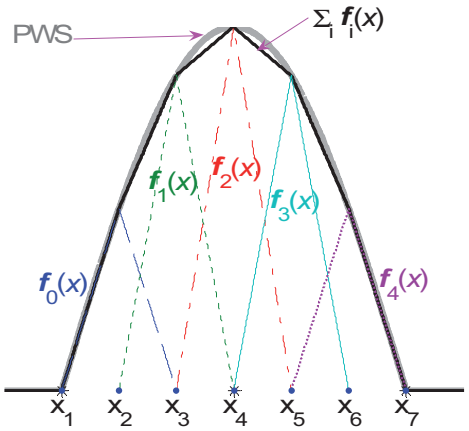

Figure 4-10. Piecewise linear (PWL) functions used to approximate a piecewise sinusoidal (PWS) function.

Note:

It is clear that the only modification required in the program to support this extension of the basis functions defined on chains is the calculation of the weights for matrix ***M****, described earlier in this section. There is no need for any modifications to the subroutines for integration and calculation of the impedance matrix elements, which are usually the most complex and difficult to change parts of a program realising MoM.*

With the approach discussed in this section, it is possible to use virtually any function for an interpolating basis function, with a simple calculation of the desired function at specified points. Furthermore, no alterations are required to the rest of the algorithms or program.

The only clear limitation of this approach is the requirement of a small electrical length for the wire segments composing a chain, so that the approximation of the applied basis function would be sufficiently accurate. This approximation will produce best results when the density of the initial mesh is high. Then, as illustrated in Figure 4-10, the difference between the piecewise linear approximation due to the PWL functions used in the computing matrix elements, and the sinusoidal profile of PWS function will not be large.

Note:

It is also possible to apply PWS basis functions selectively, only to the last segments of long structures (to free ends of wires), and fill the remainder of the structure with the chains of PWL functions.

4.9 Changes required to a standard MoM program in order to implement the compression technique

These are shown in the form of a flowchart provided in Appendix D. The changes include three steps additional to the standard MoM procedure:

- Identification of chains, processing them to ensure that the maximum electrical length is kept to a reasonable limit, and generation of the matrix **M**. This may include considering the remaining single wires as chains (of one wire only), as to unify the algorithms.

- Compute new impedance matrix. Section 4.11 provides discussions on approaches to lower computational burden for this procedure.
- Compute a new excitation vector for a given source, solve the new system of linear equations, and compute the contributions to the original (old) unknowns.

4.10 Finding the Relation between the Polynomial Basis Functions in a Shifted Co-ordinate System

This section outlines the mathematical basis for using the higher order polynomial basis functions within the scheme of composite multiple domain basis functions [Lysko, 63].

In this section, a transformation matrix is derived that transforms the original polynomial basis functions defined on individual wire segments into a new set of multiple domain polynomial basis functions. The new composite basis function is a multiple domain basis function and is defined on an aggregated domain of a chain.

The transformation matrix **M** obtained in a series of hierarchical steps. The steps include a decomposition of the matrix into sub-matrices **m**. The matrix **m** corresponds to an individual chain, and is a product of three matrices. One of these matrices expresses the relationship due to a linear shift between the coordinate systems of a chain and its wire segments. The other two matrices model two reverse processes: formation of a polynomial out of individual power terms, and decomposition into individual terms.

The method proposed can be applied to arbitrary sets of polynomial-based basis functions. Furthermore, the framework for obtaining the transformation matrix **M** can be readily extended to take advantage of the least squares or the MoM procedures. In the case of the latter, this would result in a MoM-in-MoM method.

4.10.1 Formulation of a Matrix Relationship between the Coefficients of the Old and New Basis Functions

The matrix **M** already discussed in Section 4.6 for the piecewise linear basis functions is in this section generalised on higher order polynomial basis functions. The matrix may still be considered as composed of sub-matrices due to the individual chains. A single sub-matrix is hereinafter denoted with the symbol **m**.

The sequence of transformations to obtain a sub-matrix **m** for one chain starts with the a new set of basis functions $[BF^{new}]$ and may be written as follows

1) Decomposition of new currents, i.e. $[BF^{new}]$, into a set of basic hierarchical polynomials, $[P^{new}]$, as $[P^{new}] = [X]^{-1} \cdot [BF^{new}]$. The basic hierarchical polynomials are assumed to be defined in an original co-ordinate system. The matrices [X] and its inverse, $[X^{-1}]$, are discussed in detail in Section 4.10.4.
2) Conversion from the hierarchical polynomials $[P^{new}]$ into an "old" set of hierarchical polynomials, $[P^{old}] = \mathbf{G} \cdot [P^{new}]$. This old set $[P^{old}]$ is defined in a co-ordinate system that has a linear shift with respect to the coordinate system of $[P^{new}]$. The matrix **G** is discussed in detail in Sections 4.10.2 and 4.10.3.
3) A composition relating the original set of basis functions $[BF^{old}]$ to the new set of basis functions $[BF^{old}]$, expressed as $[BF^{old}] = [X] \cdot [P^{old}]$.

The result of these manipulations may be combined into a relationship between the coefficients of the original (old) basis functions and the coefficients for the new set of basis functions $[BF^{new}]$:

$$[BF^{old}] = [X] \cdot \mathbf{G} \cdot [X]^{-1} \cdot [BF^{new}] = \mathbf{m} \cdot [BF^{new}].$$

This finally defines the sub-matrix **m** as

$$\mathbf{m} \equiv [X] \cdot \mathbf{G} \cdot [X]^{-1},$$

The matrices [X] and **G** and their formulation are discussed in the sections following.

4.10.2 Shifting the Local Coordinate System for Polynomial Sets of Equal Order

This section focuses on the derivation of a matrix equation which can express a linear shift in the co-ordinate system between two sets of polynomial basis functions defined on the same chain.

The relationship between the piecewise linear (PWL) basis functions within the context of the original and chained basis functions has already been established in Section 4.6. In order to utilise the full power offered by the concept of aggregating the basis

functions and respective domains, the relationships derived now need to be extended for the higher order polynomial basis functions.

In the context of the method of moments, a convenient solution would be to derive a matrix which maps the new coefficients A_k to the old ones a_k, as $[a_k] = \mathbf{G}[A_k]$, like it was done with the piecewise linear functions in Section 4.6.

Note:

In practical terms, this requires a high degree of integration between this technique and the particular realisation of the method of moments.

The multiple domain basis functions (MDBF) cover the joint/united domains of definition of the original basis functions. Each original basis function may be defined in its own, local co-ordinate system placed along a respective chain. These local co-ordinate systems may be considered as being joined at the borders of their domains, thus introducing a new, unified, piecewise linear co-ordinate system. The new co-ordinate system on the same chain can then be related to the original local co-ordinate systems by a simple linear shift in the coordinates.

This may be illustrated with a simple example. An extended current function $F_c(x)$, shown in Figure 4-11, covers the interval from x_1 to x_4, and consists of three original current functions defined in the sub-intervals $x_1 < x < x_2$, $x_2 < x < x_3$, and $x_3 < x < x_4$. The subscript c in $F_c(x)$ reflects the relation of this function to the chain basis functions. One of the 3 original current functions, $F_1(x)$ is highlighted (shown as a thick dashed curve), and will be used for an illustration.

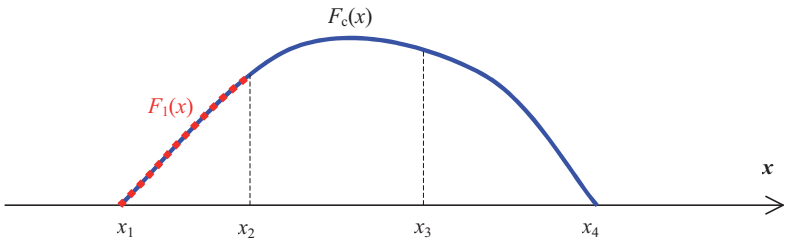

Figure 4-11. Example of an extended basis function based on a polynomial function.

The old and new basis functions are considered to be polynomials. Each of the original current distribution functions is comprised of n_b+1 polynomial basis functions with coefficients a_k:

$$F_1(x) = \sum_{k=0}^{n_b} a_k (x - x_{c1})^k, \quad x \in [x_1, x_2].$$

The new set of basis functions has the same form as the original set of basis functions. That is:

$$F_c(x) = \sum_{k=0}^{N_b} A_k (x - x_c)^k \text{ , defined on the interval } x \in [x_1, x_4].$$

The degree of polynomial and its coefficients in the new set are denoted with N_b and A_k, respectively.

For the polynomial basis functions, the difference in the coefficients comes from the difference in the origin for the respective co-ordinate systems. The new and the old basis functions may be inter-related, so that the new coefficients of the polynomials are expressed via the coefficients of the original basis functions.

In order to express the function $F_c(x)$ in the same form as the function $F_1(x)$, the parameters x_c and x_{c1} can be related to each other through a displacement, denoted with Δ:

$$x_{c1} = x_c + \Delta.$$

Then the function $F_c(x)$ may be rewritten as

$$F_c(x) = \sum_{k=0}^{N_b} A_k (x - x_c)^k = \sum_{k=0}^{N_b} A_k \left((x - x_{c1}) + \Delta \right)^k$$

The expression in the inner brackets, $(x - x_{c1})$, is the same as the argument in the series $F_1(x)$. To simplify writing the expressions, it will be given a temporary dummy name, $\xi = x - x_{c1}$. The resulting expression $(\xi + \Delta)^k$ may be rewritten using the binomial expansion. This brings the function $F(x)$ to the following form:

$$F_c(x)=\sum_{k=0}^{N_b}A_k\left(\xi+\Delta\right)^k=\sum_{k=0}^{N_b}A_k\sum_{n=0}^{k}C_n^k\Delta^{k-n}\xi^n=\sum_{k=0}^{N_b}A_k\sum_{n=0}^{k}C_n^k\Delta^{k-n}\left(x-x_{c1}\right)^n$$
$$=\sum_{n=0}^{N_b}B_n\left(x-x_{c1}\right)^n,\quad where\quad B_n=\sum_{k=n}^{N_b}A_kC_n^k\Delta^{k-n}\qquad,$$

and the factor C_n^k is the binomial coefficient defined [Råde, 93] as $C_n^k\equiv\binom{k}{n}\equiv\frac{k!}{n!(k-n)!}$.

The values of the coefficients B_n were deducted by considering the structure of the series, and with the help of Table 4-4.

Table 4-4. Structure of the series for coefficients $B_n=\sum_{k=n}^{N_b}A_kC_n^k\Delta^{k-n}$ relating the old and new sets of polynomial basis functions.

	$n=0$	$n=1$	$n=2$	$n=3$	…
$k=0$	$A_0\cdot\mathbf{C}^0{}_0\cdot\Delta^0\,\xi^0$				
$k=1$	$A_1\cdot\mathbf{C}^1{}_0\cdot\Delta^1\,\xi^0$	$A_1\cdot\mathbf{C}^1{}_1\cdot\Delta^0\,\xi^1$			
$k=2$	$A_2\cdot\mathbf{C}^2{}_0\cdot\Delta^2\,\xi^0$	$A_2\cdot\mathbf{C}^2{}_1\cdot\Delta^1\,\xi^1$	$A_2\cdot\mathbf{C}^2{}_2\cdot\Delta^0\,\xi^2$		
$k=3$	$A_3\cdot\mathbf{C}^3{}_0\cdot\Delta^3\,\xi^0$	$A_3\cdot\mathbf{C}^3{}_1\cdot\Delta^3\,\xi^1$	$A_3\cdot\mathbf{C}^3{}_2\cdot\Delta^1\,\xi^2$	$A_3\cdot\mathbf{C}^3{}_3\cdot\Delta^0\,\xi^3$	
$k=$…	…	…	…	…	…

Thus, the coefficients B_n are expressed through the coefficients A_k of the new basis functions as $B_n\left(\left[A_k\right]\right)=\sum_{k=n}^{N_b}A_kC_n^k\Delta^{k-n}$.

In its new form, the expression $F_c(x)=\sum_{n=0}^{N_b}B_n\left(A\right)\left(x-x_{c1}\right)^n$ may now be compared with the original set of polynomial basis functions $F_1(x)=\sum_{k=0}^{n_b}a_k(x-x_{c1})^k$. For the functions $F_c(x)$ and $F_1(x)$ to produce the same values, their coefficients must match:

$$a_k=B_n(A).$$

Thus, the relationship between the old and new coefficients may be established.

Note:

Another method to obtain the coefficients is to require the function and all its derivatives to match within the domain of definition: $F_1(x)= F_c(x)$, $F_1'(x)= F'_c(x)$, $F_1''(x)= F''_c(x)$, ..., for all $x_1 < x < x_2$. Then, as the first step, the relation between the coefficients for the highest order terms can be obtained. This will lead to determining the coefficients for the next lower order terms, and so on, until the slope and intercept coefficients are obtained.

It may also be noted that the coefficient of the term with the highest degree is always transferred without any modifications. This can be easily proven by requiring the function's highest derivative to match within the domain of definition: $F_1^{(k)}(x)= F_c^{(k)}(x)$, for all $x_1 < x < x_2$.

The coefficients used in the function $F_1(x)$ can be written as a column vector $[a_k]$. The same can be done with the coefficients $[A_k]$ in the function $F_c(x)$. Having done all the transformations described in the above, it is possible to write the relationship between the old $\left[a_i\right]_{i=0,1,\ldots,M-1}$ and new coefficients $\left[A_j\right]_{j=0,1,\ldots,N-1}$ as a matrix multiplication with a matrix **G** of size M x N, with elements $\left[G_{ij}\right]$:

$$\begin{bmatrix} a_0 \\ a_1 \\ \vdots \end{bmatrix} = \mathbf{G} \begin{bmatrix} A_0 \\ A_1 \\ \vdots \end{bmatrix}.$$

In an expanded form, the expression for each of the coefficients a_i may be written as:

$$\begin{aligned} a_0 &= G_{11}A_0 + G_{12}A_1 + G_{13}A_2 + G_{14}A_3 + \ldots \\ a_1 &= G_{21}A_0 + G_{22}A_1 + G_{23}A_2 + G_{24}A_3 + \ldots \\ &\vdots \\ a_{i-1} &= G_{i1}A_0 + G_{i2}A_1 + G_{i3}A_2 + G_iA_3 + \ldots \end{aligned}$$

Recalling that the coefficients in the left-hand side vector may also be written as $a_i = B_i(A) \equiv \sum_{k=i}^{N_b} A_k C_i^k \Delta^{k-i}$, the matrix coefficients [G_{ij}] relating the old and new higher order sets of polynomial basis functions may be expressed as

$$G_{ij} = C_{i-1}^{j-1} \Delta^{k-i}.$$

It may be noted from the expression for the coefficients $B_i(A)$, that for a single set of polynomial basis functions (later referred to as a partial set), the resulting partial matrix **G** is upper triangular, with all the elements below the main diagonal equal zero.

The transformation matrix for the complete system, including multiple partial sets of basis functions (a set per each individual wire/chain) may then be composed by appending the respective matrices, in the order defined by the order in which the unknown coefficients are numbered. With an appropriate numbering scheme, the complete compression matrix may still remain upper triangular. Utilisation of this property helps to reduce the number of floating point operations (e.g. addition, multiplication) required.

It may also be noted that in order to utilise this approach, the order of the new polynomial (for a chain) must be equal or higher than the order of the polynomial for any wire within the chain. Otherwise, the unutilised coefficients may be ignored by setting the respective element of the compressing matrix to zero.

Note: a Simple Approach for Identifying the Individual Coefficients of a Polynomial From a Composite Polynomial

The technique derived in the above addresses situations where the value of the integral corresponding to each individual term in a polynomial basis function is known. In practice, the situation is frequent where the tight degree of integration is not possible and only the final impedance matrix is available. Each element of this matrix is usually based on a composite polynomial including several terms, where each term has a different power. In order to separate the individual coefficients it might be possible to set up a linear system. If the number of unknowns in this system exceeds the number of equations available, it is possible to re-compute the missing terms for a few of the lowest powers of each polynomial.

Note:

The matrix **G** *is lower triangular and has* $\frac{1}{2}n_b(n_b+1)$ *non-zero entries.*

It may be readily verified that, when the co-ordinate systems coincide, i.e. $\Delta=0$*, the matrix* **G** *reduces to a unitary diagonal matrix. This may be considered as an indication of the correctness of the derivations.*

The other particular case of interest is when $\Delta=1$*. Then, the matrix* **G** *is essentially a table of binomial coefficients. Taking an example of* $n_b=7$*, the matrix* **G** *is*

$$\mathbf{G}=\begin{bmatrix} 1 & & & & & \vdots & \\ 1 & 1 & & & \cdots & 0 & \cdots \\ 1 & 2 & 1 & & & \vdots & \\ 1 & 3 & 3 & 1 & & & \\ 1 & 4 & 6 & 4 & 1 & & \\ 1 & 5 & 10 & 10 & 5 & 1 & \\ 1 & 6 & 15 & 20 & 15 & 6 & 1 \end{bmatrix}.$$

Note:

This transformation may be generalised on transforming old and new polynomial sets that have different number of terms and/or powers. This requires an approximate method, such as a variational [Kantorovich and Krylov, 37] or least-square [Kolundzija, 45] technique, and is not included in this thesis.

4.10.3 On Optimal Calculation of Matrix **G**

In a practical implementation, the matrix **G** is computed for each wire. It is therefore important to try to minimise the number of operations required for building this matrix. It is clear that the factors C_{j-1}^{i-1} may be pre-computed and stored. It may also be noted that the main diagonal of the matrix is always unitary, and does not require calculations. This leaves the calculation of various powers of Δ^k, k=0,1, …, n_b-1, and $\frac{1}{2}(n_b-2)(n_b-1)$ multiplications to scale the coefficients of a stored triangular matrix of rank n_b-2 by these Δ^k. Thus, filling in the matrix **G** requires a total of $n_b-2+\frac{1}{2}(n_b-2)(n_b-1) = \frac{1}{2}(n_b-2)(n_b+1)$ floating-point operations (FLOPs).

Note:

The total number of FLOPs required to obtain all matrices **G** *for a system as a whole may be substantially reduced if the mesh uses points spaced equidistantly.*

4.10.4 Conversion between Terms of a General Polynomial and Polynomial-Based Function

The algorithm discussed in the beginning of Section 4.10.1 requires the ability to decompose a polynomial-based function into its power terms, using a matrix form. In addition, the algorithm also requires composing a basis function from the individual power terms, also in a matrix form. This section describes these transformations.

The transformation between a polynomial set $\{x^i\}_{i=1,2,\ldots,N}$ represented as a column vector $[P]_{N\times 1}$ and the set of nodal and singleton basis functions $\{N_i,S_j\}_{i=1,2;j=3,4,\ldots,N}$ defined in (2.40)-(2.42) and represented as a column vector $[BF]_{N\times 1}$ may be written in a matrix form as

$$[BF]=[X]\cdot[P].$$

Expanding this notation for the basis functions defined in Table 2-3, the above expression is written as

$$\begin{bmatrix} \frac{1}{2}(1-x) \\ \frac{1}{2}(1+x) \\ x^2-1 \\ x^3-x \\ x^4-1 \\ x^5-x \\ \vdots \end{bmatrix} = \left[\begin{array}{c|c|cccc|c} \frac{1}{2} & -\frac{1}{2} & 0 & 0 & 0 & 0 & \\ \frac{1}{2} & \frac{1}{2} & 0 & 0 & 0 & 0 & \\ -1 & 0 & 1 & 0 & 0 & 0 & \cdots \\ 0 & -1 & 0 & 1 & 0 & 0 & \\ -1 & 0 & 0 & 0 & 1 & 0 & \\ 0 & -1 & 0 & 0 & 0 & 1 & \\ \vdots & \vdots & & \vdots & & & \ddots \end{array}\right] \cdot \begin{bmatrix} x^0 \\ x^1 \\ x^2 \\ x^3 \\ x^4 \\ x^5 \\ \vdots \end{bmatrix}.$$

Note:

The matrix [X] *of rank* n_b *has only* $2n_b$ *non-zero entries, and may, especially when* $n_b>>2$, *be considered as a block or sparse matrix, i.e. storing non-zero blocks or entries only. When* n_b *is large, this may speed up calculations since matrix multiplication subroutines for sparse matrices will not try to multiply zero elements.*

The inverse conversion

$$[P] = [X]^{-1} \cdot [BF]$$

from the column vector of basis functions $[BF]_{N\times 1}$ back to the column vector of polynomial set $[P]_{N\times 1}$ may be calculated by inverting the matrix [X]. This may also be accomplished by doing the decomposition manually (filling in the entries of the matrix manually, without resorting to a numerical inversion of matrix [X]):

$$\begin{bmatrix} x^0 \\ x^1 \\ x^2 \\ x^3 \\ x^4 \\ x^5 \\ \vdots \end{bmatrix} = \left[\begin{array}{c|c|cccc} +1 & +1 & 0 & 0 & 0 & 0 \\ \hline -1 & +1 & 0 & 0 & 0 & 0 \\ \hline +1 & +1 & 1 & 0 & 0 & 0 \\ -1 & +1 & 0 & 1 & 0 & 0 \\ +1 & +1 & 0 & 0 & 1 & 0 \\ -1 & +1 & 0 & 0 & 0 & 1 \\ \vdots & \vdots & & \vdots & & \end{array}\right] \cdot \begin{bmatrix} \frac{1}{2}(1-x) \\ \frac{1}{2}(1+x) \\ x^2-1 \\ x^3-x \\ x^4-1 \\ x^5-x \\ \vdots \end{bmatrix}.$$

Note:

The matrix $[X]^{-1}$ *of rank* n_b *has only* $3n_b$-2 *non-zero entries. Thus it also may be considered as a sparse matrix, provided that* $n_b >> 2$.

4.11 Computational Complexity Evaluation

In the following, computational complexity in terms of the number of floating point operations (FLOPs) is estimated for the direct and compressed (MDBF) methods discussed in previous sections and chapters. The obtained estimates are then used to compare the performance of the methods.

The derivations made in this section are based on an assumption that a geometrical structure consists of N_w single geometrical current-defining segments (wires). It is assumed that each segment requires n_b basis functions.

It is also assumed that these N_w wires may be divided into n_c chains, and each chain also requires n_b basis functions. The ratio of the number of wires to the number of chains is denoted with letter K, symbolising a compression ratio. The value of K also tells the average number of wires in a chain.

NB! In the derivations, the memory traffic [Golub, 24] is neglected.

4.11.1 The Original System

The number of unknowns in the original uncompressed system is expressed as $N=(n_b\text{-}1)\cdot N_w$. The original system of linear equations represented in matrix form as $\mathbf{Z}\cdot\mathbf{I} = \mathbf{V}$ requires approximately $1/3\cdot N^3$ complex floating-point operations (FLOPs) to solve and obtain N unknown currents represented with a column vector $\mathbf{I}$. An opportunistic scenario of a complex multiplication is considered. It requires 4 real multiplications and 2 real additions as compared to a complex division that requires 5 additional real FLOPs. Thereby, the total number of FLOPs will be of the order of $2\cdot N^3$. In terms of the number of wires and basis functions per wire, this translates into $2\cdot(n_b\text{-}1)^3\cdot N_w^3$.

4.11.2 Compressed System

The new compressed system will have $n=N/K$ unknowns. Conversion of the original system of N linear algebraic equation $\mathbf{Z}\cdot\mathbf{I} = \mathbf{V}$ into a new compressed form $\mathbf{Z}^{new}\cdot\mathbf{I}^{new} = \mathbf{V}^{new}$ with n, $n\leq N$ unknowns requires the following steps:

1 Form chains.

This operation requires on the order of N_w manipulations for identifying and establishing chains as a set of structures.

In addition, identifying and splitting electrically long chains into shorter chains requires (a) a calculation of a cumulative sum for each chain (K FLOPs per chain), (b) comparisons to establish optimum ratios ($2K$ FLOPs per chain). The last remark is based on the assumption that a pseudo-optimum algorithm C (refer to Section 4.4.6) is used.

The total count of FLOPs is estimated as $n_c\cdot(3K) = 3N_w$.

2 Obtain an N×n transformation matrix $\mathbf{M}$ relating the old set of N variables $\mathbf{I}$ to a new set of n variables $\mathbf{I}^{new}$ with $\mathbf{I} = \mathbf{M}\cdot\mathbf{I}^{new}$.

As already mentioned in Section 4.6, the matrix $\mathbf{M}$ is formed with sub-matrices $\mathbf{m}$. corresponding to the sets of basis functions.

Sub-matrices are required for (a) each junction of wires, where the respective old and new doublet-related variables need to be inter-linked, and (b) each wire, where the coefficients of old singletons are to be related to the coefficients of new chain-based singletons.

This step may be considered in the following sequence:

- Form an array for a cumulative length of wires in a chain in order to evaluate the distances between the old and new co-ordinate systems, and calculate the respective values of Δ.

  This requires $2K$ real additions for each chain.

  Note:

  Part of this operation may also be done already during the process of forming chains, since it is necessary there for identifying and splitting up electrically long chains.

Each sub-matrix **m** is a product of matrix **X** (transforming hierarchical polynomials into polynomial basis functions), matrix **G** (converting the co-ordinate system used as argument of polynomials), and an inverse of matrix **X**. This product is $\mathbf{m} = \mathbf{X}\cdot\mathbf{G}\cdot\mathbf{X}^{-1}$. Thus, this step includes 2 matrix multiplications of a sparse matrix, lower triangular matrix, and another sparse matrix.

- Calculation of matrix **G**.

  As discussed earlier, calculations involved in obtaining one matrix **G** requires n_b-2+½(n_b -2)(n_b-1) = ½(n_b -2)(n_b+1) FLOPs.

- Matrix product $\mathbf{t} = \mathbf{G}\cdot\mathbf{X}^{-1}$. (sizes $[n_b \times n_b] \cdot [n_b \times n_b]$)

  A matrix product of real matrix **G** and real sparse matrix $\mathbf{X}^{-1}$ results in summations $t_{i,j} = \sum_{k=1}^{q} Z_{i,k} M_{k,j}$, where q depends on the known number of non-zero entries in the i–th row of the triangular matrix **G**, for j=1,2. These add up to n_b^2 FLOPs.

For values of index $j>2$, there is only 1 non-zero element in the respective column of $\mathbf{X}^{-1}$, and the sum reduces to a single product of the respective element of **G** and unity, and does not need a computation.

- Matrix product $\mathbf{X}\cdot\mathbf{t}$. (sizes $[n_b\times n_b]\cdot[n_b\times n_b]$)

  This product may be considered in a similar manner. Therefore, it will also take n_b^2 FLOPs.

Note:

The resulting matrix **m** *is nearly lower triangular. In the upper triangle, it has only one element that is not equal to zero. That is*, $M_{1,2}=-M_{2,1}=-\frac{1}{2}\Delta$. *The 2 other "standing out" elements are* $M_{1,1}=1-\frac{1}{2}\Delta$ *and* $M_{2,2}=1+\frac{1}{2}\Delta$.

- The last three steps in obtaining sub-matrices **m** are repeated for each junction and for each wire (in total, $N_w+N_w\cdot(n_b-2)$ times) in order to complete the matrix **M**.

  Adding all FLOPs gives a total of

$$2K+(N_w+N_w\cdot(n_b-2))\cdot(n_b-2+\tfrac{1}{2}(n_b-2)(n_b-1)+n_b^2+n_b^2)$$

$$=N_w\cdot(7/2n_b^3-5n_b^2+5/2n_b-1)+2*K \text{ FLOPs.}$$

  Note:

  Most of the multiplications do not require any actual multiplication since one of the factors in the products is ±1.

  Moreover, considering the particular presentation in the matrices, it is possible to avoid matrix multiplications, and, instead, fill in the resulting matrix **m** *directly.*

  This may be illustrated with Figure 4-12 *on the example of matrix* **m** *including the elements of matrix* **G** *explicitly, generated for* $n_b=5$. *This example shows the main features for the structure of matrix* **m** *(first two rows are the same for any number of basis functions* n_b, *and the remaining rows have a simple hierarchical structure).*

```
> t3:=X.G.X^(-1);
```

$$t3 := \begin{bmatrix} \frac{1}{2}G[1,1] - \frac{1}{2}G[2,1] + \frac{1}{2}G[2,2] & \frac{1}{2}G[1,1] - \frac{1}{2}G[2,1] - \frac{1}{2}G[2,2] & 0 & 0 & 0 \\ \frac{1}{2}G[1,1] + \frac{1}{2}G[2,1] - \frac{1}{2}G[2,2] & \frac{1}{2}G[1,1] + \frac{1}{2}G[2,1] + \frac{1}{2}G[2,2] & 0 & 0 & 0 \\ -G[1,1] + G[3,1] - G[3,2] + G[3,3] & -G[1,1] + G[3,1] + G[3,2] + G[3,3] & G[3,3] & 0 & 0 \\ -G[2,1] + G[4,1] + G[2,2] - G[4,2] + G[4,3] - G[4,4] & -G[2,1] + G[4,1] - G[2,2] + G[4,2] + G[4,3] + G[4,4] & G[4,3] & G[4,4] & 0 \\ -G[1,1] + G[5,1] - G[5,2] + G[5,3] - G[5,4] + G[5,5] & -G[1,1] + G[5,1] + G[5,2] + G[5,3] + G[5,4] + G[5,5] & G[5,3] & G[5,4] & G[5,5] \end{bmatrix}$$

Figure 4-12. Example of sub-matrix m (here denoted with *t3*) transforming a column vector [BF^{new}] of new basis functions into a column vector [BF^{old}] of old basis functions with [BF^{old}]=m·[BF^{new}], where m=X·G·X^{-1}. The example has been generated for five hierarchical polynomial basis functions, n_b=5 using Maple [Maple, 68]. Elements of the matrix G are shown as G[i,j].

It is possible to show that such a reduced approach requires less than approximately $8+2\cdot\frac{1}{2}(n_b+3)(n_b-2)+\frac{1}{2}(n_b+3)$ real additions and only 4 multiplications. These add to a total of $n_b^2+1.5n_b+7.5$ FLOPs. This estimate will be taken as the final.

3 Compress the original $N\times N$ impedance matrix **Z** to obtain a new $n\times n$ impedance matrix **Z**^{new} by **Z**^{new} = **M**^{T}·**Z**·**M**.

- Matrix product **t** = **Z**·**M**. (sizes $[N\times N]\cdot[N\times n]$)

  A matrix product of complex matrix **Z** and real matrix **M** results in summations $t_{i,j}=\sum_{k=1}^{N} Z_{i,k}M_{k,j}$, where each summation requires $2N$ real multiplications and $2(N-1)$ real additions. This summation is repeated $N\cdot n$ times (corresponding to the number of elements in the resultant matrix **t**). Thus, the total number of FLOPs consumed by the product is $N\cdot n\cdot(4N-2)$.

- Matrix product **Z**^{new} = **M**^{T}·**t**. (sizes $[n\times N]\cdot[N\times n]$)

  This matrix product of complex matrix **t** and real matrix **M** results in $Z_{i,j}^{new}=\sum_{k=1}^{N} M_{k,i}t_{k,j}$, and requires requiring $2N$ real multiplications and $2(N-1)$ real additions. This summation is repeated $n\cdot n$ times (corresponding to the number of elements in the resultant matrix **Z**^{new}). The total number of FLOPs here is $n\cdot n\cdot(4N-2)$.

- The total count of FLOPs for the product $\mathbf{M}^{\mathrm{T}}\cdot\mathbf{Z}\cdot\mathbf{M}$ is thus $n\cdot(N+n)\cdot(4N\text{-}1)$.

  Using the identity $n=N/K$, this may be written as

  $$N^2\cdot(4N\text{-}1)\cdot(1+1/K)/\mathrm{K},$$

  thus showing the third power of N.

Note:

When the dimensions of a geometrical structure are large in terms of wavelength, and the structure itself is not complex, the matrix ***M*** *should have most of its entries null, and, asymptotically, be a sparse matrix.*

The sparseness of the matrix is expected to come from the spatial grouping of the original basis functions (in terms of new basis functions), and from a low spatial overlap between the domains of the (new) basis functions. Therefore, only on the order of K entries in each column of $\mathbf{M}$ *are not zero (the number of wires attached to a junction times K). Each row of* $\mathbf{M}$ *has only on the order of the number of wires joining a junction non-zero entries.*

Thus, the matrix product $\mathbf{M}^{\mathrm{T}}\cdot\mathbf{Z}\cdot\mathbf{M}$ *is expected to take significantly fewer FLOPs than the derived quantity. Considering that 2K entries in each column and 2 entries in each row are not zero, it is possible to show that the number of FLOPs reduces to*

$$2N^2(4K+3).$$

4 Compress the excitation vector $\mathbf{V}^{\mathrm{new}} = \mathbf{M}^{\mathrm{T}}\cdot\mathbf{V}$. (sizes $[n\times N]\cdot[N\times 1]$)

This matrix product results in $V_j^{new} = \sum_{k=1}^{N} M_{k,i}V_{k,1}$. Each element $V_{\mathrm{j}}^{\mathrm{new}}$ takes $2N$ real multiplications and $2(N\text{-}1)$ real additions. To fill in the vector $\mathbf{V}^{\mathrm{new}}$ requires n repetitions of that procedure. Thus, the total count of FLOPs here is $n\cdot(4N\text{-}2)$.

5 Solve the new system of linear equations $\mathbf{Z}^{\mathrm{new}}\cdot\mathbf{I}^{\mathrm{new}} = \mathbf{V}^{\mathrm{new}}$.

This operation requires $2\cdot n^3$ real-valued FLOPs.

6 Obtain currents in terms of original unknowns by $\mathbf{I} = \mathbf{M}\cdot\mathbf{I}^{\mathrm{new}}$. (sizes $[N\times n]\cdot[n\times 1]$)

This step takes a total of $N\cdot(4n\text{-}2)$ FLOPs.

Adding the counts from steps 1 to 6 up results in

$$n_c\cdot(3K) + n_b^2+1.5n_b+7.5 + n\cdot(N+n)\cdot(4N\text{-}1) + n\cdot(4N\text{-}2) + 2\cdot n^3 + N\cdot(4n\text{-}2) \text{ FLOPs} \quad (4.4)$$

required to obtain a solution with the compressing technique (under a presumption of a full matrix **M**).

4.11.3 Comparison

When the number of unknowns is small, i.e. $N\sim1$, the compression technique has an overhead that increases the solution time by over 100%. However, this inefficiency is unimportant for most practical situations, since the total number of operations is low and the total time to solve the system is usually negligible.

For large N, the estimate (4.4) may be simplified to the leading terms

$$2n(2N^2 + 2nN)) \approx 4N^3/\mathrm{K}.$$

It is possible to show that the leading term is due to the step 3 (compression of the original impedance matrix, with $n\cdot(N+n)\cdot(4N\text{-}1)\approx4N^3/\mathrm{K}$), and is computationally the most demanding.

This may be compared with about $2\cdot N^3$ FLOPs required to solve the system directly.

The ratio of the former and latter FLOP count estimates shows that, for a large number of unknowns $N>>1$ and basis functions per wire $n_b>>1$, and the ratio of the number of wires to the number of chains K, the compression technique provides a relative performance gain of about

$$(4N^3/\mathrm{K}) / (2\cdot N^3) = K/2\ (1\text{-}3/n_b). \quad (4.5)$$

This factors K and $(1\text{-}3/n_b)$ indicate that efficiency, even in the asymptotic sense, strongly depends on the ability to unite the wires (through the factor K), and on the order of approximation n_b. A higher number of wire segments aggregated into each chain, and a higher order polynomial of the MDBF, should offer a lower number of unknowns and a better compression for the impedance matrix.

Note:

It may be shown that, whether the matrix multiplications for $\mathbf{m}=\mathbf{X}\cdot\mathbf{G}\cdot\mathbf{X}^{-1}$ *are considered in a reduced form, or even as a multiplication of full matrices, the performance gain still arrives to K/2 (also in an asymptotic sense). This indicates that more or less arbitrary polynomial basis functions may be used in these transformations.*

Note:

In practical situations, this technique is efficient when the geometrical structure has curvatures that may not otherwise be modelled accurately in a piecewise manner. It is also helpful in treating the electrically small elements, and improving the condition number. With these in mind, it is probably not recommended to apply the technique blindly to an arbitrary situation, since the overhead operations may decrease performance. At the least, one should compare the number of FLOPS in terms of the exact expressions first.

Note:

Considering the note to step 3, the technique may provide the performance gain up to

$$K^{3}\cdot(1-3/n_b) - 4K^{7}/N,\ \ N\rightarrow\infty.$$

4.12 Transfer of Algorithms for Wires onto Plates, Chains of Wires and Chains of Plates

This section introduces an approach of extending a MoM based code written for wires onto more complex structures. The approach is based on an introduction of virtual wires, based on end points, and requires only a minor amount of additional coding related to generation of the virtual wires.

Thus, the algorithms developed for automatic processing of individual wires, and assigning the doublet and singleton basis functions to them can be easily adopted to apply them to the chains of wires, to plates (quadrilaterals) and to the chains of plates (quadrilaterals).

Note:

In this section, it is assumed that the compressing matrix is created in a step separate to the filling in of the compressed matrix (e.g. it follows the creation of the original uncompressed impedance matrix).

4.12.1 From Wires to the Chains of Wires

The idea is based on the analogy between the single wires and wire chains. A wire is defined with 2 nodes, designating the beginning and the end of the wire, as shown in Figure 4-13a. The notation of the *beginning* and *end* is used to define the direction of the current through the wire.

The Matlab code realising the MoM uses a data structure, where each wire is assigned two nodes (for the beginning and the end, respectively), wire radii of the beginning and the end, and other parameters. A 2-dimensional array *Wires* is used to store these data.

```
node1 = Wires(1,wn)    % obtain number of the first node for the wire number wn
node2 = Wires(2,wn)    % obtain number of the second node for the wire number wn
```

A wire chain is composed of several wires connected in series, as shown in Figure 4-13b. Considering these wires as one virtual wire (defined by the end points of the chain), one can identify the first and the last nodes. These nodes can then be used to define the direction for the flow of current through the chain, just as it is done with single wires.

Note:

In a practical realisation, it is also necessary to take into account that some of the wires in a chain may have the direction of the current flow defined on them such that it is opposite to the direction defined for the chain. In effect, this must then translate into changing the sign of the coefficients in the compressing matrix **M**.

Note:

It should be highlighted that the virtual wires are not used for the actual electromagnetic modelling, but only to be able to mimic the data structure, and utilise the already existing and proven algorithms.

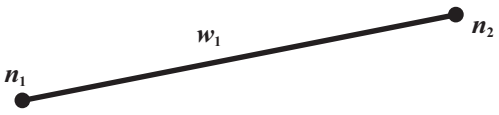

(a) Wire $\mathbf{w}_1$ defined with end nodes $\mathbf{n}_1$ and $\mathbf{n}_2$.

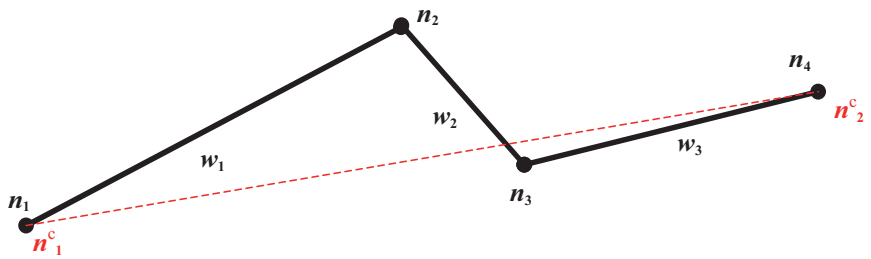

(b) Chain $\mathbf{c}_1$ composed of 3 wires $\mathbf{w}_1$, $\mathbf{w}_2$, and $\mathbf{w}_3$. The chain is defined with end nodes $\boldsymbol{n}^c_1$ and $\boldsymbol{n}^c_2$. The wires are defined with nodes $(\mathbf{n}_1,\mathbf{n}_2)$, $(\mathbf{n}_3,\mathbf{n}_2)$ and $(\mathbf{n}_3,\mathbf{n}_4)$, respectively. Note that the direction of the middle wire is thus opposite to the direction of the chain. The end nodes $\boldsymbol{n}^c_1$ and $\boldsymbol{n}^c_2$ correspond to the nodes $\mathbf{n}_1$ and $\mathbf{n}_4$. The dashed red line represents a virtual wire whose data representation is used as an equivalent to the chain.

Figure 4-13 . Steps in the analogy between the wires, wire chains, plates and plate chains.

The following Matlab code illustrates the usage of such equivalency:

```
% structure Chain(i).{wires(:),wends(:)}

wiren1 = Chain(i).wires(1)          % first wire
wend1  = Chain(i).wends(1)
wiren2 = Chain(i).wires(end)        % last wire
wend2  = Chain(i).wends(end)

node1 = Wires(wend1, wiren1)   % first node
if wend2==1, wend2==1; else wend2=2; end;
node2 = Wires(wend2,wiren2)    % last node
```

Note:

The data structure used for storing chains utilises the flexibility of Matlab, which takes care of dynamic memory management. In a practical realisation, it is also possible to

use one of the more classical data structures to store the data. For example, a one-dimensional array may keep the sequences of wires, stored in a linear fashion. Then another array may be used for indexing the elements in the first array (to define the beginnings of the chains).

Otherwise, one may use pointers and allocate memory dynamically, as it is done in Matlab. This is an easier but somewhat slower approach.

Before the compressing matrix **M** may be created, the basis functions must be assigned to the chains. It is possible to write special sub-routines to handle this. However, the concept of virtual wires enables the use of exactly the same algorithms and subroutines as for wires. The only requirement for this is to create an array of virtual wires (corresponding to the sub-divided chains).

4.12.2 From Wires to Quadrilaterals and to the Chains of the Latter

The concept of virtual wires may also be used to assign basis functions to quadrilateral geometrical elements (herein, further referred to as *plates*) and to the chains of plates. Again, the same algorithms and subroutines may still be used as for wires and chains of wires, respectively.

A two-dimensional structure like a plate, requires 2 virtual wires, as illustrated in Figure 4-14.

The two virtual wires correspond to a decomposition of the surface current into two currents flowing through the plate's surface.

Note (repeated):

The virtual wires are not used for the actual electromagnetic modelling, but only to be able to mimic the data structure, and utilise the already existing and proven algorithms

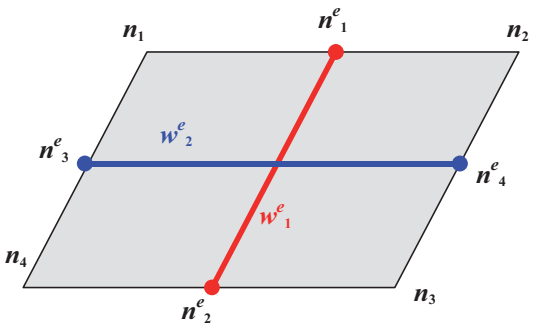

Figure 4-14. A plate and two virtual wires reflecting two current flow directions. A plate defined with the nodes n_1-n_4. The sides of this plate are divided into two halves with new, equivalent nodes n^e_1 to n^e_4 placed, for example, in the middle of each side. Effectively, the plate is replaced with two virtually equivalent wires w^e_1 and w^e_2, defined with nodes (n^e_1,n^e_2) and (n^e_3,n^e_4), respectively.

4.13 Application to the Wire Meshes

The ideas related to the aggregation of wire segments may also be applied to a more general class of wire structures, such as a fine wire mesh, where electrically small cells may be united [Lysko, 64]. A fine wire mesh is used in wire-only programs, such as SuperNEC [105] by Poynting, South Africa, to model solid conducting plates. In that scenario, the aggregation of the fine cells into larger ones may be equivalent to disjoining the crossing wires in a cell, illustrated in Figure 4-15. There, the thin wires that cross but do not have a node at the crossing point are not connected electrically. The current on the wires inside the cells shown in Figure 4-15b with thick lines may be estimated (interpolated) through the values at the nodes. This is shown with thick lines in Figure 4-15b. Summarising, this process the current inside the new cells is decomposed into vertical (see Figure 4-15c) and horizontal (see Figure 4-15d) components. Those components may be interpolated from the values on the new rougher grid, and this interpolation may be readily used in the context of the grouping/compressing the impedance matrix.

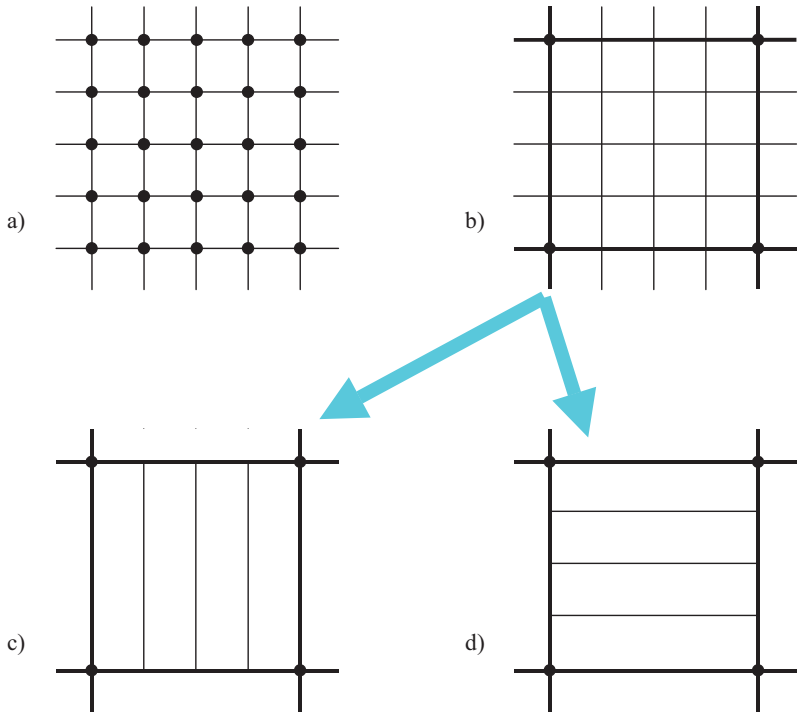

Figure 4-15. Possible aggregation of a grid that is electrically fine. (a) Original fine mesh. (b) The result of aggregation process, where unknowns are assigned only on the new rougher mesh (on the wires shown with thick lines); the current on the inner wires (with respect to the "thick" wires) is interpolated from the "thick" wires (and is used in the context of the grouping). In the simplest form, this process is equivalent to a decomposition of the currents on the inner mesh into independent vertical (c) and horizontal (d) components. In all plots, the nodes (where electrical connections are taken into account) are shown with dots.

NB The transformation from (a) to (b) is restricted by the maximum dimensions of a cell in the original mesh (bounded by four neighbouring dots). The maximum dimension of a cell must be much smaller than the wavelength.

4.14 Summary

This chapter introduces several original derivations and discussions related to a novel class of basis functions named "multiple domain basis functions" (MDBF). These basis functions allow covering one to several individual wire segments with a single set of basis functions. In doing so, the number of unknowns is decoupled from the number of geometrical segments, permitting more efficient modelling of structures with curvatures

and with electrically small features. Application of the MDBFs to such structures results in a smaller number of unknowns and a smaller rank impedance matrices (termed "compressed"), regardless of how fine the mesh (i.e. the piece-wise linear geometrical approximation of the structure) around a curvature is.

The chapter starts with a motivation for and an overview of the approach. The new compressed column-vector of unknowns is described as a product of a compression matrix and the original column-vector of unknowns.

In order to simplify treatment, a concept of chains is introduced. A chain is defined as a series of wire segments, all connected in series. The process of applying the MDBFs begins with identifying the chains of wire segments, and then splitting these chains into shorter manageable sub-chains. The latter part is similar to the division of long wires into shorter segments, often used by commercial modelling software. The chapter introduces original algorithms for both identification and splitting processes. All the algorithms are fully automatic. The splitting process is guided by the splitting parameter, which is the maximum permitted electrical length of any single sub-chain. An in-depth set of discussions and comparisons have been made with regard to differentiating between the algorithms. In addition, the results produced by these algorithms have been compared against the results produced by searching through the complete set of possible splits and using various metrics. The comparison indicated a sense of optimality for the mesh generated, and highlighted that the algorithms are able to achieve desired goals (e.g. uniformity of mesh). Even more discussions on the comparison between the algorithms can be found in the subsequent chapters.

The chapter then gives an example of applying the MDBFs to a geometrical structure composed of five wires, continuing on the example from Chapter 3. In the example, the error in the input impedance computed through the compressed solution was found to be within 0.5% of the impedance due to the traditional MoM. The example of applying the MDBFs includes a discussion on the comparison between the results obtained via a direct method of moments and the proposed compressing technique. It was found that by minimizing the condition number, the impedance due to the new (compressed) solution can be made to be within 0.02% of the traditional calculation.

Next, the technique just applied to the MDBFs of piecewise linear (PWL) profile is extended to the piecewise linearly-interpolated piecewise sinusoidal (PWS) basis functions. Moreover, it has also been concluded that the method can be further extended onto arbitrary piecewise linear-interpolated shapes of basis functions at no additional computational cost. Furthermore, a finer mesh will result in a better approximation of the shape, with no increase in the rank of the compressed linear system.

This is followed by a derivation and discussions on a new method for computing the compression matrix when both the original and the new basis functions are polynomials. This method includes the three main steps describing the decompositions between the polynomial forms and a shift of the coordinate system. Each step is discussed in detail. Subsequently, a derivation and discussion on the computational complexity of the proposed method are made. It is shown that the reduction in the number of unknowns is proportional to the number of wires per chain. It is also shown that the reduction in the number of unknowns can also be improved by increasing the degree of polynomial approximation, although this improvement quickly becomes smaller, with the growth in the degree of polynomial approximation.

At the end of the chapter, it is shown how the method can be applied to the plates and wire meshes with virtually no additional code required.

Chapter 5. Application Examples

The chapter focuses on the application of the matrix compression technique developed in Chapter 4. This chapter starts with a brief reference to the programming code developed. This is followed by illustrating the application of the compression technique on several detailed examples, ranging from a small monopole to a coil-loaded antenna. Both piecewise linear and piecewise sinusoidal basis functions are considered, together with all three chain splitting algorithms A, B, and C. A similarity between the behaviour of the error convergence curves of the compression technique with PWL and PWS basis functions, and a direct MoM with 1st and 2nd degree polynomial basis functions, respectively, is discussed. The compression technique's ability to reduce the number of unknowns with no sacrifice in accuracy is demonstrated on a coil-loaded antenna, an object which includes curved structures. Guidelines and suggestions end the chapter.

5.1 Note on the Code Realizing the Compression Technique

The code uses a thin wire method of moments (MoM) theoretical framework based on the works [Kolundzija et al., 45-47] and described in Chapter 2 and Chapter 3. Multiple domain basis functions (MDBFs) introduced in Chapter 4 have been implemented and permit to reduce the number of unknowns. The code also includes other modules also based on original ideas, e.g. the computation of the radiation pattern described in Section 3.10 and Appendix B [Lysko, 66], and memoization [Lysko, 61].

The code was written to be file-compatible with WIPL-D [Kolundzija et al., 47]. In addition, two modules for trans-coding the geometry between WIPL-D and PCAAD [84] have been written. This extra work afforded the author the possibility to compare the results between his own Matlab code, WIPL-D and PCAAD. In addition, the company WIPL-D d.o.o., Serbia, the owner of WIPL-D software, kindly provided a special feature in WIPL-D Pro v.6.1 that permits storing the impedance matrix generated by WIPL-D, in a file. This saved a significant amount of time in generating relatively large impedance matrices (sized to over 5000 unknowns).

The total size of the Matlab-based programming code created for this thesis, including the routines to manipulate and present data, amounts to over 20000 lines of code. Some

details on the functionality, structure of the code, and its testing can be found in Appendix C.

5.2 Introducing the Application Examples

A number of examples were selected in order to consider various aspects important in effective application of the compression technique. The selection criteria included the need to demonstrate features and behaviour of the compression technique and compare them against the direct MoM and measured data.

The examples include the following:

- **Two electrically short dipoles (one thin and one thick)**

This first example served as a proof-of-concept example, where the compression technique is shown to deliver results matching both an available theoretical reference and the results produced by the direct MoM. It also shows that the ability of the compression technique to enforce the required shape of the current distribution can be used to counteract some of the restrictions of the thin wire approximation and delta gap generator.

- **Meander monopole**

This example builds up the complexity of the geometrical structure under consideration. A meander monopole is first optimized with respect to its length. The resulting structure is then used to investigate the properties of the compression technique. A piecewise linearly interpolated PWS basis function (pwliPWSbf) serving as a multiple domain basis function (MDBF) is compared to the piecewise linearly interpolated PWL basis function (pwliPWLbf), already tried in Example 1. The chain splitting algorithms *A*, *B*, and *C* are inter-compared.

- **Half wave straight dipole**

This example, of a very thin dipole, serves to illustrate that the results of the compression technique converge into the reliable and well proven results from the direct MoM. Here, the study starts with a revision of the properties of the PWL and higher order polynomial basis functions applied to the dipole. This prepares a basis for comparing results with those obtained by the compression technique. The convergence

of obtained accuracy versus the number of used unknowns is then used to illustrate the equivalency between (a) the interpolated PWL (pwliPWLbf) serving as MDBF, and (b) the traditional PWL basis functions [Balanis, 5], as well as between (c) the interpolated PWS serving as MDBF (pwliPWSbf) and (d) 2^{nd} degree polynomial basis function.

- **Thin wire monopole loaded with a choke**

This practical example is used to demonstrate the advantages of the compression technique when modelling structures that include curved elements. The example starts with a thorough numerical study of the structure using the direct MoM. This also prepares a basis for comparing the results from direct MoM to the ones obtained by the compression technique. The application of the compression technique is then characterized in terms of used MDBFs, meshing algorithms and symmetry considerations. The discussions include details of modelling with different meshing and basis functions. The consequences to the impedance matrix condition number, current distribution approximation, and convergence of the results are also discussed. For this coil-loaded monopole, the compression technique is shown to require much fewer unknowns than a direct MoM, at the same level of required input impedance accuracy.

In addition to the above-mentioned examples, the references [Rogers and Butler, 97] and [Rogers and Butler, 96] give other samples of successful application of a similar impedance matrix compressing technique, based on piecewise linear basis and pulse testing functions. The examples demonstrated in these two references are a resonant loop antenna, normal and axial mode helices, and a spiral antenna.

It is noted that this work extends on the samples of applications shown in the above-mentioned references [Rogers and Butler, 97] and [Rogers and Butler, 96]. This work includes detailed investigations with regards to the effects of the meshing and different basis functions on the result. Furthermore, it considers the condition number, and implements the piecewise linearly interpolated piecewise *sinusoidal* basis functions.

5.3 Example 1: Two Short Dipoles

In this subsection, two 1 m long dipoles are independently modelled at the frequency of 1 MHz. Of the two dipoles considered, one is very thin with wire radius of 1 μm, and

the other is very thick with wire radius 0.5 m. The thin dipole is used to provide a preliminary validation for the compression technique, as the traditional direct method of moments (MoM) can solve this problem. Also, an analytical solution is available. The thick dipole is modelled to illustrate how grouping the individual segments can help with getting around the limitations of both a thin wire approximation condition and the problem associated with delta gap generators (discussed in Section 3.3).

Several models were built for simulating the behaviour of the dipoles.

Some models composed a dipole with 10 wire segments. For the thick dipole, this breaks a condition of having the length of a wire segment much larger than the diameter of the wire, due to the thin wire approximation (the conditions are listed in Section 2.4), and also permits the current to have a large capacitive component near the generator.

1) Some other models were made up of only two wire segments, improving on the conditions mentioned in (1).
2) Two metallic plate-based models of the think dipole were designed to avoid reliance on the thin wire kernel normally used for wire modelling, and to obtain more robust results. One of the two models included the end caps covering the otherwise hollow model of the wire.
3) Own Matlab code was applied to the wire models to obtain results and for comparison against the other models.

Table 5- shows a summary of the obtained results.

Analysis of these results shows that the dipole made of very thin wire is modelled very well by any of the available methods, including the compression technique. The other, very thick dipole cannot be modelled with the thin wire kernel based traditional MoM accurately, if it is represented by ten wire segments, as the input impedance obtained in this way is far from the values obtained by more advanced methods (e.g. plate models). This result is the same whether WIPL-D or own Matlab code are applied.

Using the compression algorithm with a sufficiently large splitting parameter (i.e. the maximum permitted length of a sub-chain must be greater than the length of the dipole's arm) forces a single rooftop basis function onto the dipole. This therefore gives the same value of the input impedance as with the direct MoM applied to a dipole modelled with two wire segments. The advantage offered by the developed compression

algorithms is in providing an opportunity to process the electrically small features systematically and automatically (including identification, grouping, splitting etc.)

Table 5-1 Input impedance of two electrically short dipoles modelled using various techniques. The dipoles are 1 m long, and are modelled at 1 MHz. By default, the total length of the dipole is split into 10 wire segments.

Model		**Wire R=1 μm**	**Wire R=500 mm**
Theoretical formula for electrically short dipole		0.219 – 16469i (reference)	0.22 – 1487i
Wire models in WIPL-D			
"as is" (traditional MoM)		0.214 – 16419i	0.11 – 1251i
Only 2 segments per dipole		0.219 – 16443i	0.22 – 1649i
Plate models in WIPL-D			
No caps			0.18 – 1700i
With end caps			0.20 – 1670i
Wire models using own MoM code			
Own program (traditional MoM)		0.214 – 16420i	0.11 – 1251i
Own program, applying the compression algorithm,		0.219 – 16444i	0.22 – 1649i

5.3.1 Summary

This example illustrates that the impedance matrix compression technique can be used to improve the quality of a solution even when the thin wire approximation can not be satisfied within the traditional MoM, or the current is allowed to vary too greatly due to a close proximity of electrically very small segments / features. The example also shows that the matrix compression can be tuned to produce results matching those due to traditional direct MoM. This offers a mechanism to decouple the number of unknowns from the number of geometrical segments (i.e. a mechanism to decouple the electromagnetic and mechanical sides of modelling).

5.4 Example 2: a Meander Monopole

A summary of the results can be found in [Lysko, 59], [Lysko, 60].

5.4.1 Geometrical Structure

The geometry of the meander is based on a basic element as shown in Figure 5-1. This element is a set of four interconnected wires, each 1 m long and with a radius of 1 mm. The ratio of wire segment length to radius, 1000:1, was set to be sufficiently large to satisfy the thin wire approximation conditions. This aims to ensure validity of the numerically obtained results, even under the finest meshing of the chain into sub-chains.

Each wire is at a straight angle with respect to the neighbouring wires. More complex structures shown in Figure 5-2, were built of this basic element. This was done by attaching the elements to one another whilst turning each next element by a constant angle with respect to the previous one. A total of 10 basic elements were used, resulting in the total height of 20 m, and equivalent to 40 m of bent wire.

The structures are modelled as being on a perfectly conducting ground plane, and are all fed with a delta gap generator (discussed in Section 3.3). Most of the simulations were performed at the frequency 2.28485 MHz (near 1st resonance).

5.4.2 Finding the Shortest Monopole

First, several versions of the monopole shown in Figure 5-2 were simulated with WIPL-D to identify which configuration provides the greatest effect in reducing the resonance frequency and minimizing the height.

The plot of the first resonance frequency versus the turning angle is shown in Figure 5-3b. The plot tells that the last structure out of the ones shown in Figure 5-2 gives the lowest resonance frequency. This is attributed to minimizing the coupling between the adjacent basic elements. The coupling is minimized by maximizing the distance between the elements, provided by the 180 degrees turning angle.

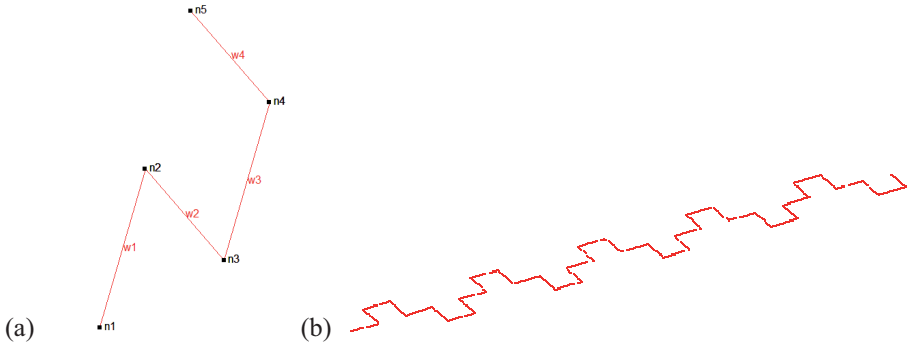

Figure 5-1 (a) Basic Element. It is composed of four wires, each 1 m long and 1 mm radius. (b) Final meander monopole.

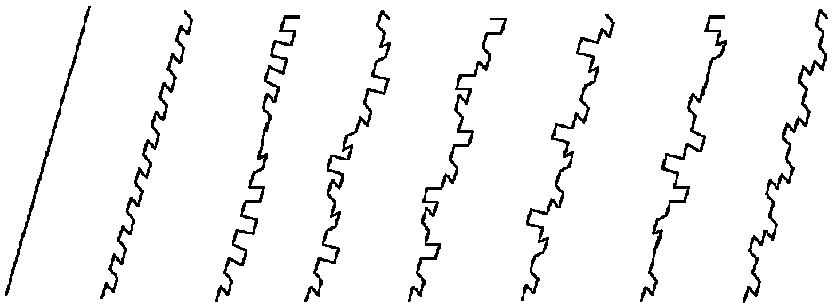

Figure 5-2 Monopole configurations tested. (a) A straight monopole used for comparison (20 m tall, 1 mm wire radius), (b)-(h) Meander monopoles of the same total height. The basic elements composing the monopoles are rotated at a linearly increasing angle with steps 0°, 30°, 60°, 90°, 120°, 150°, and 180°.

These resonance frequencies can be compared against the first resonance frequency of a straight monopole of the same total height, as shown in the first configuration in Figure 5-2a. This monopole has a resonance at 3.655 MHz. This means that the height of a straight monopole (0.25λ) must be nearly 1.5 times more than that of this meander monopole (0.1523λ). The wire length used for the monopole is 0.3047λ.

In the next step, the resonance properties of the resulting structure were investigated.

As seen from Figure 5-3a, the horizontal dark strip at the last segment (number 40) corresponds to zero current at the end of a monopole. The vertical bright feature seen in the same figure around 2.3 MHz corresponds to the first resonance in the monopole. A

dark diagonal stripe observed in the bottom right-hand side corner is due to a low level of current magnitude and is attributed to the null in a standing wave current pattern.

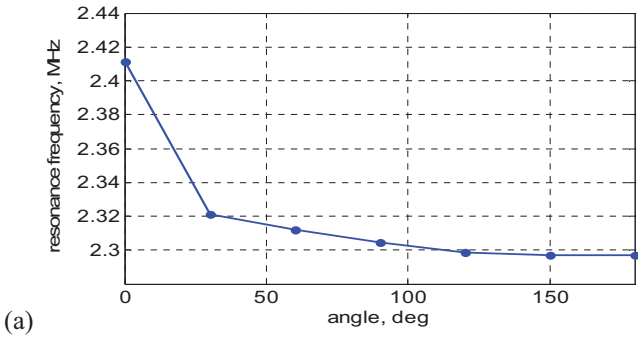

(a)

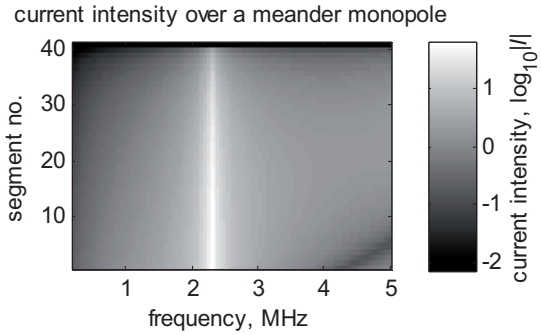

(b)

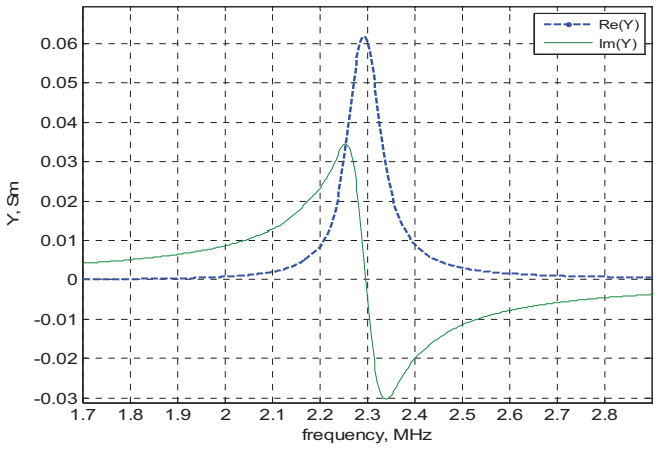

(c)

Figure 5-3 (a) Resonance frequencies of the meander monopole samples versus the angular shift between the basic elements of a meander monopole. (b) Current intensity on the wire against frequency. (c) Input conductance and susceptance of the final meander monopole versus frequency.

The plot of admittance of the selected meander monopole against frequency is shown in Figure 5-3c. The behaviour is similar to other classical resonant antennas.

5.4.3 Application of the Piecewise Linearly Interpolating PWL and PWS Basis Functions

In applying the compression technique to the meander monopole, it is possible to choose the maximum permitted electrical length of a sub-chain (i.e. the chain splitting parameter) within a wide range of values. The minimum useful value is defined by the electrical length of the shortest segment of the structure. The maximum useful value is the total electrical length of all wire segments in the meander monopole. It is also possible to use a smaller or larger range but this will not provide a complete picture or will not add any additional information, respectively.

The meander monopole consists of 40 wire segments of equal length. From this, the minimum value of the splitting parameter was chosen to be the same as the electrical length of a single segment. In order to obtain comprehensive information about the behaviour of the compression technique when it is applied to this meander monopole, the complete range of 1 to 40 lengths of a wire segment must be covered. Thus, 40 simulations with different values of the splitting parameter were prepared.

In each simulation, the compression technique was applied to the impedance matrix obtained from the direct MoM. This results in a new compressed impedance matrix, excitation vector, and a respective solution.

In total, 40 possible solutions became available for comparison against the reference solution. The reference solution is the solution resulted from full uncompressed impedance matrix generated by the direct MoM.

The results were processed together to obtain a set of various parametric plots, where either the number of unknowns or the maximum permitted electrical length was used as the parameter.

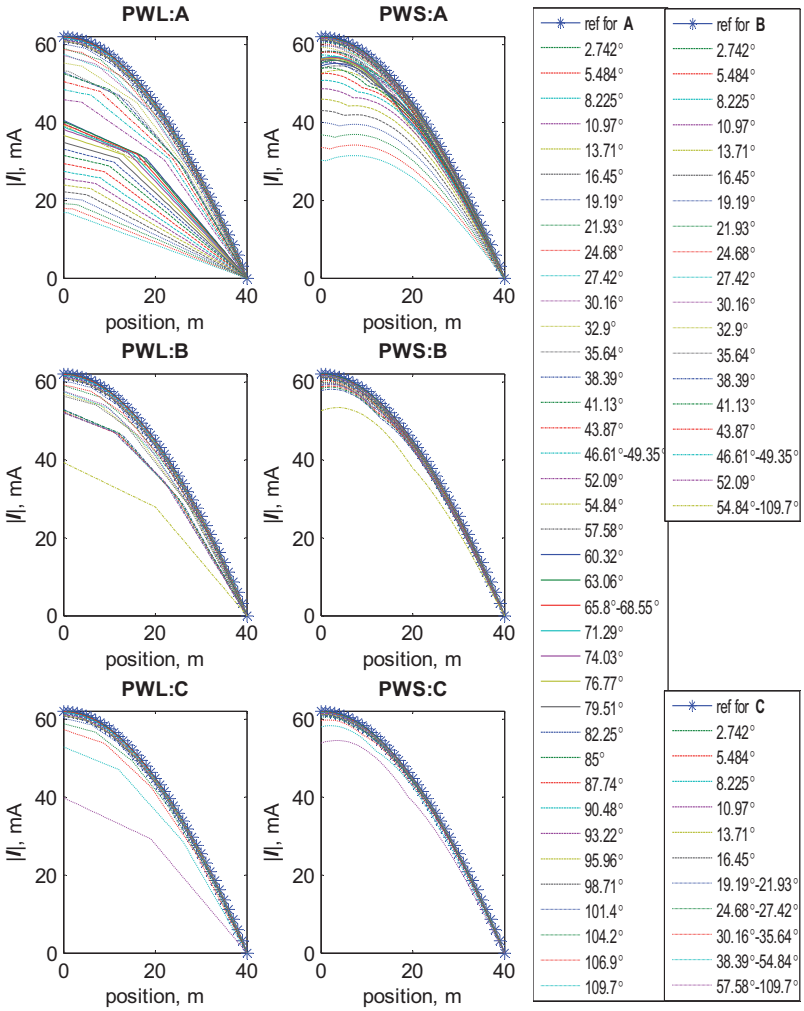

Figure 5-4 Current distribution along the meander monopole at frequency 2.28485 MHz, calculated using the impedance matrix compression technique. The sub-titles "PWL" and "PWS" stand for piecewise linear and piecewise sinusoidal interpolating functions assigned to chains. The letters "A", "B", or "C" in the sub-titles denote the co-named algorithm used to split an electrically long chain into shorter sub-chains. The horizontal axis marks the distance along the wire, starting from the feed point. The vertical axis specifies the current magnitude. The curves which trace the same current profiles have been collected under the same legend. Stars (*) denote the most accurate (reference) solution using a direct method of moments solution.

The above procedure was repeated for each combination of the piecewise linearly interpolating basis functions (PWL and PWS) and the selection of segmenting/chain splitting algorithms (*A*, *B*, or *C*).

Figure 5-4 shows how the choice of an interpolating basis function (PWL and PWS) and the selection of a segmenting algorithm (*A*, *B*, *C*), influences the calculated current distribution along the meander monopole. The distribution of curves with respect to the reference curves (solutions) indicate that the algorithms *B* and *C* are preferred in comparison to the algorithm *A*, as there are only a few curves belonging to the algorithms *B* and *C* that are relatively far away from the reference curve. Also, a comparison of the lengths of the legends between algorithms *A*, *B* and *C* indicate that the algorithm *C* achieves the narrowest, most grouped distribution with respect to the reference solution.

The plots (a) and (b) in Figure 5-5 show that there is a strong correlation between the ratio of the maximum and minimum length of wire segments used in the structure and the impedance matrix condition number. A visible correlation between the peaks in the just mentioned ratio of longest to shortest segments, and in the condition number, with the peaks in the solution error shown in Figure 5-5c for PWL:*A*, confirms the initial assumption that the algorithm *A* cannot avoid overly short segments from being singled out.

Furthermore, Figure 5-5c demonstrates that the usage of algorithms B and C is preferred to A in terms of minimizing the average solution error. Out of the algorithms B and C, the same figure indicates that the algorithm C performs better, at least for this specific structure.

The same figure shows a drastic difference between usage of PWL and PWS basis functions. The PWS basis function shows consistently better accuracy as compared to PWL basis functions. This is valid for any value of the splitting parameter, as shown in Figure 0 5c.

It may also be important to note that the error curves are mostly monotonically increasing with the growth in the roughness of the mesh (i.e. with an increase in the value of the splitting parameter).

(a)

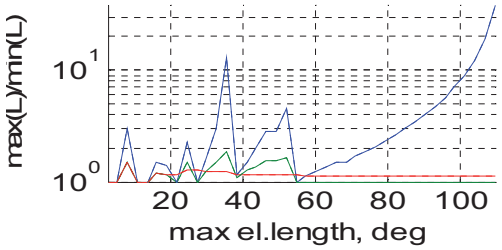

(b)

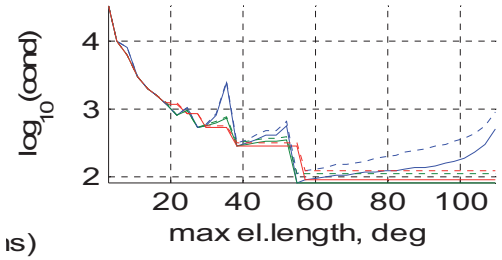

(c)

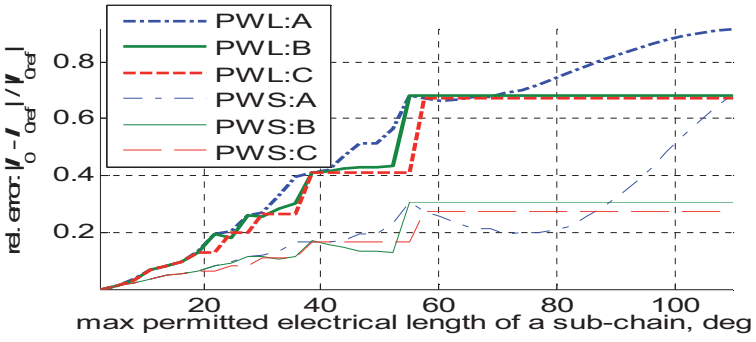

Figure 5-5 (a) Error in current at the feed point, (b) Degree of non-uniformity in splitting a long chain into shorter sub-chains, and (c) Condition number versus the chain splitting parameter "maximum permitted electrical length of a sub-chain", i.e. max(*kL*). The error was estimated with respect to an equivalent WIPL-D model. (c) A convergence plot of error in the current at the feed point against the solution due to the direct MoM. In all plots, blue, green and red curves correspond to algorithms A, B, and C, respectively. The solid lines (—) are generated using piecewise linear (PWL) basis functions on sub-chains, whilst the dashed lines (- - -) are generated using piecewise sinusoidal (PWS) basis functions on sub-chains.

5.4.4 Summary

This example compares the results of using the linearly interpolated PWL and PWS profiles for the multiple domain basis functions (MDBF) applied to a meander monopole on a perfectly conducting ground plane.

A meander monopole is first optimized with respect to its length, and the resulting structure is then used to investigate the properties of the compression technique.

The compression method for grouping sub- and large domain basis functions into multiple domain basis functions (MDBF) is expanded to support piecewise linearly interpolated piecewise sinusoidal basis functions (pwliPWSbf), as compared to the piecewise linearly interpolated PWL basis functions (pwliPWLbf) used in the previous example. This example compares the results of using linearly interpolated PWL and PWS profiles serving as the MDBF and applies to a meander monopole on a perfectly conducting ground plane.

The results for the pwliPWSbf have demonstrated notable improvements in the current distribution estimation, as compared with the pwliPWLbf. This includes a narrower spread in the current distribution plots, symbolizing better average stability of the PWS function with respect to the mesh, even though this function is interpolated linearly.

In addition, it was noticed that there exist a clear correlation between the ratio of the longest and shortest segments, impedance matrix condition number, and accuracy of results. This helps to explain the failure of chain splitting algorithm *A* at certain values of the splitting parameter. In this example it was found that, among the three developed algorithms (*A*, *B* and *C*), the algorithm *A* is the least stable or accurate, whilst the algorithm *C* was found to be the most promising in terms of both stability and accuracy.

5.5 Example 3: Straight λ/2 Dipole

This model expands on the previous examples by increasing the number of unknowns under consideration and by a direct comparison to alternative commercial computational electromagnetics software PCAAD v6.0 [84], in addition to WIPL-D Pro v.6.1 [39].

The total length of the dipole is 0.4907λ (0.1472 m). It is composed of 1000 identical wire segments, 500 per arm. The wire radius is 1 μm. The dipole is fed with a delta gap generator of amplitude 1 Volt. The dipole is modelled at the frequency of 1 GHz.

5.5.1 Modelling with WIPL-D

In order to obtain reference data, a set of models of the dipole were first generated in WIPL-D compatible format, using own Matlab script. The following configurations have been modelled (differing in the number of wire segments used; degree of polynomial applied to the segments; and usage of the current expansion option, controlling the automatic assignment of the polynomial degree to a wire segment):

- **CE**: 2 fixed wire segments; the current expansion (CE) level was varied from 1 to 50. This should result in the required variation in the number of unknowns from 1 to 100.
- **Pn**: 2 fixed wire segments; the degree of polynomial assigned to each wire segment, Pn, was varied from 1 to 99. This should result in the required variation in the number of unknowns from 1 to 197.
- **Nw**: the number of wire segments per arm (segments of equal length) was varied from 1 to 1000. The polynomial of the degree 1 was used: Pn = 1; this should result in the variation in the number of required unknowns from 1 to 1999.
- The previous step was repeated for several other values of the degree of polynomial (applicable to each of the wire segments). In total, the polynomials of the following degrees were used: Pn = {1, 2, 3, 5, 9}; This should result in the variation in the number of required unknowns from 1 to over 5000, depending on both the number of wire segments per arm and the degree of polynomial per segment.

A summary of the simulation results is shown in Figure 5-6. The plots of input impedance in Figure 5-6a,b show the following:

An attempt to control the current expansion level (please refer to the red dashed curve with squares), whilst letting WIPL-D split the two wires into appropriate segments of its choice automatically, showed a very quick convergence towards the expected true solution. The WIPL-D stopped increasing the degree of polynomial at 29 unknowns. This is probably a safety boundary for achieving stable results under the automatic control of the program.

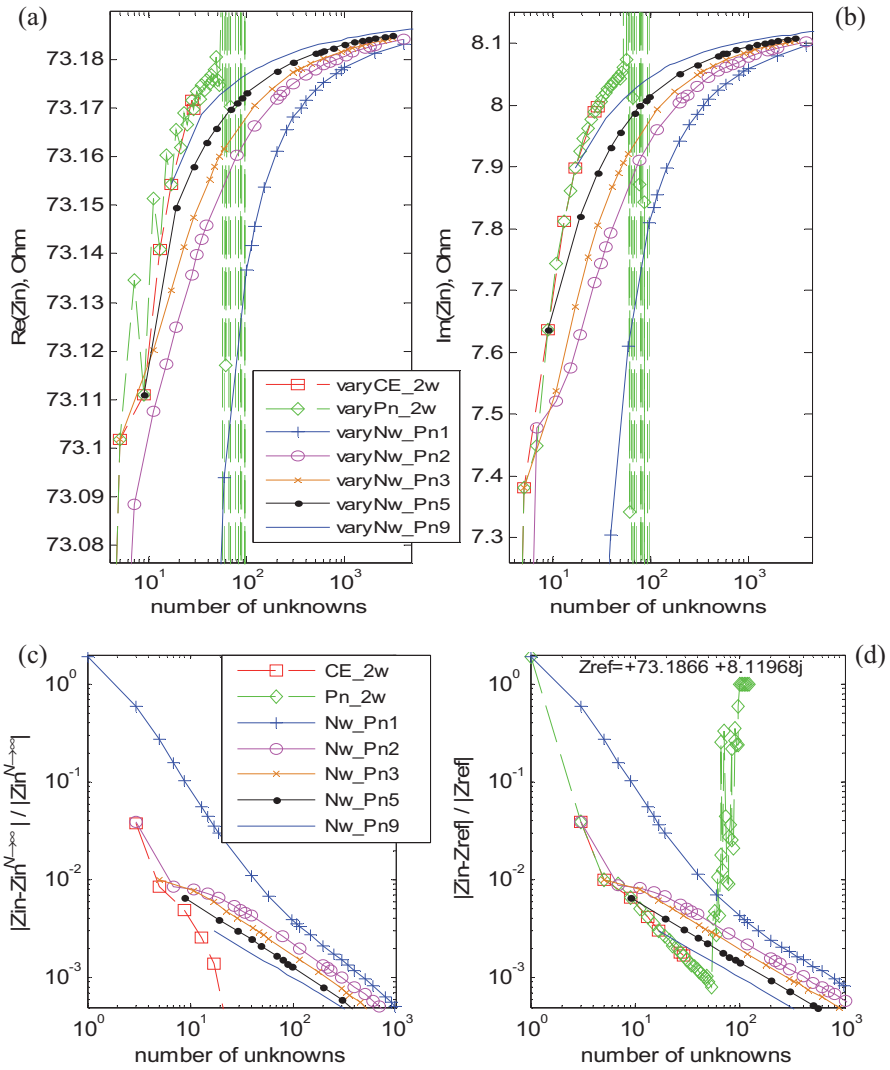

Figure 5-6 Convergence plots for a thin half-wave dipole modelled using several WIPL-D options. (a), (b): Input impedance versus number of unknowns. (c) Error per curve (with respect to the most accurate value per curve) versus number of unknowns. (d) Error with respect to a common reference versus number of unknowns. The legend entries specify which parameter was varied to increase the number of variables: current expansion option for *CE_2w*, polynomial degree for *Pn_2w* (keeping only *2* wire segments), number of wire segments for *Nw_PnX* (*X* is the degree of polynomial per segment). Double precision was used in all simulations.

The next curve, shown as the green dashed line with diamonds, describes the scenario where the automatic control was turned off, and polynomial basis functions of increasing order were assigned to only two wire segments (i.e. the number of wires was fixed). The attempt to increase the degree of polynomials worked well for relatively low degrees of polynomials. At higher degrees, the curve "varyPn_2w" first starts to oscillate around the intended values, indicating a numerical instability which leads to an unusable random oscillation over very large ranges of both resistance and reactance. This behaviour is attributed to the quick growth in the condition number of the impedance matrix, as the degree of a non-orthogonal polynomial basis function is increased. As soon as the result of this growth exceeds the threshold of machine precision (as discussed in Section 3.8), the solution becomes unusable. This result confirms that the degree of a non-orthogonal polynomial basis function must be chosen with care in order to take advantage of a quick convergence in the solution [Kolundzija et al., 51], and also explains the need for a safety boundary mentioned earlier.

Each one of the remaining five curves, denoted with "varyNw_Pn*X*", results from multiple simulations, where the number of unknowns is increased by increasing the number of sub-divisions for each arm of the dipole. At the same time the degree of the polynomial basis function, applied to the segments resulting from the sub-division, remained constant for each curve.

Notes:

a. These five curves start at different number of unknowns. This is because the number of unknowns in this scenario approximately equals to a product of the number of wire segments used for the dipole and the degree of polynomial assigned to each wire segment. This means that the initial number of unknowns increases with an increase in the degree of polynomial.

b. The higher order basis functions show a better convergence to the expected true solution. This can also be confirmed in Figure 5-6c,d.

c. The relative error shown in Figure 5-6c is calculated by comparing the value of the input impedance at a given set of parameters against the value of input impedance at the

set of parameters giving the greatest number of variables (within the same dataset/curve).

d. The relative error shown in Figure 5-6d is calculated by comparing the value of the input impedance at a given set of parameters against the value of input impedance at the set of parameters indicating the best combination of stability, convergence and accuracy. The input impedance value of Zref = 73.1866 + 8.1197i Ohm was used as the reference input impedance. This value was calculated for the dipole divided into 600 wire segments, where each segment was assigned a 9^{th} degree polynomial. This resulted in a total of 5399 unknowns.

e. In Figure 5-6d, the asymptotic behaviour of the curves shows that the higher degree basis functions offer a better convergence of the solution. Increasing the degree of polynomial by one can improve accuracy of the solution by about 80%, with the same number of variables (as long as the dynamic range of the used machine precision is sufficiently large).

Having obtained certainty in the type and range of results to be expected, the next step was to apply the impedance matrix compression technique.

5.5.2 Application of the Compression Technique

A detailed description of the procedure followed to obtain the complete set of solutions from all the combinations of the basis functions, splitting parameter and the splitting algorithm is available in the previous example, in Section 5.4.3 on page 211.

As this dipole uses 500 segments for each arm, 500 different values of the splitting parameter were prepared (ranging from the electrical length of one wire segment all the way up to the full length of the dipole's arm). In total, 500 simulations were done (each using own value of the splitting parameter) for each possible combination of the basis functions, splitting parameter and the splitting algorithm. In addition, as the direction of propagation also affects the results, the above procedure was repeated for each of the 4 possible combinations in propagating an algorithm along 2 arms of the dipole.

The results were presented as a function of a parameter, which was either the maximum electrical length of a sub-chain (splitting parameter) or the total number of unknowns in the compresses system. Selected samples of those results are presented in this text.

Figure 5-7 provides the plots for the ratio of the shortest and longest sub-chains versus the chain splitting parameter in the upper plot, and the order of magnitude of the condition number for the compressed impedance matrix in the lower plot.

The upper plot in Figure 5-7 shows that the high peaks in the ratio of the shortest sub-chain and longest sub-chain are mostly associated with the chain splitting algorithm *A*. The algorithm *B* also experiences slight increase in the ratio, but to a significantly lower degree.

The compressed matrix's condition number, as displayed in the lower plot in Figure 5-7, is affected by the peaks in the ratio of maximum and minimum sub-chain lengths. The mesh produced by the algorithm *A* leads to the worst peaks in the condition number.

Figure 5-7 tells that the condition number is higher when the spitting parameter is lower, i.e. when most of the sub-chains are short and the number of unknowns in the compressed system is high. As the splitting parameter is increased, permitting larger sub-chains and reducing the rank of the compressed system, the effect of the peaks becomes more evident. As the amplitude of the peaks in the ratio in the middle of the plot is just slightly smaller than for the high maximum permitted electrical length, the condition number seems to be more influenced by the size of the system than by the peaks in the ratio of sub-chain lengths.

The condition number for the original uncompressed impedance matrix is the leftmost point on the condition number plot in Figure 5-7.

Figure 5-7 presents the six plots of the current distribution over the complete length of the dipole for all combinations of two interpolating basis functions and three splitting algorithms. The combination PWL:*A* shows to be the most inaccurate or most sensitive to the peaks in the ratio of the longest and shortest sub-chains.

The interpolated PWL multiple domain basis function in combination with algorithms *B* and *C* shows nearly as good convergence to the reference solution as the combinations involving the piecewise linearly interpolated PWS MDBF. The triangle like current

profiles in the plots for PWL:B and PWL:C correspond to the solution with one unknown.

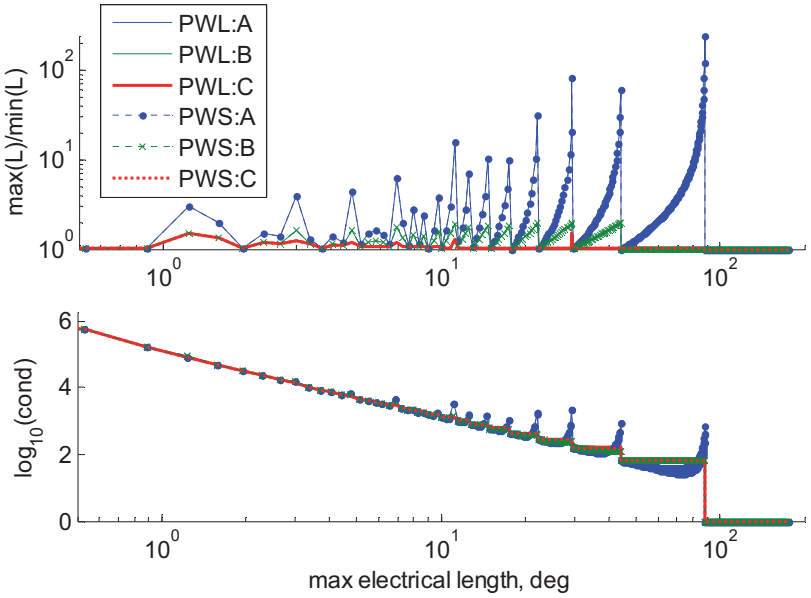

Figure 5-7 Ratio of the lengths for the longest and shortest sub-chains (in the upper plot), and the compressed impedance matrix condition number (in the lower plot) versus the splitting parameter for a half-wave dipole. The chain splitting algorithm propagated from the feed point outwards for both arms of the dipole. PWL and PWS stand for linearly interpolated piecewise linear and sinusoidal basis functions used as multiple domain basis functions (MDBF). The letter following that, *A*, *B*, or *C*, denotes the splitting algorithm used.

A careful inspection of all plots can reveal that the combination PWS:*C* supplies the thinnest set of curves. This indicates that this combination should provide the most stable and probably the most accurate results in modelling a dipole.

The convergence plot in Figure 5-9 confirms the conclusion made in the previous example, i.e. the linearly interpolated piecewise sinusoidal (PWS) basis functions offer a much better convergence rate compared to the piecewise linear (PWL) basis functions.

The two lines with big circle markers denoted with “varyNw_Pn1,2” are obtained by applying a direct (traditional) MoM to the same dipole. This confirms that application

of linearly interpolated PWL basis functions to a straight structure like a dipole is fully equivalent to application of a traditional MoM with the same number of variables.

It can also be noticed that application of linearly interpolated PWS basis functions to a straight structure like the one considered, is similar to application of a traditional MoM with the same number of variables.

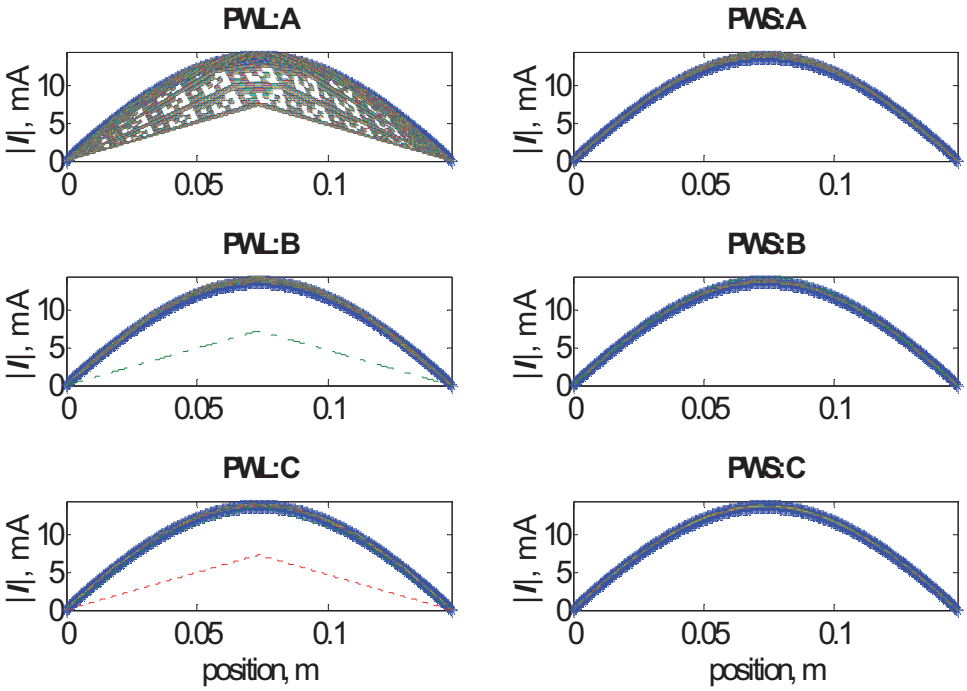

Figure 5-8. Current distribution over the dipole obtained with the compression technique for various chain splitting algorithms (A, B and C), linearly interpolated piecewise linear (PWL) and sinusoidal (PWS) basis functions. Each subplot includes a reference solution (denoted with the blue stars) and solutions due to compressing the impedance matrix with different values of the splitting parameter (i.e. maximum permitted electrical length of a sub-chain). The reference solution is obtained from the finest mesh applied.

These conclusions have been expected, as the compression technique cannot reduce the number of unknowns on a straight structure, in comparison to the traditional MoM. This is because the traditional MoM can already and easily take advantage of re-meshing such a structure. Otherwise, still within the traditional MoM, one can also apply arbitrary, including higher order, basis functions to the structure, as it has been

successfully done in WIPL-D [Kolundzija et al., 47]. The strength of the compression technique comes to play when there are (a) smooth bend approximated piece-wisely with straight segments, and/or (b) electrically small[54] and possibly repeating features.

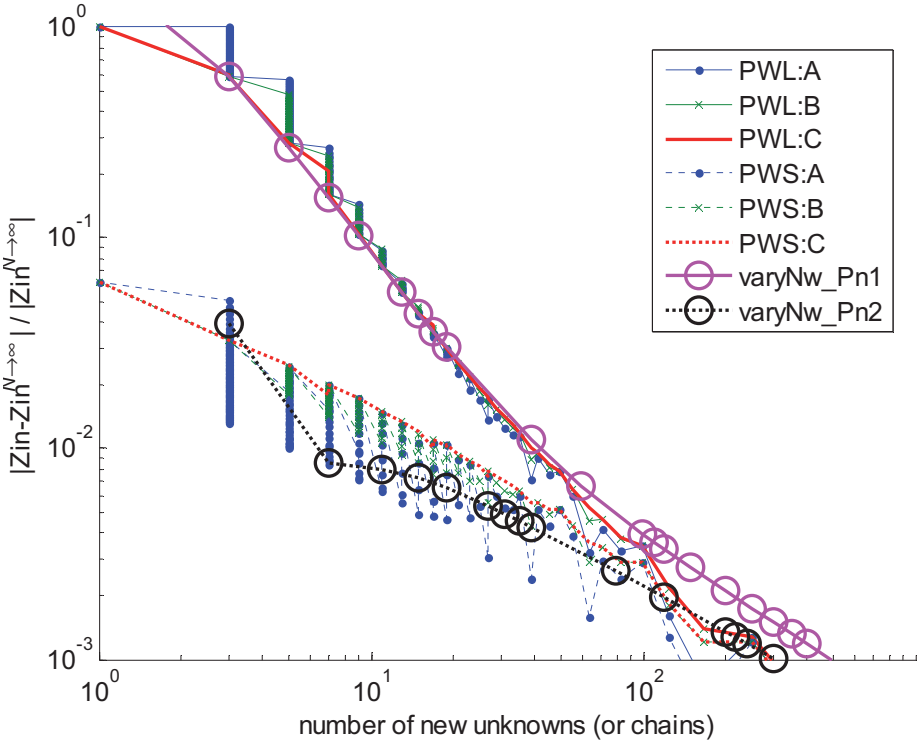

Figure 5-9 Error versus the number of unknowns due to compression. The abbreviations PWL and PWS stand for piecewise linear and sinusoidal basis functions, respectively. The letters A, B and C in the legend refer to the co-named algorithms for splitting a chain into finer sub-chains. The in splitting the chains (arms of the dipole) into sub-chains (smaller wire segments), these algorithms propagated from the feed outwards. The relative error was calculated with respect to the solution from the finest mesh applied to the structure. The lines "varyNw_P1,2" are convergence lines for applying 1st and 2nd degree polynomial basis functions to the same dipole within the direct MoM.

[54] The efficiency requirement for the features to be small is due to restrictions of the PWL and PWS basis function, as they cannot be applied over a sufficiently long segment.

5.5.3 Comparison against Reference Software

The compression technique was compared against the program PCAAD[55] version 6.0 [84] for piecewise sinusoidal (PWS) basis functions and against WIPL-D Pro version 6.1 [39] for piecewise linear (PWL) basis functions. In addition, WIPL-D Pro was used to produce the convergence curve for higher order polynomial basis function. In particular, the 9th degree polynomial was tested for comparison purposes.

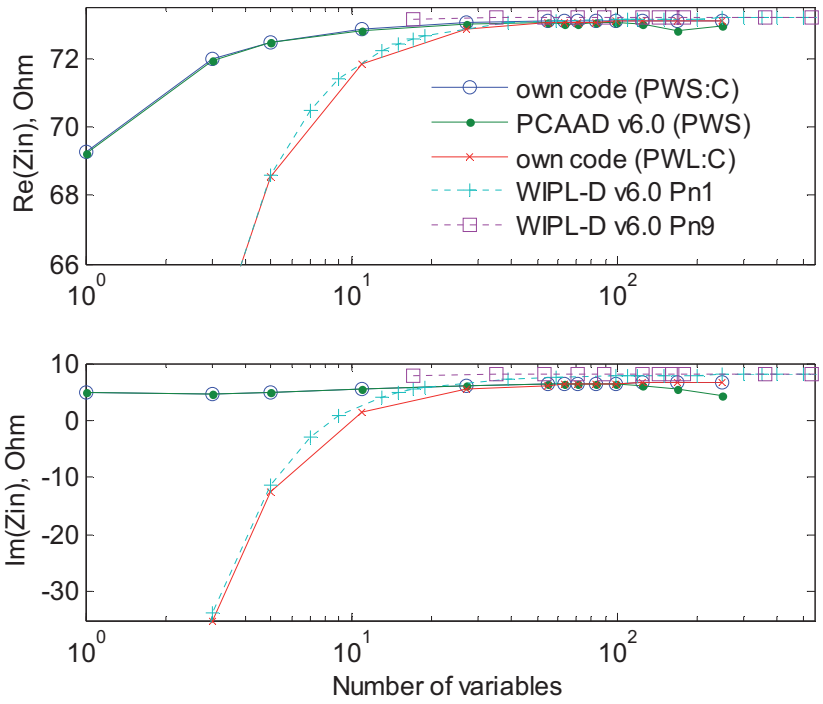

Figure 5-10 Convergence curves for the input impedance of a thin dipole. The compression technique was applied when using "own code". The PCAAD v.6.0 gave the convergence curve for piecewise sinusoidal (PWS) basis functions. The WIPL-D Pro v.6.1 was used to obtain the reference convergence curves for piecewise linear (PWL) basis functions, i.e. 1st degree polynomial denoted with Pn1, as well as the 9th degree polynomial basis functions (denoted with Pn9).

[55] PCAAD stand for Personal Computer Aided Antenna Design [84].

The plots in Figure 5-10 show that the compression technique, in applying linearly interpolated PWL basis functions (shown with red line with diagonal crosses), produced results very close to the ones produced by WIPL-D Pro using 1st degree polynomial basis functions (cyan curve "Pn1" with crosses). The match between the curves "Pn1" and "PWL:*C*" is perfect to excellent for low number of variables (most of this range is out of the graph). For a high number of variables, the match between the two curves is excellent to good, as the difference between the "Pn1" curve and "PWL:*C*" curve has a trend of increasing with an increase in the number of unknowns. This is attributed to the unequal accuracy in computing impedance matrix elements in the own code compared to WIPL-D Pro v.6.1.

The same figure also provides a visual comparison between the results produced by PCAAD v.6.0, which uses only PWS basis functions, and the results due to using the linearly interpolated PWL basis functions for applying the impedance matrix compression technique. The match is excellent for low to intermediate total number of variables. The PCAAD v.6.0 starts to diverge from the ~~correct~~ trend at about 100 variables.

Note:

This has been investigated by analyzing the impedance matrix produced by PCAAD v.6.0, and also by comparing the same to the impedance matrix produced by own Matlab code. Both programs generate very closely matched values for the main diagonal of the impedance matrix. The difference starts to increase as one move away the main diagonal. In the following argument, it is assumed that the basis functions in PCAAD are numbered in the same manner as in author's own Matlab code, i.e. linearly, from one end of the dipole towards the other end. Provided so, the magnitude of the matrix elements must decay monotonically as one moves away from the main diagonal, since the coupling between the wire segments must decrease with the distance. The impedance matrix for this dipole is a Toeplitz matrix. Thus, it is necessary to check the decay on one row or column only. The impedance matrix produced by PCAAD v.6.0 showed a slight deviation from the decay requirement, as the elements far away from the main diagonal started to have noisy pattern. NB! This behaviour is only

observed in PCAAD when the diameter of the wire in a dipole is extremely small, like in the example under consideration.

The curve "Pn9", based on applying 9th degree polynomial basis functions to the same structure, was added to the plots in Figure 5-10 to illustrate the advantage of using higher order basis functions. As it may be seen from Figure 5-10, this curve demonstrates an excellent convergence in the results, which is expected to benefit the compression technique as well. *NB!* Application of the higher order basis functions have not been implemented in author's programming code, as yet.

5.5.4 Summary / Conclusions

The model of a straight very thin half wave dipole has been investigated using both traditional direct method of moments (MoM) and the compression technique developed.

The direct MoM was used with several basis functions differing in the degree of polynomial used. The polynomial basis functions of degrees 1 (i.e. piecewise linear basis function: PWL BF) to 9 were tested. This produced the necessary comparison data and also confirmed the argument in [Kolundzija et al., 46] – the convergence of higher order polynomial basis functions is much better than that of the PWL BF.

In modelling utilizing the compression technique, only the combination of the chain-splitting algorithm *A* with the PWL multiple domain basis function (MDBF) has shown a significant dependence of the results on the quality of the mesh applied, often leading to very poor quality of the solution. The rest of the combinations of the PWL and PWS MDBFs with splitting algorithms *A*, *B* and *C* have demonstrated much better stability.

Convergence plots, showing dependence of the solution error versus the number of unknowns (and so versus the density of mesh), were plotted for both direct MoM and the results produced by the application of the compression technique. These **plots confirmed that the interpolated PWL BF serving as MDBF is equivalent to the traditional PWL BF. The same was concluded with regards to a close equivalency between the interpolated PWS BF serving as MDBF and the traditional PWS BF**.

The convergence plots have also shown that although the interpolated PWS BF is usually better than the interpolated PWL BF, in this example, the combination of PWS

with algorithm *C* often produced error higher than the combinations PWS:A and PWS:B.

A comparison against reference software was also performed. The program WIPL-D Pro v.6.1 [39] was used to serve as a reference for the PWL BFs, whilst the program PCAAD v.6.0 was used to produce comparison data for the PWS BFs.

Both interpolated PWL and PWS functions used as MDBF, matched results of the respective reference software within a small explainable margin. This serves to confirm the validity of the results produced by the compression algorithm with respect to the ability to degenerate the interpolated PWL and PWS BF serving as MDBFs into the traditional PWL and PWS BFs.

It was also noticed that the PWS MDBF converges quicker than the PWL counterpart does. This convergence rate was however found to be still much slower than what the higher order basis functions can offer.

5.6 Example 4: Modelling a Coil-Loaded Thin Wire Antenna

The antenna to be considered in this section is a thin wire monopole loaded with a coil. It has been considered previously in works such as [Taguchi et al., 107] and [Sakitani and Egashira, 99]. The purpose of this investigation is to see how the compression techniques developed in Chapter 4 apply to an antenna whose structure consists of several different substructures, i.e. two straight wire segments and a helical coil. A summary of this study is also reported in [Lysko, 65].

The geometry of the antenna is shown in Figure 5-11a. The drawing shows the two straight wire segments joined by a coil. Both straight segments as well as the coil are modelled by straight thin wire sub-segments. At the bottom, the monopole is fed with a delta gap generator.

Throughout this section, only one of the examples considered in [Taguchi et al., 107] is discussed. The geometrical parameters for this example are as follows: number of turns=8, length of the lower straight segment L_{a1}=15.02 cm, length of the upper straight segment L_{a2}=6.68 cm, length of the coil L_c=3.3 cm, wire radius for all wires a=0.15 cm, inner radius of the coil a_c=0.8 cm. Unless stated otherwise, the frequency is 300 MHz.

The numerical models considered in the remainder of this section use a 1 Volt delta gap generator to feed the antenna. Also, in all numerical models the radius of the wire ends touching the feed point is zero for both monopole and dipole models.

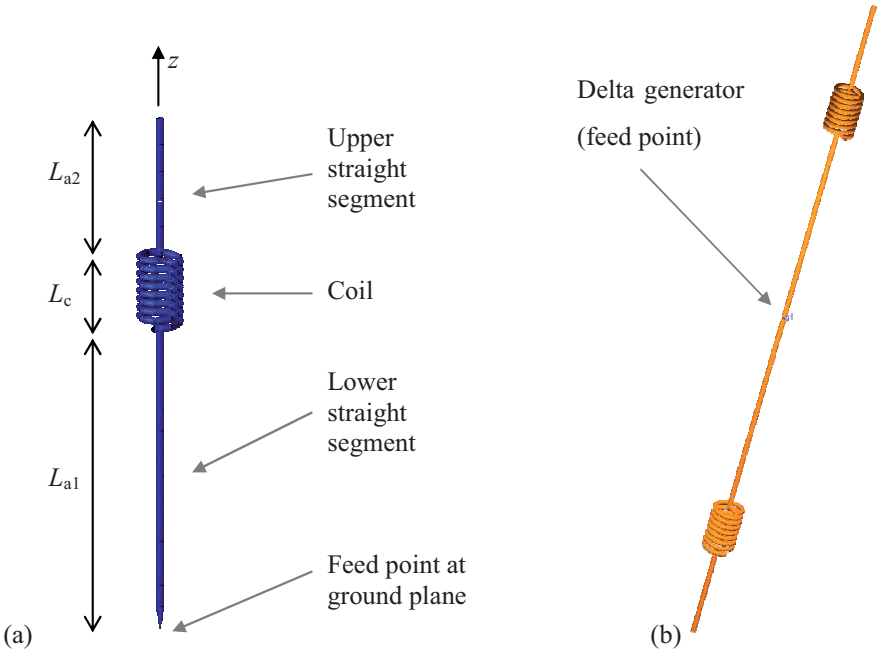

Figure 5-11 Geometry of the monopole loaded with coil (a), and (b) an equivalent dipole like structure. Note: (i) The scales for the drawings in (a) and (b) are not the same . (ii) The radius of wire ends touching the feed point is zero for both monopole and dipole.

In order to assess the reliability of numerical results, the monopole loaded with a coil was first modelled with the software package WIPL-D Pro [39]. Figure 5-12 shows the results of wide-band modelling. The figure confirms that an excellent agreement

between the measurements from [Taguchi et al., 107] and WIPL-D model has been achieved[56].

With a reference to Figure 3b from the original paper [Taguchi et al., 107], it is also possible to note that the simulation results produced by WIPL-D are closer to the measured points than the simulation results from [Taguchi et al., 107]. This is attributed to the usage of a more robust computing scheme, namely the Galerkin technique combined with higher order basis functions, when compared to the approach used in the paper [Taguchi et al., 107].

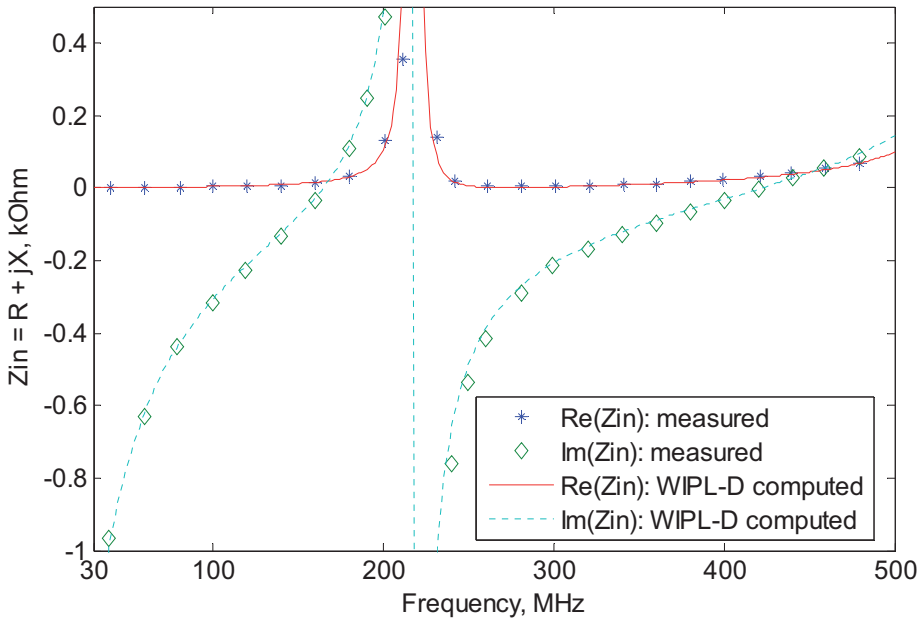

Figure 5-12 Input impedance of the coil loaded monopole antenna versus frequency, as computed by WIPL-D and measured [Taguchi et al., 107]. WIPL-D simulation was set to have a basis function based on a 2nd degree polynomial applied to each individual segment. WIPL-D model used 8 straight wire segments per one turn of the coil.

[56] In absence of tabulated data, the values of the measured data had to be extracted from [Taguchi et al., 107] using own image processing techniques. A brief description of the process is given in Appendix E.

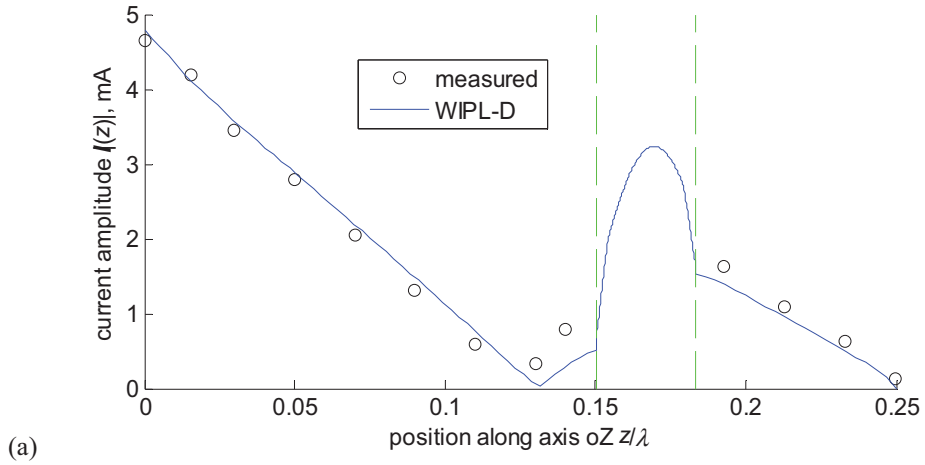

(a)

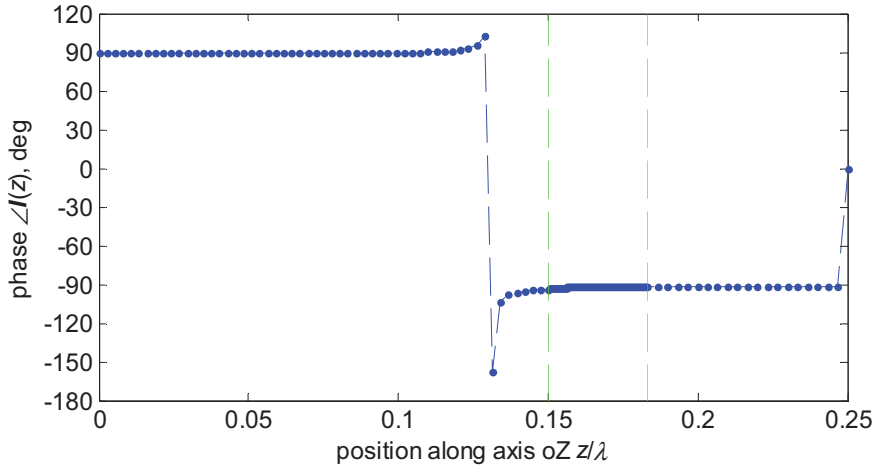

(b)

Figure 5-13 Current distribution profile along z axis. The current intensity is shown in the upper plot and the phase of the current is in the lower plot. The two vertical dashed lines indicate the boundaries of the coil. WIPL-D simulation was set to have a basis function based on a 2nd degree polynomial, applied to each individual segment. WIPL-D model used 8 straight wire segments per one turn of the coil. The input impedance at the same frequency of 300 MHz, as captured from the previous figure, is 5.915 - j214.5 Ohm.

In the next step, the current distribution on the antenna was computed with WIPL-D for a fixed frequency of 300 MHz, and plotted. A comparison between the WIPL-D simulation results and the measurements from [Taguchi et al., 107] is shown in Figure

5-13. The plots also confirm that the WIPL-D simulation has provided a reliable solution.

Several WIPL-D performance tuning parameters, such as “integral accuracy” and “current expansion” options were also tried to ensure reliable results comparable to the measurements.

The results of modelling, shown in Figure 5-13a, confirm the validity of the numerical WIPL-D model and resulting simulations.

The outlook given in Figure 5-13a, shows a relatively fast variation of the current magnitude over the coil. This is due to the circumference of each turn multiplied by multiple turns of wire in the coil. This leads to a larger electrical distance between the ends of the coil, as compared to the direct distance between the same two points. Instead of plotting the current profile against the z coordinate, the current intensity can be shown against the position along the wire. This is illustrated in Figure 5-14a. In this figure, the actual current intensity variation seen is much lower than in Figure 5-13a.

The main parts of the current distribution are smooth, as seen from Figure 5-14. It can therefore be expected that the compression technique developed in Chapter 4 could be applied to the antenna under consideration, and is likely to improve accuracy or reduce the number of unknowns required for a numerical electromagnetic analysis by means of MoM.

5.6.1 On Accuracy and Convergence of Results Due to the Direct MoM

In order to establish quantitative boundaries for the validity of the reference (WIPL-D) models, the effect of the model accuracy on modelling the coil was investigated using a direction MoM solution by means of WIPL-D Pro [39].

The coil was modelled using from 3 to 128 straight thin wire segments per turn. The result computed with 128 segments per turn was used as a reference result Y_{ref} to compute the relative error as $(Y - Y_{ref})/Y_{ref}$.

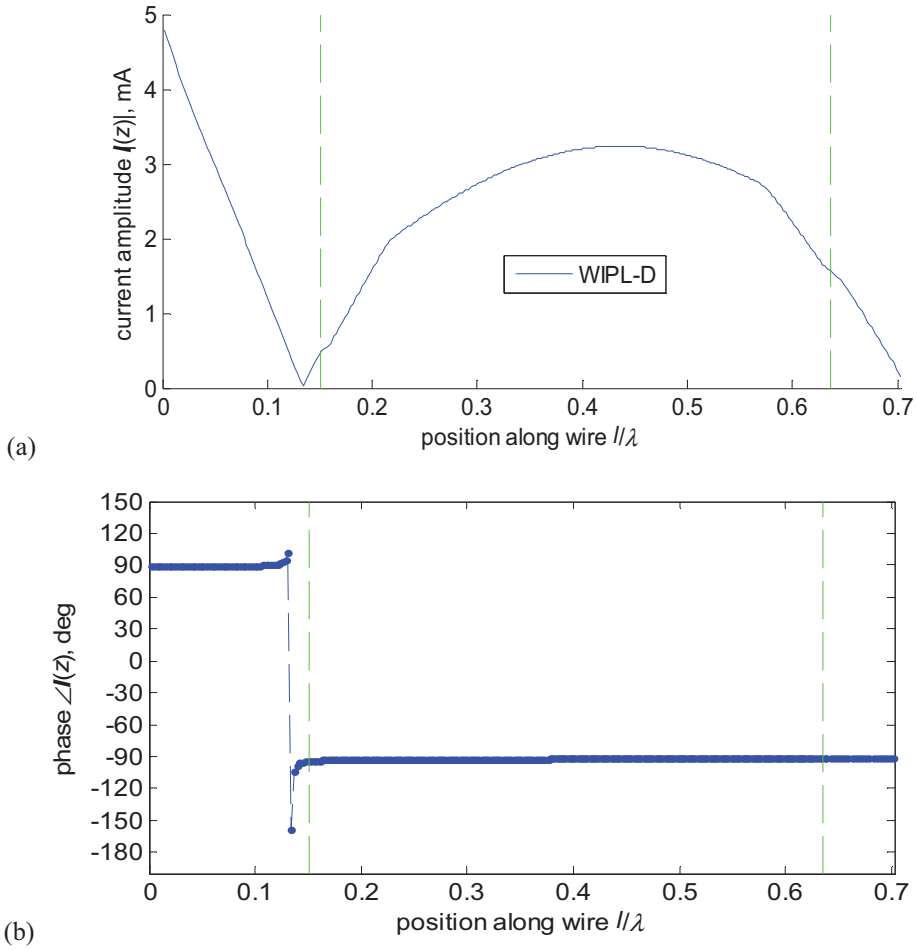

Figure 5-14 The distribution of current intensity along wire. The intensity and phase of current are shown in the upper and lower plots, respectively. The two vertical dashed lines mark the boundaries of the coil. WIPL-D was set to have a basis functions based on a 2nd degree polynomial applied to each individual segment. WIPL-D model used 8 straight wire segments per one turn of the coil.

The compression technique developed in Chapter 4 is able to reduce the number of variables required for solving a problem having electrically small features. In order to compare the direct MoM solution against the compression technique, a valid comparison criterion needs to be introduced, for example a convergence curve.

In order to quantify such a criterion, several alternative settings were tried in WIPL-D. The convergence of the results calculated by WIPL-D was estimated for two different values of a WIPL-D option "*current expansion*" (defining the degree of polynomials assigned to the segments[57]). This test resulted in the curves demonstrated in Figure 5-15.

Plots in Figure 5-15 show how the direct MoM solutions obtained with WIPL-D converge towards the correct solution. When the number of wire segments per coil's turn is too small (and so the total number of unknowns is small), the geometry of the coil becomes too distorted, and the solutions become useless. As the number of segments approximating the coil is increased, the total length of wire segments starts to become closer to the length of curved wire in an ideal helical coil. The same happens to the cross-section of the coil[58]. Thus, the numerical solutions begin to approach the ideal numerical solution obtainable with an infinite number of unknowns. One can also observe in the Figure 5-15 that the imaginary part of the ideal numerical solution does not seem to match the measurement result accurately, especially for susceptance. This can be explained with the following argument: (i) possibly, the geometrical model does not reflect the actual geometry accurately enough, and/or (ii) the measurement error could have been too great (for instance, the measured value of input resistance, 5.9 Ohm, is less than 3% of the measured value of input reactance, -214.5 Ohm).

In Figure 5-15, there is also an artefact associated with the high order "current expansion" option d8. The semi-closed loop and zigzag made by the curves in (a) and (b) around 153 unknowns are due to a switch from 301 unknowns (at 8 segments/turn) to 205 unknowns (at 10 segments/turn). The reduction in the number of unknowns is due to the automatic subroutines in WIPL-D, which trace the electrical length of each segment and assign an appropriate number of unknowns per a unit of wavelength. An increase in the number of segments per coil's turn leads to a decrease in the length of

[57] Level 0 is the default level used in WIPL-D. Levels 1 to 9 (99 in Professional version) force WIPL-D assign a basis function that has greater degree of polynomial per wavelength.

[58] Please refer for details to Appendix A.

each segment. As soon as a threshold is crossed, the degree of polynomial per segment is reduced from 2 to 1, thus reducing the total number of unknowns from 301 to 205.

Figure 5-15a compares the convergence with respect to a common absolute value. Figure 5-15b below compares the convergence curves expressed as a relative error calculated with respect to the finest available mesh size (in this section, this usually corresponds to 128 segments per coil's turn). The error is thus calculated with respect to the finest mesh for a pre-set "current expansion" parameter. This type of convergence is associated with / localized to the pre-set value of the "current expansion" parameter.

From Figure 5-15b, it is clear that using a model based on a monopole (denoted in the figure with the letter *m*) offers the best accuracy at any given number of unknowns (and so it offers better efficiency in terms of the time required to solve the system for a fixed level of required accuracy), as compared to a dipole based solution.

This level of efficiency is followed by the convergence curve derived from modelling a coil-loaded dipole, like the one shown in Figure 5-11b. The coil-loaded dipole can be replaced with an equivalent coil-loaded monopole and vice versa. Refer to Figure 5-11 for the geometry details. The curve "$m1_{eq.dip.}$" is an approximation, where it is assumed that the relative error in the input admittance of a monopole is the same as the relative error in the input admittance of a dipole, as long as their geometries match (and in particular, the number of segments per turn is the same). Replacing a monopole with a dipole should keep the value of relative error the same as for an equivalent dipole. However, it should be noted that the dipole requires nearly double an amount of unknowns, ($2N$-1), so as to reflect that a dipole needs double the number of segments compared to a monopole. One additional unknown is subtracted because, at the feed point, a dipole needs the same number of basis functions as a monopole (one basis function in this particular case). As it may be seen from Figure 5-15b, this approximation is very accurate.

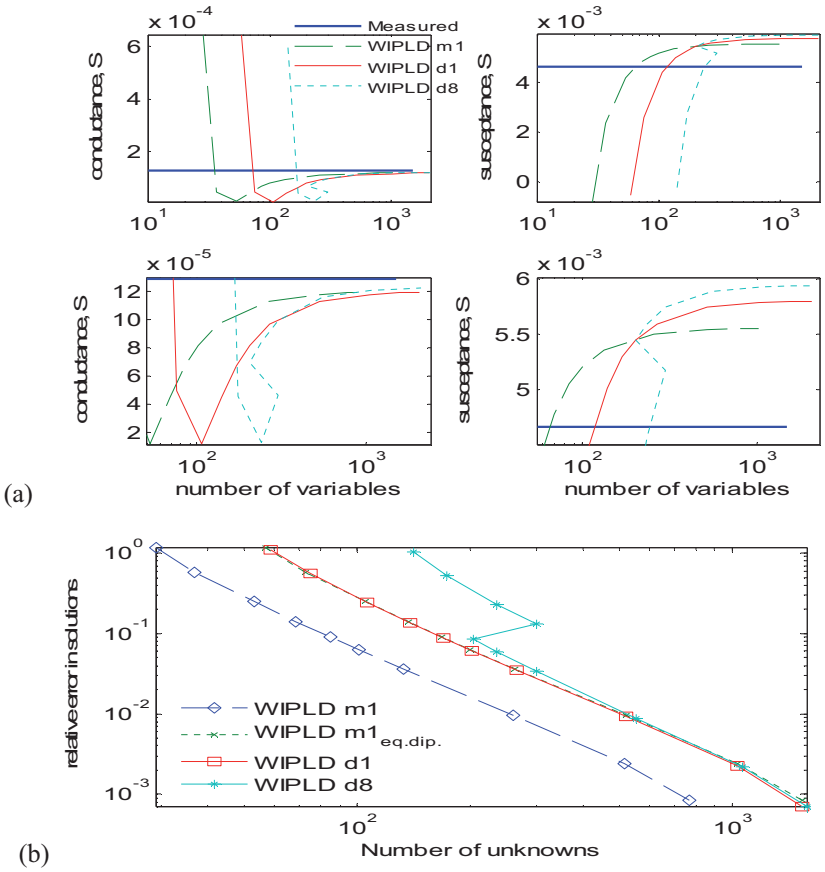

Figure 5-15 Convergence of the WIPL-D simulation results (a) with respect to the measured value of Z = 5.92 - j214.5 Ohm [Taguchi et al., 107]., and (b) with respect to own most accurate value (at the highest number of unknowns, i.e. for 128 segments per coil' turn). The two lower sub-plots in (a) are zoomed-in copies of the respective upper two sub-plots (the region with higher number of variables is zoomed into). The legend entries shown with m*n* and d*n* denote monopole and dipole WIPL D models with a parameter referred to as "current expansion" option (affecting the polynomial degree per wavelength). *Note 1*: In (a), the admittances obtained from the equivalent dipole based models have been doubled to correspond to the admittances derived from the monopoles. *Note 2*: The 2nd entry in (b), $m1_{eq.dip.}$ is obtained from the entry m1 by shifting m1 to the right by 2*N*-1, where *N* is the number of unknowns. Note 3: All calculations were done using level 5 of the "integral accuracy" option in WIPL-D.

5.6.2 Creation of model for evaluating the compression technique

In order to see how the compression technique affects the computations, the initial model of a coil-loaded monopole was first re-meshed to have a much finer mesh (length of a segment from 0.93 mm for the segments composing the coil, and up to 1.6 mm for the upper and lower straight segments of the monopole; the original model used 10.7 mm per each of the lower wire segments). The length of a segment for the new mesh was also made with the intention to break the validity criteria of the think wire approximation (as the wire radius is 1.5 mm becomes comparable to the length of a segment 1.6 mm).

The new model was made without a symmetry plane. This uses an electromagnetic equivalency between the original structure shown in Figure 5-11a and the new equivalent structure shown in Figure 5-11b. The absence of the symmetry plane permitted to take advantage of the ability of WIPL-D Pro to compute the impedance matrix exceptionally quickly, as compared to the own Matlab code[59].

An illustrative example of such a dipole is shown in Figure 5-11b.

The results of simulations were obtained following the same guidelines as described in the Section 5.4.3 "Application of the Piecewise Linearly Interpolating PWL and PWS Basis Functions" on page 211 and Section 5.5.2 "Application of the Compression Technique" on page 219.

[59] The details of assignment of the basis functions to the elements of geometrical structure and the numbering technique used for the same in WIPL-D are unknown to the author, at least for a general case scenario. However, if the nodes and wires in the geometrical structure are numbered sequentially, in series, then the order of elements in the impedance matrix produced by WIPL-D Pro and own Matlab code match.

The geometrical structure under consideration has all segments connected in series. This permits to take advantage of a much speedier computation of a large impedance matrix (1519 unknowns for the given problem) when this is executed by WIPL-D Pro rather than by own Matlab code.

5.6.3 Some Intermediate Results Relevant to the Functioning of the Compression Technique.

As described in Chapter 4, the compression technique includes several stages. During the first stage, chains (i.e. wires connected in series) are identified. As some of these chains may have very large electrical length, the chains are split into sub-chains as a part of the next stage. Three algorithms, referred to as *A*, *B* and *C* have been developed in Section 4.4

It may be noted that the algorithms *A* and *B* are sensitive to the choice of the starting point. Whether a chain is split into sub-chains starting from one end or the other, the resulting split may be very different. For instance, the algorithm *A* may produce very short sub-chains that are undesirable in numerical electromagnetic modelling. A simplified example of the splitting (where fewer unknowns are used in order to keep the picture readable) is shown in Figure 5-16. This example uses "outwards" stepping, i.e. propagating the algorithm from the feed point towards the free ends, on one dipole's arm at a time.

The three maps shown in Figure 5-16 correspond to application of the three chain splitting algorithms, *A*, *B* and *C* to a symmetrical dipole with two arms (the position of the feed point in the pictures is assumed to be cutting through the middle of the map). The horizontal axis is the coordinate along the dipole's wire and follows the curvature of the wire. For a dipole symmetrically loaded with two coils, this coordinate will also follow the coil. This is similar to the way the current distribution shown in Figure 5-13a was expanded into the one shown in Figure 5-14a. As an electrically continuous wire (a chain) is modelled with segments connected in series, the same concept will apply to splitting the chain into sub-chains.

The vertical axes for plots A, B, and C in Figure 5-16 denote the value of the splitting parameter, i.e. the maximum permitted electrical length of a sub-chain. Thus, a fixed value of this parameter selects a line of dots at the level of that value.

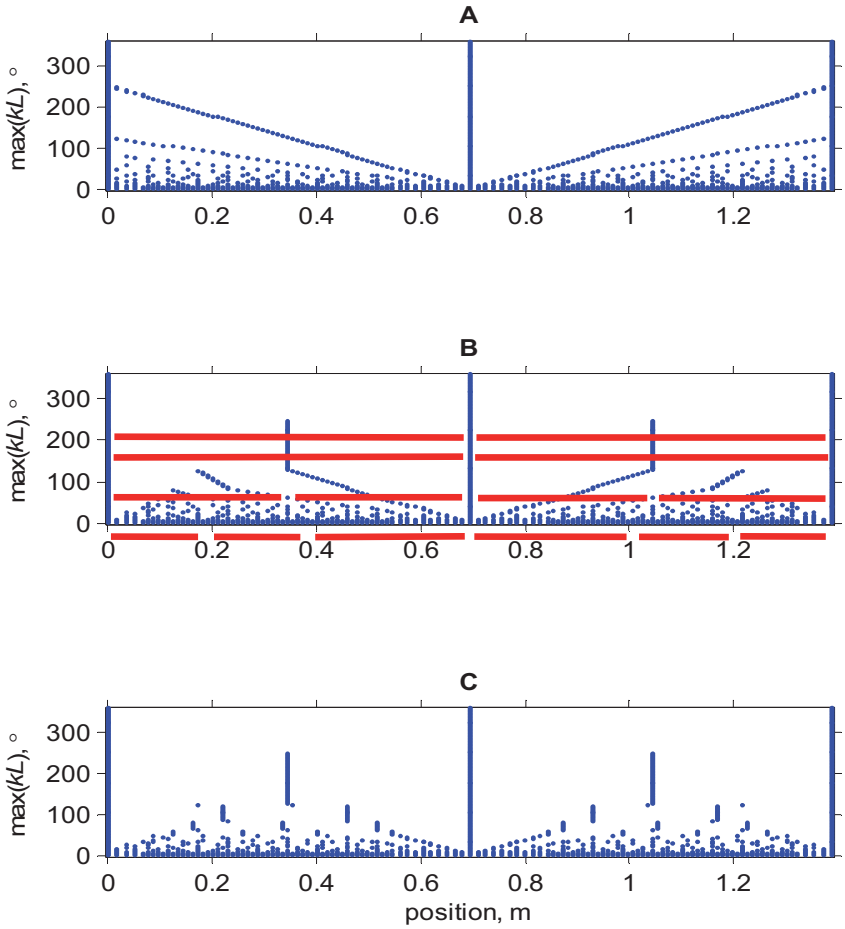

Figure 5-16 Maps showing the splitting of a dipole into sub-chains due to the algorithms *A*, *B*, and *C*. The horizontal axis indicates the position along the wire composing the dipole. The vertical axis denotes the splitting parameter (maximum permitted electrical length). The dots mark the positions of the splits introduced into previously continuous arms of the dipole (chains). The shown splits (at the dots in the plots) were produced by the algorithms applied to the chains from the centre of the dipole towards the free ends ("outwards" propagation). This may be compared against the next figure. The red horizontal lines (with thickness of one dot) are added to the middle plot and used solely for explanations in the text. They are not a part of the actual splitting map.

The dots indicate the positions of the splits. As per the algorithms developed in Chapter 4, the positions of these splits are defined as the positions where the wire segments join each other.

A map is built as follows. At a fixed value of the maximum permitted electrical length, say 300 deg, the two arms do not require any internal splitting, so there are 3 dots at the level of 300 deg. Two of these are located at the free ends of the dipole and one is in the centre. This type of splitting can be illustrated in subplot B of Figure 5-16 by any one of the two upper red lines/intervals (added to the map for illustration purpose only). These red intervals correspond to the unbroken chains.

If the maximum permitted electrical length is 200 degrees, then each of the two arms (chains) should be split into two sub-chains. The lengths of these sub-chains are approximately the same for the algorithms *B* and *C*. The algorithm *A* produces a different split, as may be noted by looking at the subplot *A* of Figure 5-16, and drawing a horizontal line through the level of 200 deg. This line will cross five dots (two correspond to the free ends, one corresponds to the feed point, and the two last points divide the dipole arms into unequal sub-intervals (sub-chains)).

A smaller the splitting parameter means the greater the number of generated sub-chains.

The maps shown in Figure 5-16 describe the results produced by the algorithms *A*, *B* and *C* for the algorithms starting at the feed point and working outwards, that is towards the other end of the respective arm (i.e. towards the outer/free end of the dipole). The same algorithm propagation direction is applied to the other arm (from the feed point towards the other free end).

There are three other options in for selecting the propagation directions. These include “inwards” propagation (the algorithm starts at the free end and propagates towards the feed point; on one dipole’s arm at a time), and two other combinations, both of which lead to asymmetrical splits of the otherwise symmetrical dipole.

The remaining three options can be pictured by cutting the subplots in Figure 5-16 into halves (along the dots corresponding to the feed point), and then re-arranging the two halves (flipping them horizontally) to obtain the remaining three options. One of the asymmetrical splits is illustrated with Figure 5-17.

It is possible to see how this affects the current distribution. Figure 5-18 presents the current intensity on the coil-loaded dipole in the form of a temperature / intensity map for the same scenario as was discussed in connection with Figure 5-16. The axes used in

the plot are the same as for the maps showing the splitting of the dipole/chain into sub-segments/sub-chains.

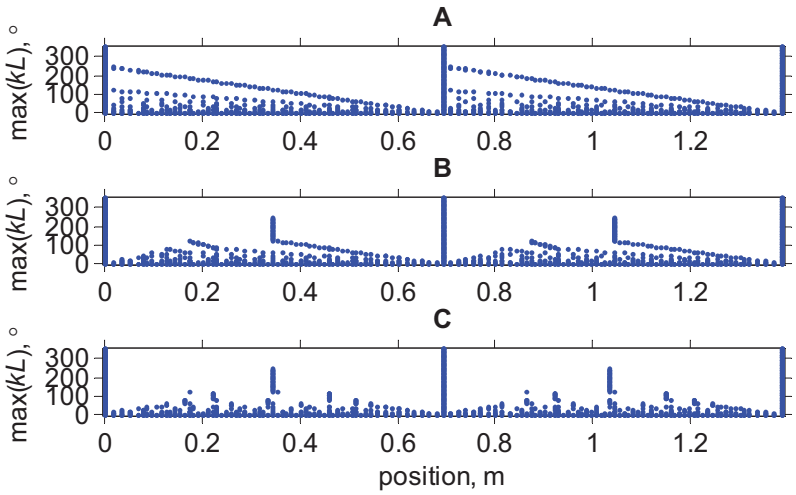

Figure 5-17 Example of an asymmetrical split: Maps showing the splitting of a dipole into sub-chains due to the algorithms A, B, and C. The horizontal axis indicates the position along the wire composing the dipole. The vertical axis denotes the splitting parameter (maximum permitted electrical length). The dots mark the positions of the splits introduced into previously continuous arms of the dipole (chains). The shown splits were produced by the algorithms applied to the two arms differently. The algorithm is applied to the left chain (left arm) from the centre of the dipole towards the left free end ("outwards" propagation), whilst to the right chain (right arm) it is propagated from the right free end towards the feed point. This may be compared against the previous figure.

Each value of the splitting parameter has a current distribution associated with it. This current distribution is shown in Figure 5-18 as a horizontal intensity strip crossing the temperature map from one side to the other side, next to the respective value of the splitting parameter. In the maps showing the splits, one strip corresponds to one row of dots. *Note*: as the simulations were run for multiple closely-spaced values of the splitting parameter, the boundary between the colour strips may be difficult to distinguish. For most part, as the current distribution over the dipole changes smoothly with the splitting parameter, this makes the individual strips look like a smoothly changing pattern. At a few certain threshold values of the splitting parameter, the

changes in the splitting are abrupt, often leading to a sharp and clear difference between the neighbouring colour strips.

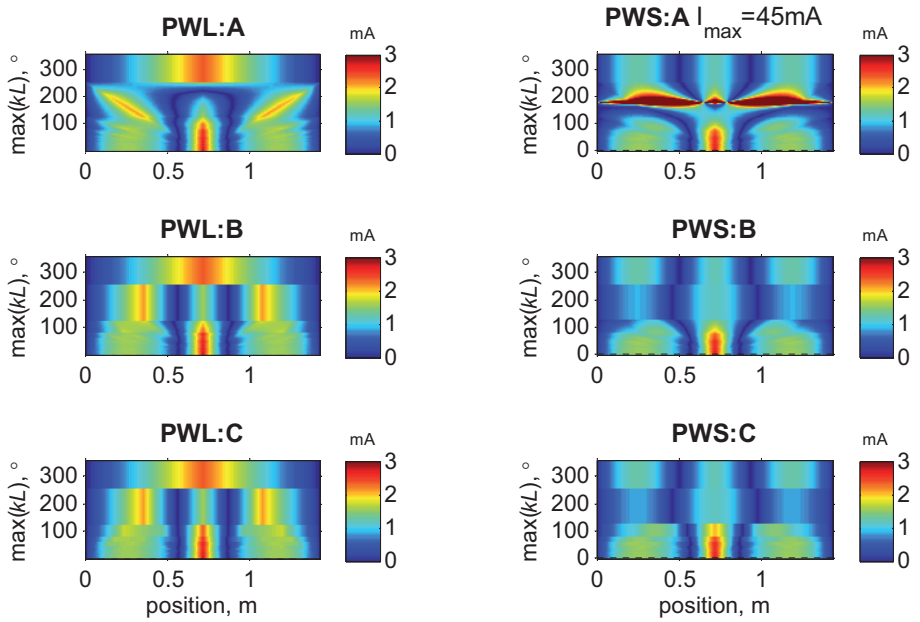

Figure 5-18 Current distribution intensity plots for "inwards" direction of algorithm application. The six subplots correspond to the six combinations of piecewise linear (PWL) and piecewise sinusoidal (PWS) basis functions, and the algorithms A, B, and C used for splitting the chains into sub-chains. The horizontal axis gives a relative coordinate along the wire's axis from one end of the dipole until the opposite end. The vertical coordinate marks the values of the chain splitting parameter (i.e. the maximum permitted electrical length of a sub-chain). Each value of the splitting parameter has a horizontal colour intensity strip associated with it and spanning from the left hand side of the intensity plot until its right hand side. Those intensity plots which had to be scaled and thresholded in the level of maximum displayed intensity, have the value of maximum current intensity shown in the title as Imax=XXmA.

The lowest colour strip on each intensity plot corresponds to the finest mesh applied to the dipole (meaning the greatest number of basis functions and unknowns). The upper colour strip corresponds to the roughest mesh applied to the dipole (typically, then a dipole is modelled with a single roof-top or a single piecewise sinusoidal basis function).

When the value of the splitting parameter is small, below 45 deg, all algorithms are able to show the presence of nulls in the current distribution. A closer inspection of the colour and intensity reveals that the shape of the current distribution around the peak at the feed point is sharp for PWL and smoother for PWS basis functions. This also follows from the nature of these functions.

As the value of the splitting parameter is increased, different algorithms and basis functions produce dissimilar results. The PWS:C keeps the amplitude of the current at the feed point longer and steadier than other algorithms under PWS BF. However, the plots indicate that the PWL BF does so as well, if the sharp peak amplitude is neglected. In addition, the PWL:C keeps the positions of the two nulls in the current distribution for a larger span of the splitting parameter.

Figure 5-18 also shows that the algorithm *A* produces results most sensitive to the specific value of the splitting parameter. Both types of basis functions, piecewise linear (PWL) and piecewise sinusoidal (PWS) are affected around the splitting parameter of 180 deg. It must however be noted that only the range 0 to 90 degrees may be considered as appropriate for the splitting parameter, if the PWL and PWS basis functions are used. If this range is exceeded, then these basis functions, and especially PWL, are not able to model the oscillation of the current appropriately.

Figure 5-19 presents the current distributions for the six combinations of the two interpolated multiple domain basis functions (of PWL and PWS type) and the three chain splitting algorithms *A*, *B*, and *C*.

As it has already been seen from Figure 5-18, the performance of the algorithm A is poor, whether it is used with PWS or PWL MDBF.

In general, the plots show that the PWL MDBF seems to provide results of better quality than the PWS MDBF. This is the opposite from what has been observed in the previous example for an unloaded dipole. This is attributed to the more complex shape of the current distribution for the coil loaded antenna compared to an unloaded one.

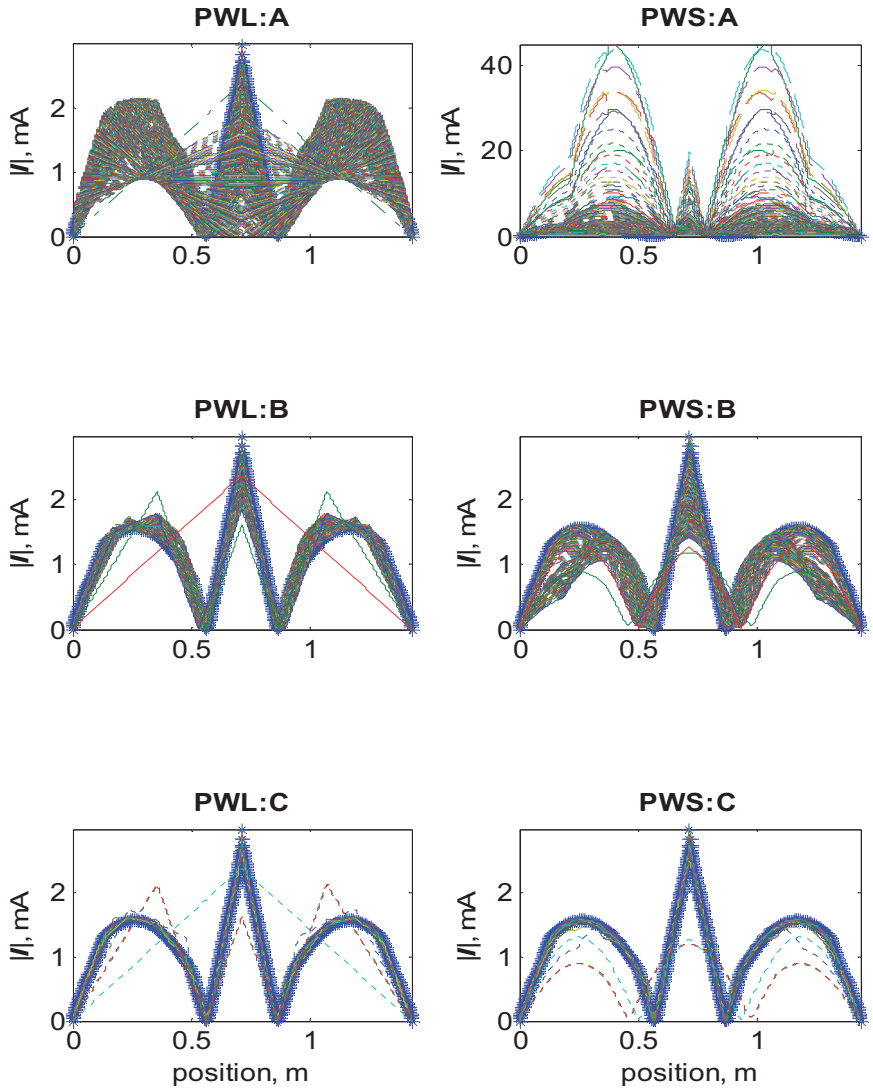

Figure 5-19 Families of the current distribution plots for the case where the splitting algorithm was applied symmetrically, in the "inwards" direction (from the ends towards the feed). The six subplots correspond to the six combinations of piecewise linear (PWL) and piecewise sinusoidal (PWS) basis functions, and the algorithms A, B, and C used for splitting the chains into sub-chains. The horizontal axis gives a relative coordinate along the wire's axis from one end of the dipole until the opposite end. The vertical coordinate is the current magnitude. The star symbol (*) denotes the reference current profile.

Note:

Another perspective could perhaps been obtained by filtering the results in accordance with the ability of a particular basis function to represent the main features in a current distribution, such as maximum and nulls. This would have limited the span of the splitting parameter to 45 degrees for a PWL MDBF and 90 degrees for a PWS MDBF.

Figure 5-20 and Figure 5-21 are included in the text to illustrate the effect caused by asymmetric application of the splitting algorithms, causing an asymmetric mesh and disturbing the current distribution. These figures are similar to Figure 5-18 and Figure 5-19, respectively, which have just been discussed.

It is clear from Figure 5-20 and Figure 5-21 that the algorithm *A* is strongly affected by the asymmetry, whilst the algorithm C shows the best resilience.

5.6.4 Comparison between the Convergence and Errors Due to the Direct MoM and Compressed Solutions

The error, i.e. the degree of deviation from a reference solution, due to a direct fine-meshed MoM solution (produced by WIPL-D) can be compared against the error produced by the code realizing the compression techniques.

The results of the comparison are shown in Figure 5-22. In that figure, the relative errors for various cases are plotted against the number of unknowns required to solve a problem. As in the previous sub-section, a relative error is computed with respect to the respective reference solution, where a problem is meshed with the shortest segments. A fine mesh of shortest wire segments must result in having the highest number of unknowns. The two straight wire segments, the upper and lower, were also sub-divided into shorter sub-segments of the length estimated as the mean of all available segment lengths.

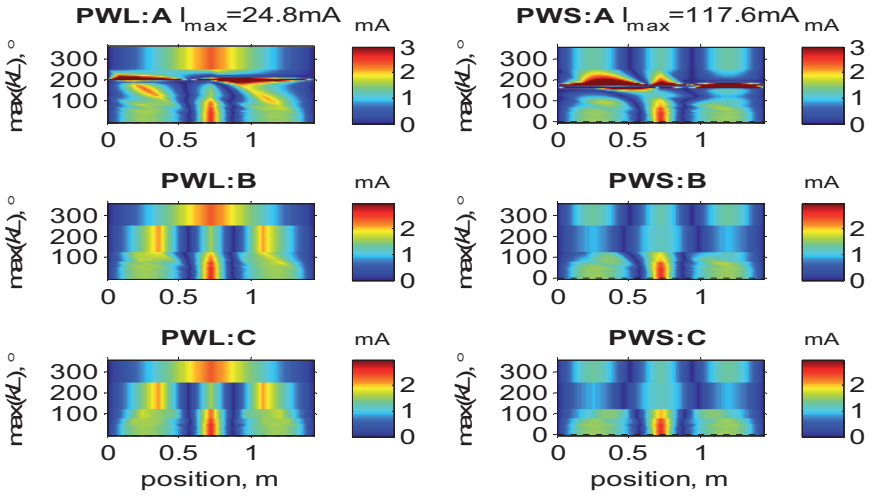

Figure 5-20 Current distribution intensity plots for an asymmetrically meshed dipole, where the "inwards" direction of algorithm was applied to the right hand side of the dipole, whilst the "outwards" direction of algorithm was applied to the other arm. The six subplots correspond to the six combinations of piecewise linear (PWL) and piecewise sinusoidal (PWS) basis functions, and the algorithms A, B, and C used for splitting the chains into sub-chains. The horizontal axis gives a relative coordinate along the wire's axis from one end of the dipole to the opposite end. The vertical coordinate marks the values of the chain splitting parameter (i.e. the maximum permitted electrical length of a sub-chain). Each value of the splitting parameter has a horizontal colour intensity strip associated with it and spanning from the left hand side of the intensity plot to the right hand side. Those intensity plots which had to be scaled and thresholded in the level of maximum displayed intensity, have the value of maximum current intensity shown in the title as Imax=XXmA.

When the chain splitting algorithm is set to operate outwards from the feed point, it is possible to observe in Figure 5-22 that the piecewise linearly interpolated piecewise sinusoidal (PWS) basis functions provide an advantage over piecewise linear (PWL) basis functions, as the observed error is smaller.

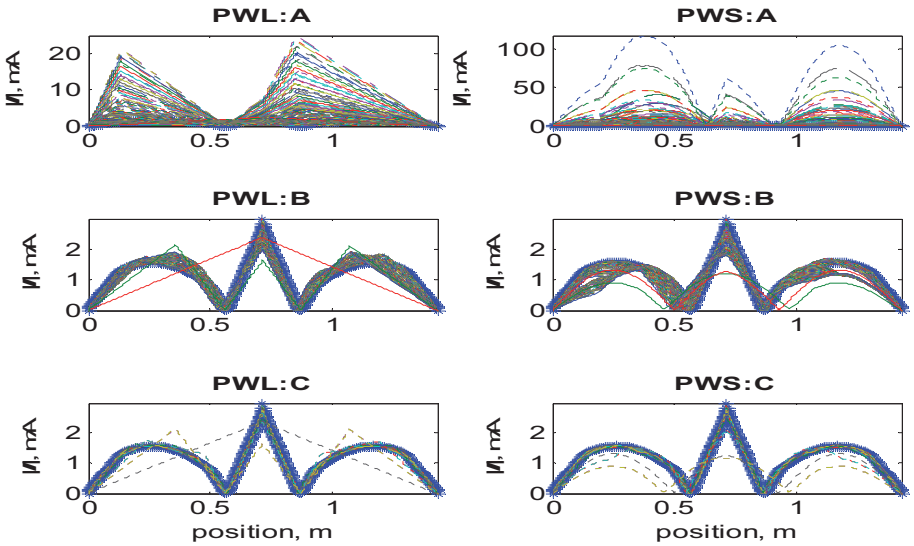

Figure 5-21 Families of the current distribution plots for the case where the splitting algorithm was applied asymmetrically, i.e. where the "inwards" direction of the algorithm was applied to the right hand side of the dipole, whilst the "outwards" direction of algorithm was applied to the other arm. The six subplots correspond to the six combinations of piecewise linear (PWL) and piecewise sinusoidal (PWS) basis functions, and the algorithms A, B, and C used for splitting the chains into sub-chains. The horizontal axis gives a relative coordinate along the wire's axis from one end of the dipole until the opposite end. The vertical coordinate is the current magnitude. The star symbol (*) denotes the reference current profile.

When the chain splitting algorithm is set to operate inwards, i.e. from the free ends towards the feed point, the same effect is hardly pronounced. It is however possible to see that, at certain points, the error goes drastically down. This is attributed to the scenarios where the meshing close to the generator is set in such a way as to get the input admittance closely matched to the value at the highest mesh density (reference value).

The same plots in Figure 5-22 also include the error curves for the solutions obtained by a direct MoM, using WIPL-D. The two respective curves, denoted with δ(Ymono) and δ(Ydip), correspond to solving a coil loaded monopole and the equivalent dipole

configurations[60]. The solutions were also obtained for various densities of the mesh applied to the coil, resulting in a different number of unknowns.

The convergence curve for a dipole is above the curves resulting from the application of the compression technique, at any given number of unknowns visible in the plot. This means that for all the tested densities of the mesh applied onto the coil, usage of the compression technique offers the same accuracy in the solution, yet requires a much lower number of variables. Moreover, if the accuracy requirements are low (permitting a relatively high error, on the order of 10-50%), then the problem can be solved using fewer unknowns than the minimum required by the direct MoM.

The curve for a monopole, shown mostly for reference purposes, indicates an interval where usage of symmetry allows further improvement of the performance in terms of the achievable error per a fixed number of unknowns even further[61].

5.6.5 Comparison of the Condition Numbers of the Impedance Matrices due to MoM and the Compression Technique

The condition number for the compressed and original impedance matrices is shown in Figure 5-23 against the total number of unknowns.

[60] As a reminder, the equivalent dipole was introduced in order to be able to take advantage of the speed in filling in the impedance matrix, offered by WIPL-D (see a footnote on the previous page).

[61] Due to time constraints, it was not possible to test the symmetry plane enabled model based on the compression technique with a sufficiently large number of unknowns (on the order of several hundred to several thousands). It is however expected that applying the symmetry to the compression technique (as it was done in other section of this Chapter) will be able to move the compression technique's convergence curves lower and to the left, thus being able to save on the number of unknowns, in comparison to the direct MoM, for any given value of error (at least for this specific geometry with a sufficient amount of electrically small elements)

Figure 5-23 demonstrates that the condition number of the matrix due to high order basis functions is very high, on the order of 10^8. Despite having this large magnitude, the condition number hardly changes as the complexity of the problems increases. In the considered scenarios of a coil-loaded monopole or dipole, the number of unknowns is increased only by increasing the density of the mesh on the coil. This means that the main contribution to the high value of the condition number for d8 is due to the lower and upper (straight) segments of the antenna, where the assigned polynomial degree is very high (13). This may be contrasted with the basis functions assigned to the segments of the coil, which have polynomial basis functions of degree 1.

The condition number for lower order systems, such as m1 and d1, on the other hand, experiences a fast monotonic growth.

The curves for the condition number at a given matrix size (i.e. at a given number of variables) can be compared to the direct MoM (m1, d1, d8) and the compression technique (PWL,PWS:*A*,*B*,*C*). Figure 5-23 shows that the condition number for the compressed system is typically lower than the condition numbers for the direct MoM solutions, at least within the tested range of mesh densities for the coil.

This serves to confirm a good numerical stability of the compression technique, well comparable to the low to intermediate order direct MoM solution.

5.6.6 Summary

The example of a coil loaded monopole antenna has been considered using both direct MoM and the compression technique. The antenna was first analyzed using the direct MoM. A very good match between the simulated and measured results was found in terms of both broadband input impedance characteristics and the specific current distribution at a fixed frequency. This served to validate the direct MoM moment, and ensured that the original computed impedance matrix can be used with the compression technique.

It was also established that a dipole equivalent of the monopole under consideration can be used in order to perform the analysis. It was noted that the monopole requires twice less the number of unknowns compared to an equivalent dipole, providing a better

convergence. A relationship relating the convergence for the dipole and monopole was developed.

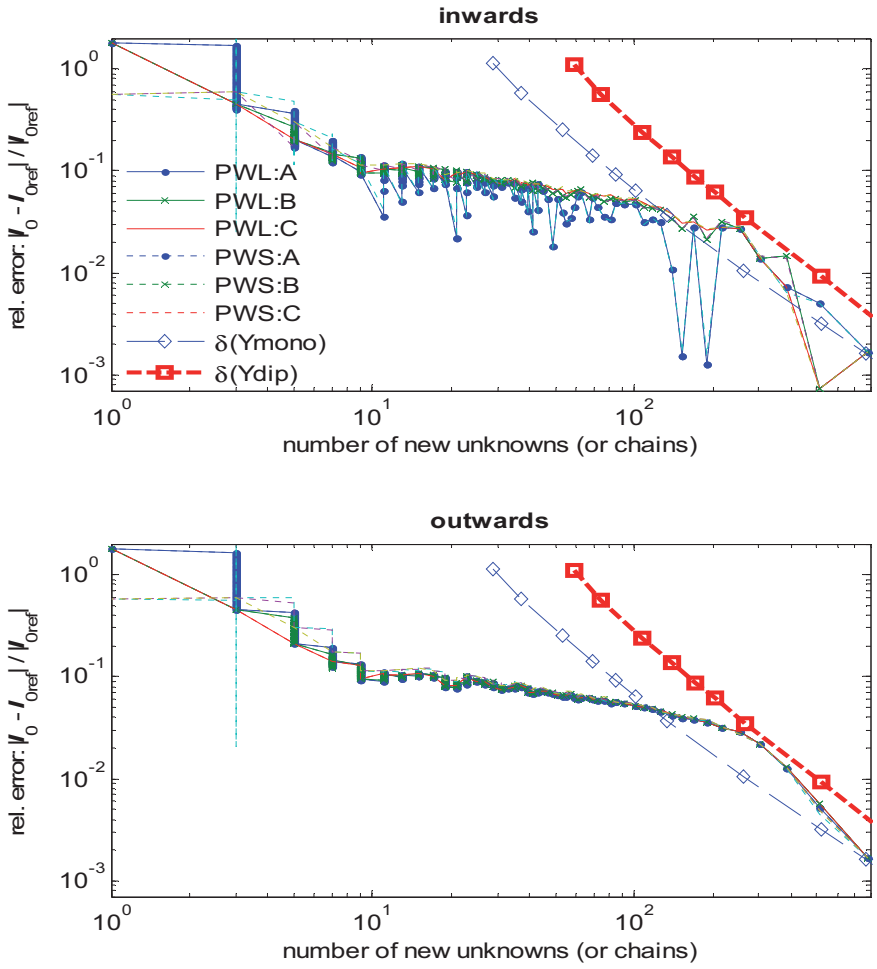

Figure 5-22 Convergence of results with growth in the total number of used variables (defined by the maximum permitted electrical length of a sub-chain). The current was compared at the feed point against a direct MoM generated reference. The upper plot corresponds to the chain splitting algorithm propagating its solution from the feed point towards the free ends. The lower plot corresponds to the chain splitting algorithm propagating its solution from the free ends towards the feed point. The notations PWL and PWS stand for piecewise linear and sinusoidal basis functions. The letters *A*, *B* or *C* following denote the splitting algorithm applied. The two last legend entries with δ denote convergence rate for a monopole and dipole modelled with WIPL-D directly.

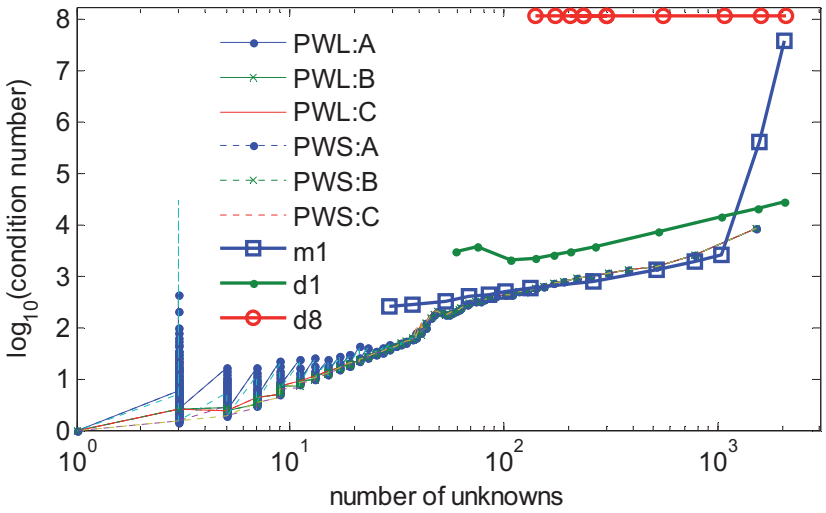

Figure 5-23 Condition number of the impedance matrix versus the number of unknowns when modelling a coil-loaded monopole and dipole. The notations PWL and PWS stand for piecewise linear and sinusoidal (basis functions used), and the letters A, B and C denote the chain-splitting algorithm applied. The first six entries in the legend describe condition number of the new compressed impedance matrix for the respective meshing scenarios. The last three entries in the legend describe the condition number for direct solutions by the MoM. The first symbol in the notations mN or dN stand for monopole/dipole and the second symbol stands for the WIPL-D "current expansion" option. There is a slight monotonic increase in the condition number for d8, which is not readily visible due to the scale of the plot.

It was also found that the higher order basis functions can provide a much better efficiency in terms of the number of unknowns per unit of length. This is valid when the mesh is not overly fine.

Next, the compression technique was applied to model the same structure. An equivalent dipole was used as the prime model.

At certain range of frequencies, the current profile on this antenna showed multiple extremes including a nearly zero current due to a standing wave pattern. The modelling has shown that the compression technique is able to handle this feature well.

A number of discussions have been made in connection with the dependence of the results on the mesh, and, thus, on the chain-splitting algorithms *A*, *B* and *C*. These discussions mostly focussed on the importance of preserving the symmetry in the meshing of a symmetrical dipole. Several means of visualization aids, such as maps showing the positions of the splits and collective current distribution plots were used.

A comparison of the performance of the direct MoM and the compressed technique in terms of the achievable error per number of unknowns has demonstrated that the compression technique provides significant savings in terms of required number of unknowns, and so in the required memory and speed of computations.

As a by product, it was noticed that, like in the previous examples, the interpolated PWS BF serving as MDBF, performs the best when applied with a sufficient number of sampling points (reflected in a lower number of unknowns). This is attributed to the quality of piecewise linear approximation for a sine function.

In addition, the condition number of the original and compressed impedance matrix were considered. It was found that the usage of algorithm *A* leads to a higher condition number than that of other two algorithms, if the number of unknowns is low. The algorithm *C* leads to a higher condition number, when the number of unknowns is high.

5.7 Concluding Remarks for All Examples

- Example 1 has shown two advantages in applying the compression technique to an electrically small structure over he direct method of moments (MoM). Specially, this is true when the segmentation of such structure breaks the thin wire approximation, as the length of a segment approaches and exceeds its radius.
- **Example 1 illustrates that the impedance matrix compression algorithm can be used to improve the quality of a solution even when the thin wire approximation cannot be satisfied within the traditional MoM, or the current is allowed to vary too greatly due to a close proximity of electrically very small segments / features. The example also shows that the matrix compression can be tuned to produce results matching those due to traditional direct MoM,**

offering a mechanism to decouple the number of unknowns from the number of geometrical segments (i.e. a mechanism to decouple the electromagnetic and mechanical sides of modelling)

- Example 2 has shown a successful application of the compression technique to a structure with multiple small size non-smooth features.
- **The results for the pwliPWSbf have demonstrated notable improvements in the current distribution estimation, as compared with the pwliPWLbf. This includes a narrower spread in the current distribution plots, symbolizing better average stability of the PWS function with respect to the mesh, even though this function is interpolated linearly**.
- Half wave dipole in Example 3 illustrated equivalence between the direct MoM and compression technique for straight objects
- **Plots confirmed that the interpolated PWL BF serving as MDBF is equivalent to the traditional PWL BF. The same was concluded with regards to a close equivalency between the interpolated PWS BF serving as MDBF and the traditional PWS BF**.
- **Both interpolated PWL and PWS functions used as MDBF, matched results of the respective reference software within a small explainable margin. This serves to confirm the validity of the results produced by the compression algorithm with respect to the ability to degenerate the interpolated PWL and PWS BF serving as MDBFs into the traditional PWL and PWS BFs.**
- Example 4, with a coil loaded monopole has demonstrated advantages of the compression technique when applying it to a structure including curved elements, namely requiring much fewer unknowns than MoM for the same required accuracy in the solution.
- **A comparison of the performance of the direct MoM and the compressed technique in terms of the achievable error per number of unknowns has demonstrated that the compression technique provides significant savings in**

terms of required number of unknowns, and so in the required memory and speed of computations.

5.7.1 Note: Summary of Observations towards Practical Implementations

- The piecewise linearly interpolated PWS basis function usually outperforms the piecewise linearly interpolated PWL basis function in terms of the number of unknowns required for a given level of solution accuracy.
- The performance of the interpolated PWS basis function may degrade if the sampling of points is very low. An interpolated PWL basis function offers a better solution under such rare circumstance.
- The chain-splitting algorithm *A* is usually the most unstable, whilst the algorithm *C*, attempting equidistant meshing, is the most stable and predictable.
- The direction of propagation for any of the algorithms plays an important role in producing stable and accurate results, as it may introduce asymmetry in describing the current distribution on an otherwise symmetrical structure.

5.8 Chapter Summary

This chapter provides several examples of applying the multiple domain basis functions (MDBF) and related techniques developed in previous chapters.

The first section provides a brief description of the programming code developed, explaining the complexity and options available.

This is followed by the application examples. These include electrically short monopole, meander monopole, half-wavelength monopole/dipole, and coil-loaded monopole/dipole. The examples compare the compression technique with the traditional method-of-moments (MoM) approach. The comparison shows that the accuracy of the results obtained using the compression technique can be set to any required value from excellent to poor, depending on the value of the splitting parameter (i.e. on the maximum permitted electrical length of a sub-chain). The examples have demonstrated

that the algorithms and techniques introduced in the previous chapter can work for a range of problems.

In the short monopole antenna example, usage of MDBFs grouped overly short individual wire segments. This helped to improve the satisfaction of the thin wire approximation conditions, and forced the current profile to match physical assumptions, improving the accuracy of the model. The straight monopole and dipole examples showed a match between the "error versus number of unknowns" curves produced by the traditional and newly devised techniques. The examples of the meander and coil-loaded monopole demonstrated that far fewer unknowns are required to obtain accurate results with the proposed compression technique. For the coil-loaded antenna including a curved structure in the form of a choke, an up to ten-fold reduction in the error was achieved. The same antenna can also be modelled using up to ten times fewer variables (translating into 100 times less memory required for the impedance matrix).

The examples also differentiated between the results obtained using the different chain splitting algorithms, *A*, *B* and *C*. In most scenarios, the algorithm *C* provided the best and most stable results.

Concluding remarks and suggestions for the successful practical use of the method and algorithms developed are provided at the end of this chapter.

Chapter 6. Discussions, Summary and Next Steps

6.1 Discussions and Summary

This work has introduced a novel extension to the traditional method of moments (MoM), offering a better way to model smoothly curved structures with no need for drastic changes to an existing MoM code based on piecewise linear geometric elements. In addition, the work proposes several other enhancements, addressing a reduction in the condition matrix of the impedance matrix, acceleration of radiation pattern computation and other aspects.

A study was performed, investigating the properties of the condition number of the impedance matrix. The study has shown that it is possible to minimize the condition number with non-to-little computational overhead. The approach proposed is novel and based on an appropriate selection of a common/reference wire at a junction with multiple wires attached. It has been shown that the choice is frequency dependent. Several solutions with different degrees of optimality and complexity have been proposed. This new and simplistic method ensures that the worst/maximum condition number is never encountered. On the other extreme, also new but more computationally demanding method minimizes the condition number. In the test examples considered, the impedance matrix's condition number has been reduced by an order of magnitude.

A new method for an accelerated computation of radiation patterns has been devised, catering for higher order polynomial basis functions. At low frequencies, the method uses Taylor's expansion of the oscillating exponential term. At higher frequencies, the method uses integration by parts. Estimates for errors have been derived and used to establish the boundary between the Taylor's expansion and the integration by parts. Although this approach has a limit on the best achievable accuracy, the tolerance offered is more than sufficient for most practical models. A comparison against commercial software has confirmed high efficiency of the technique proposed.

The main focus of this thesis has been on the realisation of novel multiple domain basis functions (MDBF) and on the development of supporting algorithms, methods and code.

Each such basis function is defined over a chain composed of one to several wire segments. This extension to the traditional MoM introduces a novel type of interpolating basis function, and separates the requirements for the geometrical model‘s mesh the from the requirements for the current distribution representation. This separation has permitted to treat curved structures with greater efficiency, and, for such structures, results in a much smaller impedance matrix. This new impedance matrix is referred to as a compressed impedance matrix. Such an aggregation of wire segments also improves the ratio of wire segment length to radius, and thus extends the boundaries of the thin wire approximation and of the wire modelling.

As a component to the above, three original mesh-grouping algorithms of different complexity, named *A*, *B* and *C*, have been developed and tested. These automatic algorithms group the wire segments into larger structures, chains, under a restriction on the maximum length of a chain. The tests have shown results indicating the quality of the resulting new rougher mesh of chains.

The multiple domain basis functions (MDBF) have also been implemented and tested. Profiles of both the piecewise linear (PWL) and piecewise sinusoidal (PWS) functions have been used as the multiple domain basis function. Application of the PWS MDBF in this scheme is novel, and has shown promising results, similar to the well-known application of PWS basis function in the wire modelling. The technique developed also permits for other arbitrary profiles of MDBF. A preliminary investigation into shaping the MDBF’s profile by a minimization of the condition number, also suggests a novel possibility to identify the correct shape of the current profile without any *a-priory* knowledge.

A comprehensive software code realising the MoM has been developed and tested in the Matlab environment. The program based on the developed code allows for application of the devised compression technique. The code also permits importing and exporting of most file formats from the commercial software WIPL-D and PCAAD.

Several examples have been used to test the algorithms and methods developed, and to quantify the improvements. A small monopole divided into very short segments dissatisfying the thin wire approximation, was successfully modelled once the segment

aggregation was applied. This has also illustrated the effect of improving the equivalent (total) length to radius ratio. Application of the MDBFs to a meander monopole and half-wave dipole have highlighted existence of a clear correlation between the ratio of the longest and shortest segments, impedance matrix condition number, and the accuracy of results. It has also demonstrated the advantages of using piecewise sinusoidal (PWS) interpolating profile over the piecewise linear (PWL) profile. Example of a coil-loaded antenna has shown an up to ten-fold reduction in the number of unknowns required for modelling a structure with a curved element. Such improvement corresponds to a hundred-fold reduction in the memory requirements. An even greater improvement can be expected for structures with a greater percentage of curved elements.

The theory developed for MDBFs was extended further to support higher order polynomial basis functions. This was accomplished by representing the transformation matrix as a product of three matrices reflecting on the shift in the coordinate system and change in the polynomial base. An estimate for computational complexity associated with the theory for MDBFs, has been derived. This estimate can provide a measure for efficient application of the technique.

Suggestions for application of the above-described methods and software code to quadrilaterals – based surface elements and meshes have also been given, paving a way from the wire based modelling into surface and towards volumetric modelling.

6.2 Next steps

There are many possible options in moving the techniques proposed in the thesis forward, towards more optimal and/or practical application. Here is an incomplete list.

- Investigate influence of local coupling effects on mesh requirements

The presence of local coupling effects, where there is no direct electrical contact between the structures, may needs a separate study, similar to [Kolundzija et al., 50] or [Gvozdev et al., 25]. Presence of such a local (with respect to the length of a long chain) effect may affect the accuracy, if the shape of the respective chain basis function does not take the effect into account.

- Develop more advanced algorithms for splitting chains into sub-chains

As it has been mentioned in the Notes in Section 4.4.7, a number of additional parameters may be taken into account when splitting the chains into sub-chains. For instance, this process may also be combined with splitting longer wires into segments, as to enhance the optimality, or it can be run iteratively. More research will need to be done in order to establish the necessary practical criteria of optimality.

- Apply the chaining technique to meshes/grids

It is believed that it may be possible to further generalise the chaining technique, and apply it to the fine meshes made of wires, as well as to surfaces made of solid plates, e.g. quadrilaterals. In both cases, it is assumed that these composite structures can be replaced by solid structures of the same dimensions, so that the higher order basis functions can then effectively approximate the current distribution on the total area.

- Investigate the influence of smoothness and corners

The main restrictions of this approach are expected to be (a) in the degree of smoothness and (b) electrical size of the initial structure. If a smooth surface is being modelled, the method should work. If, on the other hand, the mechanical structure has sharp bends that could create strong reflections, the outcome is not so obvious, and requires additional investigation. The investigation should address the question of computing the maximum effective electrical length as a function of curvature.

The electrical size of a fine mesh made of wires, or a surface made of solid quadrilaterals, i.e. two-dimensional (in terms of surface currents) structures, should have similar restrictions as for the chains. However, the degree of curvature may again give rise to the differences and errors. In order to achieve a preset accuracy with a limited set of basis functions, a strongly curved plate may be required to have a smaller permitted electrical size compared to a flat plate. The algorithms for aggregating into new, more intelligent type of chains/meshes also need to be developed.

- Extend the concept of chains onto the RWG basis functions

The other very exciting direction of extending the aggregating technique is to apply it to triangular surface elements. These elements developed by Glisson, Wilton and Rao

[Rao, 94] are usually referred to as RWG basis functions, and are very popular today due to their flexibility in covering curved surfaces. The elements support piecewise linear approximation in the direction of current flow and piecewise constant approximation in the orthogonal direction. The RWG basis functions usually require several times more unknowns per square wavelength compared to quadrilateral surface elements [Kolundzija, 42, 44, 43]. The application of the aggregating technique may help to eliminate this inefficiency. Some work in the direction of RWG has already been done by an Italian group – see for example [Vipiana, Vecchi, and Pirinoli, 108], and also [Yla-Oijala et al., 113].

- Consider different polynomial basis functions

One more topic that can be readily implemented and may provide a wealth of improvement when modelling electrically large objects is the choice of basis functions. With an increase in the number of unknowns (and the basis functions used), the hierarchical polynomial basis functions lead to a rapid growth in the condition number. This may be followed by a loss in accuracy. More orthogonal set of basis functions is expected to reduce the problem.

- Support for a linear combination of sine and cosine basis functions in combination with polynomial basis functions.

Such a combination can prove to be a very efficient way to model large smooth bodies of arbitrary shape. If the sine and cosine functions are interpolated linearly, the implementation of the model is expected to be easy to implement.

- Compare the MDBF against the characteristic basis functions

The so-called characteristic basis functions [Mittra et al, 77, 91] have an advantage of being self-adaptive to the true profile of current distribution, at least in the local sense. On the other hand, the characteristic basis functions require additional computations in comparison to the MDBFs. On smooth surfaces, it is likely that the additional computational burden due to the characteristic basis functions does not provide extra accuracy, at least when the mesh is fine. This hypothesis needs to be verified and quantified.

- Implement/support inclusion of losses and excitations into the chains

This is a practically important topic.

- Extend the investigation on the reduction of the condition number

There are several expansions that may be necessary. In a first step, a more thorough numerical investigation may be accomplished by considering a wider range of geometrical structures made of wire. As a follow up, this investigation may be extended onto the plates (quadrilaterals, triangles etc.). In addition, establishing a theoretical groundwork may prove to be highly beneficial in order to reduce the quantity and diversity of numerical experiments otherwise required.

Also, it is possible to check the applicability of a scaling technique [Yla-Oijala et al., 114], which could help to address the low frequency breakdowns even more efficiently.

- Implement support for dielectrics

This extension could be based, for instance on the works [Kolundzija, 44,45,46,47,48], [Notaros et al., 82, 83], [Yla-Oijala, Taskinen, 115], [Jung, Sarkar, Chung, 35].

- Compare the developed method for calculating radiation pattern against quadratures

An investigation must be made to establish an optimum approach to combine the developed technique with the numerical quadratures (such as trapezoidal and Gaussian quadratures). It is expected that the quadratures should be able to provide the best accuracy and efficiency for relatively short to intermediate lengths of wire segments. It is also anticipated that a combination of the analytical and quadrature approaches may offer the best accuracy and/or speed and efficiency.

- Enhancing the functionality of the program

It would be important to extend the code to support quadrilateral elements. Also, it would be highly beneficial to improve the subroutines for calculating the impedance matrix elements, as to accelerate the calculations. A forward-going step would be to incorporate a frequency interpolation method as to be able to calculate wide-band parameters faster, and also to be able to perform the sensitivity analysis.

References

1. **Abraham** M., „Die elektrischen Schwingungen um einen stabförmigen Leiter, behandelt nach der Maxwell'schen Theorie," *Ann. Physik und Chemie (Wiedeman)*, N.F., Vol. 66, Oct 20, 1898, pp. 435-472.

2. **Abramowitz** M., and **Stegun** I.A., *Handbook of Mathematical Functions*.- Dover Publications, 1965.

3. **Awadhiya** A., **Barba** P., and **Kempel** L., "Finite Element Method Programming Made Easy???," *IEEE Antennas and Propagation. Magazine*, vol. 45, Aug. 2003, pp. 73-79.

4. **Balanis** C.A., *Advanced Engineering Electromagnetics*, John Wiley & Sons, 1989, 1008 pages.

5. **Balanis** C.A., *Antenna Theory: Analysis and Design*, 2nd Ed., 1997, 960 pages.

6. **Burke** G.J., **Miller** E.K., and **Poggio** A.J., "The Numerical electromagnetics Code (NEC) - A Brief History," *IEEE AP-S International Symposium and USNC / URSI*, National Radio Science, Monterey, California, June 20 -25, 2004, pp. 2871- 2874.

7. **Burke** G.J., and **Poggio** A.J., "Numerical electromagnetics Code (NEC) – Method of Moments. Part II: Program Description – Code." *Report UCID* – 18834, Lawrence Livermore Laboratory, January 1981.

8. **Butler** C.M., and **Wilton** D.R., "Analysis of Various Numerical Techniques Applied to Thin-Wire Scatterers," *IEEE Trans. Ant. Propagat*., Vol. 23, No 4, July 1975, pp. 534-540.

9. **Caorsi** S., **Moreno** D., and **Sidoti** F., "Theoretical and numerical treatment of surface integrals involving the free-space Green's function." *IEEE Trans. on Antennas and Propagation*, Vol. 41, no. 9, 1993, pp. 1296-1301.

10. **Chew** W.C., **Jin** J., **Michielssen** E., and **Song** J., *Fast and Efficient Algorithms in Computational Electromagnetics*, Artech House, 2001, 931 pages.

11. **Collin** R.E., "An Introduction to the Classic Paper by M. I. Pupin," *Proceedings of the IEEE*, Vol. 85, 1997, pp. 301-305.

12. **Davidson** D.B., ``A Review of Important Recent Developments in Full-Wave CEM for RF and Microwave Engineering", ICCEA2004, 3rd Int'l Conf. on Comput. Electromagnetics and its Applications, China, Nov 2004, pp. PS1-PS4.

13. **Davidson** D.B., Computational Electromagnetics for RF and Microwave Engineering. –Cambridge Univ. Press, 2005, 430 p.

14. **Daniels** D.J., *Ground Penetrating Radar*, Published by IET, 2004, 726 pages.

15. **Djordjevic** A.R., **Bazdar** M.B., **Vitosevic** G., **Sarkar**, T.K., and **Harrington**, R.F., *Analysis of Wire Antennas and Scatterers*. -Artech House, 1990.

16. **Djordjevic** A.R., **Bazdar** M.B., **Sarkar** T.K., and **Harrington** R.F., *AWAS for Windows: Analysis of Wire Antennas and Scatterers*. -Artech House, 1995.

17. **Djordjevic** A.R., **Bazdar** M.B., **Sarkar** T.K., and **Harrington** R.F., *AWAS for Windows Version 2.0: Analysis of Wire Antennas and Scatterers, Software and User's Manual*. - Artech House, 2002.

18. **Djordjevic** A.R., **Bazdar** M.B., **Sarkar** T.K., **Harrington** R.F., "Solution of Two-Potential Equation for Wire Structures Using Polynomial Expansion and Pulse Testing Functions." *IEE Seventh International Conference on Antennas and Propagation, ICAP 91*, Vol. 1, 15-18 April 1991, pp. 540-543.

19. **Djordjevic** A.R., and **Notaros** B.M., "Three types of Higher Order MoM Basis Functions Automatically Satisfying Current Continuity Conditions," *Proc. IEEE AP-S Int. Symp.*, Vol. 4 , 2002, pp. 610-613.

20. **Duffy** M.G., "Quadrature over a pyramid or cube of integrands with a singularity at a vertex." *SIAM Journal on Numerical Analysis*, 19(6), 1982, pp. 1260-1262.

21. **Encycopedia Britannica**, Available online at http://www.britannica.com/.

22. **Forsythe** G.E., Malcolm M.A., and Moler C.B., *Computer Methods for Mathematical Computations*, Prentice-Hall, 1977.

23. **Gamage** J.K., *Efficient Space Domaine Method of Moments for Large Arbitrary Scatterers in Planar Stratified Media*, Doctoral thesis, NTNU, 2004.

24. **Golub** G.H. and **Van Loan** C.F., *Matrix Computations*. 3rd Ed., The John Hopkins University Press, 1996, 698 pages.

25. **Gvozdev** V.I., **Kouzaev** G.A., and **Nefedov** E.I., "Balanced Slotted Line. Theory and experiment." *Radio Engineering and Electronics Physics (Radiotekhnika i Elektronika)*. Vol. 30, No 5, 1985, pp. 1050-1057.

26. **Hallén** E., "Theoretical Investigations into the Transmitting and Receiving Qualities of Antennae," *Nova Acta Regiae Soc. Sci. Upsaliensis*, Ser. IV, 11 No. 4, 1938, pp. 1-44.

27. **Harrington** R.F., "Matrix Methods for Field Problems," *Proc. IEEE*, Vol. 55 , No. 2, Feb. 1967, pp. 136-149.

28. **Harrington** R.F., *Field Computation by Moment Methods*, Macmillan, 1968. Reprinted by IEEE Press, 1993.

29. **HFSS** (by Ansoft, LLC, USA). Producer's web site: http://www.hfss.com, and http://www.ansoft.com/products/hf/hfss/ .

30. **Hua** Y., and **Sarkar** T.K., "Generalized pencil-of-function method for extracting poles of an EM system from its transient response," *IEEE Trans. Ant. Propag*., Vol. 37, Feb. 1989, pp. 229-234.

31. **IEEE 145-1993**: Standard Definitions of Terms for Antennas, 1993.

32. **IEEE 754-1985**: Standard for Binary Floating-Point Arithmetic, 1985.

33. **Itoh** T., **Pelosi** G., **Silvester** P.P., *Finite Element Software for Microwave Engineering*.- Wiley, 1996, 504 pages.

34. **Järvenpää** S., **Taskinen** M., and **Ylä-Oijala** P., "Singularity extraction technique for integral equation methods with higher order basis functions on plane triangles and tetrahedral." -*Intl. J. Numer. Meth. Eng*., Vol. 58, 2003, pp. 1149-1165.

35. **Jung** B.H., **Sarkar** T.K., and **Chung** Y.-S., "A Survey of Various Frequency Domain Integral Equations for the Analysis of Scattering from Three-Dimensional Dielectric Objects," Progress In Electromagnetics Research, PIER 36, 2002, pp. 193–246.

36. **Kantorovich** L.V., and **Akilov** G.P., *Functional Analysis in Normed Spaces*, Oxford: Pergamon Press, 1964, 773 pages.

37. **Kantorovich** L.V., and **Krylov** V.I., *Approximate Methods of Higher Analysis*, John Wiley & Sons, 1964, 681 pages.

38. **King** L.V., "On the Radiation Field of a Perfectly Conducting Base-Insulated Cylindrical Antenna Over a Perfectly Conducting Plane Earth, and the Calculation of the Radiation Resistance and Reactance," *Phil. Trans. R. Soc. (Lond.)*, 236, 1937, pp. 381-422.

39. **Kolundzija** B.M. et al., *WIPL-D Pro v6.1: 3D Electromagnetic Solver, Professional Edition. User's Manual*, WIPL-D d.o.o., 2006.

40. **Kolundzija** B.M., "Comparison of a Class of Subdomain and Entire Domain Basis Functions Automatically Satisfying KCL," *IEEE Trans. Ant. Propagat.*, Vol. 44, No. 10, Oct., 1996, pp. 1362-1366.

41. **Kolundzija** B.M., "Effect of a Wire End in Thin Wire Analysis," *in Proc. IEEE AP-S Symposium,* Syracuse, NY, (Vol. 2 in Digest) 1988, pp. 843-846.

42. **Kolundzija** B.M., "General Entire-Domain Galerkin Method for Electromagnetic Modeling of Composite Wire to Plate Structures," *Proc. of 20th EuMc*, Budapest, Hungary. Pt. 1, 1990, pp. 853-858.

43. **Kolundzija** B.M., "On the Locally Continuous Formulation of Surface Doublets," *IEEE Trans. Ant. Propagat*., Vol. 46, No. 12, Dec. 1998, pp. 1879-1883.

44. **Kolundzija** B.M., and **Popovic** B.D., "Entire-Domain Galerkin Method for Analysis of Metallic Antennas and Scatterers," *Proc. IEE, Pt. H*, Vol. 140, No. 1, Feb. 1993, pp. 1-10.

45. **Kolundzija** B.M., and **Popovic** B.D., "Entire-Domain Galerkin Method for Analysis of Generalised Wire Antennas and Scatterers," *Proc. IEE, Pt. H*, Vol. 139, No. 1, Feb. 1992, pp. 17-24.

46. **Kolundzija** B.M., and **Djordjević** A.R., *Electromagnetic Modeling of Composite Metallic and Dielectric Structures*, Artech House, 2002, 481 pages.

47. **Kolundzija** B.M., **Ognjanovic** J.S., and **Sarkar** T.K., *WIPL-D: Electromagnetic Modeling of Composite Metallic and Dielectric Structures – Software and Users Manual*, Artech House, 2000, 300 pages.

48. **Kolundzija** B.M., and **Popovic** B.D., "Entire Domain Galerkin Method for Analysis of Generalised Wire Antennas and Scatterers," *IEE Proc.-H*, Vol. 139, No 1, Feb. 1992, pp. 13-18.

49. **Kolundzija** B.M., and **Sarkar** T.K., "On the Choice of Optimal Basis Functions for MoM/SIE, MoM/VIE, FEM and Hybrid Methods," *Proc. IEEE AP-S Int. Symp*., Vol. 1, Jun. 1998, pp. 278-281.

50. **Kolundzija** B.M., **Tasic** M.S., and **Sarkar** T.K., "Optimal Meshing of Polygonal Surfaces in Case of Pronounced Proximity Effect," *Proc. IEEE AP-S Int. Symp*., Vol. 4, 22-27 June 2003, pp. 73-76.

51. **Kolundzija** B.M., and **Popović** B.D., "A New, Rapid and Accurate Method for Evaluation of Potential Integrals in Thin-Wire Antenna Problems," *Proc. 5th ICAP*, York, Pt. I, 1987, pp. 35-38.

52. **Kraus** J.D., and **Marhefka** R.J., *Antennas for All Applications*, 3rd Ed., McGraw-Hill, 2002, 938 pages.

53. **Kyle** R.H., "Mutual Coupling Between Log-Periodic Antennas," *IEEE Trans. Ant. Propagat.*, Vol. 18, No 1, Sep. 1971, pp. 15-22.

54. **Lysko** A., and **Aas** J.A., "GPR-Directed Study of a Dipole on Lossy Ground." Proc. of the XXVIth General Assembly of the Intl. Union of Radio Sci., University of Toronto, Toronto, Ontario, Canada, Aug. 1999.

55. **Lysko** A., *AM1D Getting Started v1.0*, 2001. - Internal for the Department of Telecommunications, Norwegian University of Science and Technology, 2001.

56. **Lysko** A., *Antenna Pattern Measurements AM1D, User's Manual*, 2001. - Internal for the Department of Telecommunications, Norwegian University of Science and Technology, 2001.

57. **Lysko** A., and **Eide** E., "A New Antenna Laboratory for 3D Antenna and RCS Measurements." *In Proc. of 23rd AMTA Meeting and Symposium (Mile Hi 2001)* in Denver, USA, October, 2001.

58. **Lysko** A.A., "Investigation of Characteristics of a Flat Dipole at an Junction of Dielectric Layers", *MSc Thesis* (in Technique and Technology), St.-Petersburg State Technical University (SPbSTU), Russia, 1998.

59. **Lysko** A.A., "On Grouping Individual Wire Segments into Equivalent Wires or Chains, and Introduction of Multiple Domain Basis Functions," *IEEE Intl Symp. on Ant. & Propagat. and USNC/URSI National Radio Science Meeting*, 2009.

60. **Lysko** A.A., "Using Piecewise Sinusoidal Basis Functions to Blanket Multiple Wire Segments," *IEEE Intl Symp. on Ant. & Propagat. and USNC/URSI National Radio Science Meeting*, 2009.

61. **Lysko** A.A., *A Method and System of Memoization*, South African Patent Application No 2008/10479, 2008.

62. **Lysko** A.A., *A Method of Operating A Computing Device to Perform Memoization*, International PCT Patent Application, PCT/IB2009/055650, Dec 2009.

63. **Lysko** A.A., "A Method of Applying Single Higher Order Polynomial Basis Function over Multiple Domains." Accepted for the 27th Progress In Electromagnetic Research Symposium (PIERS 2010) to be held on March 22–26, 2010 in Xi'an, China, 2 pages.

64. **Lysko** A.A., "Modelling a Wire Mesh Reflector by Grouping into Sub-meshes." Accepted for the 27th Progress In Electromagnetic Research Symposium (PIERS 2010) to be held on March 22–26, 2010 in Xi'an, China, 2 pages.

65. **Lysko** A.A., "Modelling of Coil-loaded Wire Antenna Using Composite Multiple Domain Basis Functions." Accepted for the 27th Progress In Electromagnetic Research Symposium (PIERS 2010) to be held on March 22–26, 2010 in Xi'an, China, 2 pages.

66. **Lysko** A.A., "On Calculation of Radiation Field Integrals for Higher-Order Basis Functions in Conical Thin Wire MoM Formulation." *Proc. of the 6th WSEAS Int. Conf. on Applied Electromagnetics, Wireless and Optical Communications (ELECTROSCIENCE '08)* in Trondheim, Norway in July 2-4, 2008, 6 pages.

67. **Makarov** S.N., *Antenna an EM Modeling with Matlab*, John Wiley & Sons, 2002, 288 pages.

68. **Maple 9.5** Getting Started Guide. Toronto: Maplesoft, a division of Waterloo Maple Inc., 2004. Web: http://www.maplesoft.com.

69. *Matlab Programming*, Version 7 (Release 14). The MathWorks, Inc., 3 Apple Hill Drive, Natick, MA 01760-2098, USA, 2004. Web: http://www.mathworks.com.

70. **Maxwell** J.C., "A Dynamical Theory of the Electromagnetic Field," *Proc. Roy. Soc. (London)*, Vol. 13, Dec 8, 1864, pp. 531-536.

71. **Medgyesi-Mitschang** L.N., and Eftimiu C., "Scattering from Wires and Open Circular Cylinders of Finite Length Using Entire Domain Galerkin Expansions," *IEEE Trans. Ant.. Propagat.*, Vol. 30, No. 4, July 1982, pp. 628-636.

72. *Merriam-Webster Dictionary*, Available online at: http://www.merriam-webster.com/dictionary/generatrix.

73. **Miller** E.K., and **Deadrick** F.J., *Some Computational Aspects of Thin-Wire Modeling, in Computer Techniques for Electromagnetics*, R. Mittra (Ed.), Pergamon Press, 1973.

74. **Miller** E.K., and **Deadrick** F.J., *Some Computational Aspects of Thin Wire Modeling, in Numerical and Asymptotic Techniques in Electromagnetics*, R. Mittra (Ed.), Springer, 1975.

75. **Miller** E.K., **Medgyesi** L., and **Newman** E.H., *Computational Electromagnetics: Frequency Domain Method of Moments*, IEEE Press, 1992, 508 pages.

76. **Mittra** R., *Numerical and Asymptotic Techniques in Electromagnetics*. New York, Springer-Verlag New York, Inc. (Topics in Applied Physics. Vol. 3), 1975. 270 p.

77. **Mittra** R., and **Du** K., "Characteristic Basis Function Method For Iteration-Free Solution Of Large Method Of Moments Problems," Progress In Electromagnetics Research B (PIERS-B), Vol. 6, 2008, pp. 307–336.

78. **Morita** N., **Kumagai** N., and **Mautz** J., *Integral Equation Methods for Electromagnetics*, Artech House, 1992.

79. **Mushiake** Y., *Self-Complementary Antennas*. Springer, 1996, 128 pages.

80. **Nakano** H., *Helical and Spiral Antennas – A Numerical Approach*. Research Studies Press Ltd. John Wiley & Sons. 1987.

81. **Nomura** Y. and **Hatta** T., "The Theory of a Linear Antenna, I," *Tech. Rep. Tohoku Univ.*, Vol. 17, Pt. 1, 1952.

82. **Notaros** B.M., **Popovic** B.D., "General Entire-Domain Galerkin Method for Analysis of Wire Antennas in the Presence of Dielectric Bodies," -IEEE Proc.-Microw. Antennas Propag., Vol. 145, No 1, Feb 1998, pp. 13-18.

83. **Notaroš** B.M., **Popovic** B.D., **Weem** J.P., **Brown** R.A., and **Popović** Z., "Efficient Large-Domain MoM Solutions to Electrically Large Practical EM Problems." -IEEE Transactions on Microwave Theory and Techniques, Vol. 49, No. 1, Jan 2001, pp. 151-159.

84. *PCAAD 6.0 – Personal Computer Aided Antenna Design*. Information available on web site http://www.antennadesignassociates.com/pcaad6.htm

85. **Peterson** A., **Ray** S.C., and **Mittra** R., *Computational Methods for Electromagnetics*, IEEE Press and Oxford University Press, 1998.

86. **Petrov** G., "Application of Galerkin's Method to a Problem of the Stability of the Flow a Viscous Liquid," (Russian), *Priklad. Matem. i Mekh*., Vol. 4, No. 3, 1949, pp. 3-12.

87. **Pocklington** H.C., "Electrical Oscillations in Wires," *in Proc. Cambridge Phil. Soc. Proc.* , London, England, Vol. 9, Oct. 1897, pp. 324-332.

88. **Popovic** B.D., and **Djordjevic** A.R., "A Comparison of Two Efficient Methods for Analysis of Wire Antennas," *in Proc. of 5th Intl. Conf. Ant. Propagat*., Apr. 1987, pp. 107-110.

89. **Popovic** B.D., **Dragovic** M.B., and **Djordjevic** A.R., *Analysis and Synthesis of Wire Antennas*, Research and Studies Press, 1982.

90. **Pozar** D., *Microwave Engineering*, 2nd Ed., Wiley, 1998.

91. **Prakash** V.V.S., and **Mittra** R., "Characteristic Basis Function Method: A New Technique for Efficient Solution of Method of Moments Matrix Equations," Microwave and Optical Technology Letters, Vol. 36, No 2, Jan 2003, pp. 95-100.

92. **Press** W.H., **Teukolsky** S.A., **Vetterling** W.T., and **Flannery** B.P., *Numerical Recipes in C++: The Art of Scientific Computing*, 2nd Ed., Cambridge Univ. Press, 2002.

93. **Råde** L., and **Westergren** B., *Mathematics Handbook for Science and Engineering*, Studentlitteratur, Sweden, 1995.

94. **Rao** S.M., **Glisson** A.W., and **Wilton** D.R., "Electromagnetic Scattering by Surfaces of Arbitrary Shape," *IEEE Trans. Ant. Propagat.*, Vol. 30, No.3, May 1982, pp. 409-418.

95. **Richmond** J.H., "Computer Analysis of Three-Dimensional Wire Antennas," Ohio State Univ., ElectroScience Lab.,Dept. of EE, Rep. 2708-4, 1969.

96. **Rogers** S.D., and **Butler** C.M., "An Efficient Curved-Wire Integral Equation Solution Technique," *IEEE Trans. Ant. And Propag*., Vol. 49, No. 1, January 2001. pp. 70-79.

97. **Rogers** S.D., and **Butler** C.M., "Reduced Rank Matrices For Curved Wire Structures," *Digest of IEEE APS/URSI Radio Science Meeting*, July 1997, pp.68-71.

98. **Rumsey** V., *Frequency Independent Antennas*. Academic Press, 1966.

99. **Sakitani** A. and **Egashira** S., "Coil-loaded dipole antenna," *Reports of the Faculty of Science and Engineering*, Saga University, Japan. No. 12, March 1984, pp. 151-156.

100. **Schwab** C., and **Wendland** W.L., "On Numerical Cubatures of Singular Surface Integrals in Boundary Element Methods." *Numerische Mathematik*, 62, 1992, pp. 343-369.

101. **Silvester** P.P., and **Ferrari** R.L., *Finite Elements for Electrical Engineers*, 3rd Ed., Cambridge University Press, 1996.

102. **Stamm** J.M. and **Breakall** J.K., "Comparison of Results for the NEC4, WIPL-D, and Eiger Antenna." Proc. of 17th Applied Computational Electro-magnetics Conf., Monterey, CA, March 2001, pp. 269-276.

103. **Storm** B., *Investigation into Modern Aerial Theory and a New Solution of Hallen's Integral Equation for a Cylindrical Aerial*, Dissertation, Imperial College, London, UK, 1953.

104. **Stutzman** W.L., and **Thiele** G.A., *Antenna Theory and Design*, 2nd Ed., John Wiley & Sons, 1998.

105. **SuperNEC** (by Poynting Software Ltd Pty, South Africa). Producer's web site: (http://www.supernec.com),

106. **Taflove** A., and **Hagness** S.C., *Computational Electromagnetics* – The Finite Difference Time-Domain Method, 3rd Ed., Artech House, 2005.

107. **Taguchi** M., **Yamashita** K., **Tanaka** K., and **Tanaka** T., "Analysis of Coil-Loaded Thin-Wire Antenna," *IEEE AP-S Intl Symp* 3, 1990, pp, 273-276.

108. **Vipiana** F., **Vecchi** G., **Pirinoli** P., "A Multiresolution System of Rao–Wilton–Glisson Functions." -IEEE Transactions on Antennas and Propagation, Vol. 55 (2), No 3, 2007, pp. 924-930

109. **Volakis** J.L., *Antenna Engineering Handbook*, 4th Ed., McGraw-Hill, 2007.

110. **Wang** J.H.H., *Generalised Moment Methods in Electromagnetics*, John Wiley & Sons, 1991.

111. **Wilton** D.R., **Rao** S.M., **Glisson** A.W., **Schaubert** D.H., **AlBundk** O.M., and **Butler** C.M., "Potential Integrals for Uniform and Linear Source Distributions on Polygonal and Polyhedral Domains." *IEEE Trans. on Ant. Propagat.*, Vol. 32, No 3, 1984, pp. 276-281.

112. **Yee** K.S., "Numerical Solution of Initial Boundary Problems Involving Maxwell's Equations in Isotropic Media," *IEEE Trans. Ant. Propagat*., 14, May, 1966, pp 302-307.

113. **Yla-Oijala** P., and **Taskinen** M., "Calculation of CFIE impedance matrix elements with RWG and n times RWG functions." -IEEE Transactions on Antennas and Propagation, Vol. 51, No 8, Aug. 2003, pp. 1837 – 1846.

114. **Ylä-Oijala** P., **Taskinen** M., "Well-conditioned Muller Formulation for Electromagnetic Scattering by Dielectric Objects." -IEEE Transactions on Antennas and Propagation, Vol. 53, No 10, 2005, pp. 3316-3323.

115. **Ylä-Oijala** P., **Taskinen** M., and **Sarvas** J., "Surface integral equation method for general composite metallic and dielectric structures with junctions," -Progress In Electromagnetics Research, PIER 52, 2005, pp. 81-108.

116. **Yuan** M., **Sarkar** T. K., and **Kolundzija** B., "Solution of large complex problems in computational electromagnetics using higher-order basis in MoM with out-of-core solvers." -IEEE Antennas and Propagation Magazine, Vol. 48, No 2, 2006, pp. 55-62

Appendix A. On Equivalent Radius of Curvature

Geometrically, a round circle may be modelled with a regular polygon. This is a piecewise linear approximation. It is very practical, and as such is widely used for modelling loops, spirals and similar antennas when a program supports only straight piecewise linear segments (e.g. straight wire segments). Figure A-1 shows an example of such approximation.

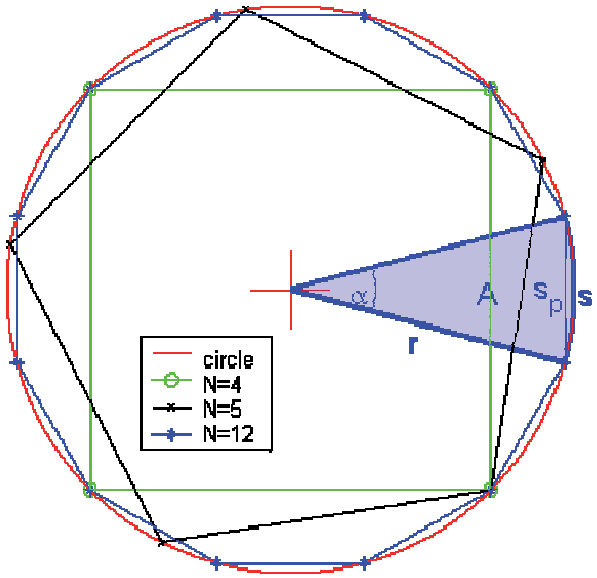

Figure A-1. Geometrical approximation of a round circle with a regular polygon. Several polygons with four, five and twelve sides are shown as drawn into the circle. The notation in the figure are: r is the circle radius, α is the opening angle of a sector with arc length s, and area A, and s_p is the length of the base of an equilateral triangle fitted into the sector.

It is possible to show that this approximation converges to a circle when the length of each of the approximating straight segments becomes infinitesimal, i.e. the number of segments goes to infinity. In practice, however, it is desirable to minimize the number of segments. This demands establishment of a relationship between the number of segments in a regular polygon and the error this approximation results in.

The derivations made below consider a loop antenna made of thin perfectly conducting wire. It is also assumed that the circumference of the wire in the loop plays a more

significant role in the error than the area of this loop. Therefore, this approximation may be inaccurate at low frequencies, where the magnetic interactions (proportional to the area of a loop) may dominate.

The *n*-th resonant frequency of a circular loop antenna in vacuum, made of a very thin wire, may be estimated as

$$f_n = n\frac{c}{C} = n\frac{c}{2\pi r}, \tag{A.1}$$

where n is the number of resonance ($n = 1, 2, \ldots$), c is the speed of light ($3 \cdot 10^8$ m/s), C is the circumference of a circle, and r is the circle radius. The resonant wavelength λ_n can be found using one of the following forms:

$$\lambda = C = 2\pi r \,, \lambda_n = c/f_n = C/n = 2\pi r/n \tag{A.2}$$

In a numerical model, a circle may be approximated with a regular n-corner polygon. Assuming that the polygon's centre is at the origin, the coordinates of polygon vertices may, for example, be calculated as

$$\begin{cases} \varphi_k = \dfrac{2\pi}{n}k, \\ x_k = r\cos(\varphi_k), \text{ where } k = 0, 1, \ldots, n-1, \\ y_k = r\sin(\varphi_k), \end{cases} \tag{A.3}$$

where φ_k is angular coordinate of the k-th vertex, and x_k and y_k are the respective rectangular coordinates.

The drawback of this approximation is in the shift in the resonant frequencies that may occur due to a decrease in the perimeter for the approximating polygon compared to the circumference of the original circle. Table A-1 based on [Råde, 93] shows a comparison of the main geometrical parameters of a circle and a regular n-corner polygon.

Table A-1. Expression for parameters of circle with radius r compared to expressions for equivalent parameters of a regular n-corner polygon with outer radius r.

Parameter \ Geometry	**Circle**	**Regular polygon with n corners**
Length of an arc/side with opening angle α	$s = \alpha r$	$s_p = 2r\sin(\frac{\alpha}{2})$
Area of sector/segment	$A = \frac{sr}{2} = \frac{\alpha r^2}{2}$	$A_p = \frac{1}{2} r^2 \sin(\alpha)$
Circumference/perimeter	$C = 2\pi r$	$P_p = ns_p = n2r\sin(\frac{\alpha}{2})$
Area	$S = \pi r^2$	$S_p = ½nr^2\sin(\alpha)$

It is possible to minimize the shift in frequency by a slight increase in the outer diameter of the approximating polygon in the model. In order to find how much of increase is necessary, it is possible to set the circle's circumference equal to the perimeter of the regular polygon (the subscript $_p$ is used to denote quantities related to the polygon):

$$C = 2\pi r = P_p = n2r_p \sin(\tfrac{\alpha}{2}).$$

This gives the desired *equivalent radius* of the polygon as $r_p = r\frac{\pi}{n\sin(\frac{\alpha}{2})} = rF_p$. In the last expression, the factor F_p was introduced to signify the relative difference in the radius of a circle and the outer radius of a regular polygon that is considered equivalent to the circle. In the same manner it is possible to derive the expression for a factor equalizing the areas of a circle and an equivalent polygon: $F_s = \sqrt{\alpha / \sin(\alpha)}$.

The factors F_p and F_s are shown in Figure A-2. Both factors converge to unity as the number of sides in the polygon increases, i.e. as the quality of geometrical approximation improves.

The final expression for the factor F_p can be written as

$$F_p = \frac{\pi}{n\sin(\frac{2\pi/n}{2})} = \frac{\pi}{n\sin(\frac{\pi}{n})} = \frac{\alpha/2}{\sin(\alpha/2)} \qquad \text{(A.4)}$$

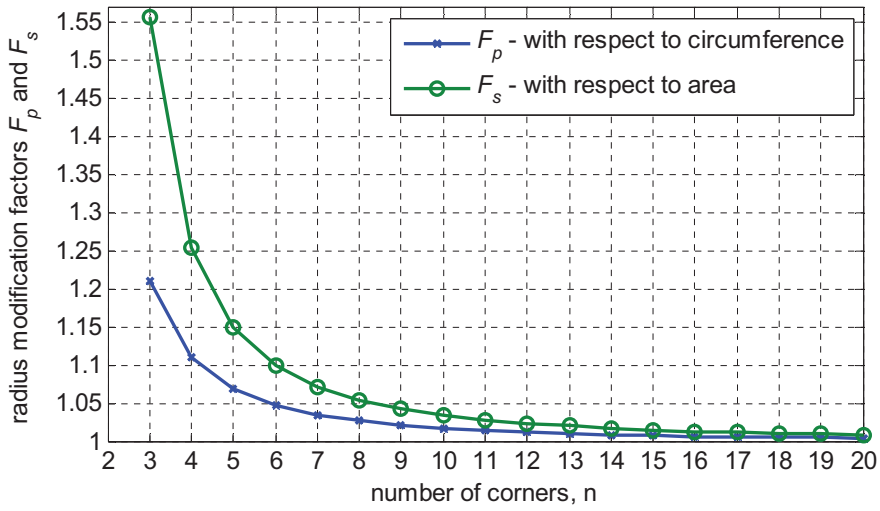

Figure A-2. Value of factors F_p and F_s as a function of the number of corners of a regular polygon, n.

It is also possible to evaluate the relative error in the resonance frequency of a loop antenna. This error may be defined as:

$$\varepsilon = \frac{f_p - f_c}{f_c}, \tag{A.5}$$

where f_p is the resonance frequency of a polygonal loop and f_c is the resonance frequency of a circular loop. The resonance frequency of a loop is assumed to be defined by its perimeter only, i.e. the phase velocity of a wave travelling around the loop periphery is assumed independent of the geometrical properties of the periphery, incl. the radius of curvature. Denoting the perimeter of the polygonal loop with C_p and the circumference of the circular loop with C_c, the expression for the relative error maybe expressed through the factor F_p:

$$\varepsilon = \frac{c/C_p - c/C_c}{c/C_c} = F_p - 1 = \frac{\pi/N}{\sin(\pi/N)} - 1, \text{ or } \frac{\sin(\pi/N)}{\pi/N} = \frac{1}{1+\varepsilon}. \tag{A.6}$$

In order to obtain the number of required segments N from the prescribed accuracy of solution ε, one would need to solve this transcendent equation. The result may be shown in the following plot.

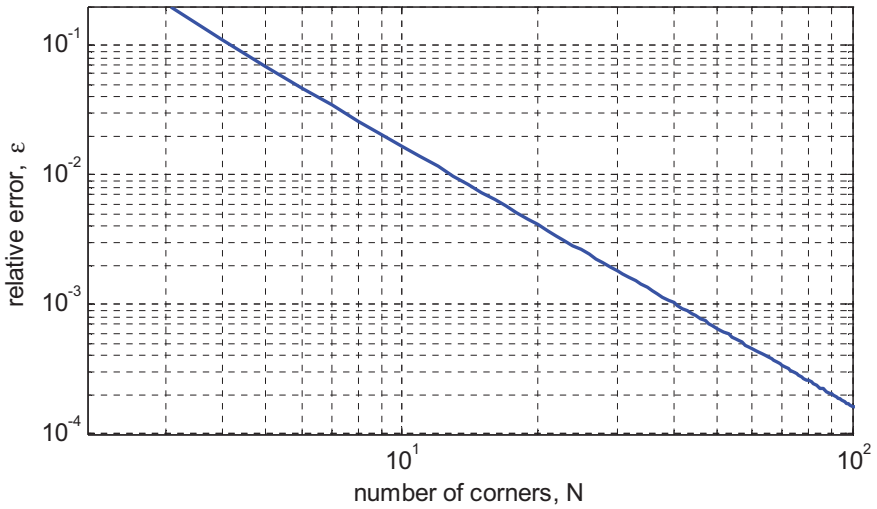

Figure A-3. Error in the first resonance frequency of a loop modelled with a regular polygon with *N* sides/corners.

Solving a transcendent equation might be inconvenient. Instead, it is possible to obtain a simple approximate solution. The right-hand side of the expression (A.6) can be expanded asymptotically for large N by using Taylor's series expansion with parameter $1/N$. Keeping only the first two terms in the expansion of the sine function results in the asymptotic estimate given by (A.7):

$$\varepsilon \cong \frac{(\pi/N)^2}{3!}, \quad N >> 1. \tag{A.7}$$

Thus, in order to achieve the relative frequency error below ε, the number of segments in a polygonal loop must be greater than the nearest higher integer of

$$N = \frac{\pi}{\sqrt{6\varepsilon}}, \text{ valid for } \varepsilon << 1. \tag{A.8}$$

The exact (A.6) and asymptotic (A.8) norms may be used to estimate the required quality of geometrical approximation based on the required accuracy in the resonance frequency.

Note:

Kolundzija at el. [46] utilised a different definition for the equivalent radius that cannot be expressed as a continuous analytical function.

Appendix B. Paper on Calculation of the Radiation Pattern

NB This is a copy of the reference [66]:

On Calculation of Radiation Field Integrals for Higher-Order Basis Functions in Conical Thin Wire MoM Formulation

ALBERT A. LYSKO
Wireless Africa group
Meraka Institute,
Council for Scientific and Industrial Research
Meiring Naude Rd, Brummeria 0001, Pretoria
SOUTH AFRICA
alysko@csir.co.za, http://www.meraka.org.za/

Abstract: - An efficient method of integration for far field calculations is derived. The method applies to the integrals arising from calculation of far field pattern with higher-order polynomial basis functions and moment method. The integral under consideration is a product of a power and exponential functions. Depending on the electrical length of the integration path and the required accuracy, either integration by parts or small parameter expansion is applied, in a recursive manner. The speed performance of a Matlab implementation indicates that the presented method is favorable compared to the commercial software "WIPL-D" used as a reference.

Key-Words: - antenna radiation patterns, moment methods, numerical analysis.

1 Introduction

There are cases when modeling of even simple antennas and scatterers may take a relatively long computing time, e.g. when optimizing the geometry with respect to radiation parameters. This often happens due to the need to calculate a radiation pattern or radar cross section (RCS) for many excitations or simply at a large number of points. Calculation of a radiation pattern typically involves a summation of partial electric fields produced by individual current components [1]. Each partial electric field is an integral of the Green's function and the respective current (basis function). It is easy to deduce that the computational complexity of this task scales as $O(N \cdot M)$, where N is the number of unknowns (directly related to basis functions) and M is the number of angular points, at which the radiation pattern is to be calculated.

The process of solving the system and obtaining unknown currents requires $O(N \cdot \log N)$ to $O(N^3)$ operations [2]. Thus, when the impedance matrix size is not large (say, under 1000 unknowns), most of the total time used for simulation is often consumed by integrations and summations involved in the far field estimation.

In the field of ultra wide bandwidth (UWB)/short pulse (SP) arrays, the synthesis techniques [3], [4], [5], often require computation of radiated fields over multiple radiators and over many steering directions.

Evaluation of the far field is often considered a trivial task. This is the case where (a) the basis function is a pulse or a piecewise linear function, or a piecewise sinusoidal basis function [1], and (b) the Green's function is a free space Green's function or may be expanded into a superposition of such [6]. The piecewise sinusoidal functions permit exact analytical integration. The general expressions for an integral of exponent and power function may be found for instance in [7]. For electrically very short segments, the expressions may be reduced to a central point rule [1]. For somewhat longer segments, as the integrand has no singularity, a simple numerical quadrature may be readily used as done by many authors [1], [8].

Traditionally, the integration for power basis functions, including those mentioned above, is performed either by a direct analytical integration or numerically [1], [8], [9]. However, such an approach is usually limited to a specific basis function and may, subject to accuracy and speed, be restricted in the electrical size of the wires. As it will be shown in this paper, the high powers of polynomial basis functions quickly give rise to large errors due to limited computer accuracy

In this paper, a different analytical approach has been applied for the integration involving higher-order power basis functions on thin wire segments. The resulting closed-form expressions, obtained by integration by parts, were found to suffer from a

rapid loss of numerical accuracy for electrically short segments. This problem has been addressed by utilizing a series expansion at low frequencies. The obtained formulae were analyzed from the point of view of numerical accuracy. Further, the error estimating expressions for low and higher frequencies were combined to give the point of optimum to separate the regions of applicability of the series and integration by parts expressions, as well as to give an estimate for the maximum error due to the developed combined approach.

To enhance performance, the recursive properties found in the expressions have been utilized and the resulting algorithm implemented in Matlab [12]. Comparison with the output from a commercial program WIPL-D [10] has shown high efficiency of this algorithm.

2 Derivations

2.1. The Function Under Consideration

Computing the far field from the polynomial-approximated current on thin-wire antennas and scatterers [8], [10], [11] leads to integrals of the form,

$$F_i^u\left(\xi\right)=\int_{z_1}^{z_2} z^i e^{\xi z}dz \qquad (1)$$

where $\xi = j\beta\vec{u}_{r'}\vec{u}_z\cos\alpha$. This integral represents the normalized electrical field produced by a straight wire segment. The geometry of the wire segment is to be modeled by a truncated cone with opening angle α and axis matching z axis of a segment's local coordinate system. The factor z^i in the integrand is a term of a higher-order power/polynomial basis function. The exponent in the integrand represents the fast-changing factor of the free-space Green's function, expanded asymptotically, in the Fraunhofer region. The integration is done from the beginning z_1 of the cone to its end z_2, along the cone axis. The wire (cone axis') unit vector is denoted as $\vec{u}_z$, and the unit vector to the observation point is referred to as $\vec{u}_{r'}$. The other notations used are: i is the order of power basis function, and β is the propagation constant. To highlight the physical meaning, the product of the unit vectors can be expressed as cosine of the angle between them: $\vec{u}_{r'}\vec{u}_z=\cos\theta$. With this in mind, the function will also be referred to as $F_i^u\left(\theta(\xi)\right)$.

2.2. Example of Numerical Instability

For a uniform current distribution (i=0), the integral (1) may be written as

$$F_0^u\left(\theta(\xi)\right)=\int_{z_1}^{z_2} e^{\xi z}dz=\left(e^{\xi z_2}-e^{\xi z_1}\right)/\xi$$

$$=\left(z_2-z_1\right)e^{j\beta\frac{z_1+z_2}{2}\vec{u}_{r'}\vec{u}_z\cos\alpha}\frac{\sin\left(\beta\frac{z_2-z_1}{2}\vec{u}_{r'}\vec{u}_z\cos\alpha\right)}{\beta\frac{z_2-z_1}{2}\vec{u}_{r'}\vec{u}_z\cos\alpha}$$

Both closed forms for this integral (with exponents and sinuses) are numerically unstable (as $\frac{0}{0}$) at angle θ equal 90 degrees and also for conical wires degenerated into disks (when the length of cone is reduced to zero). The exponential form of the expression is also prone to errors due to subtraction of closely valued exponents. This happens when $\beta\left(z_2-z_1\right)\vec{u}_{r'}\vec{u}_z\cos\alpha\approx 0$, for example (a) for electrically short wires, (b) for values of angle θ close to 90 degrees, and (c) for the cones that are close in shape to disks. The accuracy in the result is lost completely when the first, linear, term in the expansion of exponent ($e^{\xi z}\approx 1+\xi z+\ldots,\ \left|\xi z\right|<<1$) becomes smaller than the uncertainty of the floating point number representation $\frac{\varepsilon_0}{2}$ used in computations. This may be written as the inequality: $\left|\xi z\right|\le\frac{\varepsilon_0}{2}$. The scenario where the accuracy is lost is equivalent to taking into consideration only the static field, i.e. $e^{\xi z}\approx 1$, and neglecting the radiating terms.

It is possible to estimate the error due to the limited accuracy of floating point number representation. The inequality may be re-written as $1\le\frac{\varepsilon_0}{2\left|\xi z\right|}$. Considering the left- and right-hand sides equal, and taking the unity as a relative error of 1, the fractional inaccuracy due to subtraction of closely-valued terms δ_{ξ_0} may be evaluated as

$$\delta_{\xi_0}\le 2\frac{\varepsilon_0}{2}\frac{1}{\left|\xi z\right|},\quad \left|\xi z\right|\ll 1 \qquad (2)$$

This expression quantifies the numerical instability due to subtraction of exponents with close powers.

2.3. Lower and Higher Frequency Formulae

In the situation described in the previous section, it is convenient to expand both exponents into a Maclaurin series with respect to the parameter ξ:

$$F_0^u\left(\xi\right)\cong\left(z_2-z_1\right)+\frac{1}{2}\left(z_2^2-z_1^2\right)\xi+\ldots,\quad \left|\xi\right|<<1.$$

Such procedure may also be repeated for higher-

order power functions. This is however a somewhat laborious task.

A simpler method to calculate the integral when the parameter ξ is small, and for arbitrary $i \geq 0$, is to expand the exponent in the integrand into a Maclaurin series and integrate the resulting combined series analytically, as shown in (3).

$$\begin{aligned} F_i^u(\xi) &= \int_{z_1}^{z_2} z^i e^{\xi z} dz \\ &\cong \int_{z_1}^{z_2} z^i \left(1 + \xi z + \tfrac{1}{2!}(\xi z)^2 + \ldots\right) dz \\ &= \tfrac{1}{i+1}\left(z_2^{i+1} - z_1^{i+1}\right) + \tfrac{1}{1!}\tfrac{1}{i+2}\left(z_2^{i+2} - z_1^{i+2}\right)\xi \\ &\quad + \tfrac{1}{2!}\tfrac{1}{i+3}\left(z_2^{i+3} - z_1^{i+3}\right)\xi^2 + \ldots \end{aligned} \tag{3}$$

It is useful to note by writing the next, $(i+1)^{\text{th}}$, term $F_{i+1}^u(\xi) = \tfrac{1}{i+2}\left(z_2^{i+2} - z_1^{i+2}\right) + \tfrac{1}{1!}\tfrac{1}{i+3}\left(z_2^{i+3} - z_1^{i+3}\right)\xi + \ldots$ that some parts of F_i^u may be reused in computing F_{i+1}^u. When computing several terms of a polynomial, the re-usage enables a partially recursive process and may therefore save some computational efforts.

At higher frequencies the electrical length of the integration interval may be too long to apply the expression (3). Then one may integrate (1) by parts. The resulting expressions shown in (4) may also be used in a recursive manner.

As shown later in the paper, the accuracy of results produced by the expansion (3) worsens for larger values of parameter ξ. On the other hand, the accuracy of formula (4) is improving with growth in ξ. Therefore, using (3) for small ξ and (5) for large ξ may be expected to give the best accuracy. The respective domains may then be separated at a break point. It is assumed that such a point exists. The coordinate of this break point, ξ_0, will be identified later in the paper.

Summarizing the above-mentioned, it is possible to write a procedure for calculating the value of the function $F_i^u(\xi)$ for all the powers of a polynomial over a specified wire segment as

$$F_i^u(\xi) = \frac{1}{\xi}\left(z^i e^{\xi z}\Big|_{z_1}^{z_2} - iF_{i-1}^u\right), \quad |\xi| > \xi_0 \tag{4}$$

$$\begin{aligned} F_i^u(\xi) &\cong \tfrac{1}{i+1}\left(z_2^{i+1} - z_1^{i+1}\right) + \tfrac{1}{1!}\tfrac{1}{i+2}\left(z_2^{i+2} - z_1^{i+2}\right)\xi \\ &\quad + \tfrac{1}{2!}\tfrac{1}{i+3}\left(z_2^{i+3} - z_1^{i+3}\right)\xi^2 + \ldots \\ &\quad + \tfrac{1}{(n-1)!}\tfrac{1}{i+n}\left(z_2^{i+n} - z_1^{i+n}\right)\xi^{n-1}, \\ &\qquad |\xi| \leq \xi_0 \end{aligned} \tag{5}$$

These expressions allow partially recursive process of calculating the radiation integrals with hierarchical power basis functions.

Now it is left to evaluate the value of ξ_0, giving an optimum with respect to the best achievable accuracy. This requires error estimates for the series expansion, as well as for the exact expressions obtained by integration by parts.

2.4. Error Estimation for Lower Frequencies

The accuracy of the approximation (5) is defined by the number of terms left in the truncated series. The series is not slowly converging (convergence is better than one of sine or cosine functions) and this promises to give advantage in both speed and accuracy for the wire segments that have a short electrical length, as compared against the direct integration by parts. This feature is particularly important for curved structures geometrically approximated with a large number of small straight wire segments.

Considering a truncated series approximation (5) of order m of the function $F_i^u(\xi)$ in (1), the fractional accuracy of (5) may be evaluated by the ratio of its $(n+1)^{th}$ term to the first one:

$$\delta_{F_i}^{\xi n} = \frac{\tfrac{1}{n!}\tfrac{1}{i+1+n}\left(z_2^{i+1+n} - z_1^{i+1+n}\right)\xi^n}{\tfrac{1}{i+1}\left(z_2^{i+1} - z_1^{i+1}\right)}.$$

To simplify further discussions, consider $z_2 = L, z_1 = -L$, where L is the half-length of the wire segment. The terms of the series (5) with even powers are zero, and only the odd-powered terms would be considered. The formula for estimating the fractional accuracy of expression (5) then reduces to

$$\delta_{F_i}^{\xi L} = \tfrac{1}{n!}\tfrac{i+1}{i+1+n}\left|L\xi\right|^n \tag{6}$$

2.5. Error Estimation for Higher Frequencies

Derivation of an error estimate for the exact formula (4) is done in an iterative manner. For a zero-order power basis function, the absolute error in the exact expression for F_0^u may be evaluated as ε^1/ξ. Continuing with the other terms (e.g. $\varepsilon^1/\xi^2 + L\varepsilon^1/\xi$ for the next function, F_1^u), the absolute error for the function F_i^u with arbitrary index $i = 0, 1, 2, \ldots$ may be written as

$$\Delta F_i^u \leq \tfrac{\varepsilon^1}{\xi^{i+1}} i!\left(1 + \xi L + \tfrac{(\xi L)^2}{2!} + \ldots + \tfrac{(\xi L)^i}{i!}\right) \cong \tfrac{\varepsilon^1}{\xi^{i+1}} i! e^{\xi L}.$$

The value of ε^1 may be found from the previously

found estimate for the inaccuracy of F_0^u:

$$\frac{\varepsilon^1}{\xi F_0^u} = 2\frac{\varepsilon_0}{2}\frac{1}{\xi L},$$

so that $\varepsilon^1 = 2\frac{\varepsilon_0}{2}\frac{1}{\xi L}\xi F_0^u \le 2\frac{\varepsilon_0}{2}\frac{1}{\xi L}\xi 2L = 4\frac{\varepsilon_0}{2}$. Then the fractional inaccuracy for the terms with odd i may be estimated as

$$\frac{\Delta F_i^u}{F_i^u} \cong \frac{\frac{\varepsilon^1}{\xi^{i+1}} i! e^{\xi L}}{\frac{1}{i+1}\left(L^{i+1} - (-L)^{i+1}\right)} = 2\frac{\varepsilon_0}{2} e^{\xi L} \frac{(i+1)!}{(\xi L)^{i+1}}, \quad (7)$$

$$i = 1,3,5,\ldots, \quad |\xi L| \to 0$$

From this expression it is easy to see that the errors may accumulate very quickly, as the degree of polynomial (i) increases. This is very different from the behavior of the truncated series approximation, which changes much slower as there is no factorial dependency on the degree of polynomial.

It may also be noted that it is possible to derive the expressions for errors due to the non-recursive closed analytical form of the expression (1). It has the same form as the expression (7). As such, it possesses the same poor properties when applied to integration of high order polynomial basis functions on short intervals.

The both error functions, (6) and (7), are depicted in Fig. 1. The change in power i from 0 to 6 does not change the error of the truncated series approximation (6) much, at the same time producing dramatic effect in the error function (7) resultant from the integration by parts (4). From the point of view of the best accuracy that should be possible to achieve by combining the functions (4) and (5), the figure illustrates existence of an optimum value of ξ_0 for each pair of i and n. Considering an example with i=0 and n=1, a better accuracy may be obtained via the truncated series until approximately $\xi_0 = 2.1\cdot 10^{-8}$. After that point either a higher degree truncated series i, or the exact expression (4) should be used.

2.6. Finding a Break Point

Setting the derived error estimates for the series (6) and integration by parts (7) equal to one another gives an equation (where the exponent is approximated with its first term only, unity):

$$\frac{1}{n!}\frac{i+1}{i+1+n}(L\xi)^n = 2\frac{\varepsilon_0}{2}(i+1)!(\xi L)^{-i-1}.$$

This leads to an estimate for an optimum position to separate the domains for applying either the exact formula or truncated series approximation, shown in the expression (8):

$$|\xi_0| = 1/L\left(2\frac{\varepsilon_0}{2} n!(i+1)!\left(1+\frac{n}{i+1}\right)\right)^{\frac{1}{(n+1+i)}} \quad (8)$$

This expression is numerically expensive. It is possible to reduce the computational costs by pre-tabulating the function of two arguments, n and i. With a careful selection of tabulated values, this approach can still lead to nearly optimal in terms of accuracy results.

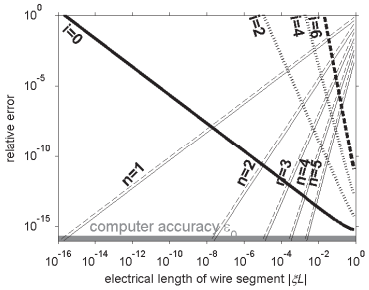

Figure 1. Relative inaccuracies in calculating integrated-by-parts functions and their truncated series approximations versus the electrical length of wire segment. Thick lines correspond to the function $F_i^u(\xi)$ with value of power *i*=0,2,4 and 6. Thin lines correspond to the truncated Maclaurin series approximation of degree *n*=1,2,3,4 and 5. These lines are either solid (*i*=0) or dashed (*i*=6). A gray strip at the bottom of the graph denotes the computer uncertainty level for double precision (i.e. $\varepsilon_0 = 2^{-53} \approx 1.1\cdot 10^{-16}$).

3 A Note On Computing the Far Field Series

The total electrical field at a point is formally calculated as a sum of fields produced by each wire segment. The field due to a single wire segment is a sum of components due to hierarchical basis functions. To compute this double series more accurately, it is better to interchange the order of summation, so that the field components corresponding to the same power i for all of the wire segments would be added up in the inner loop:

$$\sum_{wires}\sum_{i} \Rightarrow \sum_{i}\sum_{wires}$$

It may be noted, though, that rearranging the summation this way may lead to a drop in speed of

summation cased by a lower efficiency of usage of cache present in most of the currently available computer systems. This note however is valid only where the amount information related to the geometry of wire requires an amount of memory that is substantially larger than the size of cache.

4 Results

Typically, the achievable accuracy for radiation pattern measurements done in an anechoic chamber is around 40dB, which corresponds to the relative inaccuracy in the electrical field magnitude of 10^{-2}. From the plots in Fig. 1, it is easy to see that the exact function (4) resulting from integration by parts is incapable of this accurate reproduction of the far field for short wire segments when high-order polynomials are used to characterize the current. For this situation, an adaptive algorithm for computing the functions (4) and (5) has been developed, implemented in Matlab [12], and tested with Maple [14].

The testing was done by comparing the numerical calculations produced within Matlab against the results of closed-form analytical calculations performed in Maple. Matlab uses double precision number representation that gives up to 16 significant figures. Maple was set up to provide reference results with over 100 significant digits. The testing has confirmed accuracy of the combined approach.

For a low number of wire segments and high number of points in far field, the performance of the calculations done within Matlab [12] (without any compilation) was found to be only 20% slower than the speed of the commercially available WIPL-D. This confirms the efficiency of the proposed algorithm. Taking into consideration (a) the speed improvement potential from code optimization and compilation [13], (b) the fact that program WIPL-D [10] does all calculations with single precision, and (c) that Matlab uses a slower double precision, it is expected that the efficiency of the proposed algorithm is superior to WIPL-D's.

As a final remark, it may be noted that the best achievable accuracy decays as the degree of polynomial is increased. At the break point, the accuracy of results cannot be improved using the present approach. However, for practically usable (up to about 9) powers referred to [11], the available accuracy still exceeds the measurement errors by a substantial margin.

5 Conclusion

The expressions for estimating far field due to higher-order polynomial basis functions within the thin wire approximation in the method of moments have been developed.

The calculations have been branched. At lower frequencies, a Maclaurin series expansion has been applied. At higher frequencies, a recursive expression based on the integration by parts has been utilized. Formulas for evaluating errors in the resulting far field estimates due to numerical round-off effects have been developed for both higher and lower frequency branches. An accuracy-optimum boundary separating the use of higher- and lower-frequency formulae has also been found.

An algorithm utilizing the recursive properties of the two approaches has been developed and implemented in Matlab. The accuracy of the results has been validated against analytical computations done in Maple with virtually unlimited accuracy.

A comparison of Matlab code against commercial electromagnetic modeling software WIPL-D has demonstrated the high performance and good potential for the proposed approach.

6 Acknowledgment

This work was supported in part by the Research Fellow's scholarship from the Faculty of Information Technology, Mathematics and Electrical Engineering at the Norwegian University of Science and Technology, Norway.

The author would like to thank his scientific supervisor Professor Jon Anders Aas, whose comments and support have been invaluable.

References

[1] Balanis, C.A., *Antenna Theory: Analysis and Design*. –New York: John Wiley & Sons, Inc., 1997

[2] Chew W.C., Jin J.-M., Michielssen E., and Song J., *Fast and Efficient Algorithms in Computational Electromagnetics*. –Artech House, 2000.

[3] A. Shlivinski and E. Heyman, Discrete array representation of continuous space-time source distributions, *Turk. J. Elec. Engin.*, vol. 10, no. 2, 2002, pp. 257–271.

[4] D. R. Hackett, C. D. Taylor, D. P. McLemore, H. Dogliani, W. A. Walton III, and A. J. Leyendecker, A transient array to increase the peak power delivered to a localized region in space: Part I theory and modeling, *IEEE Trans.*

Antennas Propag., vol. 50, no. 12, 2002 pp. 1743–1750, pp. 1743–1750.

[5] S. Yang, Y. B. Gan, and P. K. Tan, "A new technique for power-pattern synthesis in time-modulated linear arrays," *IEEE Antennas Wireless Propag. Lett.*, vol. 2, July 2003, pp. 285–287.

[6] Jagath K.H. Gamage, *Efficient Space Domain Method of Moments for Large Arbitrary Scatterers in Planar Stratified Media*. Dr.ing. thesis, NTNU, 2004.

[7] Råde L., and Westergren B., *Mathematics handbook for science and engineering*. – Birkhauser Boston, Inc., 1995.

[8] Djordjevic A.R. et al., AWAS for Windows 2.0, Software and Users Manual. –Northwoood MA, Artech House, 2002.

[9] Makarov S.N., *Antenna and Electromagnetic Modeling with Matlab*. –New York: John Wiley & Sons, Inc., 2002

[10] Kolundzija B.M., Djordjević A.R., *WIPL-D: Electromagnetic Modeling of Composite Metallic and Dielectric Structures. Software and User's Manual*. –Boston: Artech House, 2000

[11] Kolundzija B.M., Djordjević A.R., *Electromagnetic Modeling of Composite Metallic and Dielectric Structures*. –Boston: Artech House, 2002

[12] Matlab Programming, Version 7 (Release 14). The MathWorks, Inc., 3 Apple Hill Drive, Natick, MA 01760-2098, USA, 2004. Web: *http://www.mathworks.com/*.

[13] Matlab Compiler User's Guide, Version 2.1 (Release 12), The MathWorks, Inc., 3 Apple Hill Drive, Natick, MA 01760-2098, USA, 2000.

[14] Maple 9.5 Getting Started Guide. Toronto: Maplesoft, a division of Waterloo Maple Inc., 2004. Web: *http://www.maplesoft.com/*.

Appendix C. About the Program

This appendix provides a brief overview of the program implementing the theoretical foundations given in the previous chapters. This is followed by two examples of the methods used to test the program and verify the correctness of the results produced by the program.

Program's Structure and Functionality

The program realising the ideas described in previous chapters was written in Matlab [Matlab, 69], a language and programming environment that has become a de-facto standard tool in numerical research. This choice was dictated by the clearness of the language, compactness of the matrix manipulations, excellent options for plotting, as well as by a positive experience with Matlab gained by the author from his past work.

Matlab is in its essence an interpreting language. It does not create a binary realisation of the code, but rather interprets the lines of code one by one and calls related libraries to execute these lines. The sacrifice in performance, arising from this, was exchanged for a convenience and compactness of programming, and is also compensated by the wide set of mathematical tools embedded in and available with the language.

At its current state, the program and all related sub-routines for data exchange and presentation, together with the functions for plotting and optimisations used to generate plots for this thesis, took about 20 thousand lines of code and consume over 800 kB of disk space. This includes the following components:

i. Program for electromagnetic analysis and modelling, including functions and scripts for geometrical modelling, computing impedance matrix, far field etc.

ii. Libraries written for data exchange with WIPL-D

iii. Libraries written for data presentation (geometry, current distribution etc.)

iv. Functions and scripts written for geometrical model generation (such as dipoles, monopoles, spirals, etc.)

The program (i) for performing electromagnetic analysis and modelling has the following structure:

1. Load set-up parameters and geometry.
2. Validate geometry (overlapping wires, invalid parameters etc.)
3. Prepare/calculate intermediate parameters to speed up calculations.
4. Estimate symmetry of impedance matrix.
5. Establish junctions of wires.
6. Establish wire variables and their relation to junctions and wires.
7. Enter a loop for stepping through frequency, set up the order of calculating the elements of impedance matrix:
   a. Define the order of calculating and filling in the impedance matrix.
   b. Calculate impedance matrix elements Z_{jp}.
      7.b.1. Evaluate 4 partial impedances:
         7.b.1.1. Each impedance is split into 3 separate integrals, one due to the vector potential $\boldsymbol{A}$, and two due to scalar potential V. Self-impedance elements are processed separately.
      7.b.2. If a ground plane is present, calculate partial impedances due to symmetry consideration.
   c. On competition, copy the lower triangular matrix to upper one, if the matrix is symmetrical.
   d. Estimate the condition number, and the error in currents to be obtained.
   e. Save the impedance matrix into a file.
   f. Calculate the load impedances $\mathbf{Z}_L$ due to loadings, and add to the impedance matrix: $\mathbf{Z} = \mathbf{Z} + \mathbf{Z}_L$. Save the matrix $\mathbf{Z}_L$.
   g. Go through the list of generators:
      7.g.1. Calculate the excitation vector $\mathbf{V}$.
      7.g.2. Solve the system of linear equations $\mathbf{Z} \cdot \mathbf{I} = \mathbf{V}$.
      7.g.3. Compute the remaining currents using Kirchhoff's current law.
      7.g.4. Save currents into a file.
      7.g.5. Obtain the network parameters:
         7.g.5.1. Calculate admittance (y) parameters, and then compute impedance (z) and scattering (S) – parameters.
      7.g.6. Compute radiation pattern:
         7.g.6.1. For each specified angle, calculate total electric field due to all wires. Add the fields due to reflections from the ground plane, if a ground plane is present.
      7.g.7. If specified in set-up, load results produced by WIPL-D, and compare with own results. Calculate the error between the two sets of parameters. The errors in the following parameters are estimated: current I, network parameters Y, Z and S, and far field pattern.
   h. Set Up Chains:
      7.h.1. Find all long sequences of wires and denote them as chains.
      7.h.2. Split electrically exceedingly long chains into shorter ones (maximum length is set with parameter k_{max}).
      7.h.3. Convert remaining wires into chains.
      7.h.4. Calculate intermediate parameters.
      7.h.5. Establish an array of equivalent wires.

7.h.6. Establish chain variables and their relation to junctions and chains.
7.h.7. Set up basis functions for chains.
7.h.8. Form compressing matrix **M** interrelating original variables and new variables with the following relationship: $\mathbf{I}^{old} = \mathbf{M} \cdot \mathbf{I}^{new}$.
7.h.8.1. For old independent variables.
7.h.8.2. For old dependent variables – establish a linear relationship with old independent variables.

i. Apply compression matrix to impedance matrix and excitation vector, and obtain new impedance matrix and voltage vector.
j. Estimate the condition matrix of new impedance matrix.
k. Solve new linear system, and obtain new currents $\mathbf{I}^{new}$.
l. Fill in the vector of old currents: $\mathbf{I}^{old} = \mathbf{M} \cdot \mathbf{I}^{new}$.
m. Calculate the error in the solution based on the compressed matrix.

8. End of the loop.

On Program Validation

Testing of the program and validation of results are essential design cycle components.

An intensive testing was done to verify that various input geometries are supported, as well as that the program produces correct results, measurable to reference formulae and comparable with the results produced by other programs for electromagnetic modelling.

A sample of one of the comparison runs when an electrically thin dipole was investigated is shown in the below.

The dipole is a symmetrical 10 m long, composed of 10 equal wire segments. It was fed with a delta gap generator, and tested at the frequency of 1 MHz. Several versions of different radius were probed, as stated in the table below. The table below shows a summary of the input impedance figures due to WIPL-D and own code. The last four rows show the results produced by the own program and compared against WIPL-D.

Model \ **radius =**	**1um**	**1mm**	**10cm**	**500mm**
Theoretical formula for el. short dipole	**0.21932 - 16469i**	0.21932 - 8582.6i	0.21932 - 3324.7i	0.21932 - 1487.2i
WIPL-D	0.21391 - 16419i	0.20753 - 8515.0i	0.17885 - 3171.7i	0.11118 - 1250.9i
WIPL-D with power balance	0.21422 - 16419i	0.20783 - 8515.0i	0.17911 - 3171.7i	0.11136 - 1250.9i

option				
WIPL-D with caps				0.16644 - 1875.1i
WIPL-D with caps zero radius				0.16684 - 1879.2i
WIPL-D with caps + power balance + zero radius				0.16698 - 1879.2i
WIPL-D with 2 segm. only + power balance	**0.21974 - 16443i**	**0.21974 - 8567.9i**	**0.21974 - 3351.1i**	**0.21974 - 1648.5i**
WIPL-D with 6 segm. only + power balance + caps				0.16792 - 1884.5i
WIPL-D plate model with end caps				0.19886 - 1669.8i
WIPL-D plate model w/o end caps				0.17674 - 1700.2i
WIPL-D plate model with power balance				0.17675 - 1700.2i
WIPL-D plate model with power balance w caps				0.19887 - 1669.7i
Own program	0.21389 - 16420i	0.20751 - 8515.0i	0.17884 - 3171.6i	0.11119 - 1251.0i
Own program + compression algorithm	0.21940 - 16444i	0.21940 - 8567.9i	0.21940 + 3351.0i	0.21939 - 1648.6i
Rel err in current at the feed point (**own prog**)	8.8e-5	7.3e-5	3.8e-5	1.6e-5
Max rel error in current at the feed point (when using the compression technique; **own**	0.019	0.038	0.12	0.48

program)				

A sample of comparing the radiation pattern (for a different antenna) is also available:

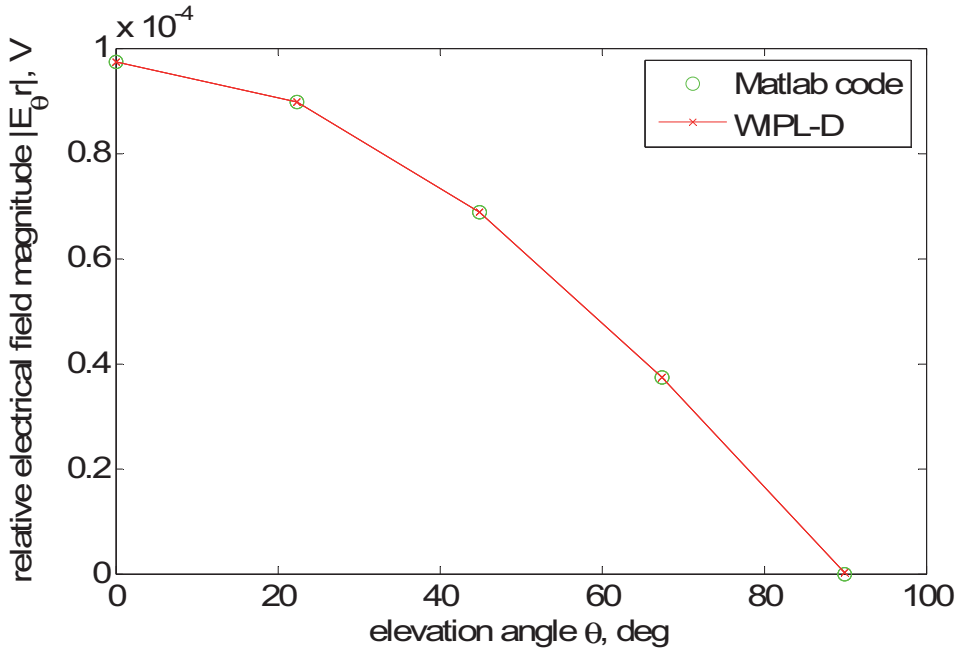

Figure D-1. E-plane pattern of a monopole on an infinite ground plane. Results of WIPL-D and own code compared. The frequency is 1 MHz, monopole length 2 m, monopole wire radius 0.1 mm.

The figure shows an excellent match between the results due to WIPL-D and the results produced by own code.

Note:

An alternative to the program WIPL-D, which could probably be also used for testing, is the program AWAS [Djordjevic et al., 17]. It is based on a similar theoretical basis [Djordjevic et al., 15, 16].

Appendix D. Flowchart of Changes Required to a Standard Program to Support Compression Technique

The flowchart for a standard method of moments code and additional components required are shown below. The additional (new) components are the three grey boxes on the right hand side.

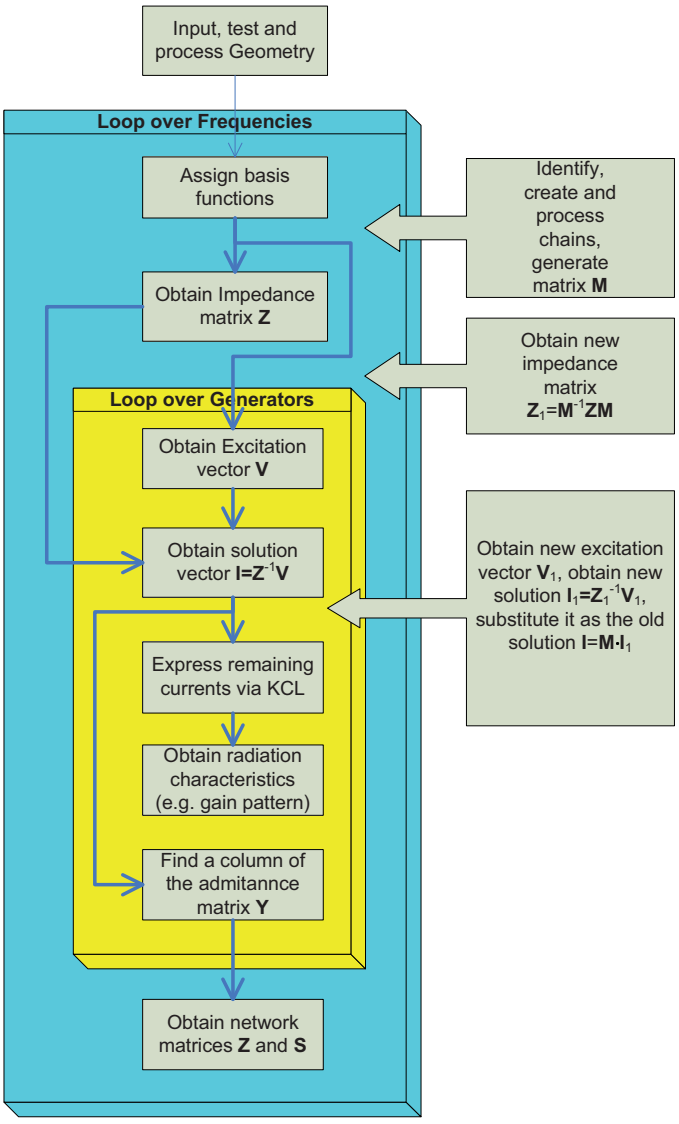

Appendix E. On Extraction of Data Points from a Scanned Source

Sometimes, for example when the paper was old, it was difficult to get hold of the original report, which could have provided access to tabulated data. Therefore, the data contained in the plots published in the [Taguchi et al., 107] was extracted from the plots and tabulated by applying image processing techniques. The procedure outlined in below describes the steps taken to extract the data (taking example of the plot of the input resistance versus frequency in Fig 3b of [Taguchi et al., 107]):

1) An image file containing the plot was rotated to align the function axis with the vertical axis.
2) The coordinates (in pixels) of the markers on the abscissa and ordinate axes were sampled and expressions generated to convert the horizontal and vertical pixel counts into the respective physical quantities
3) Reference image of a circle (denoting the real part of the input impedance in the plot) was generated, based on the pixel counts estimated from the image file of the plot
4) A two dimensional convolution between the image of the plot and the image of reference circle was applied to obtain estimations for the positions of the measured data points. The convolution produced an image with peaks corresponding to the positions of the circles (and a few additional peaks due to other parts of the image in the plot)
5) A threshold of 30 intensity counts (relative to the maximum intensity count in the convolution image) was applied to enhance the visibility
6) The positions of the measured data points (in terms of the pixel counts) were extracted by searching for the points of maximum; a small area around each detected point was immediately cleared to permit finding the next peak
7) The extracted positions were then manually filtered to eliminate the few false data points

8) The obtained set of positions was then converted from pixel counts into physical quantity units to produce a table of measured data points